The role of low oxygen on the self-renewal and neural differentiation of human pluripotent stem cells.

A thesis submitted for the degree of Doctor of Philosophy

by

Rachel L Steeg (BSc)

2014

Cardiff School of Biosciences, Cardiff University

Declaration

This work has not been submitted in substance for any other degree or award at this or any other university or place of learning, nor is it being submitted concurrently in candidature for any degree or other award.

STATEMENT 1

This thesis is being submitted in partial fulfilment of the requirements for the degree of PhD.

STATEMENT 2

This thesis is the result of my own independent work / investigation, except where otherwise stated. Other sources are acknowledged by explicit references. The views expressed are my own.

STATEMENT 3

I hereby give consent for my thesis, if accepted, to be available for photocopying and for inter-library loan, and for the title and summary to be made available to outside organisations.

Signed …… (candidate) Date 01.10.2014

Abstract

Human embryonic stem cells are derived from the pre-implantation blastocyst, residing in an extremely low oxygen environment. Application of this *in vivo* oxygen concentration to an *in vitro* setting has previously shown to be essential for driving the self-renewal and directed differentiation of human pluripotent stem cells. However, studies on hESCs at low oxygen have been frequently contra-indicatory. Here, comparative analysis of a hESC and iPSC line at a low oxygen concentration resulted in divergent effects across the two cell lines. Augmented TGFβ signalling was observed in conjunction with up-regulated transcription of pluripotency markers NANOG and POU5F1 in hESCs but not iPSCs. IPSCs also shifted to a state of increased proliferation whereas hESCs did not. It was also observed that exposure of hESCs and iPSCs to light throughout low oxygen culture induced large amounts of apoptosis, highlighting the requirement for careful selection of cell culture equipment for environmental oxygen control.

Both the embryonic and adult brain retain tissue specific oxygen concentrations far below that at atmospheric oxygen concentrations. Previous studies showed that embryonic silencing of factors responsive to low oxygen caused a range of embryonic abnormalities, including deformation of the neural plate and tube. Here, differentiation of hESCs to an early neuroectodermal identity at low O_2 did not definitively augment production of NPCs but did additively suppress BMP signalling above that at atmospheric O_2. A concordant rise in apoptosis was also observed in a manner both independent of, and augmented by, exogenous BMP inhibition. Subsequently, neurogenesis at low oxygen produced terminal neurons with accelerated and augmented synaptic and induced excitability. This was characterised by a rise in the rate of membrane depolarisation, increased action potential overshoot and accelerated expression of pre-synaptic marker Synaptophysin. These results highlight a novel, critical role for low oxygen in augmenting the excitability of hESC derived neurons.

Acknowledgements

Huge thanks to Prof Paul Kemp and Prof Nick Allen for your advice and support over the last few years, couldn't have done it without you! My thanks also to the team at Baker-Ruskinn for the unwavering technical support provided throughout my PhD, particularly Samir Patel and Greg May who gave me fantastic opportunities and steadfastly supported the project.

Thanks to Prof Joachim Fandrey and Dr. Teresa Otto for inviting me to your lab and helping with the HIF staining.

I'd like to thank Dr. Julia Griffiths for the electrophysiology and advice - Team Hypoxia for the win! Also thanks to Dr. Christian Schnell and Dr. Dave Rushton for helping out with the electrophysiology and to Shona Joy for all of her cell culture wisdom. Thanks also to Dr. Belinda Thompson for all your advice and support.

I'd like to say a huge thank you to everyone that I've been lucky enough to spend the last few years working with. It's a family that I will miss enormously when I leave Cardiff and you've all contributed massively to keeping me at least mostly sane throughout. Dani, Tom, Emma, Irene, Sali, Becky, Lydia, Martin, Polly and Seva, its been a pleasure! Stu, thanks for my good luck charm Flamango Frank and Sarah thanks for constantly telling me that it would all come together in the end - look it did! Also thanks to my partner in crime Charlie, you've been a solid friend throughout and I definitely wouldn't have retained any level of sanity without you.

Finally, my biggest thanks go to my family who have been a constant source of steadfast love and support. Thanks Mum, Dad, Claire, Jo, Sarah and Redrobe-Steeglets - you gave me the belief that I could actually do it! I'd like to dedicate this thesis to you.

Abbreviations

ALK	Anaplastic Lymphoma Kinase Receptor
AP	Action potential
ATP	Adenosine triphosphate
bHLH	Basic helix-loop-helix
BMP	Bone Morphogeneic Protein
BMSC	Bone marrow stem cells
BSA	Bovine Serum Albumin
CBP	CREB Binding Protein
CDK	Cyclin Dependent Kinases
CITED2	CBP/P300 Interacting Transactivator Carboxy Terminal Domain 2
CNS	Central nervous system
Cp	Capacitance
CREB	cAMP response element binding protein
CT	Cytotrophoblast cells
CTAD	C-Terminal Activation Domain
DKK1	Dickkopf-1
EB	Embryoid Body
ECL	Enhanced chemiluminescent substrate
ECS	Extracellular solution
EPO	Erythropoeitin
ESC	Embryonic stem cell
FACS	Fluorescence Activated Cell Sorting
FBS	Fetal Bovine Serum
FGF2	Fibroblast Growth Factor-2
FIH	Factor Inhibiting HIF
FSC	Forward Scatter
GD	Gestational Day
GFAP	Glial fibrillary acidic protein
HCG	Human Chorionic Gonadotropin
hESC	human embryonic stem cell
HIF	Hypoxia Inducible Factors
HP-NPC	Hypoxia preconditioned NPC
HRE	Hypoxia response element
hTERT	Human Telomerase Reverse Transcriptase
I	Current
iAPs	Induced action potentials
ICM	Inner cell mass
ICS	Intracellular solution
IK^+ Max	Peak current density of K^+ channels
INa^+ Max	Peak current density of Na^+ channels
iPSC	Induced pluripotent stem cell
KSR	Knockout Serum Replacement
LEF	Lymphoid Enhancer Binding Factor

MAP2	Microtubule assembly protein-2
MEFi	Irradiated mouse embryonic fibroblast
mEpiSC	Mouse epiblast stem cell
MSC	Mesenchymal stem cell
NPC	Neural Progenitor Cell
NSC	Neural Stem Cell
NT-ESC	Nuclear Transfer Embryonic Stem Cell
NTAD	N-Terminal Activation Domain
ODDD	Oxygen Dependent Degradation Domain
PBS	Phosphate Buffered Saline
PFA	Paraformaldehyde
PHD	Prolyl hydroxylases
PI	Proliferative Index
PSC	Pluripotent stem cell
PSD95	Post-synaptic density protein 95
pVHL	Von Hippel-Lindau protein
RB	Retinoblastoma protein
R_{in}	Input Resistance
ROS	Reactive oxygen species
s100B	S100 Calcium Binding Protein-B
sAP	Spontaneous action potential
SDS	Sodium dodecyl sulphate
SDS-PAGE	Sodium dodecyl sulphate polyacrylamide gel electrophoresis
SGZ	Subgranular zone
siRNA	Small interfering RNA
SSC	Side Scatter
SSEA	Stage Specific Embryonic Antigen
SVZ	Subventricular zone
TBS	Tris Buffered Saline
TCF	T-Cell Factor
TGFB	Transforming Growth Factor Beta
TRA	T cell Receptor Alpha locus
TUNEL	Terminal deoxynucleotide transferase dUTP
VEGF	Vascular Endothelial Growth Factor
V_m	Resting membrane potential
VZ	Ventricular zone

Table of Contents

List of Figures

List of Tables

1. Introduction

1.1 Pluripotent Stem Cells

1.1.1 Clinical applications of post-embryonic stem cells.

One of the major challenges facing medical therapeutics is the replacement of organs and tissues that either due to injury or illness have become dysfunctional. The majority of tissue or cells used in transplantation are currently supplied by living or 'dead' donors ('dead' donors have blood flow and oxygen supply maintained externally to keep organs viable until removed for the recipient). This reliance on person to person donation has many issues, the main being a huge inadequacy of supply to meet demand with only 30-40% of the patients on the waiting list for transplantation actually receiving organ donation annually (Abouna 2008; Aulisio et al. 2007; POST 2013). The risk of autoimmune transplant rejection and the unsuitability for all tissues to undergo transplantation in this way, particularly neural tissue, increase complexity (Abouna 2008; Aulisio et al. 2007; Dunnett et al. 1997). Achieving a supply of cells which are of defined identity, from a known genetic background and from a limitless supply has huge implications for aiding research into disease modelling, high throughput drug screening and toxicity testing, in addition to phasing out current reliance on animal use with its associated ethical objections (Ebert et al. 2012).

To counterbalance the lack of available tissue suitable for transplant, stem cells are now widely investigated as an alternative cell source. Stem cells have a remarkable ability to form fully functioning cells and tissues, with the degree of plasticity and possible lineage formation dependent on the stem cell populations used. The populations shown to have the most success in human transplants so far are bone marrow stem cells (BMSCs), including haemotopoietic and mesenchymal stem cells. Although both populations were first discovered in the

bone marrow as bone cell precursors, they have now been isolated from multiple sources in the human body including adipose tissue, peripheral blood supply and embryonic products such as the placenta and umbilical cord. As well as undergoing self-renewal to maintain the undifferentiated stem cell population, they can also be directed to form somatic cell populations, a process termed 'differentiation'. After over 200 clinical trials to investigate safety and efficacy of transplantation, BMSCs have been shown to be largely effective with minimal levels of toxicity and side-effects (Ren et al. 2012; S. Wang et al. 2012). Transplantation for the treatment of haematological disorders (e.g. sickle cell disease) and cancers of the blood and bone marrow (e.g. leukaemia) have been performed since the 1960's with great success (Kearney & Richardson 2005). More recently transplantation has been shown to improve cardiac function after ischemic infarcts, liver function in patients with end-stage liver failure, motor and nerve function after injury to the central nervous system and increased survival after Graft vs Host disease (an autoimmune reaction after hematopoietic stem cell transplantation), indicating large potential for the use of stem cells in therapeutic cell replacement (S. Wang et al. 2012; Ren et al. 2012; Jiang et al. 2013; Szabó et al. 2013; S. Wang et al. 2013)

1.1.2 Clinical applications of human embryonic stem cells.

Classically, mesenchymal stem cells (MSC) differentiate to chondroblasts (cartilage), adipocytes (fat) or osteoblasts (bone), a fairly limited range of cell types specific to the mesodermal lineage (Ren et al. 2012). Alternatively, human embryonic stem cells (hESC) retain a higher level of plasticity and are capable of forming all germ layers and tissues present post-natally, a quality known as 'pluripotency'. Because of this, hESC have the potential to supply an indefinite amount of human cells which have been specifically produced for purpose. They were initially derived from the inner cell mass (ICM) of pre-implantation embryos *(Figure 1)* (Thomson 1998). Explant and culture of the ICM allows for the pluripotent state to be captured before differentiation and embryonic development, and derived to form a stable hESC line. The hESC line can then be

maintained indefinitely, either undergoing self-renewal to form identical daughter cells or directing cell fate to form fully functional somatic cells and tissues (Kumar 2010; Camarasa et al. 2012; Thomson 1998).

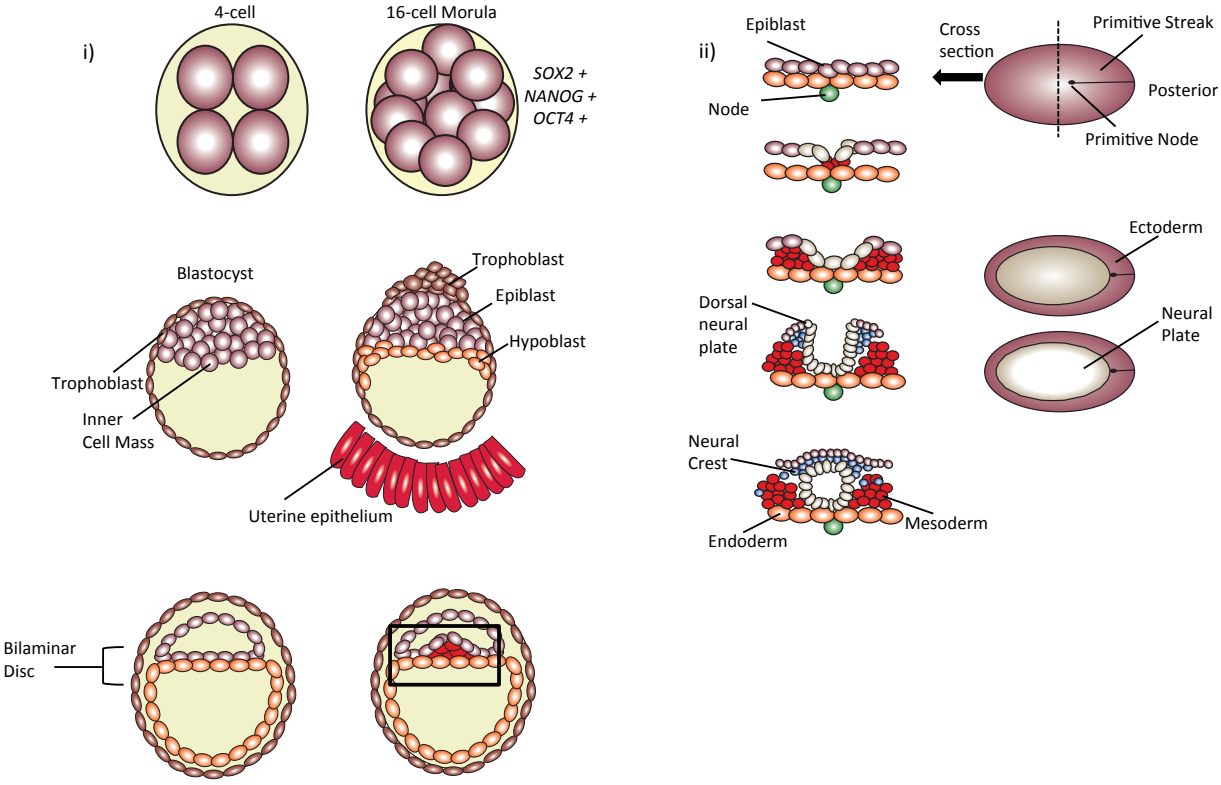

Figure 1.1. Early embryonic development.

(i) Post-fertilisation, the 2 cell zygote undergoes rounds of cell division to increase cell number. The 16-cell Morula then gives rise to the blastocyst, a transient structure consisting of an outer shell of trophoblast cells (which will develop into the placenta and extra-embryonic tissues) and the Inner Cell Mass (ICM). Invasion of the trophoblast into the maternal uterine epithelium forms foetal vascular connections allowing implantation of the blastocyst. In the immediate post-implantation period of development, the ICM (a pluripotent population of cells) gives rise to the epiblast and hypoblast. The epiblast subsequently forms the primary germ layers responsible for embryonic development, outlined in black. The outlined black cross-section can be viewed in more detail as in (ii). Cells in the posterior region of the epiblast begin to migrate towards the central point, causing the epiblast to thicken and invaginate, a formation known as the Primitive Streak. Movement ventrally into the hypoblast leads to formation of the Endoderm and Mesoderm germ layers and the remaining epiblast becomes the Ectoderm. The thickened point of the Primitive Streak (known as the Node) now lies in the dorsal Mesoderm layer and provides signals to the overlying ectoderm to form the neural plate, and subsequent folding to form the neural tube.

Because of their ability to endlessly self-renew and efficiently differentiate, the possibilities for their use in replacing degenerated or injured tissue are vast. In 2012, the first successful trial of transplantation of hESC derived cells was completed in the human eye. A number of degenerative disorders lead to loss of visual photo-receptors and subsequent blindness, Stargardt's macular dystrophy and age-related macular degeneration being the two most common in the developing world. In patients suffering from these diseases, transplantation of hESC-derived retinal pigment epithelium cells into a region of the eye with functioning photo-receptors resulted in integration of the graft and improved visual function with early signs indicating no adverse side effects (Schwartz et al. 2012).

Although research using human recipients has been slowed due to fears of tumour formation (a common concern of pluripotent cells due to high rates of self-renewal which may be addressed by prolonging the maturation of transplanted cells, hence avoiding the introduction of highly proliferative multipotent progenitors), many studies have reported functional improvements after insertion of hESC derived somatic cells into animal models of degenerative disease (Baker 2009; Doi et al. 2012; Brederlau et al. 2006). Grafts of hESC derived cardiomyocytes, (the cells which make up cardiac muscle) not only integrated and formed connections with the damaged host muscle but also vastly improved myocardial function after experimental infarct, although incidences of tumour formation were observed (Dai et al. 2007; Leor et al. 2007; Cai et al. 2007; Caspi et al. 2007). Cell replacement also improved behavioural deficits induced in a rodent model of Parkinsons Disease, a disorder responsible for striatal depletion of dopaminergic neurons and severe loss of motor control. After transplantation, hESC-derived dopaminergic neurons were shown to have integrated into the existing neural circuitry with concomitant increases in depleted neurotransmitters and correction of behavioural deficits (Cho et al. 2011; Ben-Hur et al. 2004). These two possible applications represent just a few of the degenerative illnesses and injuries, which could be targeted and alleviated using targeted stem cell therapy.

1.1.3 Reprogramming somatic cells as an alternative source of pluripotent stem cells.

The introduction of induced pluripotent stem cells (iPSC) has taken the potential of hESCs one step further. It has now been extensively demonstrated that through epigenetic reprogramming, easily accessible somatic cells (such as CD34+ blood cells or dermal fibroblasts) could be transitioned into a pluripotent state, whilst retaining the donor's genetic background (Takahashi & Yamanaka 2006; Ye et al. 2009). This has critical implications for the modelling of diseases with contributory genetic causes, allowing large-scale production of cell populations from a diseased genetic background. When modelling human injury and illness, animal models do not always acutely reflect the human disease. For example, the pathology of Alzheimer's Disease in humans is not fully understood but familial cases are due to mutations in the Amyloid Precursor Protein gene (APP), Presenilin-1 and -2 (PS-1, 2) and ApolipoproteinE (ApoE). The disease state has been characterised by accumulation of extracellular amyloid plaques, intracellular neurofibrillary tangles and a loss of acetylcholine transmission with distinct memory and behavioural impairments. Models in multiple species including guinea pigs, rodents and dogs have been investigated but no single model accurately reflects the human disease progression and pathology, at least partly underlying the slow progress in pharmaceutical targeting of the disease. Those that most accurately reflect Alzheimer's Disease require triple mutations of the named genes, a genotype which has not been observed in humans so is not a genotypically accurate reflection of the diseased state (Duff & Suleman 2004; Bales 2012). Moreover, familial cases of Alzheimer's Disease represent only a tiny minority of total cases, the use of iPSCs allows for modelling of sporadic cases without prior knowledge of underlying genetic causes (Lambert & Amouyel 2011; Israel et al. 2012)

IPSCs are now being used to tackle this issue by generating pluripotent stem cells (PSCs) derived from individuals with genotypes of interest. Specific cell populations, which are sensitive to degeneration can then be made by directing

stem cell differentiation to a somatic cell of interest; this may be extremely useful in two regards. Firstly, disease modelling for therapeutic cell replacement can be targeted with the individual's own cells, so hypothetically reducing the risk of immune rejection (Scheiner et al. 2014; de Almeida et al. 2014). Secondly, testing of pharmaceuticals can be performed on cultured human cells with a physiologically relevant disease genotype. The initial landmark study by Yamanaka et al., which generated the first iPSCs required forced expression of four key genes that regulate pluripotency, POU5F1, KLF4, c-myc and SOX2 into fetal fibroblasts. Due to this genetic manipulation, these somatic cells underwent epigenetic reprogramming, transitioning from a tissue specific gene expression to a re-established pluripotent state (Takahashi & Yamanaka 2006). Recent advances have avoided the use of the oncogene c-myc, circumventing the risk of increased incidences of tumour formation. Advances in methods of non-integrative gene expression have also avoided random gene integration with its consequential risks to downstream disease modelling (Wu & Hochedlinger 2011; Saha & Jaenisch 2009; Nakagawa et al. 2008; Hou et al. 2013; O'Malley et al. 2009). Once reprogrammed, iPSCs have exhibited many of the hallmarks of hESCs, importantly including the capacity for differentiation down a specific cell lineage. Use of iPSCs also circumvents ethical issues that surround ESCs, as the use of adult somatic cells not require destruction of a donated embryo.

In an exciting development, Tachibana et al. recently demonstrated cell reprogramming through transfer of a somatic cell nucleus into the cytoplasm of human oocytes, forming pluripotent ESCs (NT-ESC) (Tachibana et al. 2013). In addition to avoiding introduction of genetic material, it was shown that in mouse cells, iPSC retained DNA methylation patterns which were reminiscent of the original donor cell and favoured differentiation along that lineage. Conversely, NT-ESCs showed methylation status' and differentiation potential which were more reflective of hESCs (Kim et al. 2010). Additionally, a comparison of iPSC and NT-ESC derived from a mouse line with telomere dysfunction showed diminished mitochondrial function and telomere lengthening in iPSCs, but not NT-ESCs (Le et

al. 2014). Hence, somatic cell nuclear transfer may be an exciting alternative for large scale production of PSCs.

1.2 Characterising human embryonic stem cells.

Pluripotent stem cells are typically characterised by a number of different markers, both transcriptional markers which are recognised as critical for maintaining the pluripotent state and cell surface markers specific to PSCs. Whilst many of these studies have been performed on ESCs, these markers are also relevant for iPSCs.

Human ESCs express a well-documented array of cell surface markers including SSEA4, TRA-1-60 and TRA-1-81, which in conjunction with stem cell colony morphology are commonly used to assess the quality of cultures (Thomson 1998; Henderson et al. 2002; Draper et al. 2002; Avery et al. 2006; Adachi et al. 2010; Rodda et al. 2005; Z. Wang et al. 2012; Stewart et al. 2006; Reubinoff, Pera, Fong, a Trounson, et al. 2000). Underlying the undifferentiated state is a network of key transcriptional regulators with POU5F1 (also known as OCT4), NANOG, KLF4 and SOX2 at its core (Avery et al. 2006; Stewart et al. 2006). Expression of these transcription factors is critical for maintenance of the undifferentiated state, so are commonly used as markers of pluripotency. As discussed below, loss of their expression indicates a commitment to differentiation. Upstream of these transcriptional regulators are a number of signalling pathways which are involved in maintaining pluripotency. Among these, TGFβ signalling (through Nodal/Activin), FGF signalling and Wnt signalling are of particular importance (Stewart et al. 2006; Xu et al. 2008; Vallier et al. 2005; Z. Wang et al. 2012; Ding et al. 2010; Li et al. 2007; Sato et al. 2004; Kühl & Kühl 2012; Besser 2004; Eiselleova et al. 2009; Mazumdar et al. 2010).

1.2.1 The regulation of pluripotency in mouse and human embryonic stem cells.

Mouse ESCs were the first embryonic stem cells to be isolated and proliferated successfully (Martin 1981; Evans & Kaufman 1981). Accordingly, much of the early work on the mechanisms of self-renewal has stemmed from mESCs. As the focus here is on the pluripotency signalling of human ESC and iPSC lines, it is worth noting that some aspects underlying the maintenance of self-renewal do differ between mouse and human ESCs. Maintaining the undifferentiated state of mESCs has been reliant on the use of Leukaemia Inhibitory Factor (LIF), a cytokine which activates STAT3, an upstream mediator of MAPK activity (Stewart et al. 2006; Avery et al. 2006). Contrastingly, it's been shown that both LIF and STAT3 activity were not sufficient for maintaining pluripotency in hESCs, or in ESCs obtained from other primates (Dahéron et al. 2004; Sumi et al. 2004). However, LIF mediated regulation of pluripotency is still reliant on POU5F1 or SOX2 mediated transcription (Stewart et al. 2006). Although both mouse and human ESCs have traditionally been generated from the pre-implantation ICM, only explanted human ICM transitioned through an epiblast-like intermediate stage before forming typical hESC colonies which then retained a developmental stage reflective of the post-implantation epiblast (O'Leary et al. 2013; Conley et al. 2005). Derivation of pluripotent cell lines from the mouse epiblast (mEpiSC) have shed light onto an underlying cause of these disparities in signalling, forming a population of cells more reflective of hESCs than mESCs (Brons et al. 2007; Tesar et al. 2007). With an adversity to single cell dissociation, maintenance of pluripotency that was LIF-independent but Activin/Nodal and FGF2 dependent and a rounded, flattened colony morphology, mEpiSCs bore greater resemblance to hESCs rather than mESCs (Brons et al. 2007). Furthermore, their epigenetic status and global gene expression was also more similar to hESCs, than mESCs (Tesar et al. 2007). Hence, the dissimilarities between human and mouse ESC may actually reflect differences in their relative developmental stage, rather than a specific species difference.

1.2.2 Activin/Nodal/TGFβ signalling.

Both Activin and Nodal act to maintain pluripotency through downstream effectors SMAD2/3, this signalling pathway has been outlined in *figure 1.2*. Direct targets of this TGFβ signalling family include NANOG and POU5F1 (Stewart et al. 2006; Xu et al. 2008). The importance of this pathway for maintaining pluripotency in hESC has been clearly demonstrated; blockage of SMAD2/3 phosphorylation resulted in transcriptional down-regulation of *POU5F1* and *NANOG* and induced spontaneous differentiation (Vallier et al. 2009; James et al. 2005). These effects were at least partly due to direct transcriptional regulation; phosphorylated-SMAD2/3 was shown to directly regulate *NANOG* transcription through a binding site in the *NANOG* promoter with overexpression of SMAD3 increasing *NANOG* transcription two-fold (Vallier et al. 2005).

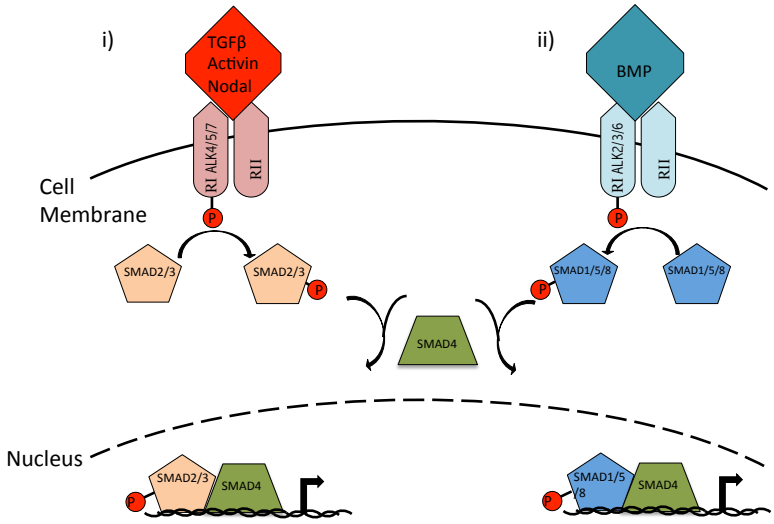

Figure 1.2. TGFβ signalling through Activin/Nodal and BMP.

TGFβ signalling can be separated into two main types. i) TGFβ, Activin or Nodal ligands bind to serine/threonine kinase type I (ALK4, 5 or 7) and II receptors, activation of receptors results allows phosphorylation of downstream transcription factor SMAD2 and SMAD3. Once phosphorylated, SMAD2/3-P translocates to the nucleus and associates with SMAD4 to regulate gene transcription. ii) The Bone Morphogenic Protein (BMP) arm is regulated in a similar manner. BMP binds type I (ALK1, 2, 3 and 6) and type II receptors, activation of kinase activity however results in phosphorylation of SMADS1, 5 or 8. Again, nuclear translocation and transcriptional regulation is performed in conjunction with SMAD4.

1.2.3 NANOG, POU5F1 and SOX2.

NANOG is a homeodomain protein recognised as a key transcription factor required for self-renewal and is a direct transcriptional target of phosphorylated SMAD2/3 (Vallier et al. 2005). ShRNA silencing of NANOG gene expression in hESCs resulted in a loss of POU5F1 and TRA-1-81 expression (Vallier et al. 2005; Z. Wang et al. 2012). It was shown to be rapidly down-regulated upon differentiation of hESCs and has been thought to maintain the pluripotent state via direct inhibitory actions on pro-endoderm transcription factors such as GATA6 and 4, in addition to repressing neuroectodermal differentiation (Vallier et al. 2005; Z. Wang et al. 2012; Mitsui et al. 2003; Rossant 2004).

In vivo, SOX2 expression was first observed at the 2-cell stage of mammalian embryonic development, retaining expression throughout ectodermal differentiation, indicating an additional role in neuronal development (Dee et al. 2007; Keramari et al. 2010; Avilion et al. 2003). It has an essential role in regulating the pluripotent state, both *in vitro* and *in vivo*. Si-RNA depletion of SOX2 in hESCs reduced expression of NANOG, POU5F1, SSEA4 and TRA-1-81 and this loss of self-renewal resulted in a trophoectodermal cell fate. (Adachi et al. 2010; Fong, K. A. Hohenstein, et al. 2008). Conversely, shRNA silencing of SOX2 maintained the pluripotent state of hESCs with no alteration to expression of TRA-1-81, NANOG and POU5F1, although a higher proportion of differentiated colonies was however observed and it is feasible that the use of feeder layers supported SOX2 KD-hESC enough to maintain the undifferentiated state in spite of the loss of SOX2 (Z. Wang et al. 2012).

Similarly to NANOG, protein expression of POU5F1 has also been widely observed in pluripotent hESCs with reduced expression upon differentiation (Gerrard, Zhao, et al. 2005). Silenced POU5F1 expression in hESCs resulted in stabilised SOX2 expression, which was recognised as a pre-requisite for the commitment of hESCs to enter the neuroectodermal lineage. Additionally, a loss of POU5F1 activity resulted in a loss of pluripotency markers SSEA4, TRA-1-81 and NANOG, solidifying that it too is essential for sustaining an undifferentiated state (Z. Wang et al. 2012). BMP/TGFβ signalling was also shown to regulate POU5F1

activity in a dose-dependent manner. In the absence of BMP signalling in mouse and human ESCs, POU5F1 remained at high levels to sustain self-renewal. In the presence of BMP, POU5F1 co-operated with phosphorylated SMAD1/5/8 in a POU5F1 concentration dependent manner. At high levels of POU5F1 transcription, POU5F1 and BMP initiated the commitment of cells towards a mesendodermal fate whereas at low transcript and protein levels POU5F1 regulated transition towards primitive endoderm and extraembryonic ectoderm (Z. Wang et al. 2012; Niwa et al. 2000). Levels of POU5F1 were modulated in concert with NANOG in a biphasic manner, whereby increased POU5F1 directly down-regulated *NANOG* transcription and vice-versa, in addition to POU5F1 repressing it's own transcription (Pan et al. 2006; Wang et al. 2006; Kashyap et al. 2009). These observations from manipulating the expression and activity levels of POU5F1, SOX2 and NANOG in hESCs are consistent with *in vivo* data from mice, whereby these genes were responsible for regulating epiblast development and the early establishment of the primary germ layers (Nichols et al. 1998).

As loss of one of these three key regulators (NANOG, POU5F1 or SOX2) resulted in the deregulation of the remaining two, it also seemed clear that they undergo auto-regulation between them. Evidence from Boyer et al. outlined this process, observing that in hetero-dimeric form they bound to each others promoters, commonly using NANOG as a regulatory co-factor although hetero-dimers of POU5F1 and SOX2 and NANOG homodimers were also observed (Boyer et al. 2005; Wang et al. 2008; Kashyap et al. 2009). This seemed to be reflected in mESCs whereby POU5F1 and SOX2 formed a heterodimer on the NANOG promoter and NANOG fed back to regulate POU5F1 and SOX2 expression (Loh et al. 2006; Boyer et al. 2005; Rodda et al. 2005). Taken together, this points to complex transcriptional regulation between these three transcription factors to sustain a pluripotent state in human and mouse ESCs.

Figure 1.3. Co-regulation between POU5F1, SOX2 and NANOG. *All three transcription factors form heterodimers to regulate transcription of each other, frequently using NANOG as a co-factor.*

1.2.4 MAPK, PI3K/AKT and NFκB as upstream regulators of pluripotency.

In addition to TGFβ signalling and the actions of downstream transcription factors NANOG, SOX2 and POU5F1, other pathways also contribute to maintaining self-renewal. Many transcripts which have been shown to be active exclusively downstream of the MAPK, PI3K/AKT and NFκB signalling pathways were enriched in pluripotent hESCs and down-regulated upon PSC differentiation (Armstrong et al. 2006; Li et al. 2007). Specific inhibition of upstream PI3K, MEK and NFκB signalling led to the subsequent loss of a pluripotent state in hESCs with down-regulated NANOG, POU5F1, SOX2 and SSEA4 expression (Armstrong et al. 2006; Ding et al. 2010; Li et al. 2007). After addition of FGF2 to FGF2 starved hESC cultures, downstream MAPK and PI3K signalling was activated and nuclear translocation of β-catenin was observed (Ding et al. 2010; Li et al. 2007). It is evident that the upstream regulation of self-renewal by MAPK, PI3K and NfκB is performed in conjunction with FGF2 and Wnt/β-catenin signalling.

1.2.5 Canonical Wnt/β-catenin signalling in pluripotency.

The canonical Wnt/β-catenin pathway has been extensively characterised and linked to maintaining pluripotency in hESC through a number of intersecting pathways. Transcriptional regulator, β-catenin, normally undergoes degradation after phosphorylation by a 'degradation complex' (Stewart et al. 2006). Inhibitors of GSK3 (a subunit of the β-catenin degradation complex) was shown to improve establishment of new hESC lines, in addition to sustaining pluripotent hESC cultures (classed as NANOG and POU5F1 positive) in the absence of the conditioned media which would otherwise be responsible for sustaining self-renewal (Sato et al. 2004; Kühl & Kühl 2012). The mode of action required for β-catenin to sustain pluripotency in this manner appeared to be dependent on the functionality of TGFβ receptors, ALK4/5/7 implying cooperation with SMAD2/3 (Besser 2004). In conjunction with this, β-catenin activity may be linked to

increased Nodal signalling, therefore aiding SMAD2/3 phosphorylation (Besser 2004; Stewart et al. 2006). This possibly underlies observations that β-catenin was responsible for up-regulating POU5F1 activity, and in response to FGF2 treatment, underwent nuclear translocation leading to increased LEF/TCF mediated transcription (Ding et al. 2010). In addition to Wnt's coordinated actions downstream of TGFβ, one of the subunits of telomerase, TERT, was indirectly regulated by active β-catenin via a key pluripotency regulator, KLF-4, so possibly contributing to the immortality of PSC lines (Hoffmeyer et al. 2012). That said, Wnt/β-catenin's role in maintaining self-renewal is debated with reports that Wnt is only involved in differentiation to somatic cell fate and not in sustaining a pluripotent state (Kühl & Kühl 2012).

1.2.6 Notch signalling

Notch signalling has been well characterised, with the Notch receptor extending throughout the plasma membrane with extracellular and intracellular domains. Upon ligand binding, the Notch Intracellular Domain is cleaved by the catalytic activity of α and γ-secretases and subsequent nuclear translocation allows transcriptional regulation (Andersen et al. 2012). Canonical Notch signalling was indicated to be vital for the undifferentiated state as inhibition of γ-secretase resulted in transition of hESCs from a pluripotent to a differentiated state signified by loss of POU5F1 expression (Prasad et al. 2009).

1.2.7 Fibroblast Growth Factor-2.

When culturing hESCs and iPSCs, FGF2 has long been used as a critical growth factor to sustain the pluripotent state, without which both hESCs and iPSCs have been shown to undergo spontaneous differentiation (Stewart et al. 2006; Vallier et al. 2005; Ding et al. 2010; Eiselleova et al. 2009). The positive effect of FGF2 on self-renewal has been linked to interactions with several previously mentioned signalling pathways. Specific co-localised expression of FGF receptors on POU5F1 positive cells was seen in both hESCs and iPSCs, inhibition of FGF receptors

resulted in subsequent down-regulation of POU5F1 expression (Ding et al. 2010). However, this drop in pluripotent marker expression was not observed when Activin/Nodal signalling was stimulated and the proportion of pluripotent cells was vastly augmented by combined treatment of FGF2 and Activin (Ding et al. 2010; Vallier et al. 2005). Treatment with Activin then up-regulated FGF2 expression, which fed-back to induce TGFβ1 and BMP antagonist expression as well as inhibiting SMAD1 activity (Stewart et al. 2006; Xu et al. 2008). This indicated that FGF2 was integral in the Activin/Nodal dependent pluripotency network.

Additional to TGFβ signalling, maintenance of pluripotency mediated through canonical Wnt/β-catenin signalling was also partly regulated by FGF signalling. WNT-ligand activation of receptors results in accumulation of the transcription factor β-catenin, which proceeded to regulate downstream transcription of target genes in conjunction with co-activators LEF and TCF (Stewart et al. 2006; Mazumdar et al. 2010). Forced stabilisation of β-catenin in the presence of FGF2 maintained pluripotency of hESCs, but subsequent removal of FGF2 rapidly attenuated POU5F1 activity and self-renewal (Ding et al. 2010). FGF2 also stimulated the transcriptional activity of TCF / LEF, downstream of Wnt and β-catenin (Ding et al. 2010). Finally, FGF2 treatment was responsible for activating the PI3K/AKT and MAPK pathways, promoting pluripotency (Stewart et al. 2006; Li et al. 2007).

1.2.8 High telomerase activity prevents senescence.

A key characteristic of *in vitro* PSCs is the ability to avoid senescence, replicating in culture indefinitely. ESCs have been shown to retain high levels of telomerase activity, an enzyme responsible for conserving the length of telomeres by capping and stabilising chromosome ends. High levels of telomerase have been correlated with immortality of human cell lines and a loss of telomerase activity with finite life-span, common in culture of somatic cells. This partly underlies the ability for pluripotent stem cells (PSCs) to remain stable for an indefinite length of time in culture (Thomson 1998; Stewart et al. 2006).

1.2.9 Pluripotency and low oxygen.

The maintenance of hESCs in a pluripotent state is regulated through interactions of multiple pathways, namely TGFβ, FGF, Wnt/β-catenin and Notch. During *in vitro* culture of hESC, maintaining this state can be labour intensive and costly. Here, the possible advantages of culturing hESC in a low oxygen environment were investigated. As discussed below, an oxygen concentration of <5% was shown to be physiologically relevant to the *in vivo* ICM. When hESC have previously been maintained under low oxygen, a family of proteins (HIFs) interacted with these signalling pathways, helping to sustain the pluripotent state. Here, the term 'low oxygen' will be used to reference oxygen at <5% O_2, rather than it being low in relevance to the 'normal' physiological oxygen concentration.

1.3 Role of Oxygen in foetal and embryonic development.

1.3.1 Reduced oxygen concentration in vivo.

Oxygen is essential for life with the vast majority of organisms relying on it for energy production. In humans, its initial key role was recognised as a vital electron acceptor during ATP production (Karp 2009). Over recent years, it has been acknowledged that oxygen is also a signalling molecule in its own right. Although oxygen makes up ~20% (~160 mmHg) of inhaled atmospheric air, its concentration decreases rapidly as it enters the lungs. Alveolar air resides at ~ 13% O_2 (100 mmHg), which then moves down its concentration gradient across the alveolar membrane, to bring peripheral blood up to ~13%. Tissue specific oxygen concentration is reliant on the distance away from the nearest vasculature, but 5% O_2 (40 mmHg) has been acknowledged as a general estimate for most tissues (Singh 2008). From immediately post-fertilization, throughout embryonic development and up to formation of fully functional adult tissues, oxygen gradients exist to regulate embryonic patterning, tissue proliferation and differentiation, and to signal pathophysiological abnormalities.

In the very early stages of pregnancy, (day 6-7 post-fertilisation in humans) the blastocyst (consisting of the ICM and outer shell of trophoblast cells) can be explanted for development of a hESC line (Camarasa et al. 2012) *(figure 1.1).* At this stage of embryonic development, the intrauterine fluid has a concentration of oxygen far lower than that found that at atmospheric conditions. Direct uterine measurements in humans are technically difficult due to the invasive nature of the electrodes and catheters used to quantify oxygen concentration but the mid-point of the menstrual cycle has been estimated to reside at ~3% O_2 (19 mmHg) (Ottosen et al. 2006). Additionally, measurements of dissolved oxygen in peripheral maternal venous blood showed a progressive increase in parallel with advancing pregnancy, residing at ~30 mmHg at 8-10 weeks and ~65 mmHg by 12-13 weeks, likely due to the establishment of foetal-maternal blood supply (Rodesch et al. 1992). Basal uterine measurements in the Rhesus monkey and rabbit were at 2% and 6% O_2 respectively (13 mmHg and 42 mmgHg) and at day 6-8 post-fertilization, uterine oxygen tension for hamsters and rabbits was constant at 5% and 3% respectively (Fischer & Bavister 1993). Oviduct oxygen tension was typically higher than that of the uterus with the Rhesus monkey at 7%, the hamster at 6% and rabbit 7% O_2 (50 mmHg, 45 mmHg and 53 mmHg respectively) (Fischer & Bavister 1993). Such consistently low uterine oxygen tensions across species are likely to have an essential biological function, playing a role in directing development of morphologically and functionally normal embryos.

1.3.2 Early embryonic development at reduced oxygen.

Indeed, examinations of embryonic development, which were performed at an O_2 concentration reflective of the physiological environment during embryogenesis, indicated that the control of O_2 *in vivo* was vital. Explanted bovine blastocysts maintained *in vitro* at 2% O_2 (compared to a 20% O_2 control) developed with a higher proportion of cells in the ICM rather than the trophoectoderm layer, in addition to altered transcriptional identity (Harvey et al. 2004). Maturation of ovine zygotes at 5% O_2 produced a higher frequency of blastocysts compared to those at 20% O_2 (Bernardi et al. 1996). Additionally, the *in*

vivo timeframe for ovine morula development was reflected *in vitro* at 5% O_2 but was significantly retarded at 20% O_2 (Tervit et al. 1972).

Alterations to embryonic and foetal development under low oxygen have frequently been linked to the actions of the Hypoxia Inducible Factors (HIFs), a family of transcriptional regulators which are hypothesised to regulate critical aspects of normal embryonic development under low oxygen. *(See Figure 1.4)* Through stabilisation of the alpha-subunits during reduced oxygen, they subsequently act to regulate gene transcription with common targets being Vascular Endothelial Growth Factor (VEGF) and Erythropoietin (EPO) (Semenza & Wang 1992; Ema et al. 1997; Hu et al. 2007; Hu, Wang, Chodosh, et al. 2003; Dutta et al. 2008). Homozygous null mutants of the HIF1A, 2A and HIFB sub-units were embryonically lethal with specific morphological malformations, emphasizing their crucial role in embryogenesis (Maltepe et al. 1997; Ramírez-Bergeron et al. 2006; Iyer et al. 1998; Ryan et al. 1998).

1.3.3 Establishment of foetal-maternal blood supply and subsequent vascular and bone development as oxygen dependent processes.

Early in human pregnancy (prior to 11 weeks), the uterine spiral arterioles responsible for providing maternal blood flow become plugged by Cytotrophoblast cells (CT) (Caniggia et al. 2000). The subsequent low oxygen environment (~2-3%) has been shown to prevent oxidative stress (the embryo at this stage would not have adequate antioxidant enzymes to protect itself) and retain HIF1A in its active state (Caniggia et al. 2000; Genbacev 1997; Gultice et al. 2009; Ietta et al. 2006; Pringle et al. 2010). It has been shown that at ~11 weeks of gestation, removal of the arteriole plug causes differentiation and invasion of CTs into the uterine wall, establishing maternal-foetal vasculature support (Pringle et al. 2010). When blood supply after this time was inadequate, an environment of pathophysiological hypoxia (~8.5% O_2) resulted in a higher probability of adverse events mid-term (Pringle et al. 2010). This balance of oxygen concentration must be maintained to allow HIF1A to control proliferation, differentiation and invasion of CTs (Caniggia et al. 2000; Genbacev 1997; Gultice et al. 2009). Evidence has suggested that at

low oxygen, HIF1A bears responsibility for retaining CTs in a proliferative, non-invasive state which when released, allows CT invasion into the uterine wall to secure blood flow to the placenta (Caniggia et al. 2000; Genbacev 1997; Gultice et al. 2009; Ietta et al. 2006; Pringle et al. 2010). This is an early demonstration of how O_2 concentration tightly regulates cell fate.

It's also been established that an essential early stage in embryogenesis was the differentiation of endothelial cells for formation of the primitive vascular network that then branched together to form a cohesive system of connections. In quail embryos, this vasculogenesis and subsequent angiogenesis was oxygen dependent with 10% O_2 forming the highest number of vascular interconnections in a VEGF dependent manner and hyperoxia (that is, higher than atmospheric O_2) proving extremely detrimental (Yue & Tomanek 1999). This effect of oxygen on vascular development was due to the actions of members of the HIF family. HIFB null mice developed with defective closure of the neural tube, under-development of the forebrain and deficient vasculature supply due to abnormal vasculogenesis and angiogenesis, possibly due to downstream VEGF activity remaining at low levels (Maltepe et al. 1997; Ramírez-Bergeron et al. 2006; Kozak et al. 1997). Additionally, mouse HIF1A knock-outs were embryonically lethal due to defects in the cardiovascular system, incomplete neural fold closures and an enlarged hind brain (Iyer et al. 1998; Ryan et al. 1998). These tissue patterns of malformations overlapped with HIF2A mutations which were also embryonically lethal due to vascular defects due to an implied role in cardiac remodelling (Peng et al. 2000). In addition, $HIF2A^{+}/^{-}$ mice presented with impaired mitochondrial function and an attenuated ability to remove reactive oxygen species (Scortegagna et al. 2003). The activities of the HIF family are thus indicated to be essential for normal vascular development, as well as further roles in in embryonic tissue patterning.

1.3.4 Neural development is oxygen sensitive.

As outlined in *section 1.3.3*, low oxygen concentration in the brain has been implicated in normal neural development. At mid-gestation in the mouse foetal

brain, the oxygen concentration was estimated at 2-5% O_2, Several studies have outlined that these reduced oxygen levels are crucial for fully functioning neural development (Mutoh et al. 2012).

Neural progenitor cells are defined by their capacity to form neurons, astrocytes and oligodendrocytes (Westerlund et al. 2003; Stiles & Jernigan 2010). Mutoh et al outlined a process whereby at 2% O_2, astrocyte specific promoters were demethylated to allow direct differentiation to an astrocytic fate, a process dependent on the actions of Notch and HIF1A and repressed at 20% O_2 (Mutoh et al. 2012). Additionally, when explanted rat and mouse embryos underwent development *in vitro*, normal and non-pathological development of the neural plate and subsequent tube formation was only possible at 5-10% O_2, with exposure to >20% O_2 between GD9-11 leading to deformation of the neural plate and neural tubes which had not fully closed, as well as development of malformed forebrain and midbrain regions (Chen et al. 1999; Morriss & New 1979). Not only does this point to the crucial effects of oxygen in neural patterning and morphologically normal development, it additionally highlights the possible use of oxygen concentration as a tool in directing stem cell fate.

1.3.5 Oxygen gradients are retained in adult tissues.

One may assume that as embryonic vasculature develops the oxygen tension in mature tissues rises accordingly. In fact, many adult organs and tissues have been demonstrated to operate in extremely low O_2 environments. The thymus and medulla of the kidney and bone marrow stem cell niches reside at ~ 1% O_2 and the O_2 concentration in the adult brain varies from ~8% to 0.55% in specific hippocampal stem cell niches (Erecińska & Silver 2001; Simon & Keith 2008). Although a large majority of research into specific cell differentiation from PSCs is commonly performed at 21% O_2, reflecting the physiologically correct environment of the terminal cell fate may be critical for accurate tissue modelling but this remains to be characterised.

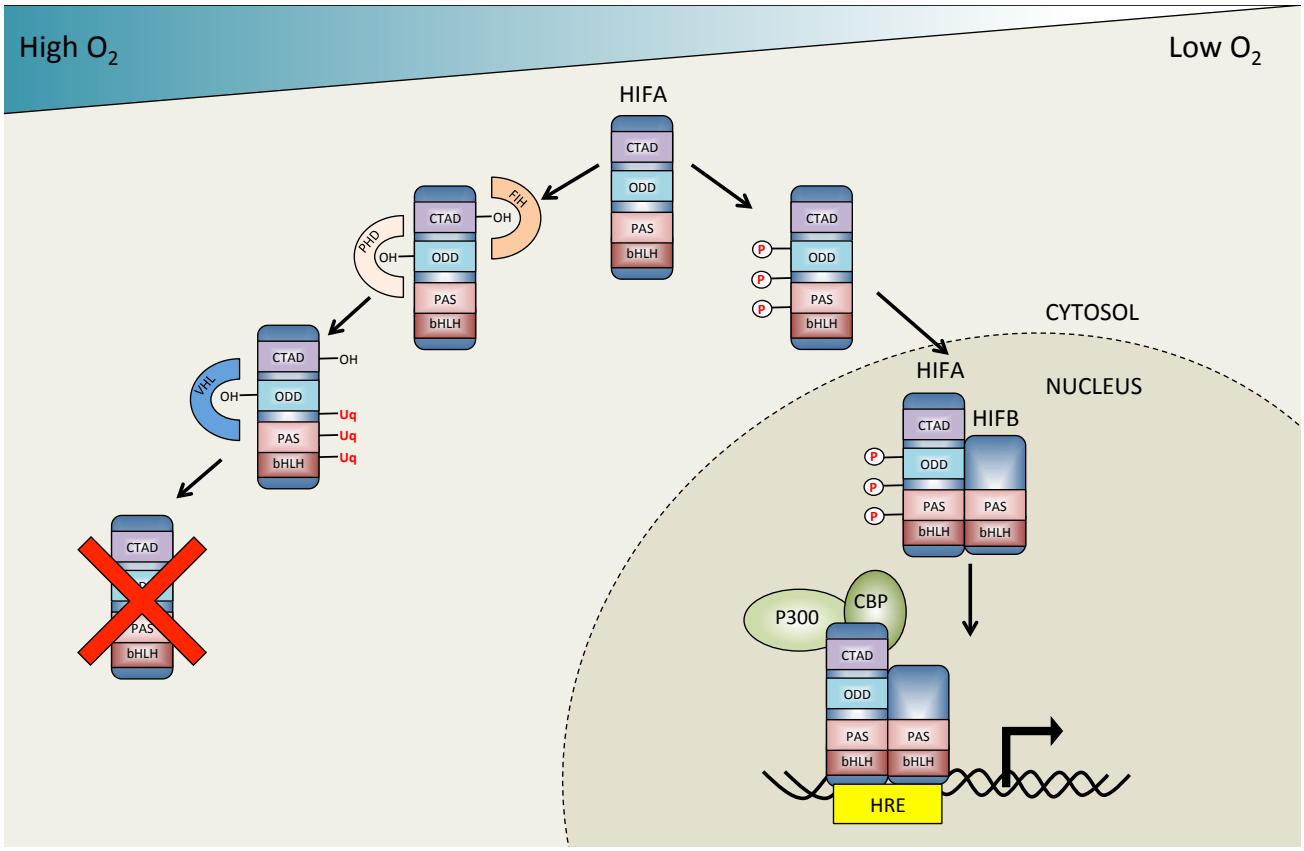

Figure 1.4. Regulation of HIF stability and transcriptional activity. *At high oxygen concentrations, both the stability and activity of HIFA subunits are modulated through hydroxylation of specific domains. Factor Inhibiting HIF (FIH) hydroxylates an Asparagine803 residue in the C-Terminal Activation Domain (CTAD) of HIFA, blocking binding with co-factors CBP and P300, required for transcriptional control of target genes. Proline Hydroxylases (PHDs) hydroxylate specific Proline402 and 564 residues in the Oxygen Dependent Degradation Domain (ODD) of HIFA subunits. This hydroxylation ensures recognition by the von Hippel Landau protein (VHL) which subsequently ubiquitinates HIFA subunits, marking them for degradation. At reduced oxygen concentrations, hydroxylation of Asparagine and Proline residues is prevented and HIFA is stabilised and accumulates cytoplasmically. After translocation to the nucleus, HIFA binds conserved promoter regions (HREs) in target genes and complexes with the regulatory subunit, HIFB which is constitutively expressed, to regulate transcription. Figure adapted from Fandrey et al, 2006.*

1.4 The role and regulation of the Hypoxia Inducible Factors.

1.4.1 Regulated expression of Hypoxia Inducible Factors.

When oxygen levels are low, whether physiologically normal or abnormal for the tissue in question, a range of cellular adaptations take place to aid cellular survival and/or apoptosis. A family of heterodimeric proteins known as hypoxia inducible factors (HIFs) modulate these cellular responses. Made up of multiple regulatory alpha (A) and a constitutively expressed beta (B) subunit, their regulation has been extensively studied *(figure 1.4).* The constitutively expressed HIFB subunit is known to bind the labile alpha subunits to allow transcription of target genes (Cejudo-Martin & Johnson 2005; Wenger 2002; Fandrey et al. 2006). Both alpha and beta subunits belong to the basic helix-loop-helix (bHLH) and PER-ARNT-SIM (PAS) family of proteins, with conserved domains for DNA binding and subunit dimerisation. Typically, reports using stem cells have indicated that HIF1A would be stabilised and transiently maintained during the initial 12-48 hours of introduction into low oxygen. HIF2A and 3A follow in the proceeding days and have different O_2 concentration stabilisation profiles, with HIF2A generally being stabilised at higher O_2 tensions in adult cell lines (Patel & Simon 2008; Zachar et al. 2010; Cameron et al. 2008; Forristal et al. 2010).

1.4.2 Prolyl Hydroxylases regulate degradation of HIFA subunits.

HIF-alpha subunits have specific domains highly involved in regulating their activity, namely, the Oxygen Dependent Degradation Domains (ODDD) located at C-terminals and N-terminals of the proteins Transactivational Domains (Appelhoff et al. 2004). Located here are two residues Pro402 and Pro564 which become hydroxylated by HIF prolyl hydroxylases (PHDs) at high oxygen concentrations. The hydroxylated ODD domain is then targeted by the von Hippel-Landau (VHL) protein, which marks HIF-alpha subunits for ubiquitination and proteasomal degradation, causing them to be undetectable in high oxygen conditions (Brahimi-Horn et al. 2005; Wenger 2002; Appelhoff et al. 2004; Nguyen et al. 2013; Ke & Costa 2006; Fandrey et al. 2006). As hydroxylation requires availability of oxygen

molecules, PHDs cannot modify the proline residues at low oxygen causing accumulation of HIF-alpha subunits (Brahimi-Horn et al. 2005; Appelhoff et al. 2004). Cell lines without functioning pVHL activity have previously showed high levels of the HIF1A and 2A subunits as well as up-regulation of *VEGF* transcripts, a downstream target of HIF1A (Iliopoulos et al. 1996; Krieg et al. 2000). A mitochondrial dependent pathway has also been implicated in regulating HIF-alpha subunit stabilisation. Cell lines with no mitochondrial activity failed to show the typical up-regulation of HIF1A and 2A targets such as *VEGF* and *EPO* at low oxygen, the expression of which were restored upon addition of Cobalt Chloride (a chemical inducer of HIF-alpha stabilisation). Repression of functional HIF1A activity in wild-type cell lines was then observed upon addition of antioxidants (Chandel et al. 2000; Chandel et al. 1998).

Three forms of PHDs have been identified (PHD1-3) each with defined roles in the regulation of HIFA subunits. Numerous cell lines showed up-regulation of PHD2 & 3 mRNA and protein after oxygen restriction (0.5%) with PHD1 showing constant or decreased expression under hypoxia (Berchner-Pfannschmidt et al. 2008; Niecknig et al. 2012; Berra et al. 2003; Appelhoff et al. 2004; Fandrey et al. 2006; D'Angelo et al. 2003). Across all lines tested, PHD2 was the most abundantly expressed both at high and low oxygen in addition to bearing the greater responsibility in targeting HIF1A for degradation; siRNA silencing of PHD2 not only stabilised HIF1A expression and its nuclear translocation but protein expression of the former was also up-regulated by reduced oxygen, possibly demonstrating a feedback loop underlying the typically short-lived expression profile of HIF1A (Appelhoff et al. 2004; Berra et al. 2003; Niecknig et al. 2012). Whilst silencing of PHD2 in combination with PHD1 or 3 showed the latter two to be non-redundant in terms of regulating the stability and expression of HIF1A, albeit at lower efficiencies than that of PHD2, PHD1 and 3 contrarily showed much greater power over HIF2A than PHD2; silencing of PHD1 and PHD3 either singly or combinatorially resulted in much greater induction of HIF2A than that caused by PHD2 repression (Appelhoff et al. 2004). These differing roles in the regulation of

HIF-alpha isoforms may be mediated via differing affinities of PHD isoforms to the N-Terminal vs C-Terminal ODD domains (Appelhoff et al. 2004).

1.4.3 Regulation of HIF-alpha transcriptional activity.

In addition to regulating the degradation and stability of HIF-alpha subunits, a number of mechanisms have been outlined to modulate transcriptional activity through binding of transcriptional co-factors CBP and P300. It was shown that Factor Inhibiting HIF (FIH) hydroxylated an Asn803 residue in the C-terminal transactivational domain of HIF1A in high oxygen, preventing binding to the above co-activators (Wenger 2002; Nguyen et al. 2013; Ke & Costa 2006). Like the PHDs, FIH was shown to be an O_2 dependent enzyme and unable to hydroxylate the asparagine residues in low oxygen (Wenger 2002). Additionally, CBP/P300 Interacting Transactivator with ED-rich Tail2 (CITED2) negatively regulated HIF1A by competing for binding to CBP/P300 (Freedman et al. 2003). As the promoter region of CITED2 contained a HRE region, which became stimulated under 'hypoxic' conditions, this may have acted as part of a negative feedback loop for HIF1A activity (Pringle et al. 2010; Bhattacharya et al. 1999).

THE *HIF3A* gene has been shown to have up to seven different splice variants, some of which have been implicated in negative regulation of HIF1A and 2A transcriptional activity (Maynard et al. 2003; Makino et al. 2002; Augstein et al. 2011; Heikkilä et al. 2011). Overexpression of HIF3A isoforms in umbilical venous endothelial cells cells repressed hypoxia induced transcription of HIF1A and 2A target genes (Augstein et al. 2011). A subset of these isoforms was also shown to accumulate in the nucleus, whereby they bound HIF1A or 2A and prevented them from regulating downstream transcription. It was also observed that when the HIF3A-4 isoform bound HIF1A in the cytoplasm, neither subunit underwent subsequent nuclear translocation (Heikkilä et al. 2011). This evidence points to an additional layer of HIFA regulatory control.

1.4.4 Expression patterns and transcriptional targets of stabilised HIFA subunits.

As oxygen becomes limiting, mechanisms targeting HIF-alpha degradation and repressing activity are blocked, shown to result in stabilised HIFA subunits. These subsequently accumulate cytoplasmically and translocate to the nucleus, forming complexes with HIFB and transcriptional co-activators p300 and CBP (Brahimi-Horn et al. 2005; Wenger 2002; Appelhoff et al. 2004; Nguyen et al. 2013; Ke & Costa 2006; Gardner et al. 2001). Phosphorylation, possibly mediated by mitogen activated protein kinases (MAPKs) have been shown to enrich transcriptional activity (Salceda et al. 1997; Richard et al. 1999; Wang & Semenza 1993)(Wenger 2002). This transcriptional complex regulates its downstream effects by binding the specific HIF Response Element (HRE) 5'-CGTG-3', found on a number of critical target genes (Pringle et al. 2010). Target genes include regulators of pluripotency, such as NANOG, POU5F1 and SOX2 and β-catenin effectors LCF and TEF (White et al. 2004; Talks et al. 2000; Moreno-Manzano et al. 2010; Mazumdar et al. 2010; Covello et al. 2006; Petruzzelli et al. 2014). Numerous studies have confirmed distinct and overlapping gene profiles for transcriptional regulation by the HIF-alpha subunits. Gene specificity of transcription between the alpha subunits was shown to be determined by their N-Terminal Activation Domain and choice of co-activators, with large homology between the 1A and 2A subunits (~83% in the bHLH domain and ~70% in the PAS) (Hu, Wang, Chodosh, et al. 2003; Tian et al. 1997; Hu et al. 2008; Lau et al. 2007). Common targets of both HIF1A and 2A include EPO and VEGF (Hu et al. 2007; Hu, Wang & Chodosh 2003; Ema et al. 1997). HIF1A was also capable of inducing glycolytic pathway genes such as phosphoglycerate kinase 1 (PGK1) and lactate dehydrogenase A (LDHA) and blocking the oxidative phosphorylation needed for aerobic glycolysis (Hu et al. 2007; Hu, Wang & Chodosh 2003; Semenza 2011b). HIF2A alone was able to up-regulate transcription of the pluripotency regulators NANOG, POU5F1 and SOX2 as well as cell-cycle regulator CyclinD1, and TGF-α (Hu, Wang, Chodosh, et al. 2003; Patel & Simon 2008; Covello et al. 2006; Moreno-Manzano et al. 2010; Petruzzelli et al. 2014). HIF1A was also expressed fairly ubiquitously throughout the body whereas HIF2A and 3A were found to be tissue specific, commonly expressed in

distinct cell populations in the lungs, heart, brain, kidney and liver (Tian et al. 1997; Zachar et al. 2010; Cameron et al. 2008; Wiesener et al. 2002; Gu et al. 1998).

There have been some cell types found (*e.g.* neural stem cells in the subventricular zone (SVZ) and subgranular zone (SGZ)) which stabilised HIF1A constitutively (Cunningham et al. 2012). In these instances, it is credible that alpha-subunit stabilisation occurred in an O_2 independent manner, particularly as it did not seem to undergo hydroxylation or ubiquitination (Roitbak et al. 2011). A couple of mechanisms are likely; it was also shown that Heat shock protein 90 (HSP90) could occupy a site in the PAS domain, leading to alpha-subunit stabilisation (Isaacs et al. 2002). Additionally, HIF1A may have been stored in cytoplasmic vesicles, avoiding the oxygen dependent degradation process entirely (Roitbak et al. 2011). Constitutive expression indicated that it was likely HIF proteins played an important role in neurogenesis or maintenance of NSCs.

1.5 Hypoxia Inducible Factors play a role in regulating pluripotency.

As derivation of hESC lines is reliant on explanting ICM from a low oxygen environment (~3-5 % O_2) deriving and maintaining hESC lines in low oxygen may increase their viability and their ability to sustain a pluripotent state (Ottosen et al. 2006; Fischer & Bavister 1993; Thomson 1998). As detailed in section 1.2, tightly controlled signalling pathways sustain the pluripotent state in hESCs, many of which have shown to be regulated upstream by the actions of HIF1A and 2A.

1.5.1 Morphological assessment of pluripotent stem cells at low oxygen.

Insufficient culture practices commonly cause PSCs to undergo spontaneous differentiation into an early germ layer progenitors, losing the ability to self-renew. This can be initially evaluated by morphological assessment of cultures. Pluripotent hESC colonies typically have tight, rounded borders with a smoothened surface. After spontaneous differentiation, the colony border is lost

and cells appear flattened, distinct and darker in addition to the appearance of large, raised clumps. An example of both pluripotent and differentiated hESC colonies can be seen in *Figure 2.1*. Numerous studies showed that after long term culture at 3-5% O_2, hESC were typically more likely to display pluripotent morphology, evaluated by visually quantifying areas of spontaneous differentiation and areas of pluripotency (Chen et al. 2010; Zachar et al. 2010; Ezashi et al. 2005; Forristal et al. 2010). Additionally, HCG, a marker for the trophoblast lineage and hence up-regulated upon loss of self-renewal, showed reduced transcription in hESCs maintained at 3% O_2 (Ezashi et al. 2005).

1.5.2 NANOG, POU5F1 and SOX2 in pluripotent stem cells at low oxygen.

As previously discussed, POU5F1 is critical for maintaining pluripotency. Whereas some reports of hESCs cultured at 1-5% O_2 indicated no increase in *POU5F1* transcript levels, others observed significant increases in both transcript levels and in protein load (Forristal et al. 2010; Lengner et al. 2010; Chen et al. 2010). Maintenance of hESCs at 5% O_2 also caused a higher percentage of colonies to remain positive for POU5F1 with fewer differentiated, SSEA1 positive areas. This pluripotent phenotype was repressed upon inhibition of Notch signalling (Prasad et al. 2009). Augmented POU5F1 transcription at low oxygen has since been attributed to the direct action of HIF2A (Covello et al. 2006; Nordhoff et al. 2001).

The gene for POU5F1 was shown to contain a promoter with highly conserved sequences across mouse, bovine and humans species. Numerous studies reported that these conserved regions contained within them multiple HRE domains which were bound and regulated directly by stabilised HIF2A (Covello et al. 2006; Nordhoff et al. 2001). Covello et al showed this neatly, with a mouse model expressing HIF2A in the place of HIF1A; this double KI had high rates of embryonic mortality at E6.5-E7.5 and viable embryos developed with over-expanded epiblast and a loss of extra-embryonic tissues. The HIF2A mediated, up-regulation of

POU5F1 mRNA and protein was subsequently abolished after removal of the HRE region in the POU5F1 gene (Covello et al. 2006).

Further to regulation of POU5F1 expression by HIF2A, NANOG and SOX2 also became up-regulated in hESCs when maintained at O_2 concentrations less than 5%. Semi-quantitative polymerase chain reaction (QPCR) showed up-regulated transcription of *NANOG* and *SOX2* in hESCs and mESCs proliferated at 3-5% O_2 (Prasad et al. 2009; Forristal et al. 2010; Sugimoto et al. 2013). Regulation of transcription due to the stabilisation of HIFA subunits also likely underlies this alteration. Si-RNA knockdowns (KD) of HIF2A and 3A in hESCs and mESCs at 5% O_2 caused a significant decrease in the levels of NANOG, SOX2 and POU5F1 RNA and protein when compared to a HIF1α KD and control (Forristal et al. 2010; Sugimoto et al. 2013). Additionally, repression of HIF2A protein stabilisation showed a dose-dependent reduction in POU5F1, SOX2 and NANOG expression (Moreno-Manzano et al. 2010; McCord et al. 2009). Further investigation revealed two HRE sites in the promoter region of SOX2, mutation of which abolished an hypoxia dependent increase and showed specific binding with HIF2A (Moreno-Manzano et al. 2010).

1.5.3 Low oxygen interacts with various signalling pathways to regulate self-renewal.

In addition to directly interacting with, and regulating the transcription of, NANOG, SOX2 and POU5F1, low oxygen has also been shown to guide cell fate through interactions with signalling upstream of these aforementioned transcription factors.

Although the role of Wnt signalling in maintaining self-renewal of hESCs is controversial, a strong link between β-catenin and oxygen tension has been observed. TCF-reporter assays indicated high transcriptional activity at 1.5% O_2 as well as increased nuclear protein concentrations of β-catenin, LEF1, TCF1 and downstream target genes. This induction of Wnt signalling was directly mediated through the stabilisation and binding of the HIF1A/B subunits, which targeted HRE domains on the LEF and TCF promoter regions. The increase in LEF/TCF protein

loads then mediated up-regulation of transcriptional targets as well as a reduction in hESC apoptosis. The stimulatory effects of low oxygen on the Wnt signaling pathway was reported to be exclusive to hESC and neural stem cell populations, with no observable effects on somatic cells (Mazumdar et al. 2010).

Numerous studies have also associated reduced oxygen with augmented Activin/Nodal/TGFβ signalling in multiple cell lines, although only Chen et al reported an increase in levels of phosphorylated-SMAD2/3 in hESCs at low O_2 (Chen et al. 2010). In human umbilical vein endothelial cells at 1-2% O_2, an increase in TGFβ production and concomitant rise in phosphorylated SMAD2/3 was related to a positive feedback loop, whereby SMAD3 bound the TGFβ promoter and stimulated transcription. It was also shown that although this binding was increased at low oxygen, it was not wholly dependent on HIF1A. However, cooperation between the two regulators at adjacent HIF1A and SMAD binding sites in the TGFβ promoter region, additively augmented transcription (Zhang et al. 2003; Akman et al. 2001). Low oxygen also up-regulated NODAL expression, causing augmented SMAD2/3 phosphorylation in a HIF1A dependent manner although this has yet to be confirmed in PSCs (Quail et al. 2011). Finally, in a hepatoma cell line, culture at 1% O_2 induced SMAD3/4 to directly bind HIF1A and act as a cofactor, driving VEGF transcription (Sánchez-Elsner et al. 2001).

As discussed previously, high levels of telomerase activity is recognised as a marker of pluripotency and one of the key regulators of indefinite self-renewal in PSCs (Stewart et al. 2006; Amit et al. 2000; Xu et al. 2001; Koshiji et al. 2004). The activity levels of telomerase can be assessed by quantifying the activity of human Telomerase Reverse Transcriptase (hTERT), the catalytic sub-unit which complexes with the constitutively expressed units to form an active telomerase complex. Low oxygen not only causes an increase in telomerase activity, but HIF1A was shown to directly interact with two HRE sites on the promoter region of hTERT (Nishi et al. 2004). Finally, maintaining hESCs in low oxygen sustained Notch activation, aiding self-renewal (Prasad et al. 2009).

1.5.4 Reprogramming of somatic cells is augmented by low oxygen.

Production of induced pluripotent stem cells from adult somatic cells (iPSC) has enormous potential to revolutionise both disease modelling and treatment. The standard techniques involve introduction of key genes responsible for pluripotency either through plasmid transfection or lentiviral infection. These have fairly low efficiency rates with colonies forming from 0.02-0.1% of transfected cells and can take up to 4 weeks for colonies to develop (Takahashi et al. 2007; Lowry et al. 2008; Takahashi & Yamanaka 2006; Park et al. 2008). Increasingly, reports have demonstrated that reprogramming somatic cells in low oxygen (~5% O_2) led to appearance of ESC-like colonies as early as day 6 after retroviral infection and TRA-1-81 positive colonies at day 10, in addition to increasing efficiency (Shimada et al. 2012; Yoshida et al. 2009). This manipulation of oxygen concentration to influence cell fate has now been patented for its ability (in combination with FGF2) to seemingly reprogram fibroblasts into multipotent stem cells without the need for forced expression of critical gene factors (US Patent 8, 524, 494). The mechanism for this oxygen dependent, augmented reprogramming has not been made clear, although HIF2A has been clearly implicated in transcriptional up-regulation of c-myc, a common gene used in early reprogramming techniques (Gordan et al. 2007). Furthermore, reprogramming has been shown to require a shift from mitochondrial oxidative metabolism to oxidative glycolysis; common transcriptional targets of HIF1A include phosphoglycerate kinase 1 and lactate dehydrogenase A, essential for glycolytic metabolism (Guillaumond et al. 2013; Panopoulos et al. 2012; Hu, Wang & Chodosh 2003; Semenza 2011a).

It is clear that the stabilisation of the HIFA subunits due low oxygen have downstream effects on the ability of PSC populations to sustain self-renewal. Whether through direct transcriptional effects on key regulators such as POU5F1 or by stimulating upstream regulatory pathways, oxygen has the potential to be a crucial tool in the maintenance of pluripotency. This is vital, not just for our understanding as to how pluripotency is regulated and maintained, but also for maximising the potential of hESC and iPSC for use in therapeutic cell replacement.

1.6 Low oxygen in the proliferation and viability of stem cells.

1.6.1 Cell-cycle regulation in pluripotent stem cells.

Cell cycle regulation has been well characterised in eukaryotes, with a full cycle typically taking ~24-32 hours in somatic cells. During chromosomal replication and cell division, a number of checkpoints exist to ensure non-sense and damaged DNA is repaired before being passed on to daughter cells. Cyclins and Cyclin Dependent Kinases (CDKs) modulate transition through the cell cycle and checkpoints. Unbound, CDKs are inactive but when partnered to a Cyclin they gain catalytic activity and are able to phosphorylate target proteins

Transition from the G1-phase into the S-phase is controlled by the E2F transcription factor and the phosphorylation status of the Retinoblastoma protein (RB). When hypo-phosphorylated, RB binds and retains E2F in an inactive state. After RB is phosphorylated by CDK/Cyclin complexes, E2F is released to up-regulate transcriptional targets required for progression into the S-phase, including polymerases and additional cyclins and CDKs. Cyc-D2 then forms a complex with CDK4 to stimulate progression through G1-phase and into the S-phase.

Overall control of G1-phase into S-phase transition is controlled by c-myc, a transcription factor responsible for transcriptional up-regulation of E2F and CycD2. C-myc also binds to the promoter regions of P21 and P27 and represses their transcription. P21 has been recognised as responsible for initiating cell-cycle arrest upon detection of imperfect duplication of DNA, before allowing movement through the cell-cycle to continue.

In hESCs, the overall cell cycle (~12-16 hours) has been shown to be considerably shorter than somatic cells, although longer than that of mESCs at ~8-10 hours (White & Dalton 2005; Becker et al. 2007). It can also be considered a marker of pluripotency; it is established that when ESCs undergo commitment to a specific cell fate, the length of the cell cycle increases concomitantly (Lange & Calegari 2010; Conklin & Sage 2009; Zeng & Rao 2007). Additionally, mature somatic cells show a proportionally longer G1-phase than S-phase, whereas the

opposite is true in hESCs which have a G1-phase of only ~3 hours (Becker et al. 2006). Increased expression of CyclinD2 and CDK4 at least partly underlies this shortened G1-phase (Becker et al. 2010; Becker et al. 2006). It has also been extensively demonstrated that mESCs and hESCs do not have an active G1 checkpoint, characterised by down-regulation of a number of cell-cycle regulators such as p21 and p27, in addition to clear hyper-phosphorylation of RB in mESCs (Stead et al. 2002; Faast et al. 2004; Savatier et al. 1994; Conklin & Sage 2009).

1.6.2 HIFA subunits regulate cell-cycle progression.

Substantial evidence has amounted for differing and opposing roles for HIF1A and 2A subunits in the cell-cycle progression of human carcinoma lines. In a renal clear cell carcinoma cell line at 0.5% O_2, HIF2A up-regulated c-myc activity which resulted in a shift of cells from G1 into S-phase, suggested to be via HIF2A aiding c-myc promoter binding, rather then direct transcriptional stimulation (Gordan et al. 2007). Concordantly, in a renal clear cell carcinoma line at 1.5% O_2, an increase in CyclinD1 and the phosphorylated form of RB was observed to be HIF2A dependent (Baba et al. 2003).

However, in a colon carcinoma cell line, HIF1A activity correlated with attenuated binding of c-myc to DNA through competitive binding of HIF1A resulting in displacement of c-myc from the promoter region of genes such as P21. This de-repression and subsequent amassing of P21 triggered a G1 stall and prevented cell cycle progression (Koshiji et al. 2004). The observed HIF1A dependent reduction in proliferation was also displayed in PSCs, whereby *HIF1A*$^{+/+}$ mESCs slowed proliferation at 1% O_2 due to up-regulation of p21 and p53, whereas *HIF1A*$^{-/-}$ did not (Carmeliet et al. 1998). There was also an increase in p27 protein and RB hypophosphorylation due to oxygen or glucose deprivation in both mESCs and various fibroblast lines, but evidence on whether this was a HIF1A dependent or independent process was not conclusive (Carmeliet et al. 1998; Gardner et al. 2001; Goda et al. 2003). Contrastingly, culture of primary human lung fibroblasts, a normally senescent population of cells, underwent large

increases in population doublings at 1.5% O_2 which was abolished after transfection with a dominant-negative form of HIF1A (Bell et al. 2007).

1.6.3 Low oxygen may modulate the proliferation and viability of stem cells.

When evaluating the possible benefits and detriments of culturing PSCs at low oxygen, any effect on proliferation and apoptosis is important to consider. A quantitative method for assessing this is vital to determine the balance of actively proliferating and apoptotic cells. Previous reports have used the diameter of colonies as an indicator of proliferation (Sugimoto et al. 2013; Forristal et al. 2010; Ezashi et al. 2005). Chen et al. reported that hESC colonies proliferated in low oxygen were thinner, so although the colony diameter may or may not have differed, it's feasible that the density and number of cells in a colony may have varied considerably (Chen et al. 2010). At 5% O_2, an increase in the proportion of hESCs which were positive for mitotic marker Ki67 was observed in addition to a rise in cell number in mouse and human ESCs (Zachar et al. 2010; Forristal et al. 2010; Mazumdar et al. 2010). Contrasting this, additional reports indicated a drop in the number of actively proliferating cells and a decrease in the total number of cells (Chen et al. 2009; Prasad et al. 2009). Observations of stem cell viability and apoptosis under low oxygen were also mixed with decreased viability of mESCs at 1-2% O_2 and comparable rates of apoptosis at 5% O_2 (Mazumdar et al. 2010; Chen et al. 2009; Carmeliet et al. 1998). Hence, the precise effect of low O_2 on proliferation and viability in hESCs is yet to be fully elucidated.

1.7 Induction of a neural fate in vivo.

1.7.1 BMP inhibition in neuroectodermal patterning of the early embryo.

As discussed in *section 1.1.2*, hESC are obtained from the ICM of the pre-implantation blastocyst and shown to retain characteristics reflective of the epiblast, i.e. a capacity to form the primary germ layers (mesoderm, endoderm and ectoderm) (Camarasa et al. 2012; Thomson 1998). This process of germ layer

formation is known as gastrulation and bears responsibility for the transition of the pluripotent epiblast population into formation of the embryonic tissues, through a regulated progression of proliferation, cell movement and differentiation (Kumar 2010). The ectodermal germ layer consists of two sub-populations; the epidermal ectodermal cells which form the skin and nail tissues and the neuroectodermal cells which are responsible for formation of the Central Nervous System (CNS) (Gilbert 2006; Lawrence et al. 2011; Stiles & Jernigan 2010).

The first evidence of organised embryonic neural induction came in the form of Spemann and Mangolds pioneering experiments in 1924. By transplanting a small, specific section of the involuting gastrula onto various sites across the early xenopus embryo, they discovered a cell population with a dorsal mesoderm identity which was capable of initiating formation of neural tissue from non-neural ectoderm (Spemann & Mangold 1924). This population of mesodermal cells (known as Spemann's organiser in amphibians and referred to as the 'primitive node' in verterbrates) has been demonstrated across species, acting to repress BMP signalling through secretion of BMP inhibitors such as NOGGIN, CHORDIN and FOLLISTATIN and signal neuro-ectodermal differentiation. As BMP antagonists are secreted to act locally, formation of BMP-negative neuroectoderm (adjacent to the organiser) and BMP-positive epidermal ectoderm occurs. These processes are common across many model organisms and form the basis for the *in vitro* signalling used in this study (Gilbert 2006; Lawrence et al. 2011).

Trophic BMP signalling from the primitive node is mediated through TGFβ ALK2/3 receptors (Klingensmith et al. 1999). Similarly to Activin/Nodal activation of TGFβ receptors, ligand binding is known to result in phosphorylation and activation of the SMAD1/5/8 transcription factors, which subsequently translocate to the nucleus and regulate target gene transcription in conjunction with SMAD4 (Smukler et al. 2006), *Figure 1.2*. Throughout the ectoderm, BMP signalling was shown to stimulate differentiation of primitive ectoderm to form the epidermis and repressing production of a neuronal fate (Levine & Brivanlou 2007; Sela-Donenfeld & Kalcheim 1999; Delaune et al. 2005; Muñoz-Sanjuán & Brivanlou 2002). Critically, the dorsal secretion of BMP antagonists such as NOGGIN,

CHORDIN and FOLLISTATIN released responsive ectodermal cells from the actions of BMP signalling. This pathway of neural induction is known to act spatially ventral to the primitive node, founding a population of columnar neuroectodermal cells known as the neural plate (Klingensmith et al. 1999; Smukler et al. 2006; Lamb et al. 1993). Inhibition of BMP activity has been extensively demonstrated as crucial for this induction of a neural identity. Mutations in SMAD4 increased the neural induction during directed differentiation of mESCs and inhibition of BMP signalling and SMAD1 activity in xenopus embryos induced a neural fate in the ectoderm bordering the neural plate (Delaune et al. 2005; Smukler et al. 2006).

1.7.2 FGF signalling in neural induction.

It's been extensively demonstrated that FGF signalling was required for functional BMP antagonism. In the pre-gastrulation embryo, signalling through the FGF receptors showed involvement in up-regulating genes required for neuroectoderm formation, in addition to supplementing BMP inhibition (Delaune et al. 2005; Launay et al. 1996). Additionally, FGF inhibition in xenopus embryos caused a complete loss of neural tissue and suppressed the neuralising effects of NOGGIN (Delaune et al. 2005; Launay et al. 1996). *In vitro*, inhibition of FGF signalling repressed the neural induction of mESCs, which otherwise could be reliably differentiated to a neural progenitor fate phenotypically similar to the neuroectodermal cells which form the neural tube (Smukler et al. 2006).

1.7.3 Wnt signalling during neural induction.

Canonical WNT signalling is also involved, although the role of WNT is more complex with evidence indicating that WNT has a role in promoting both proliferation of NPCs and differentiation to terminal neurons suggesting that WNTs role in neural induction is multi-faceted. Baker et al. reported that during early gastrulation, WNT facilitated BMP inhibition and the subsequent formation of the neural plate, with TCF-null xenopus embryos developing with a complete loss of neural tissue (Baker et al. 1999). This correlated with reports that that

WNT/β-catenin signalling was required prior to gastrulation in xenopus and zebrafish to ensure that antagonistic BMP signals released from the organiser were functional, although the exact mechanism has yet to be elucidated (Wessely et al. 2001; Kelly et al. 2000). These pro-neural effects are temporally limited, as later in gastrulation WNT signalling has demonstrated an inhibitory role, acting to repress neural induction.

Reports also suggested that later in gastrulation, the spatial expression patterns of secreted WNT and WNT antagonists remained vital for physiologically normal neural patterning. WNT antagonists were found to be secreted by the xenopus organiser in conjunction with BMP antagonists and were implicated in de-repressing WNT's blockage of neural induction (Pera & De Robertis 2000). Additionally, xenopus embryos with an inactivated form of Dickkopf-1 (DKK1, an inhibitor of WNT signalling) developed with attenuated neural structures and WNT ligands directed epiblast cells to an epidermal fate, blocking neural conversion (Wilson et al. 2001; Mukhopadhyay et al. 2001). During mouse gastrulation, forced disruption of WNT signalling increased the levels of neural induction and in mESCs, WNT antagonism resulted in a 40% conversion to neural progenitors (Yoshikawa et al. 1997; Kelly et al. 2004; Aubert et al. 2002). Finally, during induced neural differentiation of mESCs, DKK1 expression not only increased during neuralisation but siRNA knockdown of DKK1 led to a large drop in the percentage of neurons produced (Verani et al. 2007). This points to a regulatory role for WNT in controlling and limiting conversion of epiblast into neuroectoderm. The full interplay between WNT and BMP signalling pathways remain to be clarified, particularly with respect to neuroectodermal conversion in humans.

1.7.4 Neurogenesis and neuronal maturation in vivo.

After BMP-inhibition driven formation of the neuroectoderm, midline folding of the neural plate and lifting of peripheral folds has been shown to form the basis of the neural tube, developing with an apico-basal (luminal-external) polarity (Abranches et al. 2009). Differentiation of ESC derived NPCs demonstrated that

this apico–basal (luminal - external) polarity was retained *in vitro* (Curchoe et al. 2012; Elkabetz & Studer 2008). In the apical region of the tube, accumulation of cell-cell junctions were observed due to amassing of N-CADHERIN, β-CATENIN and ZO-1 proteins, all involved in cell-cell communication (Hierholzer & Kemler 2010; Aaku-Saraste et al. 1996; Detrick et al. 1990). This regulated polarity has been revealed to be essential for controlled cycles of apical NPC proliferation and basal region differentiation. Regulation was shown to be via by Notch signalling across adjacent cells, with γ-secretase inhibition inducing rapid differentiation of progenitors to a neural fate and a loss of proliferation (Abranches et al. 2009), *Figure 8*.

Additional to an apical-basal polarity, trophic signalling was shown to result in opposing morphogen gradients across the neural tube. Anterior-posterior gradients of WNT, BMP, FGF and Retinoic Acid signalling lead to separation into the primary compartments of the developing brain – the forebrain (which avoids caudalising signals), midbrain, hindbrain and spinal cord. A dorsal-ventral axis due to dorsal BMP and WNT secretion in juxtaposition with SHH secretion from the anterior-ventral telencephalon allowed for a range of cellular identities dependent on their axonal position (Dhara & SL. 2009).

Closure of the neural tube was shown to be initiated in the center, with anterior and posterior ends being the last segments to close. Prior to full closure, the anterior tube expands to produce the three primary brain segments; anterior prosencephalon, mesencephalon and the posterior rhombencephalon. Further development causes separation into additional distinct sub-populations, including segmentiation of the prosencephalon into the dorsal (pallial) and the ventral (subpallial) telencephalons (Hoch et al. 2009; Germain et al. 2010). Upon completion of the neural tube, the interior was found to be lined with a single cell layer of NPCs, classed as neuroepithelial cells. As the interior will later develop into the ventricles, this region is widely recognised as the ‘ventricular zone’ (VZ), a region of active neurogenesis (Stiles & Jernigan 2010). The ventricles consist of a chain of connected vesicles filled with cerebrospinal fluid and have various vital

functions, importantly, they are also a critical site for NPC proliferation and neuron production during early brain development.

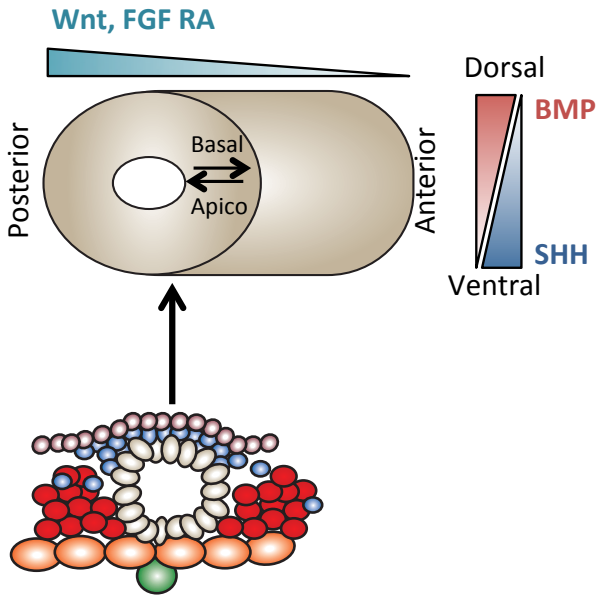

Figure 1. 5. The neural tube in vivo is reflected *in vitro*.

(i) The neural tube retains an apico-basal polarity throughout, allowing spatially regulated cycles of proliferation and differentiation. The neural tube also retains morphogen gradients for regionalisation of the developing brain. This apico-basal polarity is reflected in vitro through the formation of neural rosettes.

To generate the vast numbers of neurons required for a fully functioning human brain, after neural tube closure neuroepithelial cells undergo rounds of symmetrical proliferative cell division, producing two identical NPCs from each round of mitosis. Nuclei move between the apical and basal surfaces dependent on cell-cycle phase, with symmetrical cell division at the ventricular apical surface and S-phase at the exterior basal area (a process known as interkinetic nuclear migration). From E42 onwards, neuroepithelial cells progress into a more developed cell type called radial glial cells, populations of neuroepithelial and radial glia cells together constitute the VZ, retain very similar proliferative potential and will be hereafter jointly referred to as apical progenitors. Asymmetric apical progenitor cell division forms one proliferative apical progenitor cell and one cell with a more committed identity, a basal progenitor

cell. This latter type have restricted proliferative and cell fate potential (only being capable of forming neurons in comparison to apical progenitors which produce both neurons and glia) and either directly differentiate to post-mitotic neurons or undergo symmetric neurogenic division, forming two committed neurons or two basal progenitors. Throughout these rounds of proliferation and fate commitment, interkinetic nuclear migration retains a gradient of proliferative>committed cells, in an apical>basal manner, whereby apical progenitors make up the VZ and basal progenitors inhabit the subventricular zone (SVZ) (Stiles & Jernigan 2010; Kazanis et al. 2013; Hardwick et al. 2014; Lange & Calegari 2010).

Radial glial cells in the VZ keep an apical process attached to the ventricular surface and an extended basal process attached to the basal pial, in this way they have been shown to act as guides for newly produced neurons. Cycles of mitosis, neuron production and migration occur in an orderly progression; the VZ consists of apical progenitors undergoing mitosis and the apical processes of radial glial cells, newly generated progenitors and neurons then move up through the subventricular zone (SVZ) and finally post-mitotic neurons are guided towards the mantle and the pial surface, additionally populated by radial glial basal processes (Stiles & Jernigan 2010; Kazanis et al. 2013; Hardwick et al. 2014; Lange & Calegari 2010). With this in mind, neural development can be generally viewed in terms of an initial surge in proliferation followed by an increase in production of terminal neurons occurring concomitantly with cell-cycle exit (Hardwick et al. 2014; Lange & Calegari 2010).

Neuronal network integration is then initiated through axonal extension and synapse formation (Stiles & Jernigan 2010). The vast majority of neurons are formed pre-natally, although a low level of neurogenesis continues post-natally in the SVZ in the lateral walls of the lateral ventricles and in the dentate gyrus of the hippocampus, whereby newly produced neurons migrate to the olfactory bulb and granular layer respectively. (Stiles & Jernigan 2010; Kazanis et al. 2013)

1.8 Directed neural differentiation of pluripotent stem cells.

Capable of forming any cell in the adult body, directing human pluripotent stem cells towards a defined cellular fate and producing a homogenous and predictable population can be a significant challenge. Due to the huge number of neuronal subpopulations, each with specific regional and phenotypic identities, forming a pure and specific population of NPCs and neurons is particularly complex.

In vitro, ESCs have been shown to undergo spontaneous differentiation to a default neuroectodermal identity in the absence of external cues (Stiles & Jernigan 2010; Smukler et al. 2006; Malchenko et al. 2014). Initial protocols exploited this inclination by transitioning ESCs and NSCs to serum free medium, but due to its dependence on spontaneous differentiation this method was not only slow and often inefficient, but also produced cells of mesodermal and endodermal lineages (Cai & Grabel 2007; Reynolds & Weiss 1996; Reubinoff et al. 2001; Joannides et al. 2007; Schulz et al. 2004). Formation of pure neural populations then required selection of cells expressing NPC specific markers using either a cell sorting method such as FACS, media which selectively propagated only neuroectodermal cells or mechanical isolations of neural rosettes (Cai & Grabel 2007; Okabe et al. 1996; Reubinoff et al. 2001). Induction of a neural fate from mouse ESCs and NSCs has also been executed by reducing the monolayer cell density in serum free conditions. This method however was also still reliant on selection of neural cells and inappropriate for hESCs as the drop in cell density would commonly result in apoptosis (Ying & Smith 2003; Fukuda et al. 2006). Alternatively, co-culture with stromal feeder cells was shown to mimic the supportive role of bone marrow stromal cells *in vivo* for maintaining hematopoietic stem cell niches (Kaushansky 2006). *In vitro*, co-culture of stromal feeders and ESCs successfully induced differentiation to a neuroectodermal identity, although selection of ESC-derived NPCs was still required (Morizane et al. 2011; Vazin et al. 2008; Lee et al. 2007; Elkabetz et al. 2008; Perrier et al. 2004; Zeng et al. 2004).

Early neural differentiation protocols for PSCs detailed the induction of a neural identity from mouse ESCs, by initiating a suspension culture whereby cells formed 3D spherical aggregates known as embryoid bodies (EB) with structural cell

arrangements reflective of the early embryo. This was based on a study where teratocarcinoma cells developed cystic EBs with organised germ layer development which was comparable to the mouse ICM (Martin et al. 1977). EBs were also shown to develop with an external sheet of extraembryonic endoderm, covering a core population of cells reminiscent of the epiblast, reflecting the bi-laminar germ disc prior to gastrulation in human embryonic development (Germain et al. 2010; Martin et al. 1977). At a later stage, an anterior-posterior axis of Wnt signalling and the development of a primitive streak like cell population was formed (ten Berge et al. 2008). Although reflective of *in vivo* embryogenesis, EB based protocols which were reliant on spontaneous differentiation were shown to be lengthy and required removal of non-neural cell subtypes (Cai & Grabel 2007; Joannides et al. 2007; Schulz et al. 2004). Adaptation of EB based neural induction in concert with directed differentiation signals such as treatment with FGF2 or Retinoic Acid have been outlined, although they too are often lengthy protocols and selection of neural subpopulations was often still required (Schuldiner et al. 2001; Itsykson et al. 2005; Zhang et al. 2001).

More recently, the homogeneity of the final neuroectodermal population in addition to the ability to monitor differentiation throughout the protocol has been enhanced for human PSCs using monolayer culture techniques. Emulating secretion of BMP inhibitors from the primitive node *in vivo*, addition of NOGGIN to EBs increased efficiency of neuralisation and when used in conjunction with adherent hESCs efficiently induced NPC populations within 2 weeks (Gerrard, Rodgers, et al. 2005; Itsykson et al. 2005). Chambers et al. improved upon this further by shortening the timeframe of neural induction through addition of ACTIVIN/NODAL/TGFβ inhibition, producing NPCs with minimal contamination from other lineages or cell types. By mimicking the dual inhibition of the ACTIVIN/NODAL and BMP arms of the TGFβ signalling pathway present during gastrulation *in vivo (see section 1.8)*, PSCs *in vitro* were efficiently differentiated to form a homogenous population of neural ectoderm with neural rosette formation reflective of the *in vivo* neural plate and tube (Chambers et al. 2009).

1.9 Neuronal induction and the role of oxygen.

1.9.1 Reduced oxygen concentration in the brain in vivo.

The ability to use PSCs for therapeutics and investigation of embryonic development hinges on their ability to differentiate into fully formed somatic cells, phenotypically similar to their *in vivo* counterparts. As mentioned previously, O_2 concentration varies throughout the body and even within a single organ, acting as a signalling molecule to regulate proliferation, metabolism and differentiation (Caniggia et al. 2000; Genbacev 1997; Schipani et al. 2001; Mutoh et al. 2012; Morriss & New 1979). Oxygen concentration in both the developing and adult brain was shown to vary widely, the Rat midbrain and pia measured at 0.8% O_2 (6 mmHg) and 8% O_2 (60 mmHg) respectively (Erecińska & Silver 2001). The mouse telencephalon at E9 was ~1% O2 and in mid-gestation (E11.5) was estimated at ~2-5% O_2 (Mutoh et al. 2012; Lee et al. 2001). Both the mouse and rat developing neural tube were estimated to reside at 1% O_2 at E9 and GD9-11 respectively (Lee et al. 2001; Chen et al. 1999). During initiation of embryonic neuronal development, placental gas resided at less than 2% O_2 with the mouse telencephalon at 2.5% O_2 (Zhou, Z 2004). Although variation in exact O_2 concentration is evident, it is clear that 20% O_2 (i.e. atmospheric O_2) is not an accurate reflection of the *in vivo* environment during embryonic neurogenesis.

1.9.2 Early neural development in vivo and the role of oxygen.

As detailed in section *1.3*, oxygen gradients exist *in vivo* acting to regulate normal development, from post-fertilisation patterning through to the regulation of adult tissues. The reduced oxygen concentrations detailed above have been heavily implicated in functionally and morphologically normal neural development. Development of mouse blastocysts at atmospheric O_2 led to malformation of the neural plate and folds and deformed segregation of the fore and mid brain regions, in contrast to morphologically normal development at a

reduced O_2 (Chen et al. 1999; Morriss & New 1979). In addition, rodent models of HIF1A or HIFB knockouts were typically embryonically lethal with incomplete closure of the neural folds and abnormal regional brain development (Iyer et al. 1998; Ryan et al. 1998; Kozak et al. 1997).

Interestingly in humans, a causative link between ROS exposure prior to establishment of foetal oxidative defences and the subsequent development of neural tube defects has strong evidence. Foetus' exposed to teratogenic antiepileptic drugs (such as Valproic acid) typically developed with neural tube defects, metabolism of which was shown to directly or indirectly produce ROS (Hill et al. 2010; Nazıroğlu & Yürekli 2013). Concordantly, mouse embryos exposed to Valproic acid also developed attenuated neural tube closure and increased production of ROS, both of which were prevented by catalase treatment (Tung & Winn 2011; B. Zhang et al. 2010). Hence, evidence indicates that precise regulation of O_2 concentration and a HIF driven cellular response *in vivo* is essential for normal neural plate and tube formation.

1.9.3 Regulation of Neural Stem Cells by Hypoxia Inducible Factors.

It was mentioned in *section 1.3.2*, that using physiologically accurate oxygen concentrations during *in vitro* culture resulted in cultures which reflected their *in vivo* counterparts more aptly (Bernardi et al. 1996; Tervit et al. 1972; Mutoh et al. 2012; Morriss & New 1979). The regulatory subunits of the HIF family of proteins, responsible for cellular adaptations to fluctuating oxygen concentration, have been shown to be vital in regulating morphologically and functionally normal neuronal development. The *in vivo* O_2 concentration of the highly neurogenic SVZ was shown to reside at ~2-5% O_2 in mice and rats and HIF1A was constitutively expressed in both pre and post-natal NSCs, escaping degradation through vesicular storage (Roitbak et al. 2011; Erecińska & Silver 2001). Additionally, the mouse SVZ had a far higher concentration of ROS than surrounding areas and it was hypothesised that both the SVZ and SGZ stem cell niches maintained their relatively high levels of self-renewal due to spatial proximity to vasculature

(Goldberg & Hirschi 2009; Shen et al. 2008; Tavazoie et al. 2008; Le Belle et al. 2011). Finally, specific deletion of HIF1A in mouse neural progenitor cells resulted in high apoptosis from E15.5 onwards and subsequent depletion of neuronal density in the cortex with adult memory deficits. These losses were restored after delivery of functional HIF1A into the embryonic telencephalon (Tomita et al. 2003).

These effects of low oxygen and Hypoxia Inducible Factors during neural induction have also been demonstrated *in vitro*. Culture of human NSCs at 2-5% O_2 increased production of neurospheres due to attenuated apoptosis. Rat E12 and mouse E15.5 NSCs cultured at 3% and 2% O_2 respectively both showed an increase in proliferation in addition to a drop in apoptosis in the latter (Studer et al. 2000; Horie et al. 2008). It must be considered that as the status of HIF1A was not determined in the above studies, alterations to proliferative/apoptotic balance may have been regulated in a HIF1-independent manner, as outlined by Clarke et al whereby HIF1A-null NSCs continued to show suppression of pro-apoptotic factors at 4% O_2 (Clarke & van der Kooy 2009).

In vitro, a process has been outlined whereby PSC derived neuroepithelial cells could be induced to form radial structures with NSC and proliferative markers aptly reflecting those commonly observed during *in vivo* post-neural tube closure, *in vitro*, these structures are known as neural rosettes (Elkabetz et al. 2008). MESC derived NPCs formed rosettes of a higher density and corresponding cell number when differentiated at 2% O_2, in addition to later increasing the yield of immature and mature neurons (marked by BIII-Tubulin and MAP2 expression respectively) (Mondragon-Teran et al. 2013). Reflecting the increased proliferation of neurosphere cultures under low O_2, mESC derived NPCs were also stimulated to increase cell growth at low O_2 (Horie et al. 2008; Studer et al. 2000; Le Belle et al. 2011; Storch et al. 2001; Rodrigues et al. 2010). These early results indicate not only a crucial role for O_2 in neuronal identity but also the possibility of its application as a tool for optimisation of differentiation protocols.

It is interesting to note, that although in many cells stabilisation of HIF1A is a transient reactionary event due to a reduction in local O_2, neural stem cells (NSC)

from the neurogenic subventricular (SVZ) and subgranular zones (SGZ) have been shown to constitutively express HIF1A, implying a functional role in NSC biology (Roitbak et al. 2011; Mazumdar et al. 2010). HIF2A was also implicated in driving neurosphere formation of mouse NSCs through augmented proliferation and apoptosis (Huang et al. 2013). In light of this information, 3% O_2 was used here to reflect the estimated physiological oxygen concentration during neurogenesis.

1.9.4 Low oxygen regulates terminal fate of Neural Stem Cells.

Further to promoting self-renewal and survival of neural progenitors, low oxygen can also regulate cell fate decisions. Under low oxygen, the co-ordinated efforts of HIF1A and Notch signalling influenced mouse telencephalic NPCs towards an astrocytic fate through demethylation of the GFAP promoter, a gene essential for astrocytic development. Astrocytic differentiation occurred at the expense of neuronal differentiation (Mutoh et al. 2012). At a later gestational timepoint, mouse NPCs, in addition to rat NPCs and an immortalised human NSC line showed increased rates of neuronal differentiation at O_2 concentrations between 2-3% O_2 (Santilli et al. 2010; Studer et al. 2000; Horie et al. 2008). The control which oxygen seemed to bear on cell fate specification has also applied to designation of the neurotransmitter subtype. Mouse NSCs switched from a GABA phenotype at 20% O_2 to a Glutamate phenotype at 2% O_2 and 3% O_2 culture of rat NSCs augmented dopaminergic differentiation (Studer et al. 2000; Horie et al. 2008). Interestingly, deletion of the HIF1A gene prevented mESC-derived NPCs and mouse NSCs from undergoing WNT driven proliferation and terminal differentiation, indicating a direct role for HIF1A in modulating terminal cell fate (Mazumdar et al. 2010). Furthermore, mesenchymal stem cells and mESCs showed augmented production of specific neuronal identities under low O_2 in a HIF1A dependent manner; repression of HIF1A in mESCs repressed this augmented differentiation and in MSCs suppressed the transcriptional identity of transitory NPCs (Kim et al. 2008; Y. Wang et al. 2013). This insight into the regulatory capabilities of HIF1A indicates a possible application in modulating terminal

neuronal fate *in vitro*. If clarified in regards to PSC differentiation, the use of oxygen has the potential to be an important tool for use in directing cell fate.

1.10 Clinical applications of low O_2 in stem cell therapies.

1.10.1 HIF1A driven neurogenesis in response to stroke.

HIF1A mediated control over proliferation and differentiation is not just relevant to embryonic neurogenesis, but is vital in the response to neural ischemic incidents. It is acknowledged that the oxidative stress due to diminished glucose supply from the middle cerebral artery results in large amounts of apoptosis; NSCs in the SVZ and SGZ niches have conclusively been shown to respond to the resulting cellular damage in a HIF1A dependent manner. The stabilisation of HIF1A, both in rodents and humans, underlies the subsequent surge in proliferation and migration of NSCs from the SVZ and SGZ towards the site of injury, acting to prevent neuronal apoptosis (Harms et al. 2010; Cunningham et al. 2012; Park et al. 2006). Deletion of HIF1A from NSC populations was shown to eradicate this protective response, signifying that NSC mediated neuroprotection was reliant on HIF1A facilitated signalling (Harms et al. 2010). Manipulation of HIF1A expression in this context could predictably have large therapeutic implications. Experimental occlusion of the middle cerebral artery can be used in rodents to mimic ischemic stroke by preventing cerebral blood flow and oxygen supply (Lipton 1999). Transplantation of NSCs constitutively expressing HIF1A at the site of ischemia not only stimulated angiogenesis adjacent to the injury site but also accelerated recovery time (Wu et al. 2010). Angiogenic responses likely resulted from up-regulation of vascular endothelial growth factor (VEGF), known to not only be a direct target of HIF1A transcription but also an observed result of neural ischemic stress (Harms et al. 2010; Cunningham et al. 2012; Roitbak et al. 2008; Forsyth et al. 2006).

1.10.2 Low oxygen in the disease modelling of Parkinson's Disease.

One of the greatest challenges in the application of stem cells for regenerative therapies and disease modelling is producing a well-defined, population of cells that accurately reflect the phenotype and functionality of *in vivo* tissues. The huge variation of regionally and phenotypically diverse adult neurons forms significant challenges in directing pluripotent stem cells towards a targeted sub-population. Whilst the majority of protocols aptly reflect the signalling cascades observed during embryonic neurogenesis, a minority are now considering mimicking of the neurogenic environment through regulation of O_2.

The neurodegeneration of the dopaminergic neurons of the substantia nigra in Parkinsons Disease is an ideal target for PSC based therapeutics as early studies have already indicated therapeutic improvement after transplant of fetal dopaminergic tissue (Clarkson 2001). Proliferation and differentiation of human foetal mesencephalic precursors at low O_2 not only aided proliferation of NSCs but augmented production of cells positive for tyrosine hydroxylase (a key marker of DA transmission), hastened maturation and increased dopamine secretion (Liu et al. 2009; Studer et al. 2000). Reliance on human fetal tissue is practically limited due to the constraints on tissue availability and access, restricting the large scale-up required for widespread clinical applications. Use of pluripotent stem cells is the logical alternative; Kim et al. succeeded in amplifying the yield of tyrosine hydroxylase positive cells produced from mESCs by using 3% O_2 throughout the differentiation process, this augmented production was repressed by silencing of HIF1A (Kim et al. 2008). Use of MSCs are an additional option for multipotent cell sourcing due to ease of biopsy and lack of immune challenges upon transplantation. Neuronal differentiation of mesenchymal stem cells under 3% O_2 formed a higher proportion of neurons in addition to also promoting a dopaminergic fate, possibly in a HIF1A dependent manner (Y. Wang et al. 2013).

1.10.3 Use of an in vivo oxygen concentration avoids transplantation induced hypoxic cell death.

In addition to promoting a specific neuronal identity, low O_2 may also support the survival, proliferation and integration required, and often lacking, after cellular transplant into a relatively hypoxic adult brain. Initially, Theus et al. summarised a protective phenotype whereby after a short period of hypoxic preconditioning (HP) (with an oxygen concentration which was hypoxic relative to physiologically relevant levels), hESC derived NPCs showed increased survival and tolerance to H_2O_2 and serum withdrawal. Transplanted HP-NPCs in a rodent model of neural ischemia subsequently showed augmented survival and caused improved behavioural recovery compared to implantation of non-preconditioned cells (Theus et al. 2008). Francis et al also showed HP-NPCs went on to form neurons with improved action potential frequency and size in addition to confirming an increased tolerance to toxic insult (Francis & Wei 2010). NPC's produced at low O_2 survived better after transplant in comparison to those formed at atmospheric O_2, reflected in the high levels of cell death seen when moving NPC's from atmospheric O_2 into 3% O_2 (Stacpoole et al. 2011b; Stacpoole et al. 2011a; Stacpoole et al. 2013). A vital study by Wang et al. put this protective phenotype into practice. NPCs derived from MSCs at 3% O_2 not only promoted a dopaminergic neuronal identity but upon transplantation into 6OH-DA lesioned rats (a common rodent model of PD), neurons showed higher survival levels, increased DA production and augmented behavioural improvements (Y. Wang et al. 2013). Survival and integration of transplanted grafts is a major issue in the translation of PSCs into a viable therapeutic avenue; it seems clear that use of physiologically relevant O_2 throughout PSC differentiation is not only beneficial for enrichment of a selected sub-population of neurons, but may also be vital to maximise clinical benefits.

1.11 Scope and specific objectives.

Previous studies on the pluripotency of hESCs showed large variability in the effect of reduced oxygen concentrations on proliferation, viability and self-renewal, and in the timeline of HIF1A and 2A stabilisation. The large variables in cell culture techniques, proliferation assays, cell lines and even equipment used to maintain low oxygen concentrations likely contributed to the contrasting reports outlined above. When viewed collectively, it indicates that any use of low O_2 as a tool in maintaining and differentiating human pluripotent stem cells requires prior clarification into the stability of proliferation and viability. Furthermore, investigations into the use of low oxygen as a tool for augmenting neural differentiation have commonly only characterised the final population. This characterisation has been heavily reliant on the use of protein markers of maturity, and not through assessing functionality and excitability of terminal neurons. Hence, the specific hypotheses for this project were outlined as follows :

- Expression of HIF1A and 2A has not previously been determined in iPSCs, therefore, are the HIF1A and 2A subunits expressed in human iPSCs in addition to hESCs? Additionally, the timeframe of protein stabilisation was variable across previous studies, so at how long after introduction to low oxygen are these proteins expressed and / or stabilised, in the cell lines examined here?
- Prior reports into the pluripotency, proliferation and viability of pluripotent stem cells have also been conflicting and inconsistent, often relying on inexact methods. These aspects have also not previously been examined in iPSCs, hence, using stringent quantitative methods, does low oxygen cause shifts in proliferation or viability in hESCs and iPSCs? And is maintenance of PSCs at low oxygen a beneficial tool to support the pluripotent state?
- Multiple *in vivo* studies have detailed a dependency on HIFA subunits for formation of a morphologically normal neural plate and tube, and although examination has been paid to formation of PSC derived terminal neurons in *vitro,* induction of early neuroectoderm has not been examined. Does differentiation of hESCs to an early neural fate at a physiological oxygen concentration increase efficiency of neural induction?

- The majority of previous studies examining the production of terminal neurons at low oxygen characterised the final population using protein expression of markers known to be specific to mature neurons. Additionally, in those studies that did examine functionality, analysis was not in depth. Here we examined whether neural differentiation of hESCs performed at an *in vivo* oxygen concentration would augment or accelerate the synaptic networking and functional activity of neural populations? Additionally, which aspects of action potential generation or propagation would be most affected?

This study was undertaken in partnership with Baker-Ruskinn, manufacturers of specialised low oxygen workstations. These workstations allow cell culture incubation in addition to cell culture processes to be undertaken in a controlled low oxygen environment. As oxygen sensitive messengers such as HIF1A have been shown as extremely sensitive to high oxygen, with a half-life of between 1-5 minutes at atmospheric oxygen concentrations, this technology is a promising alternative to exposing cell cultures to oxygen fluctuations through the use of hypoxic incubators and laminar flow hoods (Wang et al. 1995; Yu et al. 1998). This study also aimed to assess this technology for the use of human PSCs. Through this partnership, development of technology complementary to low oxygen incubation was also undertaken in addition to product optimisation, namely a unit designed to reduce dissolved oxygen concentration in liquids required for cell culture processes.

2. Methods and Materials

Consumables were purchased through various suppliers, further information regarding catalogue codes and suppliers can be found in *section 2.8.*

2.1 Cell culture.

2.1.1 Media

MEFi Medium

DMEM-Glutamax	Base media	Life-Technologies, Paisley, UK
Fetal Bovine Serum	10% v/v	Life-Technologies, Paisley, UK
Penicillin-Streptomycin	10 U/ml	Life-Technologies, Paisley, UK

PSC Medium

Knockout DMEM	Base media	Life-Technologies, Paisley, UK
Knockout Serum Replacement	15% v/v	Life-Technologies, Paisley, UK
Non-essential amino acids	1% v/v	Life-Technologies, Paisley, UK
Penicillin-Streptomycin	10 U/ml	Life-Technologies, Paisley, UK
L-Glutamine	2 mM	Life-Technologies, Paisley, UK
β-mercaptoethanol	100 μm	Sigma-Aldrich, Dorset, UK
Fibroblast Growth Factor2 (FGF2)	20 ng	Peprotech, London, UK

Neural Differentiation Media

Neural Induction Medium

Advanced DMEM/F12	Base media	
Penicillin-Streptomycin	10 U/ml	Life-Technologies, Paisley, UK
L-Glutamine	2 mM	Life-Technologies, Paisley, UK

Neurobrew21 without Vitamin A	2% v/v	Life-Technologies, Paisley, UK
Addition of small molecule inhibitors as required :		
LDN193289 (LDN)	0.25-0.5 μM	Milteny, Surrey, UK
SB431542	10 μM	Abcam, Cambridge, UK

Neural Rosette Medium

Advanced DMEM/F12	Base media	Life-Technologies, Paisley, UK
Penicillin-Streptomycin	10 U/ml	Life-Technologies, Paisley, UK
L-Glutamine	2 mM	Life-Technologies, Paisley, UK
Neurobrew21 without Vitamin A	2% v/v	Milteny, Surrey, UK

SCM1

Advanced DMEM/F12	Base media	Life-Technologies, Paisley, UK
Penicillin-Streptomycin	10 U/ml	Life-Technologies, Paisley, UK
L-Glutamine	2 mM	Life-Technologies, Paisley, UK
Neurobrew21 with Vitamin A	2% v/v	Milteny, Surrey, UK
PD0332991	2 μM	Tocris, Abingdon, UK
DAPT	10 μM	Tocris, Abingdon, UK
BDNF	10 ng/ml	Milteny, Surrey, UK
Forskolin	10 μM	Tocris, Abingdon, UK
CHIR99021	3 μM	Tocris, Abingdon, UK
GABA	300 μM	Tocris, Abingdon, UK
$CaCl_2$	1.8 mM	Sigma-Aldrich, Dorset, UK
Ascorbic Acid	200 μM	Sigma-Aldrich, Dorset, UK

SCM2

Advanced DMEM/F12	50% Base media	Life-Technologies, Paisley, UK
Neurobasal A	50% Base media	Life-Technologies, Paisley, UK
Penicillin-Streptomycin	10 U/ml	Life-Technologies, Paisley, UK
L-Glutamine	2 mM	Life-Technologies, Paisley, UK

Neurobrew21 with Vitamin A	2% v/v	Milteny, Surrey, UK
PD0332991	2 μM	Tocris, Abingdon, UK
BDNF	10 ng/ml	Milteny, Surrey, UK
CHIR99021	3 μM	Tocris, Abingdon, UK
$CaCl_2$	1.8 mM	Sigma-Aldrich, Dorset, UK
Ascorbic Acid	200 μM	Sigma-Aldrich, Dorset, UK

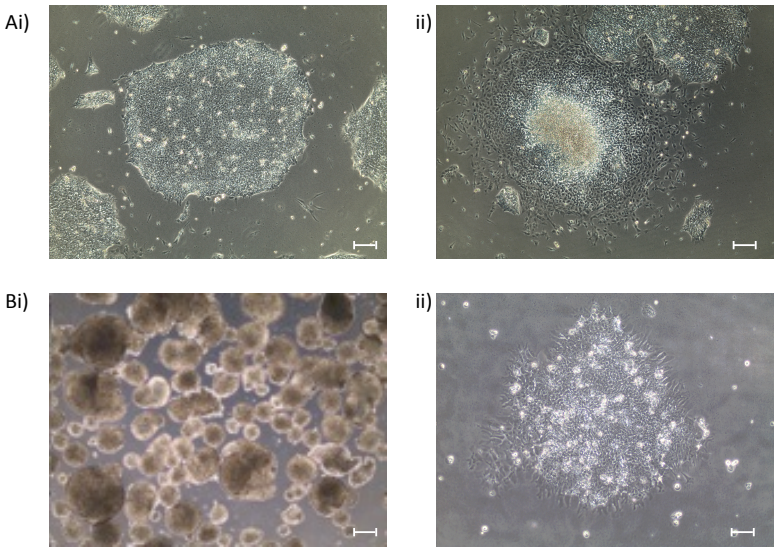

Figure 2.1 Representative images of PSC based culture methods.

HESC colonies showing typical pluripotent morphology (i) and spontaneous differentiation (ii). Pluripotent colonies typically retained defined colony borders with a homogenous surface texture. Those which displayed loss of colony borders with thick, darkened areas and visibly separate cells were deemed to have undergone uncontrolled spontaneous differentiation and were removed. (B) HESC undergoing directed differentiation to a neural fate. Classically, many protocols for directed differentiation of PSCs to germ layer progenitors used a 3D spherical aggregate (i) known as Embryoid Bodies (EBs). These allowed for structure formation in the vertical and horizontal planes (Martin et al. 1977; Germain et al. 2010; ten Berge et al. 2008). *However, use of monolayer cultures during directed differentiation theoretically allowed gas exchange and drug delivery in a more controlled and homogenous manner (ii). Scale bars represent 200μm.*

Here, the 34D6 (iPSC) and the H9 (hESC) lines were used for investigation into the effect of low oxygen. The H9 hESC line has been widely used in many studies of stem cell pluripotency and neural differentiation, including investigations into the use of low oxygen for maintaining self-renewal. Hence, its use allowed comparison with previous reports. To investigate the effects of low oxygen on a reprogrammed pluripotent cell line, a non-diseased control iPSC line was required. The 34D6 line was gifted by Professor Siddharthen Chandran and obtained using fibroblasts from a 56-year old non-diseased male, using retroviral transduction of POU5F1, SOX2, KLF4 and c-MYC. After reprogramming, all transgenes were silenced and activation of endogenous POU5F1, SOX2 and KLF4 was certified (Bilican et al. 2012).

2.1.2 Pluripotent Stem Cells

The undifferentiated state of hESCs and iPSCs was maintained using a typical monolayer culture method. Both cell lines were cultured on 60mm diameter, adherent Nunc plates (Fisher Scientific, Loughborough, UK Scientific, Loughborough, UK), coated with Matrigel (VWR, Leicestershire, UK) (diluted in cold Knockout-DMEM (Life-Technologies, Paisley, UK) at manufacturer recommended dilutions) for 1 hour at 37°C before cell seeding. When ~80% confluent, H9 and 34D6 populations were assessed to ensure only pluripotent colonies were propagated. Using standard morphological analysis *(for 'pluripotent' and 'differentiated' morphology see Figure 2.1A)* differentiated colonies were removed from the population using a pipette tip (a practice known as 'pruning'). Plates received 1 x wash with Phosphate Buffered Saline (PBS, Life-Technologies, Paisley, UK) and colonies with pluripotent morphology were dissociated from the Matrigel covered plastic using 1U / ml of a protease enzyme, Dispase (Stem Cell Technologies, Grenoble, France). Inclusion of 10 μm Y27632 dihydrochloride (Y27632, Abcam, Cambridge, UK), an inhibitor of Rho-associated kinase prevented dissociation induced apoptosis in PSCs (Gauthaman et al. 2010). Cells were incubated with Dispase and Y27632 for 15-30 minutes at 37°C before fresh PSC medium (described above) was used to gently wash colonies off the plate. Cells

were collected in a 15ml falcon tube and centrifuged at 230 x g for 3 minutes, the cell pellet was then washed with fresh PSC medium and re-centrifuged to remove residual traces of Dispase. Cells from one confluent plate were reseeded onto 4 fresh plates in PSC medium (which had been conditioned with feeder cells for additional trophic support, see below). Medium was supplemented with 20 ng Fibroblast Growth Factor-2 (Peprotech, London, UK) and Y27632 was added to plating medium for the first 24 hours after seeding. Conditioning of PSC medium was performed as detailed below.

Before use with hESC and iPSC lines, medium was conditioned overnight with mouse embryonic fibroblasts that had been irradiated to prevent further proliferation (MEFi, VH-Bio, Gateshead, UK). Using MEFi conditioned medium has been shown to sustain pluripotency in human PSCs without direct MEFi contact, allowing for subsequent analysis of gene and protein expression levels to be performed on pure populations of pluripotent human ESCs and iPSCs (Xu et al. 2001). Frozen vials of MEFis were thawed into MEFi medium, centrifuged at 230 x g for 3 minutes, washed with fresh, warmed medium and re-centrifuged at 230 x g to ensure adequate removal of the medium in which cells were frozen. MEFi were plated at a density of 1.25 x 10^5 cells per 60 mm Nunc plate which had been pre-coated with 0.1% Gelatin (Millipore, Herfordshire, UK) for one hour at 37°C. After seeding, MEFi were left for at least 6 hours to attach and form a monolayer. Once cells had adhered, the MEFi medium was removed from the cells, which were then washed with PBS. To condition PSC medium, PBS was removed and 5 ml PSC medium was added to each dish for overnight incubation at 37°C, 5% CO_2 and 95% atmospheric air. After conditioning, medium was collected, medium was filtered through 0.2 μm pore diameter filters and warmed to 37°C prior to use.

2.1.3 Neural differentiation of human embryonic stem cells.

For differentiation to a neural progenitor fate, cells underwent 3-day incubation as pluripotent cultures (described above) at either atmospheric (20% O_2) or 3% O_2. When ~80% confluent, neural induction was initiated as a non-adherent suspension (Embryoid Body) culture or as a monolayer.

For formation of Embryoid Bodies, 1 x 60 mm Nunc plate of pluripotent colonies was lifted off as outlined above, centrifuged at 230 x g for 3 minutes and the pellet transferred to a 90 mm Sterilin non-adherent dish (Fisher Scientific, Loughborough, UK) in neural induction medium as above. Y27632 was used for the first 2 days of culture to minimise cell death and was removed from culture medium thereafter. After ~12 hours in a non-adherent culture dish, cells formed Embryoid Bodies (EBs), 3D spherical aggregates of cells *(Figure 2.1b).* Differentiation was directed using small molecule inhibitors SB431542 (Abcam, Cambridge, UK) and LDN193289 (Milteny, Surrey, UK) to block SMAD2/3 regulated pluripotency and SMAD1/5/8 regulated differentiation to epidermal ectoderm and neural crest fate respectively (Chambers et al. 2009; Levine & Brivanlou 2007; Sela-Donenfeld & Kalcheim 1999; Delaune et al. 2005). The regime of drug treatment was: 10 μm SB431542 during days 1-4, 0.5 μM LDN193289 during days 1-8. On day 2 and day 4 of differentiation, 100% medium changes were performed to remove Y27632 and SB431542 respectively, from cultures.

For monolayer differentiation protocols *(Figure 2.1b)*, pluripotent hESC were pre-conditioned as outlined above. When cultures had reached 60-70% confluency, PSC medium was removed, plates were washed once with PBS and replaced with neural induction medium.

At D8, both as EBs and monolayer cultures, cells were re-plated either for immunofluorescence or for further differentiation. For immunofluorescence, cells were dissociated to single cells using TrypLE (Life-Technologies, Paisley, UK) with 10 μm Y27632 and incubated for 5-15 minutes at 37°C before washing and collecting cells in Advanced DMEM/F12 medium (Life-Technologies, Paisley, UK). Cells were then re-plated at $5x10^4$ cells per 13 mm glass coverslip (VWR, Leicestershire, UK), which had been coated with Matrigel for 1 hour at 37°C before use.

For differentiation to neural rosettes, Day 8 -NPC's were dissociated to a single cell state as outlined above and re-plated at a ratio of 1:2 in 4 ml Neural Rosette medium per 6 cm plate with 10 μm Y27632 for the initial 24 hours post-plating. Between D8-16 of differentiation, cells were fed daily.

For differentiation to terminal neurons, neural rosettes were pre-treated with 10 μm Y27632 for 1 hour and dissociated as outlined above. Cells were re-plated onto coverslips (see preparation below) at a density of 4 x 10^4 cells per coverslip in a 50 μl droplet and left to adhere for 1.5 hours before adding 500 μl media per well. Coverslips were fed with SCM1 medium for the first week post-platedown and SCM2 medium thereafter with bi-weekly media changes.

To aid long-term cell adherence, the external covering of borosilicate present on glass coverslips required removal. To etch coverslips and aid long-term cell attachment, coverslips were incubated in neat Nitric Acid (Fisher Scientific, Loughborough, UK) overnight on a rocker at room temperature. Subsequently, coverslips were washed five times with distilled water and sterilised by a 100% ethanol wash (Sigma-Aldrich, Dorset, UK) and overnight baking at 150°C (Beaudoin et al. 2012). Once placed into a 24-well plate, coverslips were coated with a 50 μl droplet of 100 μg/ml PDL (Sigma-Aldrich, Dorset, UK) and incubated for at least 1 hour at 37°C, washed with dH_2O and left to dry overnight. One hour before seeding cells, a 50 μl droplet of Matrigel was added to coverslips and left to incubate at 37°C, cells were seeded at desired density immediately after removal of Matrigel.

2.1.4 SiRNA knockdown.

Small interfering RNA (siRNA) were used to repress expression of specific gene products. SiRNA were designed with specific sequences complementary to target mRNA. When transfected into cells, siRNA have been shown to be unwound into ssRNA, bind target mRNA products and induce their degradation, preventing subsequent protein expression (Perdew et al. 2006). HIF2A gene products (SMARTpool: siGENOME EPAS1 siRNA) were silenced in conjunction with a scrambled control (siGENOME Non-Targeting siRNA #2, both Thermo Scientific, Massachusetts, USA). H9 hESCs were pre-treated with 10 μm Y27632 for 1 hour prior to dissociation as detailed above. After dissociation, cells were replated in PSC medium at high density. As per manufacturers instructions, RNAiMax

lipofectamine was incubated with 20 pm siRNA for 5 minutes at room temperature in Opti-MEM medium (both Life-Technologies, Paisley, UK) before direct addition to freshly seeded cells. Twenty-four hours later, transfection of siRNA was repeated as above but cells were not dissociated beforehand.

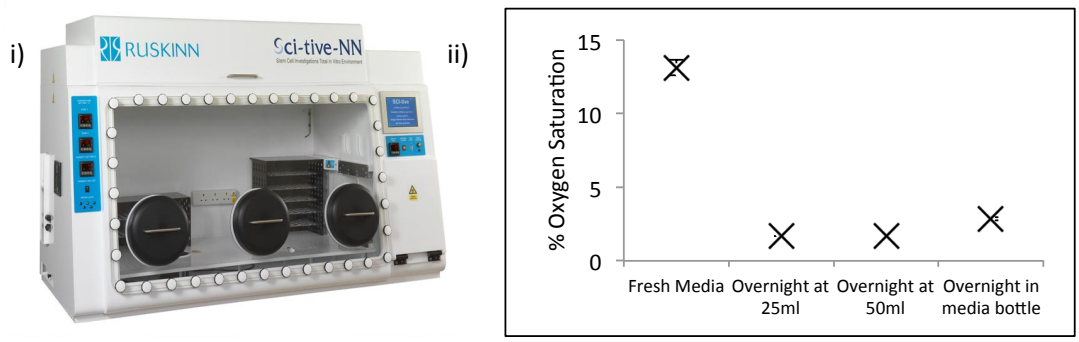

Figure 2.2 Maintenance of low oxygen conditions for comparison of 3% O2 with atmospheric O2.

(i) The Sci-tive was used to maintain low oxygen conditions throughout experiments. The large work area allowed for all cell culture processes including passaging and medium changes to be performed at 3% O_2. ii) All liquids used in low oxygen cell culture were equilibrated overnight in the Sci-tive at 3% O_2.

2.2 Control of low oxygen environment.

For atmospheric oxygen cell culture, cells were maintained in a standard incubator and laminar flow hood at 5% CO_2 and atmospheric O_2, ~20%. For examination of low oxygen conditions, gaseous concentrations of 3% O_2 and 5% CO_2 were used. Preliminary assessment of previous reports identified the use of 3% O_2 as the most likely to be beneficial for maintaining pluripotency and was reflective of the reported uterine O_2 concentration during early embryogenesis (Ottosen et al. 2006; Rodesch et al. 1992; Fischer & Bavister 1993). For control of low oxygen concentrations, a Sci-TIVE workstation was used to maintain consistent conditions at 3% O_2 and 5% CO_2 (provided by Baker-Ruskinn) *(figure 2.2).* An all-in-one unit, the Sci-TIVE was a combined workspace and incubator. The unit was completely sealed with arm sleeves to allow access for medium changes

and passaging whilst keeping O_2, CO_2, temperature and humidity completely stable. Oxygen levels were specified at 3% O_2 with 5% CO_2. Humidity was set at 70% in the Sci-TIVE with a water tray in the 'normal' incubator. In low oxygen, all liquids used during cell culture (e.g. medium, PBS and H_2O) were equilibrated overnight in petri dishes before use to maintain O_2 levels throughout experiments (Sies & Bruene 2007) *(Figure 2.2ii).*

Using a Dissolved Oxygen Bench Meter (HI2400, HANNA Instruments, UK), it was confirmed that overnight incubation of liquids in the Sci-TIVE was sufficient to bring dissolved oxygen concentration down to 2-3% O_2. This occurred both in a full bottle of fresh medium (lid off), a petri dish containing 25 ml and a petri dish containing 50 ml. The HANNA dissolved oxygen meter was calibrated between 0-20% O_2 using the provided zero oxygen solution and atmospheric oxygen concentration for the bottom and top of the range respectively. The percentage readout (y) was then corrected to be relative between 0-100% O_2 by : (y / 100) x 20.

When discussing the O_2 concentration used in cell culture, it is prudent to recognise what is being defined; the concentration of oxygen within the gaseous atmosphere of the chosen incubator and within the liquid phase of the cell culture media are not necessarily the same. Firstly, the use of percentage will not always correlate to concentration; for example, the percentage of O_2 present is the same at both high and low altitudes whereby ~20% of the gases present is oxygen. That said, at extremely high altitudes it becomes hard to breathe as the increase in pressure reduces the number of gas molecules present. The concentration (ppm or mg/L) has decreased but percentage remains constant. Secondly, liquid exposed solely to a gaseous phase with reduced oxygen concentration will take ~5-10 hours of incubation to reach equilibrium without shaking/stirring of the media, reportedly forming oxygen gradients within tissue culture dishes (Fernandes et al. 2010). A further decrease in O_2 concentration may be observed in pericellular spaces within cultures themselves (Pettersen et al. 2005). Commonly, reports of a chosen O_2 percentage during *in vitro* cell cultures refer to the percentage specified for the gaseous phase of the incubator, and not the

dissolved oxygen concentration in cell culture media. For clarity and consistency, reports of the applied oxygen concentration in preceding studies have been discussed here in terms of how they were originally reported, which was generally in relative percentage terms. Additionally, '3% O_2' which has been used throughout this study refers to the gaseous phase of the workstation.

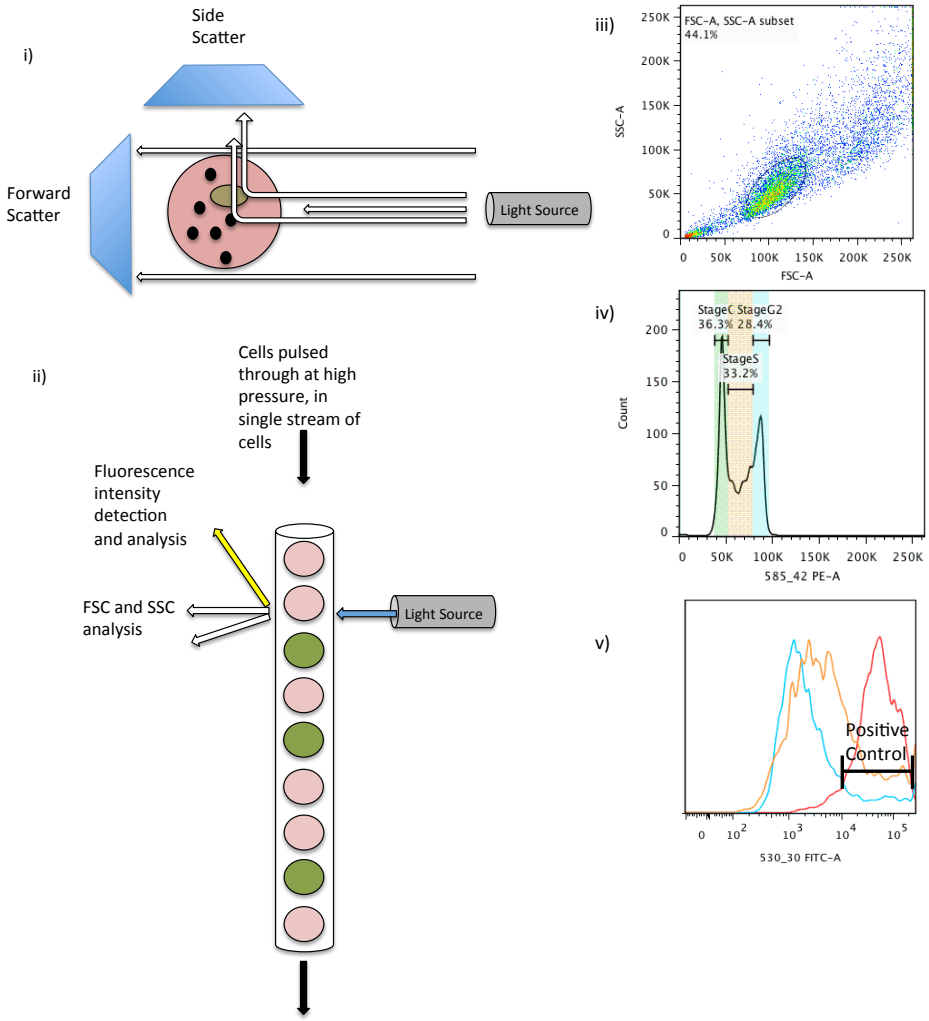

Figure 2.3 Measuring size, complexity and intensity of fluorescence using flow cytometry.

Cells moving in single file were forced through tubing adjacent to a light source and multiple detectors (i, ii). Light which was not refracted by collision with internal organelles (hence, has travelled externally around the cell) was picked up by the Forward Scatter Detector (FSC), indicating the size of the cell. Light which hit the cell directly was refracted by internal cellular structures and detected by the Side-Scatter Detector, indicating cellular complexity. Additionally, excitation of fluorescent markers were excited by selecting the relevant wavelength emission, allowing separation of cells according to fluorescent intensity. (iii) A typical SSC vs FSC plot was used to exclude debris and doublets, ensuring only whole cells were included in analysis. (iv) When performing cell cycle analysis, typically a double peaked histogram was observed, whereby the G2 peak formed at twice the fluorescent intensity (~90K) than the G1 peak (~45K). (v) Positive (red) or negative controls were used to aid separation of cell populations dependent on fluorescence. Shown here is a representative histogram of cells labelled with AnnexinV-FITC conjugate with a positive control (pre-treatment with apoptotic inducer Staurosporine).

2.3 Flow Cytometry

2.3.1 Buffers and antibody dilutions.

FACS Buffer		
Phosphate Buffered Saline		Life-Technologies, Paisley, UK
Fetal Bovine Serum	2% v/v	Sigma-Aldrich, Dorset, UK
Sodium Azide	0.1% w/v	Sigma-Aldrich, Dorset, UK
Saponin	0.14% w/v	Life-Technologies, Paisley, UK

Antibody Dilutions

Antigen	**Supplier**	**Dilution**
POU5F1	Santa Cruz	1:100
NANOG	Abcam	1:500
SOX2	Abcam	1:500
SSEA4	Developmental Studies Hybridoma Bank	1:58
Anti-mouse IgG, AF-488	Life Technologies	1:400
Anti-rabbit IgG, AF-488	Life Technologies	1:400

2.3.2. Cell dissociation.

Flow cytometry allows for separation of a population of cells into distinct sub-populations dependent on size, granular cell content and/or expression of a chosen protein marker *(Figure 2.3).*

Use of flow cytometry is reliant on dissociation of cell populations into single cells, throughout experiments hESCs and iPSCs were prepared for analysis in the same way. Two or three days after seeding (dependent on assay), medium was removed from PSCs and cells were washed once with PBS to remove remnants and floating dead cells. TrypLE with 10 μm Y27632 was added and incubated with cells at 37°C for 5-15 minutes until cells began to float off, before collection with

PSC medium and centrifugation at 230 x g for 3 minutes. PSC cultures should have at this point become single cells, if clumps were present then an additional 5 minutes of TrypLE and Y27632 treatment was given. For all experiments, 1 x 10^4 cells were recorded and the initial Forward Scatter vs Side Scatter plot *(Figure 2.3c)* was used to include only single, whole cells for analysis. Analysis of data after scanning of cells was performed using FlowJo 7.6.3 software.

2.3.3 Cell-cycle assay.

To quantify the proportion of cells actively proliferating, cells were collected when ~50-60% confluent, to ensure that analysis occurred whilst in the exponential stage of growth, normally 2 days after passaging. Once in a single cell suspension, cells were resuspended and fixed in 70% Ethanol (Sigma-Aldrich, Dorset, UK) for 60 minutes at 4°C. After fixation, cells were centrifuged at 230 x g for 3 minutes and washed once in PBS. A repeat centrifugation removed PBS and cells were then stained with 40 μg/ml Propidium Iodide and 100 μg/ml RNase A (both Sigma-Aldrich, Dorset, UK) in PBS for 30 minutes at 37°C. The fluorescent dye Propidium Iodide was used due to its property of intercalating between nucleotide bases, both RNA and DNA. To assess the proportion of cells which were actively undergoing DNA duplication and cell division, RNaseA treatment was used to remove RNA content, preventing inclusion of RNA-Propidium Iodide complexes in analysis. After incubation, cells were put on ice and samples were run immediately. Propidium Iodide is excited at ~536 nm and emits at ~617 nm so a 585-42 PE filter was used to measure fluorescence intensity. Data was displayed as a histogram of 585-42 PE fluorescence with a linear x-axis. This showed as a distinctive 2 peak graph, each peak representing a population of cells containing similar concentrations of DNA. Cells in G2/M stage of the cell cycle are pre-cell division so contain twice the amount of DNA (so considered to be actively dividing), reflected as twice the intensity of fluorescence as those with one set of DNA in G1. *(Figure 2.3D)* An algorithm within the FlowJo software separated these peaks and determined the proportion of cells in G1 and G2/M. Here, the Watson (Pragmatic) model was used to fit Gaussian curves to the G1 and G2/M peaks due

to its focus on the distribution of the two peaks, rather than the S-phase (Watson et al. 1987). The Proliferative Index (PI) was used as an estimation of the overall proliferative activity, calculated by (the proportion in G2 / the proportion in G1), any increase therefore reflected an increase in proliferation.

2.3.4 Apoptosis assay.

For analysis of apoptosis and cell death, the percentage of cells staining as positive for apoptotic marker phosphatidylserine and live/dead stain, Propidium Iodide was quantified. Phosphatidylserine is an early apoptotic cell surface marker that efficiently binds AnnexinV, conjugation of AnnexinV with FITC (excited at 496 nm and emits at 519 nm) exploits this property to positively mark apoptotic cells. Propidium Iodide is membrane impermeable so in a live cell population only marks dead cells. Once cell populations were in a single cell suspension, cells were counted and aliquoted at 1 x 10^5 cells per sample. For AnnexinV-FITC (Abcam, Cambridge, UK) and Propidium Iodide staining, cells were incubated with the dyes and buffer provided for 5 minutes in the dark at room temperature, as per manufacturers instructions. A positive control was used for gating purposes; this was obtained by pre-treating cells with an apoptotic inducer, 1 mM Staurosporine (Sigma-Aldrich, Dorset, UK) for 24 hours before analysis. *(Figure 2.3v).*

2.3.5 Antibody staining.

In addition to proliferation and apoptosis, flow cytometry was used to quantify the percentage of the cell population which maintained protein expression of specific pluripotency markers, intracellular POU5F1, SOX2, NANOG and cell surface marker SSEA4. Once in a single cell suspension, cells being stained for intracellular markers were resuspended and fixed with 4% Paraformaldehye (pH7.4, Sigma-Aldrich, Dorset, UK) for 10 minutes at 4°C. Staining was then carried out as follows: 3 x PBS wash, addition of primary antibody diluted in FACS Buffer for 30 mins at 4°C, 3 x PBS wash, secondary antibody diluted in FACS Buffer for 30 mins at 4°C, 3 x PBS wash. Each change in solution was performed by centrifugation at

230g, for 3 minutes. FACS Buffer was used to keep live cells (for surface marker expression) stable and viable whilst staining in addition to the serum blocking non-specific antibody binding. Antibody dilutions were carried out as listed above. Primary IgG antibodies from mouse were linked to Alexa Fluor 488 anti-mouse IgG, primary IgG antibodies obtained from rabbits were co-stained with Alexa Fluor 488 anti-rabbit IgG. A negative control was also produced as a sample with no primary antibody added, just the in-use secondary antibody.

2.4 Immunofluorescence

2.4.1 Block and antibody dilutions.

Block

Phosphate Buffered Saline		Life-Technologies, Paisley, UK
Bovine Serum Albumin	3% w/v	Sigma-Aldrich, Dorset, UK
Normal Goat Serum	0.1% v/v	Dako, Stockport, UK
Internal markers only, Triton-X	0.0025-50% v/v	Sigma-Aldrich, Dorset, UK
Internal markers only, Tween20	0.05% v/v	Sigma-Aldrich, Dorset, UK

Antibody Dilutions

Antigen	**Supplier**	**Dilution**
POU5F1	Santa Cruz	1:100
NANOG	Abcam	1:500
SOX2	Abcam	1:500
PAX6	Developmental Studies Hybridoma Bank	1:10
NESTIN	Millipore	1:500
HIF1A	Abcam	1:100
HIF2A	Novus Biologicals	1:100
PHD2	Novis Biologicals	1:100
MAP2	Sigma	1:500

βIII-Tubulin	Abcam	1:200
Synaptophysin	Abcam	1:200
PSD95	Abcam	1:100
Anti-mouse IgG, AF-594	Life Technologies	1:400
Anti-rabbit IgG, AF-594	Life Technologies	1:400
Anti-mouse IgG, AF-488	Life Technologies	1:400
Anti-rabbit IgG, AF-488	Life Technologies	1:400

2.4.2 Immunofluorescence staining.

Immunofluorescence was used to label cells with a primary antibody specific for a particular marker and a complementary secondary antibody with a fluorescent tag. Binding of the secondary antibody to the primary allowed visualisation of the target protein's expression levels and cellular location.

For staining to take place, cells were seeded onto glass coverslips pre-coated with Matrigel for one hour at 37°C. Once at the point of analysis, coverslips were washed in PBS and fixed with 4% Paraformaldehyde for 10-15 minutes at 4°C. After removal of PFA and 3 x PBS washes, cells being stained for intracellular markers underwent cell membrane permeabilisation for antibody access with either 100% ethanol for 10 minutes (POU5F1, NANOG, SOX2 staining), 0.05-0.25% Triton-X in PBS for 10 minutes (MAP2, βIII-Tubulin, HIF1A, HIF2A, PAX6 and Nestin) or 0.05% Tween (Synaptophysin and PSD95). Coverslips were incubated in block solution for one hour at room temperature to reduce non-specific antibody binding. Block solution was used with 0.05% Tween (Synaptophysin and PSD95) or 0.05% Triton–X (all remaining intracellular antigens) for intracellular markers with no permeabilising agent required for surface markers. After blocking, primary antibodies were diluted in blocking solution and added to coverslips for overnight incubation at 4°C as listed in *Table 2.3*. 3 x PBS washes were performed before adding the secondary antibody diluted at 1:400 in block solution for 2 hours at room temperature, in the dark. Anti-rabbit or anti-mouse IgG subtypes of AlexaFluor 594 or 488 secondary antibodies were used for fluorescent labelling.

The nuclear stain Hoechst (Thermo Scientific, Massachusetts, USA) was incubated for 10 minutes at room temperature at a concentration of 1 ng/ml in PBS. Coverslips were then inverted and mounted onto a glass slide with Fluoromount-G mounting medium (Cambridge, Cambridge Bioscience, UK).

Where cell counts have been performed, the majority of each coverslip was visualized at 10x or 20x magnification with an Olympus BX61 fluorescent microscope. The CellProfiler cell counting software quantified the number of cells positive for red antibody labelling and for blue nuclear staining, allowing a percentage of the cell population positive for a specific marker to be calculated.

2.5 Western Blots

2.5.1 Buffers, gel formulation and antibody dilutions.

Lysis Buffer		
RIPA Buffer	10 ml	Sigma-Aldrich, Dorset, UK
PhosSTOP Tablet	1 x	Roche, Sussex, UK
Complete MINI	1 x	Roche, Sussex, UK
10 x Running Buffer		
Tris Base	0.25 M	Sigma-Aldrich, Dorset, UK
Glycine	1.92 M	Sigma-Aldrich, Dorset, UK
SDS	0.1% w/v	Sigma-Aldrich, Dorset, UK
dH_2O	1L final volume	
1 x Transfer Buffer		
Tris Base	0.25 M	Sigma-Aldrich, Dorset, UK
Glycine	1.92 M	Sigma-Aldrich, Dorset, UK
Methanol	20% v/v	Sigma-Aldrich, Dorset, UK

dH_2O	1L final volume	

1 x Stripping Buffer

1M Tris-HCl pH7.5	6.25% v/v	Sigma-Aldrich, Dorset, UK
SDS	2% w/v	Sigma-Aldrich, Dorset, UK
dH_2O		
β-mercaptoethanol	0.77%	Sigma-Aldrich, Dorset, UK
(addition immediately prior to use)		

Ponceau S Stain

Ponceau S	0.1% w/v	Sigma-Aldrich, Dorset, UK
Acetic acid	5% v/v	Fisher Scientific, Loughborough, UK
dH_2O		

10 x Tris Buffered Saline

Tris Base	10 mM	Sigma-Aldrich, Dorset, UK
NaCl	150 mM	Fisher Scientific, Loughborough, UK
dH_2O	1L final volume pH	
0.05% Tween for TBS/Tween (TBS/T)		Sigma-Aldrich, Dorset, UK

7.5% Running Gel

30% Acrylamide	2.5 ml	Biorad, Hertfordshire, UK
dH_2O	4.8 ml	
1.5M Tris pH8.8	2.5 ml	Sigma-Aldrich, Dorset, UK
10% SDS	0.1 ml	Sigma-Aldrich, Dorset, UK
10% APS	100 µl	Fisons, New Delhi, India
TEMED	20 µl	Sigma-Aldrich, Dorset, UK

Stacking Gel

30% Acrylamide	1.67 ml	Biorad, Hertfordshire, UK
dH_2O	5.83 ml	
0.5M Tris pH6.6	2.5 ml	Sigma-Aldrich, Dorset, UK
10% SDS	0.1 ml	Sigma-Aldrich, Dorset, UK
10% APS	50 μl	Fisons, New Delhi, India
TEMED	10 μl	Sigma-Aldrich, Dorset, UK

Antibody Dilutions

Antigen	**Supplier**	**Dilution**	**Block**
P-SMAD1/5/8	Cell Signalling	1/1000	5% BSA, 1% Ovalbumin in TBS/T
SMAD1/5/8	Santa Cruz	1/2000	5% Milk in TBS/T
P-SMAD2/3	Cell Signalling	1/1000	5% BSA, 1% Ovalbumin in TBS/T
SMAD2/3	Cell Signalling	1/2000	5% BSA, 1% Ovalbumin in TBS/T
HIF1A	BD Bioscience	1/1000	5% Milk in TBS/T
HIF2A	Novus Biologicals	1/1000	5% Milk in TBS/T
β-Actin	Sigma-Aldrich	1/10,000	1% Milk in TBS/T
Anti-Rabbit IgG HRP Secondary	GE Life Sciences	1/20,000	TBS/T
Anti-Mouse IgG HRP Secondary	GE Life Sciences	1/20,000	TBS/T

2.5.2 Protein extraction.

Western blots allow detection and quantification of specific proteins in a given cell sample. To examine the relative concentrations of specific proteins in a cell population, protein cell lysates were obtained, separated according to size using

sodium dodecyl sulphate polyacrylamide gel electrophoresis (SDS-PAGE) and subsequently transferred onto blotting paper and probed with specific antibodies.

Initially, cell populations underwent lysis and protein extraction to ensure a pure lysate containing only proteins. Growth medium was removed and cells were washed once with PBS. TrypLE was added and incubated at 37°C for five minutes to lift off adherent cells, which were then collected with fresh medium and spun at 230 x g for 3 minutes to obtain a cell pellet. After an additional PBS wash to remove remnants of growth medium, the pellet was resuspended in lysis buffer. The detergents included in the buffer allowed for efficient lysis of cells and solubilisation of proteins by disrupting protein-protein interactions so as to allow movement of individual proteins during electrophoresis. Phosphatase and protease inhibitors were included in the buffer to prevent digestion from naturally occurring enzymes in the cell population. Snap freezing at -80°C at this stage aided lysis and samples could be stored for future protein extractions. Due to the high sensitivity to oxygen and the labile nature of the HIF1A and 2A proteins, lysates required to assess concentrations of these proteins could not be obtained in this manner. Alternatively, medium was removed from adherent cell cultures which were then washed with PBS. After removing PBS, lysis buffer was added straight to the cells and a scraper used to aid lysate collection. At this point, they were then snap frozen at -80°C.

All protein preparation from this point onwards was carried out at <4°C to prevent protein degradation. To separate the cellular proteins from the remaining cellular components, each sample underwent centrifugation at >10,000 x g for 20 minutes in a temperature controlled centrifuge at 4°C. The supernatant (now containing purely protein) was removed, aliquoted and stored at -20°C until further use. Samples obtained to assess HIF protein extraction were run on a gel immediately after protein extraction to prevent degradation.

Each sample was assessed for total protein concentration using the Pierce BCA Protein Assay Kit (Thermo Scientific, Massachusetts, USA), based on the traditional Bradford assay. Bovine Serum Albumin (BSA) was used as a standard to create a standard curve of protein concentrations. This standard curve was defined using

y=mx+c (whereby y=Absorbance, m=gradient of the line, c=the intercept and x=protein concentration) and subsequently re-arranged as x=(y-c)/m to enable calculation of total protein in unknown samples *(Figure 2.4, A)*. 20-25 μg of each protein lysate was loaded in combination with a Sample Loading Buffer (Sigma-Aldrich, Dorset, UK) and treated at 95°C for 5 minutes before loading onto the Gel. Sodium dodecyl sulphate and β-mercaptoethanol (both Sigma-Aldrich, Dorset, UK) in the sample loading buffer denatured the proteins and imparted a negative charge to each protein (essential for electrophoresis). Glycerol and Bromophenol Blue also aided loading of the wells by increasing the sample density and sample visibility respectively.

i)

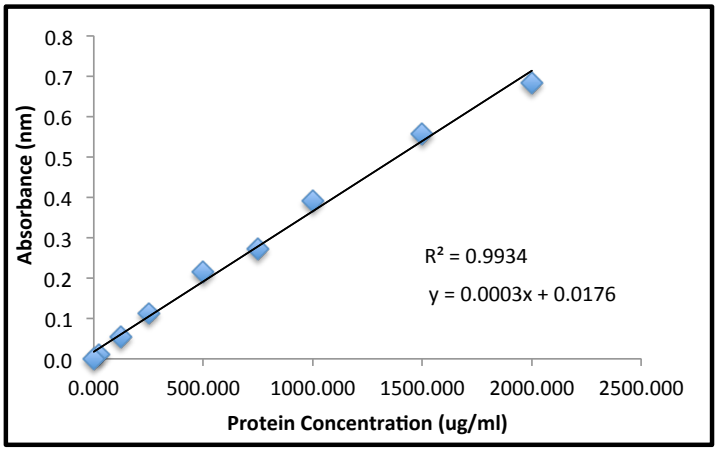

ii)

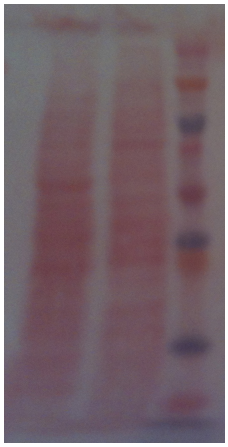

Figure 2.4 Analysis of protein concentration and protein transfer. *(i) Standard curve of known protein concentrations were formed and the equation of the curve determined from y=mx+c, where y defines absorbance and x defines protein concentration. ii) Ponceau S staining of nitrocellulose membrane after protein transfer. Right to left, protein ladder shows size of proteins, red protein ladders confirm protein has transferred onto membrane successfully.*

2.5.3 SDS-PAGE and transfer.

Protein electrophoresis was carried out on a 7.5% Acrylamide gel with standard stacking gel. Gel plates were scrupulously cleaned with water and ethanol prior to use. Once cast, gels were placed into the electrophoresis tank and central reservation filled with running buffer in preparation for protein loading. A protein marker ladder (Novex Sharp prestained protein standard, Life-Technologies,

Paisley, UK) was run alongside samples for easy visualisation and comparison of protein size across samples. Each gel was run at 120 V with running time dependent on the size of the protein to be probed. The negatively charged proteins migrate through the acrylamide gel towards the positively charged electrode and as the smaller proteins encounter less resistance and move more quickly, separation based on protein size occurs.

Separated proteins were then electro-transferred onto a Nitrocellulose membrane (GE Lifesciences, Buckinghamshire, UK) using the wet transfer method. Briefly, the nitrocellulose membrane was placed between the gel and positive electrode, held together tightly with layers of filter paper and sponges. Keeping the size-based arrangement formed during SDS-PAGE, proteins move across to the membrane and bind in a stable manner. This was performed at 120V for 70 minutes whilst using an ice-pack to prevent heat accumulation.

2.5.4 Antibody probing.

Following transfer, the membrane was stained with Ponceau S to confirm protein transfer was successful *(Figure 2.4ii)* and blocked for 1 hour at room temperature to prevent non-specific antibody binding. Block consisted of 5% non-fat milk in TBS + 0.05% Tween (TBS/T, Sigma-Aldrich, Dorset, UK) or when probing for specific anti-phosho antibodies, 1% Ovalbumin (Sigma-Aldrich, Dorset, UK) + 5% BSA in TBS/Tween. Membranes were incubated overnight at 4°C with primary antibodies diluted in block solution at 1/5 in TBS/T. Appropriate secondary Horseradish Peroxidase (HRP)-conjugated antibodies (GE Life Sciences) were diluted at 1:20,000 in TBS/T and incubated with the membrane for 1 hour at room temperature. After both primary and secondary antibody probing, the membrane underwent 4 x 3 minute TBS/T washes. An Enhanced Chemiluminescent substrate containing luminol (which emits light in combination with HRP) was used to detect specific bands of protein. After addition of ECL, bands were detected in one of two ways; the membrane was either exposed to X-Ray film, wherein the specifically probed protein bands gave out light and formed darkened bands on light sensitive

x-ray film, or for HIF1A and HIF2A westerns, the bands were visualized using a ChemiDoc XRS+ imaging system (Bio-Rad, Hertfordshire, UK).

When probing for multiple antigens on the same blot (such as sequential staining for phosphorylated SMAD1/5/8 and non-phosphorylated SMAD1/5/8), the blot was stripped after initial band exposure. Following removal of chemiluminescent substrate through 3 x TBS washes, blots were incubated at 55°C in stripping buffer for 20 minutes. Blots were then washed thoroughly with fresh TBS to ensure complete removal of β-mercaptoethanol. At this stage, the blot was then ready for sequential blocking and antibody probing as previously detailed. In specific circumstances, protein band densitometry was performed using ImageJ software.

2.6 Polymerase Chain Reaction

To compare mRNA levels of specific genes, complementary DNA (cDNA) was generated from RNA and quantitative polymerase chain reaction (QPCR) amplified mRNA specific sequences to compare their expression levels between samples. This technique relies on the basic principles of DNA amplification whereby specific oligomers (or primers) specify genomic sequences for amplification. Use of a fluorescent dye allowed quantification of the amount of starting product.

2.6.1 RNA extraction and reverse transcriptase PCR.

Initially, cells were removed from medium and washed with PBS before extracting RNA using the RNeasy Mini Kit (Qiagen, Manchester, UK) as per manufacturers instructions. This process included removal of genomic DNA before RNA was converted to complementary DNA (cDNA) using the reverse transcriptase enzyme SuperScript II (Life-Technologies, Paisley, UK). The conversion was performed using a Techne TC412 Thermal Cycler as follows: 1 x 25°C 10 minutes, 1 x 42°C 50 minutes, 1 x 70°C 15 minutes. For qPCR, cDNA was used at a final concentration of 0.5 ng per reaction with 0.5 mM dNTPs.

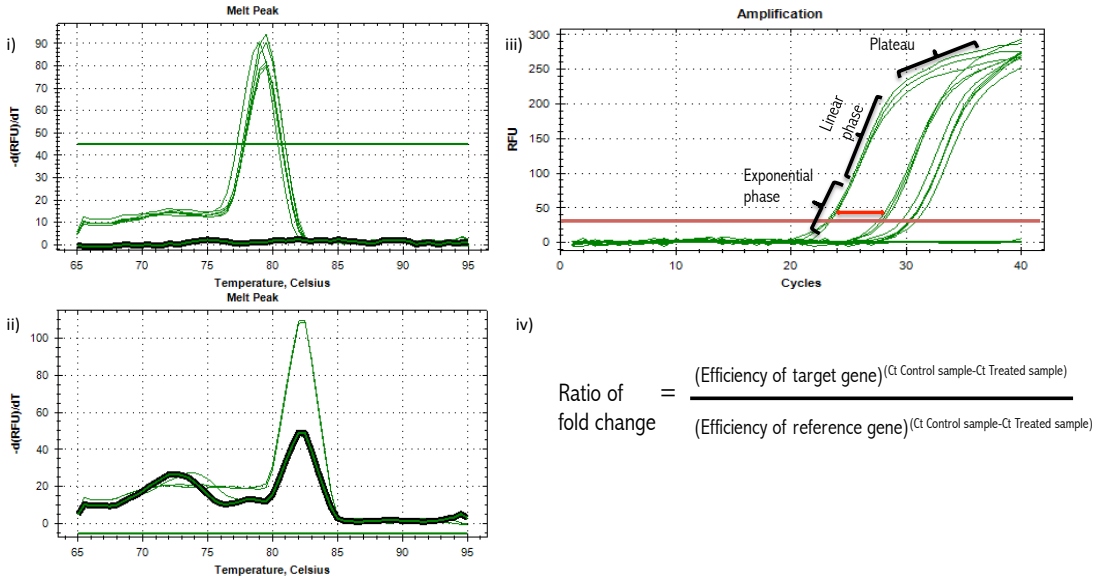

Figure 2.5 QPCR is quality controlled and quantified using a fluorescent marker to represent double stranded DNA. *The melt curve shows the temperature at which the amplicon is denatured into single strands, graphed as differential (relative fluorescence unit) / differential (temperature). Primers which were shown only to form a single product (i) had only one peak when the PCR was performed with template (pale green lines) and no product at all when performed without template added (dark green lines). Poorly designed primer sets (ii) amplified multiple sequences due to primer-primer binding and / or from non-intentional complementary sequences in the template. Any primers found to be performing in this manner were not used for analysis c) Quantification graph plots RFU vs. the number of cycles. The Ct value was measured as the number of cycles taken to reach exponential amplification, indicated by the red line. (iii) The fold change is then calculated by the difference between Ct in the untreated control sample and the treated test sample, indicated by the red arrow. (iv) The Pfaffl method of semi-quantitatively calculating fold change.*

2.6.2 Quantitative PCR.

To quantify concentrations of specific mRNA sequences, a fluorescent dye was used (Sybr Green, Thermo Scientific, Massachusetts, USA), which only fluoresced when intercalated between bases of double stranded DNA. As each cycle of amplification increased levels of the target amplicon, fluorescent signal increased accordingly. This was plotted as Relative Fluorescence Units (RFU) on the y-axis vs. the number of cycles on the x-axis, forming a typical growth response plot with exponential, linear and plateau phases. *(Figure 2.5, iii)* The number of cycles

required to reach the exponential stage of sequence amplification (where theoretically, each cycle resulted in a doubling of product) was defined as the Cycle Threshold value (CT). CT was calculated here using regression analysis. A lower CT reflected higher amounts of the target mRNA sequence in a sample, as fewer cycles were required to reach exponential amplification.

QPCR was run in cycles of 1 x 95^{o}C 15 mins, 39 x [95^{o}C for 30 seconds (denaturation of strands), 60^{o}C for 30 secs (primer annealing), 72^{o}C for 30 secs (optimal for polymerase activity)], 1 x 65°C 0.05 secs, 1 x 95°C 0.5 secs (melting curve). The melting curve was used to ensure only product was present after a full QPCR protocol. Due to the sharp increase in temperature to 95°C from 65°C, dissociation of double stranded DNA resulted in a decrease of fluorescent intensity. When plotted as differential fluorescence / differential time, peak dissociation can be pinpointed, allowing melting point comparison of multiple samples (*Figure 2.5i, ii*).

Quantitation of the relative fold-change in transcript levels comparative to a control sample was calculated using the Pfaffl method (Pfaffl 2001), *Figure 2.5iv*. This was an adapted version of the Delta-Delta-Ct method which additionally took into account the efficiency of the primers in use but still calculated the fold-change in mRNA levels relative to a control sample (for example, an untreated sample compared to a treated sample) and a reference gene which was stable throughout experiments, to account for unavoidable small variances in the starting cDNA concentration. The reference gene TATA box binding like protein 2 (TATA) was used here. Primer efficiencies were calculated through plotting CT values across a standard curve of template concentrations. Computation of the 'r^{2}' value indicated the quality of fit of the curve against the equation of the curve, i.e. the closer to 1, the more likely the primers were to duplicate product at all tested template concentrations. Primers were classed as acceptable for use if r^{2}>0.95. (*Figure 2.6*) All primer sets were also checked for target gene specificity using NCBI-Primer Blast and accepted if they had no unintended gene targets. See *Table 2.1* for primer sequences. As gene transcription was quantified relative to a control sample, a fold change of 1.0 indicates no change compared to control, fold

change of > 1.0 indicates an increase in transcription compared to control and <1.0 indicates decrease in transcription compared to control.

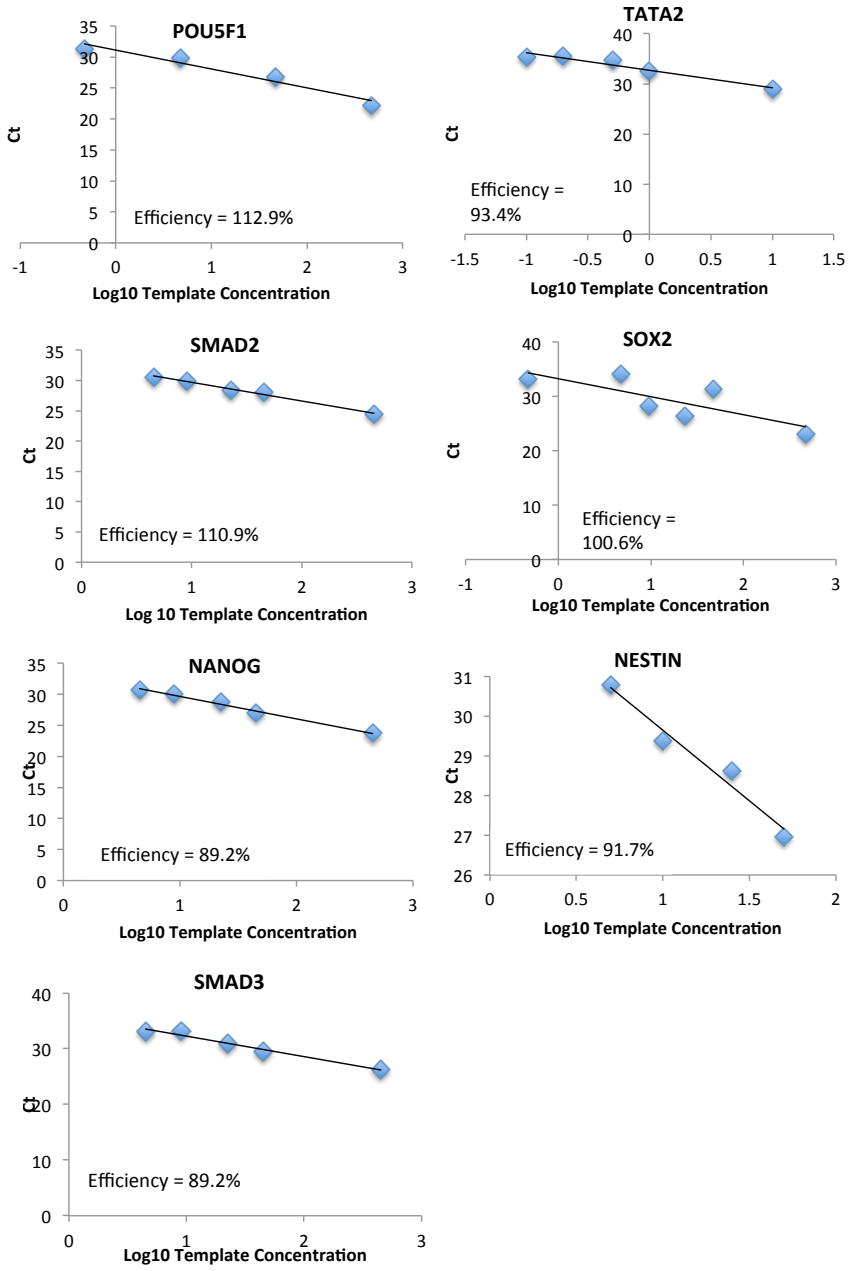

Figure 2.6 All primers showed acceptable efficiency of template amplification. *Efficiency of primer pairs was assessed using a standard curve of template dilutions. Each primer pair was assessed and accepted if efficiency of amplification exceeded* R^2*=0.95.*

Gene	Accession number	Forward and Reverse Primers
SOX2	NM_003106	F 5' - TAC AGC ATG TCC TAC TCG CAG R 5' - GAG GAA GAG GTA ACC ACA GGG
NANOG	NM_024865	F 5' - ACG CAG AAG GCC TCA GCA CCT A R 5' - CCC AGT CGG GTT CAC CAG GCA
POU5F1	NM_001173531.1	F 5' – CTC ACC CTG GGG GTT CTA TT R 5' – CTC CAG GTT GCC TCT CAC TC
TATA	NM_003194	F 5' - TGC AGT GAC CCA GGG TGC CAT R 5' - TGT GGG GTC AGT CCA GTG CCA
B-ACTIN	NM_001101	F 5' - TAG GCA CCA GGG TGT GAT GG R 5' - CAT GGC TGG GGT GTT GAA GG
SMAD2	NM_001135937	F 5' – GGC AAT TGA AAA CTG CGA AT R 5' – GTC GGG GCA CTA ATA CTG GA
SMAD3	NM_005902	F 5' – CCC TGG CTA CCT GAG TGA AG R 5' –GCT CGC AGT AGG TAA CTG GC
NESTIN	NM_006617	F 5' – GTT CCA GCT GGC TGT GGA GGC R 5' – GCT GCT GCC GAC CTT CCA GG

Table 2.1. Forward and reverse primer sequences.

2.7 Electrophysiology

2.7.1 Electrophysiological Solutions

Extracellular Solution

NaCl	135mM	Fisher Sci, S/3160/53
KCl	5mM	Sigma-Aldrich, P9333
HEPES	5mM	Sigma-Aldrich, H3375
Glucose	10mM	Sigma-Aldrich, G8270

$MgCl_2$	1.2mM	Sigma-Aldrich, M2393
$CaCl_2$	1.25mM	Fluka, 21114
pH to 7.4 using NaOH		

Intracellular Solution

NaCl	10mM	Fisher Sci, S/3160/53
KCl	117mM	Sigma-Aldrich, P9333
HEPES	11mM	Sigma-Aldrich, H3375
EGTA	11mM	Sigma-Aldrich, E4378
Na.ATP	2mM	Sigma-Aldrich, A7699
$MgCl_2$	2mM	Sigma-Aldrich, M2393
$CaCl_2$	1mM	Fluka, 21114
pH to .2 using KOH		

Additional Reagents

Tetrodotoxin (TTX)	1μm	Tocris, 1078.
Nifedipine	1μm	Tocris, 1075.

2.7.2 Whole cell patch clamp.

Whole cell patch clamping was performed on neurons at weeks 1, 2, 3 and 4 post-plate down (at day 16 neural rosette stage). All recordings were carried out at room temperature using an Axon Axopatch 200A amplifier and Digidata 13320A/D interface (both from Molecular Devices, Sunnyvale, California, USA), on an anti-vibration table, inside a Faraday cage to reduce external noise interference. Neurons grown on coverslips (see General Methods) were placed onto the stage of an inverted Olympus CK40 microscope under constant perfusion with Extracellular Solution (ECS), hereafter referred to as the 'bath'. Additional solutions (such as Nifedipine and TTX) were applied using a Rapid Solution

Changer (RSC, RSC-200, Bio-Logic, France) in a controlled and automated manner. All protocols were applied using pClamp 10.0 software.

Glass micropipettes were made from borosilicate glass tubing, pulled on a 2-stage puller (PP-81, Narishige, Japan) to form patch pipettes with a resistance of 2-3 MΩ when filled with intracellular solution. Pipettes were then inserted over a silver/silver Cl^- cathode, fixed to a CV 201AU headstage and positioned over the neuron cell body using a micromanipulator. An additional silver/silver Cl^- electrode connected to the headstage acted as a reference bath electrode. Tubing connecting the headstage and a syringe allowed control over patch pipette pressure for formation of the seal.

Seal formation was achieved in voltage-clamp configuration of the path-clamp technique. Upon insertion of the pipette into the bath, slight positive pressure prevented mixing of ICS in the pipette and ECS in the bath, and ensured bubbles and/or particles from the bath did not accumulate on the pipette tip, potentially hindering seal formation. Any pipette capacitance currents were compensated for with capacitance compensation in MultiClamp Commander software to improve the chances of sealing and maintaining a whole-cell patch. A seal test protocol then continuously measured the resistance between the two electrodes in the pipette and bath (10mV step for 10ms, at 50Hz). Pipette voltage offset was set to zero using MultipClamp Commander software. At this point, the pipette (using the micromanipulator) was brought into contact with the neuron cell body membrane. Contact was confirmed by a noticeable decrease in current amplitude due to an increase in resistance as the cell membrane covered the pipette tip. A switch from applied positive pressure to slight negative pressure caused formation of a seal between the pipette and the cell body, and the area covered by the pipette was held at -60mV to prevent cell depolarisation upon formation of whole-cell configuration. Together, this ensured a seal with resistance >1GΩ (cell attached configuration), seals of less than this were discarded and the protocol started again with a fresh pipette.

Whole-cell patch clamp was then initiated. A light increase in the pipettes negative pressure on the cell membrane caused large whole cell capacitance

currents to appear in the seal test trace, confirming whole-cell access. Capacitance is a measure of the cells ability to store charge and hence is recognised as indicative of cell membrane area. The MultiClamp Commander software measured and compensated for this using a 10mV, 10ms voltage step. Series resistance was compensated or at 80%. Junction potential was not compensated for as solutions remained constant across all experiments. Dr. Julia Griffiths performed the majority of electrophysiological recordings, with the remainder carried out by Dr. Christian Schnell. Voltage- or current-clamp protocols were applied using pClamp 10.0 software (see below). All data analysis was performed by myself using pClamp 10.0 and Microsoft Excel software. (See appendix 7.2 for summary of data with n numbers.)

2.7.3 Current Clamp Protocols

Continuous current clamp recording with zero current injection.

Current clamp controlled membrane current and measured the resulting changes in membrane potential. Measurement of resting membrane potential (V_m) and observations of spontaneous action potentials (sAP) were performed at zero current injection (I=0) during a continuous current clamp recording for a minimum of 60 seconds. Spontaneous action potentials were classed as depolarising spikes overshooting 0 mV with subsequent return to baseline, sAP trains were classed as multiple action potentials in quick succession. V_m was calculated as a mean over the last 60 seconds of the voltage recording. In cells displaying spontaneous trains of action potentials, the Vm was assessed, where possible, from a section of the recording which contained no electrical activity. If necessary, it was estimated from the trace baseline. Abortive AP's (i.e. depolarising spikes which did not overshoot 0 mV) were not included in the analysis.

Current Step Protocol.

Current step protocols were used to induce action potentials by stepping the Vm from -70 mV to threshold. Thus, current injection was employed to

hyperpolarise the membrane potential to -70 mV before the application of depolarising current steps (from 0 to +180 mV in 10 mV increments for 1s per sweep, to a total of 19 sweeps. Input Resistance (R_{in}) was calculated as the slope of voltage vs. current relationship during over the last 50ms of the first 5 sweeps, ensuring that no AP activity was induced in this period. The relationship between current and voltage (an I-V graph) was calculated using y=mx+b, whereby m=R_{in} in Ω. For analysis of induced AP properties, the first sweep with a successful AP / AP train was used. ClampFit software was employed to determine overshoot and after-hyperpolarisation. After-hyperpolarisation data were then used as the baseline value for subsequent calculation of AP height (Spike Height, mV), the AP width at half the spike height (Half-Width, ms), and the rates of depolarisation and hyperpolarisation (both V/secs). The AP activation threshold was calculated using a differential of the voltage with respect to time recording, between the chosen sweep and the last current sweep in the protocol, to calculate the highest rate of change in the rate of change of the rate of change of voltage, recognised here as threshold value. (*Figure 5.1*)

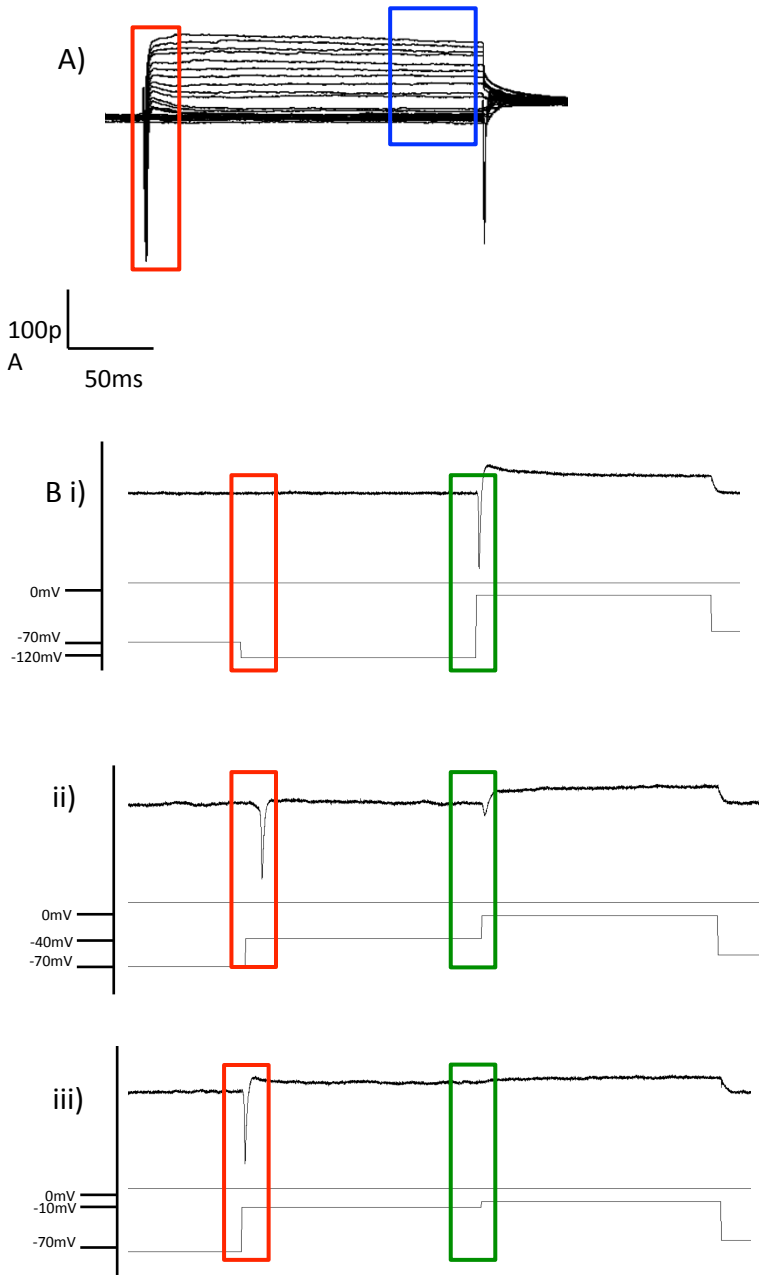

Figure 2.7 Representative traces of voltage clamp steps. *(A) Maximal induced Na^+ currents were calculated from activation of voltage-gated Na^+ currents which occurred in the initial stage of membrane depolarisation (outlined in red). Mean K^+ channel currents and maximal induced K^+ currents were calculated from the last 50ms of each sweep (outlined in blue). (B) Hyperpolarising voltage clamp step from -70 mV to -120 mV (i) shows no activation of voltage-gated Na^+ channels seen as inward current (outlined in red) but subsequent step from -120 mV to 0 mV does (green). Depolarising step from -70 mV to -40 mV (ii) induces activation, subsequent step from -40 mV to 0 mV shows smaller activation as depolarised holding potential is determining channel conductance. Larger depolarising step from -70 mV to -10 mV (iii) induces larger inward Na^+ current, subsequent step to 0 mV shows no additional current, indicating inactivation of voltage-gated Na^+ channels.*

2.7.4 Voltage Clamp Protocols

Voltage Clamp was used to manipulate membrane potential and measure resulting current flow across it. The voltage dependent activation and inactivation profiles for Na^+ and K^+ currents were measured using a voltage step protocol which depolarised the cell membrane. Thus, the cell was voltage-clamped to -70 mV and stepped from -120 mV to 50 mV in 5 mV increments, over 35 sweeps. Each sweep lasted 200 ms and then returned to 0 mV at the end of each sweep for an additional 200 ms. Activation of voltage-activated Na^+ channels (*figure 2.6A*) was seen as an initial inward current (downward peak) due to Na^+ influx. Induced K^+ channel currents were seen as constant current across the initial 200 ms sweep (*figure 2.6A).* The maximal induced Na^+ and K^+ currents (INa^+Max and IK^+Max respectively) were measured at each sweep and normalised to capacitance (pA/pF).

Activation and inactivation of voltage-gated Na^+ channels was mapped across progressively depolarising voltage steps. (*Figure 2.6B*) Na^+ conductance upon channel activation was mapped during initial membrane depolarisation steps (between -120 mV to 0 mV). Depolarisation of membrane potential to 0 mV at the end of each sweep pinpointed the voltage required for Na^+ channel inactivation. Na^+ conductance during activation was normalised to cell size using capacitance values and corrected for Na^+ driving force (66.68). Induced currents were then corrected to the maximal current size between -120 mV to 0 mV, giving normalised conductance G/Gmax. Na^+ conductance during channel inactivation underwent the same analysis but was not normalised for capacitance. The average induced K^+ current was calculated from the last 50 ms of the initial 200 ms of each sweep and normalised for cell capacitance.

2.8 Statistics

All statistics were performed using PASW Statistics v20.0. Initial analyses sought to confirm a normal distribution within data sets using the Kolmogorov-Smirnov and Shapiro-Wilk tests of normality. Data sets were considered normally

distributed if P>0.05. For data sets with three or more counterparts (*e.g.* analysis of short term proliferation with three different culture conditions of 20%, 3%-Light and 3%-Dark) one-way ANOVAs were used to assess statistical differences between and within collective means. This was reliant on equal variance across data sets, accepted as such if p>0.05. If p<0.05 (and hence unacceptable) then means were compared using the *unequal variance t-test*, the Welch Test.

When variance was acceptable, the Post-Hoc Tukeys test assessed which sub-populations had statistically significant differences between them. Data for One-Way ANOVAs was displayed as (degrees of freedom between groups, within groups)=F-value, p=p value.

Independent T-tests were used to compare 2 distinct sub-populations (*e.g.* the percentage of cells expressing SSEA4 at 20% O_2 and at 3% O_2). Significance was taken dependent on equal variances assumed / not assumed, assessed using the Levene's Test. Data for Independent T-Tests was displayed as (degrees of freedom)=t-value, p=p-value.

For all tests performed to compare the means of sub-populations, significance was set at p<0.05. Data is shown as mean ± standard error of the mean. Unless otherwise mentioned, n=3 biological replicates.

2.9 Materials

Table 2.2 General Consumables.

Product	Catalogue no.	Supplier
60mm Nunc dish	10789241	Fisher Scientific, Loughborough, UK
2 x Sample Loading Buffer	S3401	Sigma-Aldrich, Dorset, UK
24 well Nunc plate	144530	Fisher Scientific, Loughborough, UK
90mm Sterilin dish	13172211	Fisher Scientific, Loughborough, UK
Acrylamide	161-0158	Bio-Rad, Hertfordshire, UK
Advanced DMEM/F12	12634-028	Life-Technologies, Paisley, UK
Albumin from chick egg white	A5378	Sigma-Aldrich, Dorset, UK
AnnexinV-FITC Staining Kit	AB14085	Abcam, Cambridge, UK
Ascorbic Acid	A4544,	Sigma-Aldrich, Dorset, UK
b-Mercaptoethanol	M3148	Sigma-Aldrich, Dorset, UK
BDNF	130-096-286	Milteny, Surrey, UK
Bovine Serum Albumin	A9418	Sigma-Aldrich, Dorset, UK
CaCl2	499609	Sigma-Aldrich, Dorset, UK
CaCl2	21114	Sigma-Aldrich, Dorset, UK
Cell scraper	734-1527	VWR, Leicestershire, UK
CF-1 Mouse Embryonic Fibroblast, irradiated.	07GSC6001G	VH-Bio, Gateshead, UK
CHIR99021	4423	Tocris, Abingdon, UK
Complete MINI, protease inhibitor	11836153001	Roche, Sussex, UK
DAPT	2634	Tocris, Abingdon, UK
Dispase	7923	Stem Cell Tech, Grenoble, France
DMEM-Glutamax	61695	Life-Technologies, Paisley, UK
EGTA	E4378	Sigma-Aldrich, Dorset, UK
Ethanol	32221	Sigma-Aldrich, Dorset, UK
Fetal Bovine Serum	10106169	Life-Technologies, Paisley, UK
Fibroblast Growth Factor-2 (FGF2)	100-18B	Peprotech, London, UK
Fluoromount-G mounting medium	0100-01	Cambridge Bioscience, Cambridge, UK
Forskolin	1099	Tocris, Abingdon, UK
GABA	344	Tocris, Abingdon, UK
Gelatin	ES-006-B	Millipore, Herfordshire, UK
Glass Coverslips	6310149	Thermo Scientific, MA, USA
Glucose	G8270	Sigma-Aldrich, Dorset, UK
Glycine	G8790	Sigma-Aldrich, Dorset, UK
HEPES	H3375	Sigma-Aldrich, Dorset, UK
Hoechst33342	62249	Thermo Scientific, MA, USA

Insulin	407709	Millipore, Herfordshire, UK
KCl	P9333	Sigma-Aldrich, Dorset, UK
Knockout Serum Replacement (KSR)	10828-028	Life-Technologies, Paisley, UK
Knockout-DMEM	10829-018	Life-Technologies, Paisley, UK
L-Glutamine	25030-024	Life-Technologies, Paisley, UK
LDN193289	130-096-226	Milteny, Surrey, UK
Lipid Concentrate	25030-031	Life-Technologies, Paisley, UK
Matrigel	734-1440	Sigma-Aldrich, Dorset, UK
Methanol	32213	Sigma-Aldrich, Dorset, UK
MgCl2	M2393	Sigma-Aldrich, Dorset, UK
Na.ATP	A7699	Sigma-Aldrich, Dorset, UK
NaCl	S/3160/53	Fisher Scientific, Loughborough, UK
NaCl	S/3160/53	Fisher Scientific, Loughborough, UK
Neurobasal A	10888-022	Life-Technologies, Paisley, UK
Neurobrew21 with Vitamin A	130-093-566	Life-Technologies, Paisley, UK
Neurobrew21 without Vitamin A	130-097-263	Milteny, Surrey, UK
Nifedipine	1075	Tocris, Abingdon, UK
Nitric Acid	N/2250/PB15	Fisher Scientific, Loughborough, UK
Nitrocellulose membrane	RPN3032D	GE Lifesciences, Buckinghamshire, UK
Non-essential Amino Acids	11140-035	Life-Technologies, Paisley, UK
Normal Goat Serum	X0907	Dako, Stockport, UK
Novex Sharp Prestained Protein Ladder	LC5800	Life-Technologies, Paisley, UK
Opti-MEM medium	31985-062	Life-Technologies, Paisley, UK
Paraformaldehyde	P6148	Sigma-Aldrich, Dorset, UK
PD0332991	4786	Tocris, Abingdon, UK
Penicillin-Streptomycin	15070	Life-Technologies, Paisley, UK
Phosphate Buffered Saline (PBS)	10010-015	Life-Technologies, Paisley, UK
PhosSTOP phosphatase inhibitor	490685001	Roche, Sussex, UK
Pierce BCA Protein Assay	23227	Thermo Scientific, MA, USA
Poly-D-Lysine	P5899	Sigma-Aldrich, Dorset, UK
Ponceau S	P3504	Sigma-Aldrich, Dorset, UK
Propidium Iodide	70335	Sigma-Aldrich, Dorset, UK
RIPA Buffer	R0278	Sigma-Aldrich, Dorset, UK
RNAi MAX	13778-150	Life-Technologies, Paisley, UK
RNAseA	R4642	Sigma-Aldrich, Dorset, UK
RNeasy Mini Kit	74104	Qiagen, Manchester, UK
Saponin	S4521	Sigma-Aldrich, Dorset, UK
SB431542	AB120163	Abcam, Cambridge, UK
siGENOME EPAS1 siRNA	M-004814-01-0005	Thermo Scientific, MA, USA
siGENOME Non-Targeting siRNA #2	D-001210-02-05	Thermo Scientific, MA, USA
Sodium Azide	S8032	Sigma-Aldrich, Dorset, UK

Sodium Dodecyl Sulphate	L3771	Sigma-Aldrich, Dorset, UK
Staurosporine	S4400	Sigma-Aldrich, Dorset, UK
SuperscriptII	18064	Life-Technologies, Paisley, UK
Supersignal West Pico ECL substrate	34077	Thermo Scientific, MA, USA
Sybr Green	F400S	Thermo Scientific, MA, USA
Tetrodotoxin (TTX)	1078	Tocris, Abingdon, UK
Transferrin	T8158	Sigma-Aldrich, Dorset, UK
Tris Base	93362	Sigma-Aldrich, Dorset, UK
Triton-X	T8787	Sigma-Aldrich, Dorset, UK
TrypLE	12604013	Life-Technologies, Paisley, UK
Tween 20	P1379	Sigma-Aldrich, Dorset, UK
Y27632	AB120129	Abcam, Cambridge, UK

Table 2.3 Antibodies.

Target Protein	**Catalogue no.**	**Supplier**
AF-488, anti-mouse IgG	A1101	Life-Technologies, Paisley, UK
AF-488, anti-rabbit IgG	A11008	Life-Technologies, Paisley, UK
AF-594 anti-rabbit IgG	A11012	Life-Technologies, Paisley, UK
AF-594, anti-mouse IgG	A11005	Life-Technologies, Paisley, UK
B-Actin	A2228	Sigma-Aldrich, Dorset, UK
HIF1A	AB16066	Abcam, Cambridge, UK
HIF1A	610959	BD Bioscience, Oxford, UK
HIF2A	NB100-132	Novus Biologicals, CO, USA
HRP-linked anti-rabbit IgG	NA934V	GE Lifesciences, Buckinghamshire, UK
HRP-linked anti-mouse IgG	ABNA931V	GE Lifesciences, Buckinghamshire, UK
MAP2	AB32454	Abcam, Cambridge, UK
MAP2	M1406	Sigma-Aldrich, Dorset, UK
NANOG	AB9220	Abcam, Cambridge, UK
Nestin	MAB5326	Merck, Hertfordshire, UK
PSD95	AB18258	Abcam, Cambridge, UK
P-SMAD1/5/8	9511	Cell Signalling, MA, USA
P-SMAD2/3	8828	Cell Signalling, MA, USA
PAX6	N/A	Developmental Studies Hybridoma Bank
Prolyl-Hydroxylase-2	NB100-137	Novus Biologicals, CO, USA
POU5F1	SC5279	Santa-Cruz, Heidelberg, Germany
S100B	2532	Sigma-Aldrich, Dorset, UK
SMAD1/5/8	6031	Santa-Cruz, Heidelberg, Germany
SMAD2/3	5678	Cell Signalling, MA, USA
SOX2	AB5603	Abcam, Cambridge, UK
SSEA4	N/A	Developmental Studies Hybridoma Bank

SMAD1/5/8	6031	Santa-Cruz, Heidelberg, Germany
SMAD2/3	5678	Cell Signalling, MA, USA
SOX2	AB5603	Abcam, Cambridge, UK
SSEA4	N/A	Developmental Studies Hybridoma Bank
Synaptophysin	AB8049	Abcam, Cambridge, UK

3. The role of low oxygen in the pluripotency and proliferation of human pluripotent stem cells.

3.1 Introduction

3.1.1 Culture of pluripotent stem cells.

When Thomson et al. derived the first human embryonic stem cell (hESC) populations in 1998, maintenance of hESC self-renewal was reliant on the use of irradiated mouse embryonic feeders (MEFi) in combination with FGF2 and serum (Thomson 1995; Thomson 1998). FGF2 signalling is critical for maintaining pluripotency, interacting with both Activin/Nodal and canonical Wnt signalling, positively regulating self-renewal (Ding et al. 2010; Vallier et al. 2005; Xu et al. 2008; Stewart et al. 2006). The historical use of Fetal Bovine Serum (FBS) was also essential for self-renewal, with it's removal leading to swift loss of pluripotency and high rates of apoptosis (Pirkmajer & Chibalin 2011). The requirement of serum whilst culturing hESC, although essential, brings with it practical issues; commonly FBS has large batch variations and additionally exposes hESC to cross-species contaminations.

As the emphasis of hESC and iPSC applications have often focused on clinical therapeutics, cell culture practices have concurrently adapted towards more defined cell culture systems. Replacement of FBS as a source of albumin, with defined serum replacements such as Knockout Serum Replacement (KSR) negated the sole reliance on variable animal bovine serum products. The development of mTESR, a defined PSC media, negated the reliance on animal based products through the use of human derived albumin and subsequent developments removed the reliance on albumin products completely by concurrently removing β-Mercaptoethanol, initially added as it was thought to augment clonal efficiency (Oshima 1978; Chen et al. 2011; Ludwig & Thomson 2007). These formulations are however expensive. As an alternative, co-culture with feeder cells have historically supported maintenance of pluripotency.

The use of feeder cells, typically fibroblasts from rodent or human sources such as murine embryonic fibroblasts (MEF), as an adherent base for PSCs has now also been routinely replaced with the use of attachment matrices consisting of a mix of structural adherence proteins such as laminin, fibronectin, vitronectin and collagen, which although still reliant on animal based products are an increasingly defined alternative to direct co-culture (Hughes et al. 2010; Hovatta et al. 2003; Chen et al. 2011). However, feeder cells were not just attachment aids, but also gave trophic support to PSCs for maintenance of pluripotency (Besser 2004; Mallon et al. 2006; Avery et al. 2006; Stewart et al. 2006). Use of MEFi Conditioned Media (MCM, *see section 2.1.2.*) replaced the need for direct cell-cell contact so subsequent analyses of hESC cultures were not contaminated with feeder cells whilst retaining trophic support (Xu et al. 2001). Finally, when examining the effect of oxygen concentration on hESC identity, the additional variability of MEF responses to low oxygen could be eliminated. Here, both iPSC and hESC were maintained in a defined medium pre-conditioned by direct contact with MEFi (MCM).

3.1.2 Defining pluripotency in pluripotent stem cells.

Cell culture techniques must be optimised to retain activity of the pluripotency signalling network, including amongst others, the transcriptional activities of key transcription factors NANOG, SOX2 and POU5F1 (*summarised in 1.2*). Active downstream of a number of pathways including the Activin/Nodal arm of TGFβ signalling, these regulators have a vital role in the self-renewal of PSCs (Z. Wang et al. 2012; Vallier et al. 2005; Boyer et al. 2005; Mitsui et al. 2003; Rossant 2004; Gerrard, Zhao, et al. 2005; Niwa et al. 2000). To maintain pluripotency, NANOG, SOX2 and POU5F1 must be synchronously co-expressed. Silencing the expression of any one of these three transcriptional regulators led to a loss of pluripotency in hESCs and subsequent deregulated activity of the remaining two transcriptional regulators (Boyer et al. 2005; Wang et al. 2012; Vallier et al. 2005). It has also been demonstrated that loss of this triple co-expression in mouse and human pluripotent cells occurred concordantly with differentiation to early germ layer

progenitors (Mitsui et al. 2003; Rossant 2004; Gerrard, Zhao, et al. 2005). Sole expression of SOX2 in hESC indicated an early ectodermal cell fate and sole activity of POU5F1 was shown to be influential in directing mouse and human ESC towards an endodermal identity (Z. Wang et al. 2012; Niwa et al. 2000). Combined expression of these three essential transcriptional regulators was used here to define a pluripotent identity.

Cell surface markers SSEA4, TRA-1-60 and TRA-1-81 are also commonly used to define a population of cells as pluripotent (Adachi et al. 2010; Draper et al. 2002; Henderson et al. 2002; Reubinoff, Pera, Fong, A. Trounson, et al. 2000; Rodda et al. 2005; Stewart et al. 2006; Thomson 1998; Z. Wang et al. 2012). Their expression is regulated upstream by the aforementioned transcriptional regulators and sole repression of either POU5F1 or SOX2 activity resulted in a loss of SSEA4 expression in hESCs (Adachi et al. 2010; Fong, K. a Hohenstein, et al. 2008; Z. Wang et al. 2012). Due to the exclusivity of SSEA4 expression in pluripotent cells and the down-regulation of expression upon differentiation, it was used here as a marker of self-renewing cells, in addition to NANOG, SOX2 and POU5F1.

3.1.3 Low oxygen in the regulation of pluripotency of PSCs.

Although hESCs are typically obtained from the pre-implantation blastocyst, pluripotent hESCs and iPSCs are more reflective of the post-implantation epiblast. During this stage, the pluripotent cells of the *in vivo* inner cell mass reside in an extremely low oxygen environment, estimated at ~3-5% O_2, with stabilised HIF1A and 2A (Pringle et al. 2010; Harvey et al. 2004; Caniggia et al. 2000). Explanted rat blastocysts which underwent maturation at 20-40% O_2 developed with gross abnormalities typically in the neural tube, whereas those at 5% O_2 did not (Morriss & New 1979). Ovine zygotes and 8-cell morula which were matured *in vitro* at 5% O_2 formed a higher number of blastocysts and reached late-stage morula in a timeframe more reflective of that observed *in vivo*, than those undergoing development at 20% O_2 (Bernardi et al. 1996; Tervit et al. 1972). In light of this, *in*

vitro fertilisation (IVF) clinics now widely use low oxygen during fertilisation of oocytes. Meta-analyses of multiple studies showed that when blastocysts were implanted, those formed in physiologically low oxygen levels showed significantly higher rates of implantation and increased the proportion of pregnancies resulting in a live birth (Bontekoe et al. 2012; Gomes Sobrinho et al. 2011). As the undifferentiated identity of hESCs and iPSCs is reflective of a stage of development similar to that of the early embryo, the evidence suggested that the use of low oxygen and subsequent stabilisation of HIFA subunits may be a critical tool in maintaining a stable, pluripotent population of PSCs.

It has already been determined that POU5F1 and SOX2 are direct transcriptional targets of stabilised HIF2A (Covello et al. 2006; Nordhoff et al. 2001; Moreno-Manzano et al. 2010). HIF1A also has synergistic effects with TGFβ in the activation of SMAD2/3, although this has not been confirmed in PSCs (Zhang et al. 2003; Sánchez-Elsner et al. 2001). In addition, both HIF1A and 2A knockout models developed with blatant and consistent malformations typically presenting as dysregulated angiogenesis, vasculogenesis and neurogenesis (detailed in *section 1.3*), indicating a critical role of HIF activity in germ layer and phenotype formation (Iyer et al. 1998; Ryan et al. 1998; Peng et al. 2000; Scortegagna et al. 2003; Maltepe et al. 1997; Ramírez-Bergeron et al. 2006). Here, pluripotent hESCs and iPSCs were maintained at 3% O_2 to initiate HIF1A and 2A stabilisation and assessed for any alteration in proliferation, viability and the expression of markers specific for a pluripotent state, namely POU5F1, SOX2, NANOG and SSEA4.

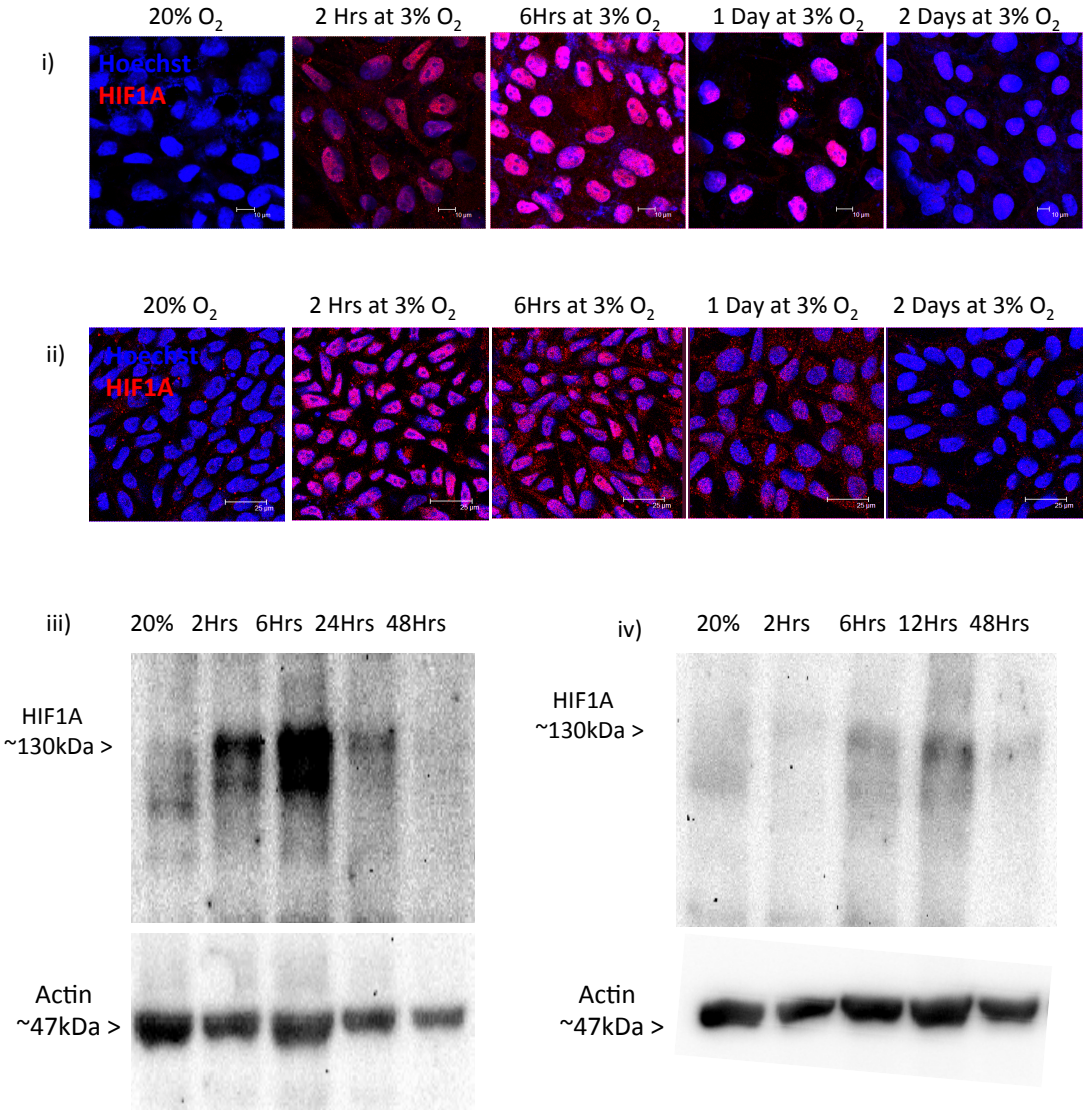

Figure 3.1 3% O_2 was sufficient to initiate transient stabilisation and nuclear translocation of HIF1A in both the hESC (i) and iPSC (ii) lines. *Immunofluorescence showed clear stabilisation of protein expression and nuclear translocation of a labile HIF subunit, HIF1A in both the hESC (i) and iPSC (ii) lines. Peak expression occurred at similar timeframes in both cell lines (6-12 hours) with stabilisation and nuclear expression subsiding thereafter. Western blots confirmed the whole population response observed using Immunofluorescence in hESC (iii) and iPSC (iv). Scale bars for H9 and 34D6 show 10 and 25 μm respectively.*

3.2 Results

3.2.1 Hypoxia Inducible Factor stabilisation in PSCs at 3% O_2.

As detailed in sections *1.5* and *1.6*, alterations to the cellular identity, viability and proliferation of PSCs resulting from incubation at low O_2 are largely mediated via the activity of HIF proteins. Reviewed in section *1.4*, HIFA subunits have previously been characterised as undergoing stabilisation and nuclear translocation at reduced oxygen concentrations, with subsequent targeted transcriptional regulation. Due to the varied timeframes of HIFA stabilisation reported previously (Forristal et al. 2010; Francis & Wei 2010; Cameron et al. 2008) and the lack of characterised HIFA activity in iPSC lines, we sought to illustrate the timeframe and pattern of the stabilisation and nuclear translocation of HIF1A and 2A after transferring hPSCs from 20% to 3% O_2 .

In both of the pluripotent hESC and iPSC lines used here (H9 and 34D6 respectively), immunocytochemistry showed HIF1A translocation from cytoplasm to nucleus within the first 2 hours of low oxygen. This reached maximal levels between 6-12 hours and by 48 hours HIF1A had returned to a cytoplasmic cellular location *(3.1i, ii)*. This confirmed that 3% O_2 was sufficient to prevent degradation of the HIF1A subunit in both cell lines, allowing it to stabilise, accumulate and translocate to the nucleus, as seen by co-staining with blue nuclear stain, Hoechst. Western blots largely confirmed this response; the H9 hESC line (*3.1iii*) showed corresponding peak signal at 6 hours post-introduction to 3% O_2 whereas the 34D6 iPSC line (*3.1iv*) showed peak signal between 6-12 hours, slightly retarded in comparison to that observed using immunocytochemistry. It is worth noting that due to the lability of both the HIF1A and 2A subunits, it was necessary to obtain protein lysis for western blot by scraping cells off cell culture plastics. This introduced an element of variability in protein content as adherent proteins in the Matrigel basement matrix would have contaminated protein samples to an unknown degree, making quantification and comparison of band density across samples unreliable, hence these results should be considered solely in terms of whether HIF1A was detectable or non-detectable using western blots.

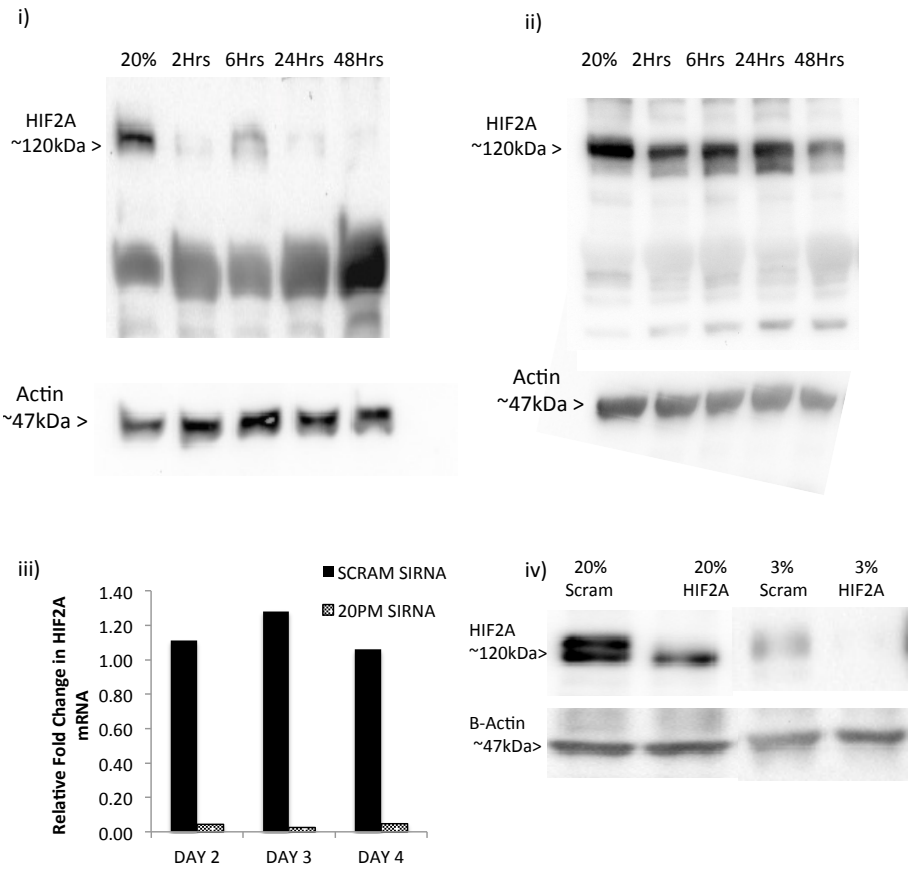

Figure 3.2 HIF2A showed variable expression at 20% and 3% O_2. *Western blot showed steady expression of the HIF2A subunit at 3% O_2 in both the hESC (i) and iPSC (ii) lines examined. Specificity of the detected HIF2A band at 120kDa was certified through siRNA knockdown at both the mRNA (20% O_2) (iii, n=1) and protein (20% and 3% O_2) level (iv) in the H9 hESC line.*

In both hESCs and iPSCs, detection of HIF2A using immunocytochemistry was not possible as the tested antibodies showed large non-specific staining, hence, investigation into the protein expression of HIF2A was performed solely using western blots. Observed with western blots, expression of HIF2A was variable across the two cell lines. In both cell lines, a band at 120kDa was detected at 3% O_2 in addition to a band at 50-60kDa at both 20% and 3% O_2. In the 34D6 cell line, expression of HIF2A appeared constitutive, with no apparent change in protein concentration across all examined timepoints at 20% and 3% O_2. In the H9 hESC line however, expression of HIF2A was variable (see *figures 3.2 and appendix figure 8.1*). All blots showed some level of expression at 3% O_2 although *figures 3.2ii* and *8.1ii* showed particularly high expression at 20% O_2 and after 6 hours at

3% O_2, with band size at other timepoints of low oxygen exposure appearing reduced. Due to this, the specificity of staining was assessed; silencing of HIF2A mRNA was carried out using short interfering RNA (siRNA) specific for HIF2A. Knockdown was initially assessed using semi-quantitative PCR and the fold-change in transcription was assessed relative to untransfected H9 cells, with thorough knockdown of mRNA achieved within 48 hours of the initial transfection (*figure 3.2iii*). Western blot of transfected cells 4 days after the initial transfection showed reduced protein concentration at both 20% and 3% O_2 after HIF2A silencing, compared to a scrambled control (*3.2iv*). Hence, it was concluded that the detected bands were correctly probing for HIF2A and that in the H9 hESC line, HIF2A underwent transient decrease and subsequent increase in protein expression at 3% O_2. This does not correlate with previous literature on HIF2A expression at low oxygen concentrations in hESCs, which reported a delayed but sustained increase in protein expression, in contrast to the immediate but transient increase in HIF1A protein expression (Närvä et al. 2013; Forristal et al. 2010).

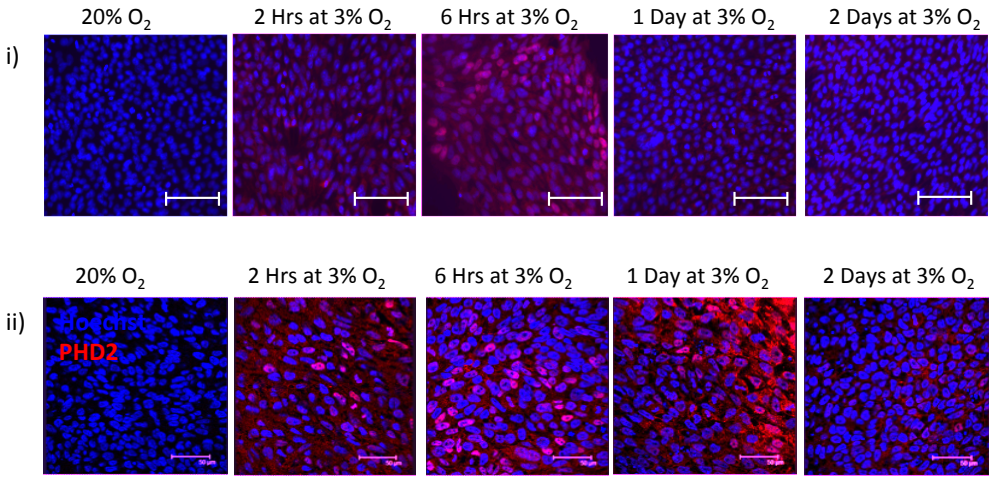

Figure 3.3 3% O_2 stimulated transient nuclear translocation of Prolyl Hydroxylase-2 (PHD2) in both hESCs and iPSCs. *Immunofluorescence of PHD2 (red) showed clear up-regulation of protein expression and subsequent localisation in the nucleus (blue) in both hESC (i) and iPSC (ii). Onset and peak of nuclear translocation occurred at similar timeframes in both cell lines (2 and 6 hours*

respectively) with nuclear accumulation subsiding thereafter. Scale bars show 50 μm.

In both cell lines, Prolyl Hydroxlase-2 (PHD2) showed transient increased protein expression and nuclear translocation in a timeframe corresponding with that of HIF1A (*Figure 3.3*). This was concordant with a reported role for PHD2 in the targeted degradation of HIF1A after hypoxia-induced stabilisation (Jokilehto et al. 2010).

3.2.2 Long term maintenance of hESCs at 3% O_2.

Within 48 hours at 3% O_2, both the hESC and iPSC cell lines underwent HIF1A stabilisation in addition to HIF2A expression. Culture of hESCs under low oxygen has been reported to induce changes in colony size and cell number (Chen et al. 2010; Mazumdar et al. 2010; Zachar et al. 2010; Prasad et al. 2009; Forristal et al. 2010; Chen et al. 2009) although the nature of these observations varied widely. With additional reported effects on cell viability (Chen et al. 2010; Mazumdar et al. 2010) it seemed vital to quantify precisely any effect of low O_2 on proliferation which may have affected subsequent colony formation or differentiation.

As HIF1A has been implicated in inducing a G1-phase stall in colorectal carcinoma cells (Koshiji et al. 2004) and HIF2A in movement from G1-phase into the S-phase in renal carcinoma cells (Gordan et al. 2007), I aimed to quantify the proportion of actively dividing cells (i.e. in G2/M) in hESCs at 3% O_2. This was performed using flow cytometric analysis to quantify the percentage of cells with one copy of DNA (G1) to those with two copies (G2/M). Those with two copies of DNA (G2/M) were classed as currently or imminently dividing, so considered 'actively dividing', as opposed to G0/1 where cells were not undergoing chromosomal duplication and/or division, hence retained only a single DNA copy. Gating algorithms allowed separation of these peaks from the S-phase mid-section and the proportion of the cell populations in G0/1 and G2/M was quantified *(Figure 3.4)*.

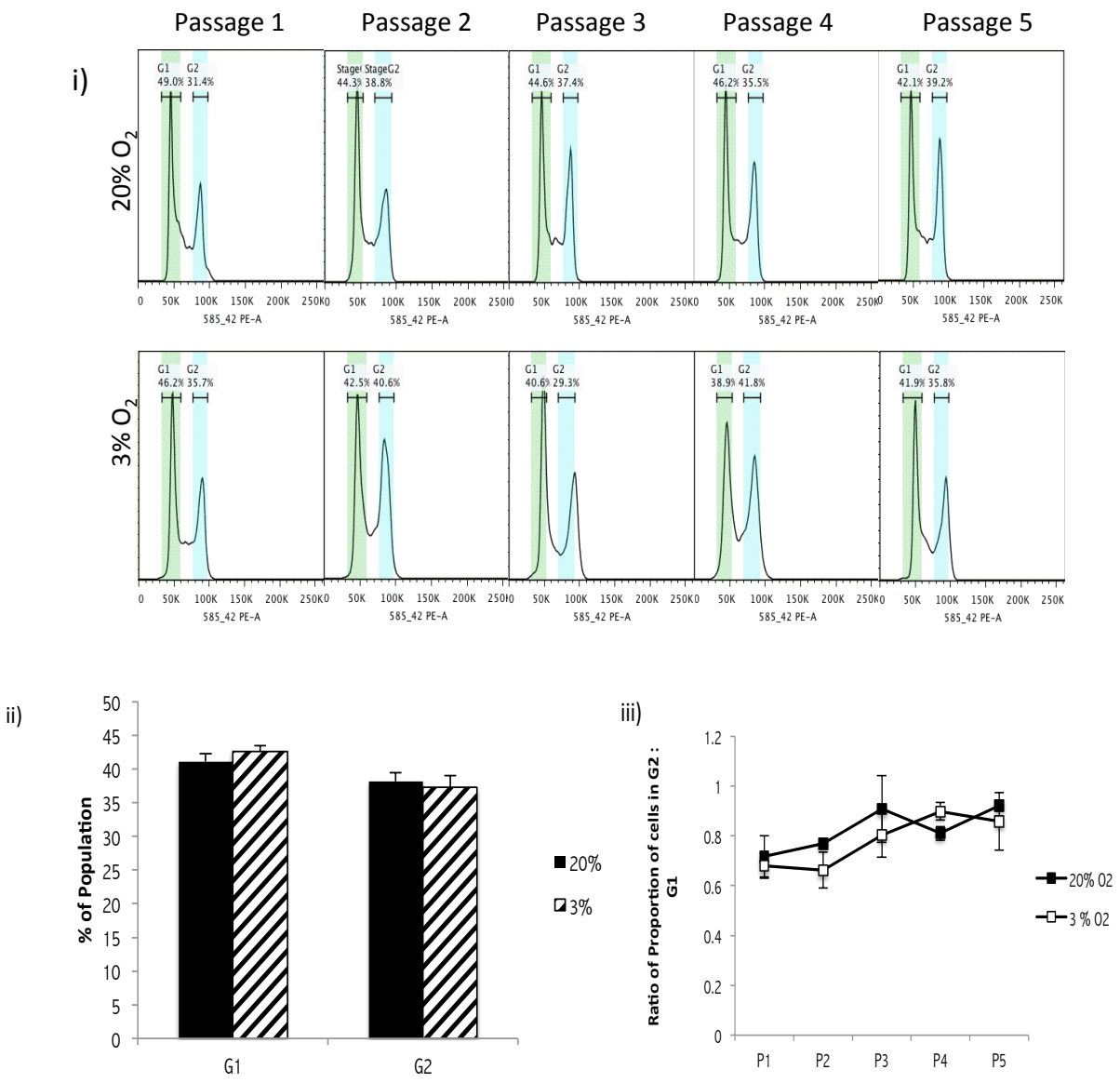

Figure 3.4 Proliferation of hESCs remained steady over 5 passages at 3% O2. *HESC populations cultured at 20% and 3% O_2 were separated into sub-populations dependent on each cells DNA content, with histograms of fluorescence separating G0-1 (one set of DNA) and G2/M (two sets of DNA) from an intermediate S-phase population (i), representative histograms of the data-set displayed. The proportion of cells in G0/1 and G2/M populations remained consistent across the entirety of the experimental period (ii). This was reflected in the Proliferative Index (PI, a ratio of G2:G1) whereby an increase in PI correlated to increased proliferation, which was consistent across both 20% and 3% O_2 (iii).*

HESCs were introduced into 3% O_2 and maintained for 5 passages, equating to ~15 days. Proliferation was assessed at each passage. The proportion of the hESC population in G0/1 and G2/M did not vary significantly after introduction to 3% O_2 and remained steady for up to 15 days, indicating that maintenance at low oxygen did not result in any clear shifts between cell-cycle phases *(Figure 3.4ii, iii).* Independent T-Tests between oxygen concentrations at each passage showed no significant differences between either the percentage in G0/1, G2/M *(3.4ii)* or overall Proliferative Index (PI) *(3.4iii)*. The PI gave an estimation of overall proliferative activity using a ratio of the percentage of cells in G2/M : G0/1, an increase in PI indicated an augmented proportion of cells undergoing cell division. Although there was a pattern of reduced proliferation rate in the first 2-3 passages, one-way ANOVA showed no significant alteration between oxygen concentrations, $F(9, 20.0)=2.36$, $p=0.053$ *(3.4,iii).*

Quantifying the proportion of cells actively dividing does not take into account the viability of the population. Flow cytometry was used to evaluate the proportion of cells positively expressing the apoptotic marker phosphatidylserine. Early after apoptosis induction, phosphatidylserine proteins flip to the outer surface of the cell and *in vivo* are used for recognition by phagocytes and subsequent cellular degradation (Fadok et al. 1998). Efficient and reliable binding of the AnnexinV protein to exposed phosphatidylserine allowed for use of fluorescently labelled AnnexinV to define live cells as apoptotic or non-apoptotic (Koopman et al. 1994). Selective permeation of propidium iodide into only dead cells was used to differentiate between live and dead cells.

Using flow cytometry, live hESC were defined as apoptotic/non-apoptotic and live/dead based on the intensity of fluorescence. *(Figure 3.5i)* Staurosporine, an apoptotic inducer through caspase and non-caspase dependent mechanisms (Belmokhtar et al. 2001) was used as a positive control to define the fluorescent intensity of apoptotic cells. As PI could not permeate into live cells, an unstained negative control was also used to aid in defining the positive population.

i)

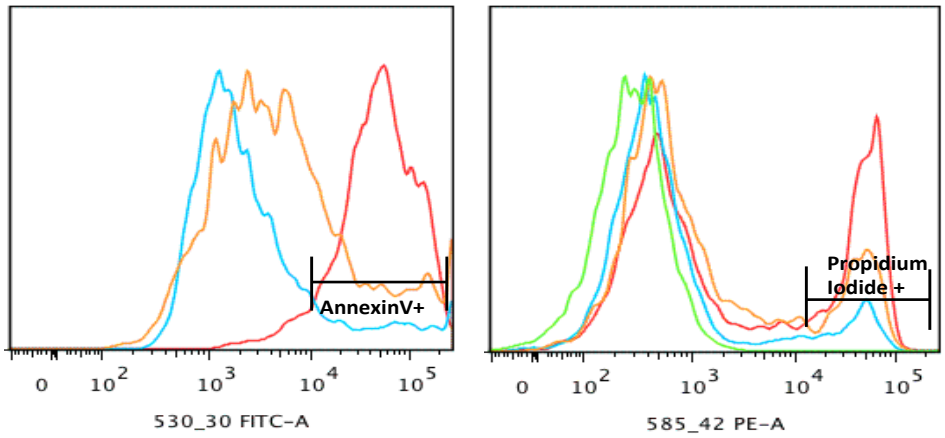

ii)

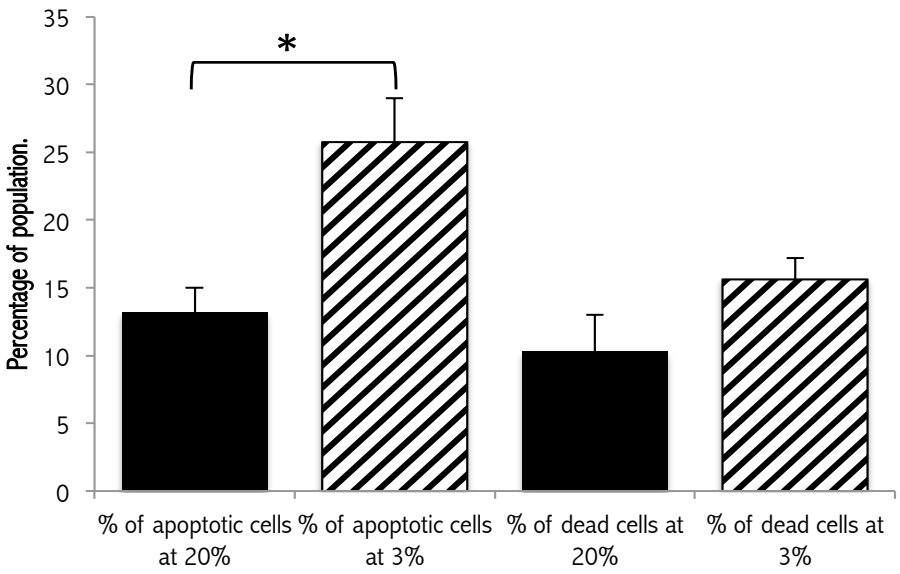

Figure 3.5 Apoptosis and cell death was augmented in hESCs at 3% O_2. *Representative histograms of hESC at 20% and 3% O_2 (i) with an unstained negative control in green, a positive control to induce apoptosis and cell death in red, 20% O_2 in blue and 3% O_2 in orange show a significant increase in both apoptosis and cell death in hESC maintained at 3% O_2 (ii).*

Apoptosis and subsequent cell death was consistently higher after culture at 3% O2 (Figure 3.5). The percentage of apoptotic cells at 3% O2 from P1-P5 (25.8 ± 3.3%) showed significant increase ($t(25)=3.2$, $p=0.004$) compared to those maintained in 20% oxygen (13.2±2.2%) (Figure 3.5ii). The levels of viability reflected this pattern with augmented cell death at 3% O2 (15.6±1.4%) compared

to 20% (10.3±2.8%), (t(28)=1.7), p=0.097) (Figure 3.5ii). This increase in apoptosis was tracked across the experimental time course, one way ANOVA showed no significant differences between groups (F(9, 20)=0.39, p=0.12) with significant difference at Passage 4 only (t(4)=3.1, p=0.036), lack of statistical significance was contributed to by large variation. A drop in viability after long-term culture of hESCs under low oxygen has been reported previously (Chen et al. 2010) although others sustained healthy and rapidly proliferating hESC cultures for as long as 18 months (Zachar et al. 2010; Forristal et al. 2010).

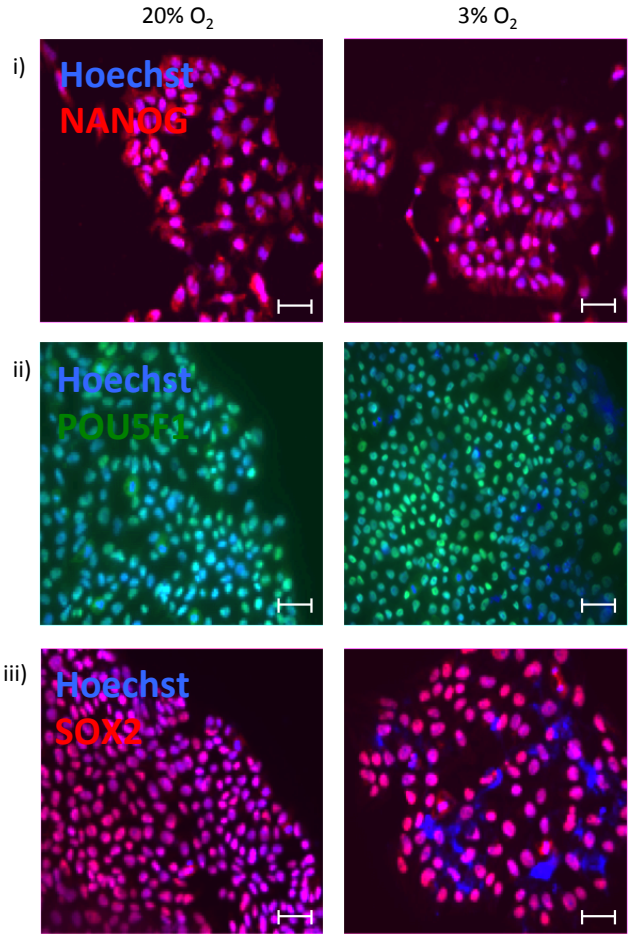

Figure 3.6 Nuclear expression of NANOG, SOX2 and POU5F1 was retained in hESCs after long-term culture at 3% O_2. *Immunofluorescence of key pluripotency regulators NANOG (i), SOX2 (ii) and POU5F1 (iii) demonstrated all specified transcriptional markers remain expressed and localised to the nucleus in the vast majority of cells. Scale bars show 50μm.*

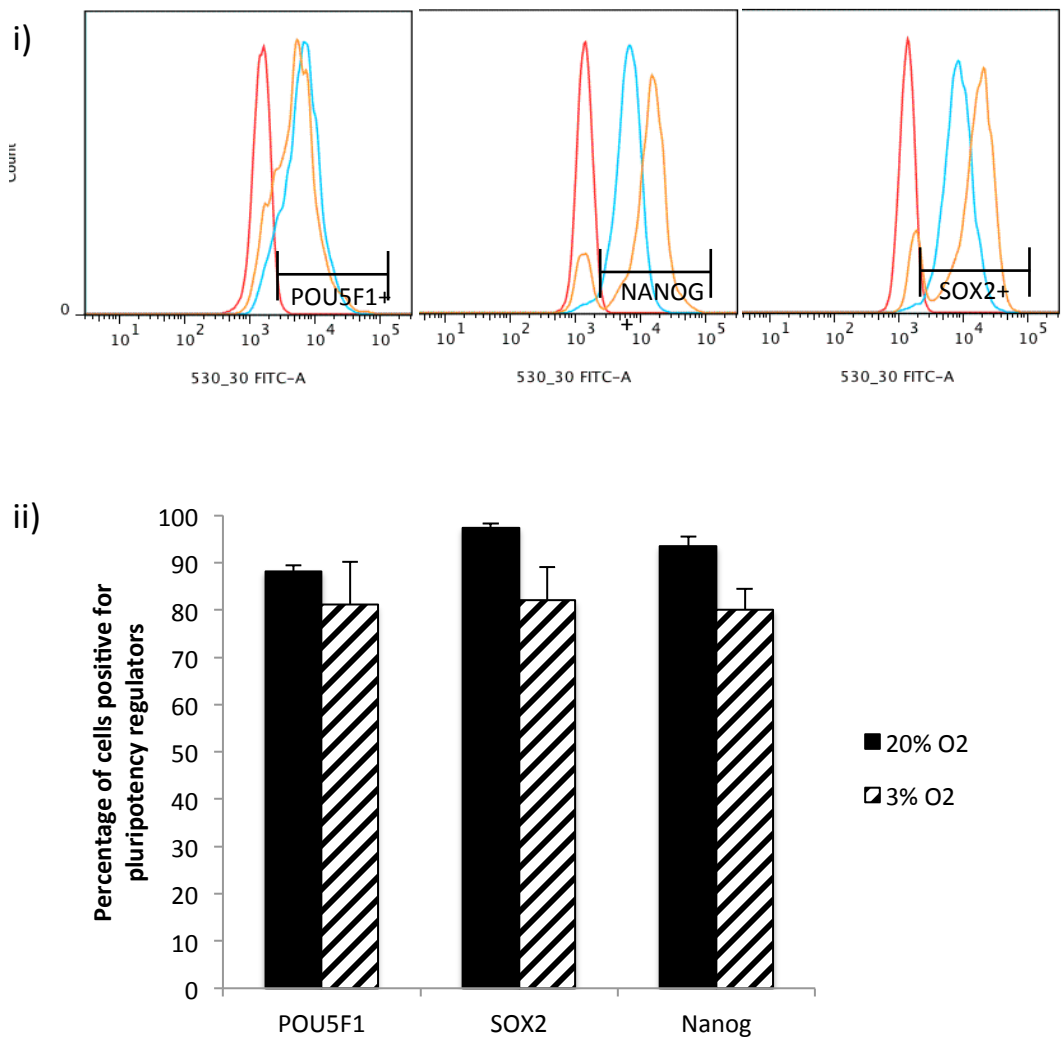

Figure 3.7 Long-term maintenance of hESCs at 3% O_2 did not induce any alteration to expression of key pluripotency markers. *Flow cytometry was used to quantify the proportion of the population remaining positive for NANOG, SOX2 and POU5F1. Representative histograms show expression of pluripotency markers was steady across oxygen conditions (i). Negative controls (red) determined gating of positive populations of hESCs maintained for 5 passages at 20% O_2 (blue) and 3% O_2 (orange). (ii) The percentage of cells positive for NANOG, POU5F1 and SOX2 after 5 passages was not significantly different although a trend of decreased percentage positive at 3% O_2 was observed, with two populations of cells (staining negative and positive) clearly evident in 530-30FITC histograms (i).*

3.2.3 Pluripotency of hESCs after long-term maintenance at 3% O_2.

In addition to determining the stability of proliferation and viability at 3% O_2, it was essential to establish if hESCs remained pluripotent throughout the experimental timecourse. Previous studies used morphological analysis to assess the percentage of differentiated colonies (Ezashi et al. 2005; Forristal et al. 2010; Chen et al. 2010), although visually assessing the pluripotent morphology of ESCs may not accurately reflect the proportion of pluripotent cells. As three critical regulators responsible for sustaining self-renewal downstream of phosphorylated-SMAD2/3 (Stewart et al. 2006; Xu et al. 2008; James et al. 2005), canonical Wnt/β-catenin (Sato et al. 2004; Ding et al. 2010) and MAPK/PI3K/NFκB signalling (Armstrong et al. 2006; Li et al. 2007; Ding et al. 2010), protein expression of POU5F1, NANOG and SOX2 was used here to define hESCs which had retained a pluripotent state. After 15 days at 3% O_2, hESCs consistently expressed these factors in the vast majority of cells *(Figure 3.6).*

To quantify this, flow cytometry using antibodies specific for these markers was performed at the conclusion of the 15-day experiment. A negative control defined the negative and positive gating *(Figure 3.7i)*. Comparably with the immunofluorescence *(Figure 3.6)*, the proportion of cells classified as positive for pluripotency markers was not significantly improved after long-term culture at 3% O_2. The percentage of NANOG positive cells showed a non-significant decrease at 3% O_2 (80.1±4.3%) compared to 20% (93.4±2%, $t(3)=3.2$, $p=0.050$) as did SOX2 with nearly uniform expression at 20% (97.3±0.89%) dropping under 3% (82.1±6.9%, $t(5)=2.2$, $p=0.079$). POU5F1 however remained consistent across 20% and 3% respectively (88.2±1.2% and 81.1±9.1%, $t(4)=0.77$, $p=0.483$), *Figure 3.7ii*. Although this suggested that long term maintenance of pluripotency at 3% O_2 was not a beneficial alternative to 20% O_2 for sustaining a pluripotent population of cells, a large majority of cells retained expression of key pluripotency markers, indicating they retain potential for trilineage differentiation.

The evidence here suggested that long-term expansion of hESC at 3% O_2 was not beneficial. Prolonged culture at physiologically low O_2 did not increase the proportion of hESC positive for pluripotency markers. In addition, proliferation

remained consistent throughout experiments with apoptosis rising over 15 days of culture, detrimentally leading to high levels of cell death. This augmented cell death may have been underlined by a number of factors, addressed here by examining short-term culture of hESC as well as an iPSC line.

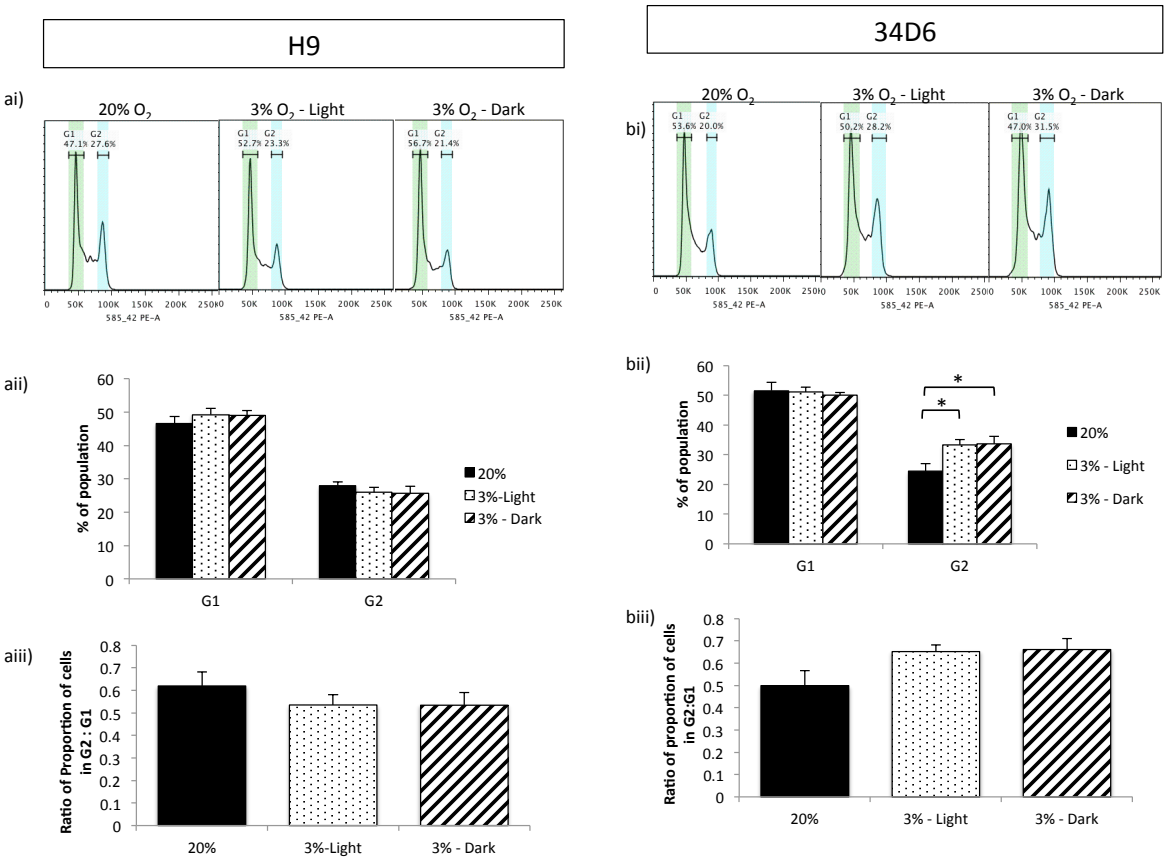

Figure 3.8 Alteration to proliferation at 3% O_2 was cell line dependent and unaffected by light exposure. *The hESC line (3.8a) in short term culture showed no significant alteration to overall Proliferative Index (aiii) or to the proportion of the population in G0/1 or G2/M (ai, ii). The iPSC line (b) did show significant increase in the proportion of cells undergoing G2/M (bii) although the pattern of increased overall proliferation at 3% O_2 (biii) was not significant. Both cell lines tested showed comparable proliferation at 3% O_2 whether maintained in the light or the dark (aiii, biii).*

3.2.4 Proliferation and apoptosis of iPSC and hESC short term at 3% O_2.

The proliferative and apoptotic effects on hESCs were determined during long-term culture at 3% O_2. The rise in apoptosis under 3% O_2 may be a reflection of

the cell line used or a consequence of introducing an established cell line which had previously undergone long-term culture at atmospheric oxygen concentrations, to reduced O_2. An iPSC cell line (34D6) at a lower passage number (between P40-55 compared to P80-95 in hESC) was used here as a comparative cell line. The controlled and consistent low oxygen concentration throughout cell culture was obtained using a Sci-TIVE workstation (Baker-Ruskinn, UK). As the front of this unit was clear and transparent, I hypothesized that the observed rise in apoptosis may be due to light exposure during culture. I have therefore examined the effects of 3% oxygen in the light and dark. Both the hESC and iPSC cell lines were introduced into 3% O_2 from previous culture at atmospheric O_2 concentrations and maintained for a short period of time only (~2-3 days) for initial assessment on the short-term effects of light exposure.

Proliferation was quantified as detailed previously by gating cell populations into G0/1 and G2/M phases of the cell cycle. The effects of low oxygen on proliferation occurred in a cell line dependent manner *(Figure 3.8).* Short term, maintenance of hESC at 3%-Light (0.54±0.05) and 3%-Dark (0.53±0.06) had no significant effect on Proliferative Index compared to 20% (0.62±0.06) *(Figure 3.8aiii)*, determined with one-way ANOVA ($F(2, 22)=0.75$, $p=0.49$), reflecting the previously examined maintenance of hESC at 3% O_2 long-term. One-way ANOVA additionally confirmed comparable proportions of cells in G0/1, and G2/M at ($F(2, 22)=0.78$), $p=0.47$) and ($F(2, 22)=0.41$, $p=0.67$) respectively *(Figure 3.8ai, ii).*

Conversely, the iPSC line did show a shift between cell cycle phases after exposure to low oxygen. The proportion of cells in G0/1 did not alter significantly between all culture conditions investigated (*Figure 3.8bi, ii,* $F(2, 13.9)=0.23$, $p=0.800$) and the observed pattern of higher overall proliferation at 3%-Dark (0.66±0.05) and 3%-Light (0.65±.030) compared to 20% O_2 (0.50±0.07) was not significant (*Figure 3.8biii*, $t(2, 18)=3.1$, $p=0.069$). This pattern of boosted proliferation was likely due to the significant increase in the proportion of cells undergoing the G2/M-phase at 3% O_2, (*Figure 3.8bi, ii*, $F(2, 24)=5.17$, $p=0.014$). Using a Tukey post-hoc test, 3%-Light (33.2±1.82%, $p=0.031$) and 3%-Dark (33.7±2.45%, $p=0.023$) showed significant increase in the proportion of cells

undergoing G2/M compared to 20% (24.2±2.56%). The proportion of cells moving through G2/M in either condition at 3% O_2 showed no difference (p=0.99), indicating that concordant with the HESC line, light exposure was not detrimental to proliferation.

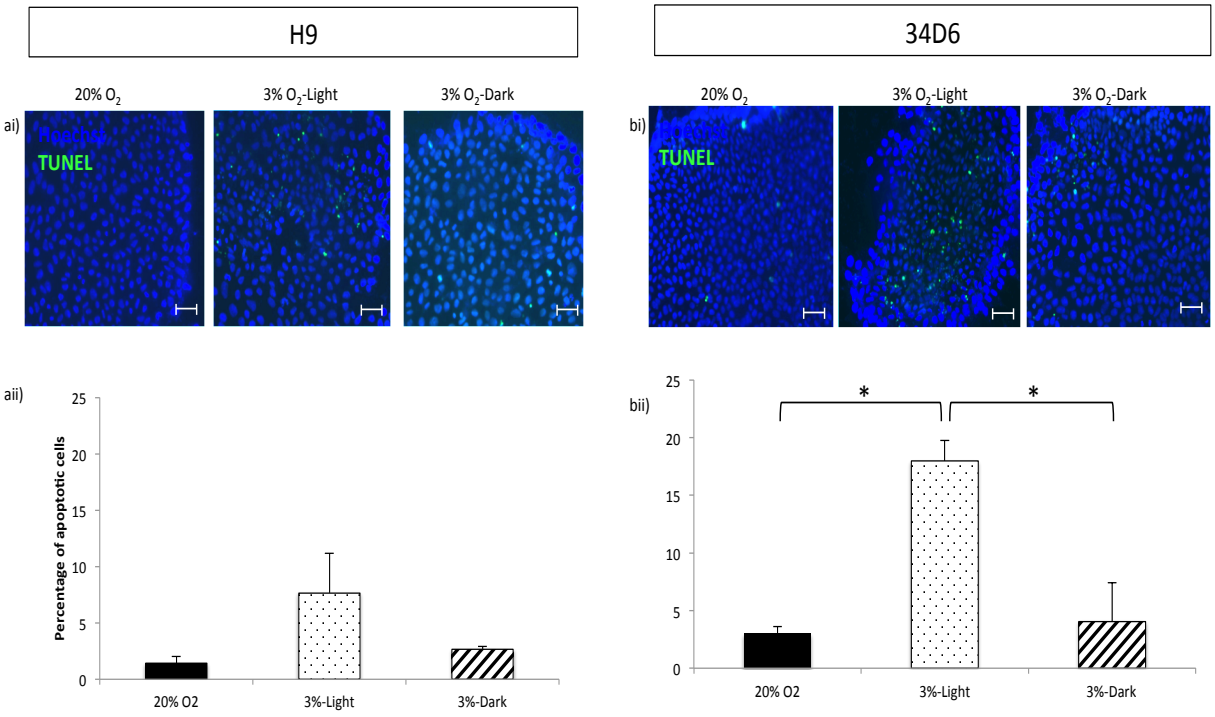

Figure 3.9 Exposure to light at 3% O_2 induced apoptosis in hESCs and iPSCs. *(ai, bi) TUNEL labelled apoptotic cells (green) showed as typically small, apoptotic bodies in comparison to viable nuclei (blue). A large increase in apoptotic cells in 3%-Light was observed both in hESC (aii) and iPSC (bii) compared to 20% and 3%-Dark. Scale bars show 50 μm.*

In previous long-term experiments, apoptotic cells were labelled using AnnexinV-FITC binding to exposed phosphatidylserine and the proportion of apoptotic cells quantified using flow cytometry. The high apoptosis rates and the known sensitivity of hESCs and iPSCs to cell dissociation led to concern that detachment into a single cell state and subsequent flow cytometry could be inducing apoptosis, thus skewing results (Watanabe et al. 2007). In the last phase of apoptosis (after phosphatidylserine exposure on the outer leaflet of cell membrane) nuclear DNA undergoes fragmentation (Ziegler 2004). TUNEL assays

(Terminal deoxynucleotide transferase dUTP nick end labelling) exploited this by using 12-dUTP coupled to FITC, binding 3'-OH ends and labelling fragmented single strand DNA *(Figure 3.9)*. The nature of the assay allowed for labelling of an entire coverslip with minimal disturbance to cell cultures, images of which were then processed by unbiased automated cell counting. In hESCs, a large increase in TUNEL positive cells was observed in 3%-Light (7.64±3.5%) compared to 20% (2.66±0.24%) and 3%-Dark (1.43± 0.58%), a one-way ANOVA determined this as non-significant due to a large SE in the 3%-Light samples ($F(2, 3)=2.5$, $p=0.23$) *(Figure 3.9a)*.

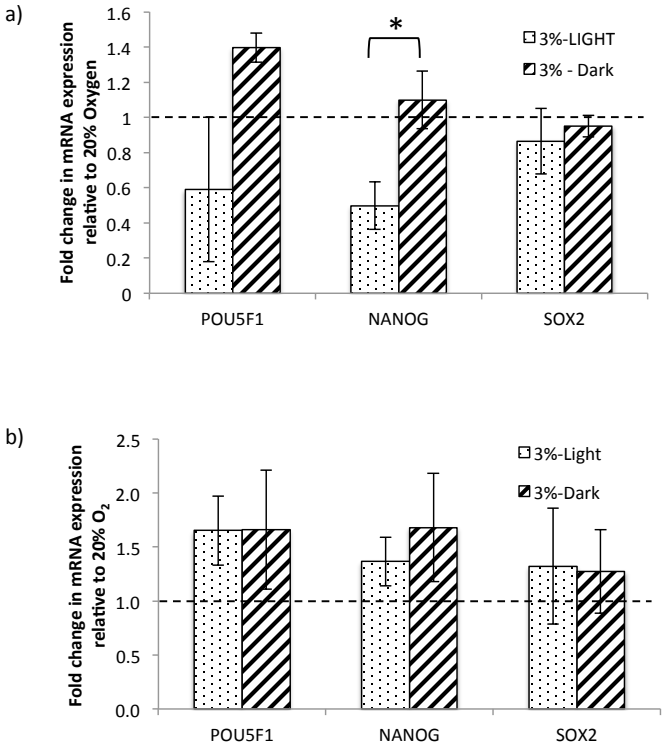

Figure 3.10 Up-regulated transcription of key pluripotency regulators due to 3% O_2 was conserved across cell lines. *Both hESC (a) and iPSC (b) showed NANOG and POU5F1 transcription at 3%-Dark above that of 20% O_2. Only hESC showed light dependent, reduced transcription, relative to 3%-Dark and 20% O_2 (a). Transcription of SOX2 remained steady across oxygen concentrations in both cell lines (a, b).*

However, the iPSC cell line confirmed that light exposure triggered this increase in cell death. A one-way ANOVA outlined a significant increase in apoptotic cell death ($F(2, 6)=14.1$, $p=0.005$) in the 3%-Light population (18.0±3.38%) compared to 20% (3.02±0.61%), $p=0.008$) and 3%-Dark (4.04±1.76%, $p=0.011$) (*Figure 3.9bii*). As long-term 3% O2 experiments were performed whilst exposed to light, it seems clear that the observed increase in apoptosis under low oxygen was underlined by long-term exposure to light. In short term TUNEL analysis, 20% and 3%-Dark cultures show comparable levels of apoptosis in both the HESC ($p=0.909$) and iPSC ($p=0.945$) lines. (*Figure 3.9*)

3.2.5 Pluripotency of iPSC and hESC short term at 3% O_2.

As apoptosis levels were comparable between 20% and 3%-Dark, the expression of key pluripotency factors were evaluated after 3 days to investigate if light exposure underlay the pattern of decrease in POU5F1, NANOG and SOX2 positive cells after long-term culture at 3% O_2. Semi-quantitative PCR allowed comparison of gene transcription between samples, normalised to hESCs or iPSCs maintained at 20% O_2. HESCs at 3%-Light showed attenuated transcription of *POU5F1* (0.59±0.40, $t(7)=1.6$, $p=0.23$) and *NANOG* (0.50±0.14, $t(7)=2.9$, $p=0.02$) in comparison to 3%-Dark (1.27±0.08 and 1.12±0.13 respectively). As samples were normalised to 20% O_2, a relative fold-change in transcription below 1.0 related to a decrease in transcription relative to the control sample used, indicating light exposure not only attenuated the up-regulated transcription at 3%-O_2 but was actively detrimental to pluripotency, relative to 20% O_2. Transcription of *SOX2* showed little alteration at 3%-Dark (0.95±0.06) relative to either 20% O_2 or 3%-Light (0.87±0.19, $t(7)=0.56$, $p=0.59$).

Interestingly, the 34D6 line showed more resilience against the effects of light exposure on low oxygen mediated transcriptional up-regulation. *POU5F1* (1.65±0.32 vs 1.66±0.55, $t(4)=0.014$, $p=0.99$) and *SOX2* (1.32±0.54 vs 1.36±0.22, $t(4)=0.07$, $p=0.95$) in particular showed no significant difference between 3%-Light and 3%-Dark respectively. Transcription of *NANOG* at 3%-Dark was slightly

increased (1.68±0.50) compared to 3%-Light (1.36±0.22) although not significantly (t(4)=0.58, p=0.596). All genes showed transcription above 1.0 at 3% O_2 (whether light or dark) which indicated consistent up-regulation relative to that at 20% O_2.

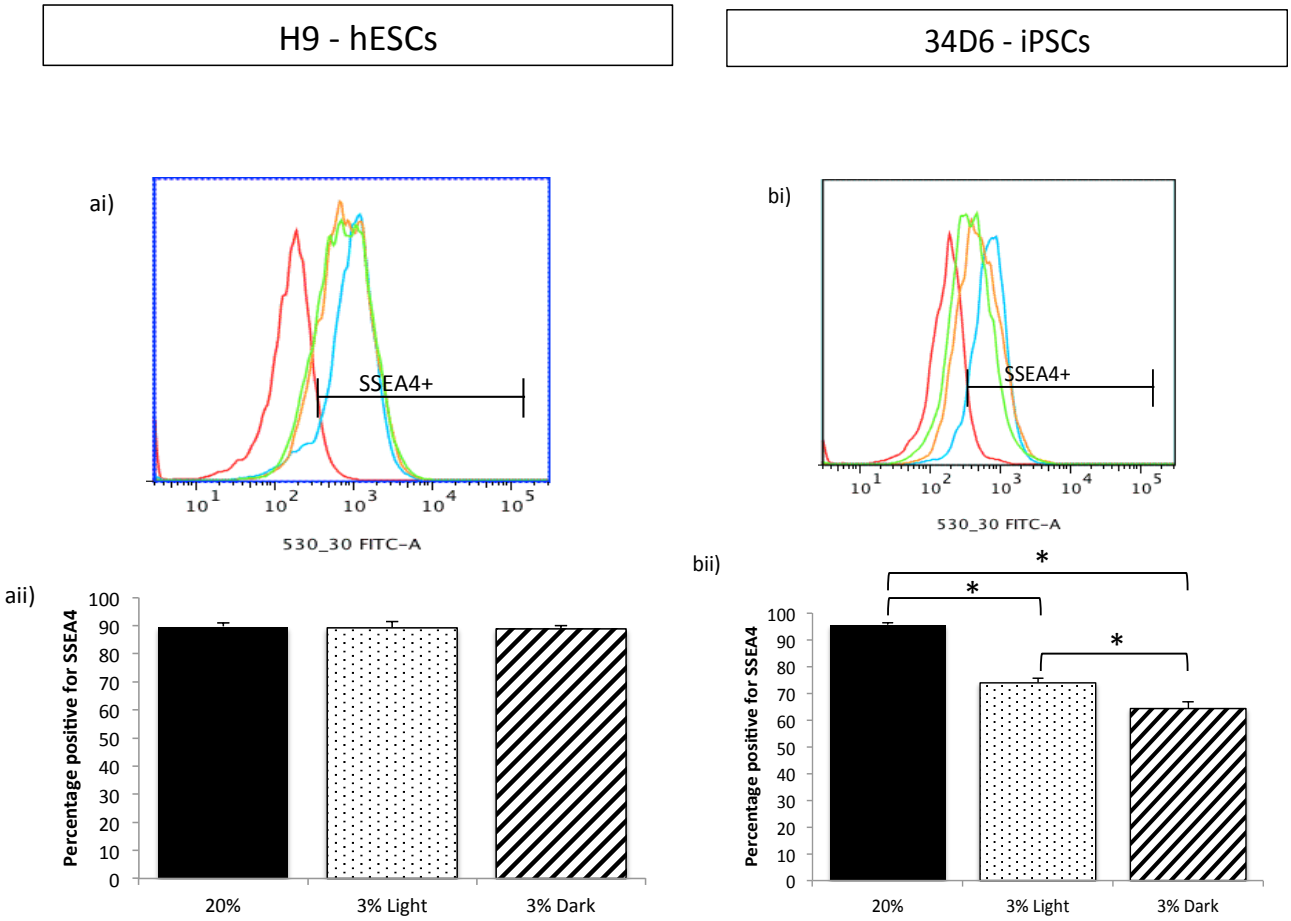

Figure 3.11 The proportion of cells retaining expression of pluripotent cell surface marker SSEA4 was cell line-dependent. *Negative controls (red) were used to determine gating of positive populations of hESC and iPSC (ai, bi) maintained for 1 passage at 20% O_2 (blue), 3%-Light (orange) and 3%-Dark (green). Expression of cell surface marker SSEA4 remained consistent across all culture conditions in hESC (aii) but was significantly attenuated in the iPSC at 3%-Light and 3%-Dark (bii).*

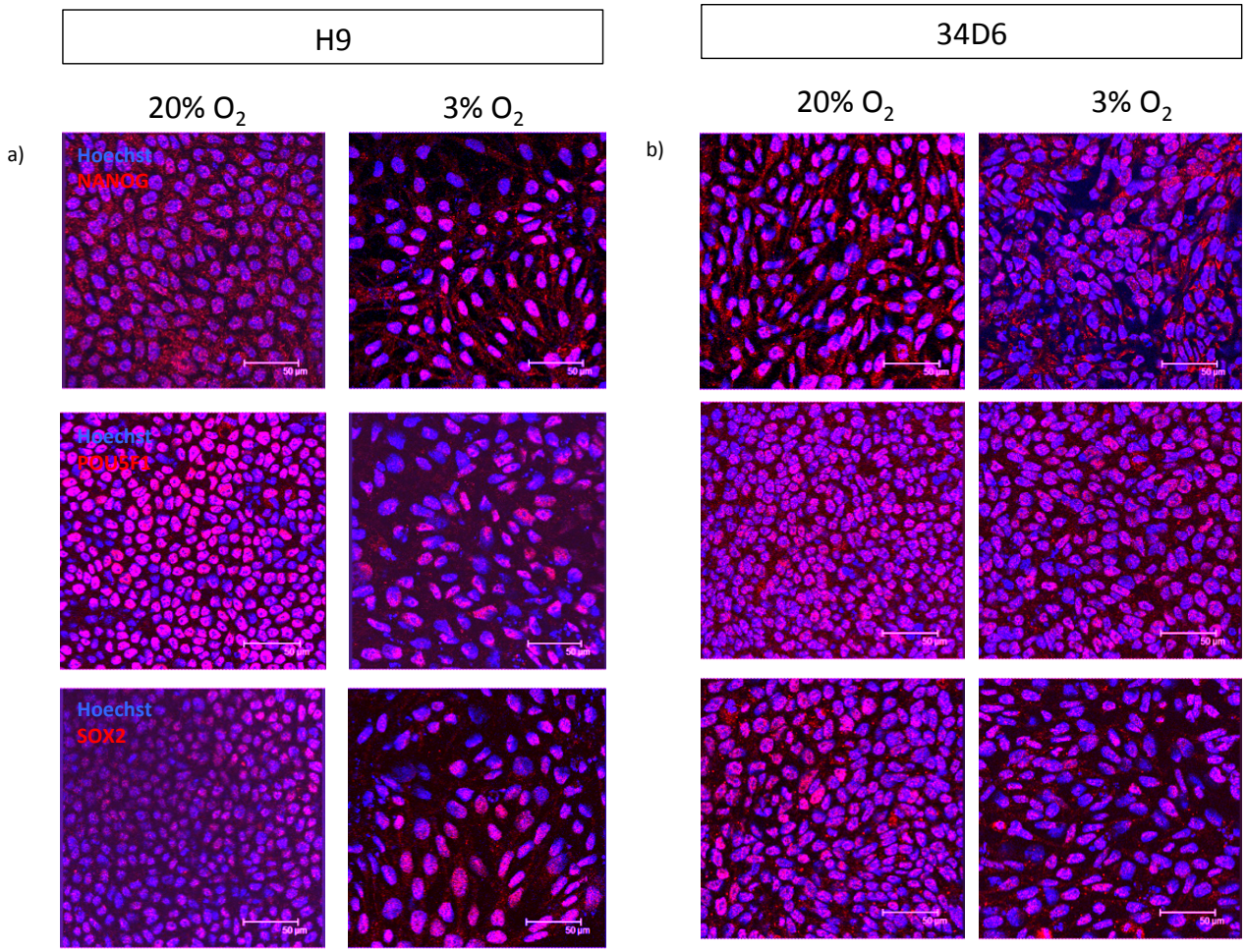

Figure 3.12 Protein expression of key pluripotency regulators NANOG, POU5F1 and SOX2 remained consistent in both cell lines at 20% and 3% oxygen. *After short-term culture of hESC (a) and iPSC (b) at 3% O_2, all specified transcriptional markers remain expressed and localised to the nucleus in the majority of cells labelled by immunofluorescence.*

Expression of SSEA4, a cell surface marker exclusive to pluripotent embryonic stem cells was used here to label cells for flow cytometry quantification (Adachi et al. 2010; Z. Wang et al. 2012; Draper et al. 2002; Henderson et al. 2002; Reubinoff, Pera, Fong, a Trounson, et al. 2000; Rodda et al. 2005; Thomson 1998; Avery et al. 2006; Stewart et al. 2006). HESCs (*Figure 3.11a*) showed comparable proportions of cell populations expressing SSEA4 ($F(2, 6)=0.07$, $p=0.938$) at 20% O_2 (89.7±1.2%), 3%-Light (89.2±2.2%) and 3%-Dark (88.9 ± 1.2%). However, the proportion of cells expressing SSEA4 in iPSCs was consistently down-regulated at 3%-Light (73.9±1.8%, $p=0.002$) and 3%-Dark (64.3±2.45%, $p=0.0004$) relative to 20% O2 (95.6±0.85%, $F(2, 5)=52.4$, $p=0.0004$). Interestingly, light exposure seemed

to have an additional effect with a significant increase at 3%-Light relative to 3%-Dark (p=0.039).

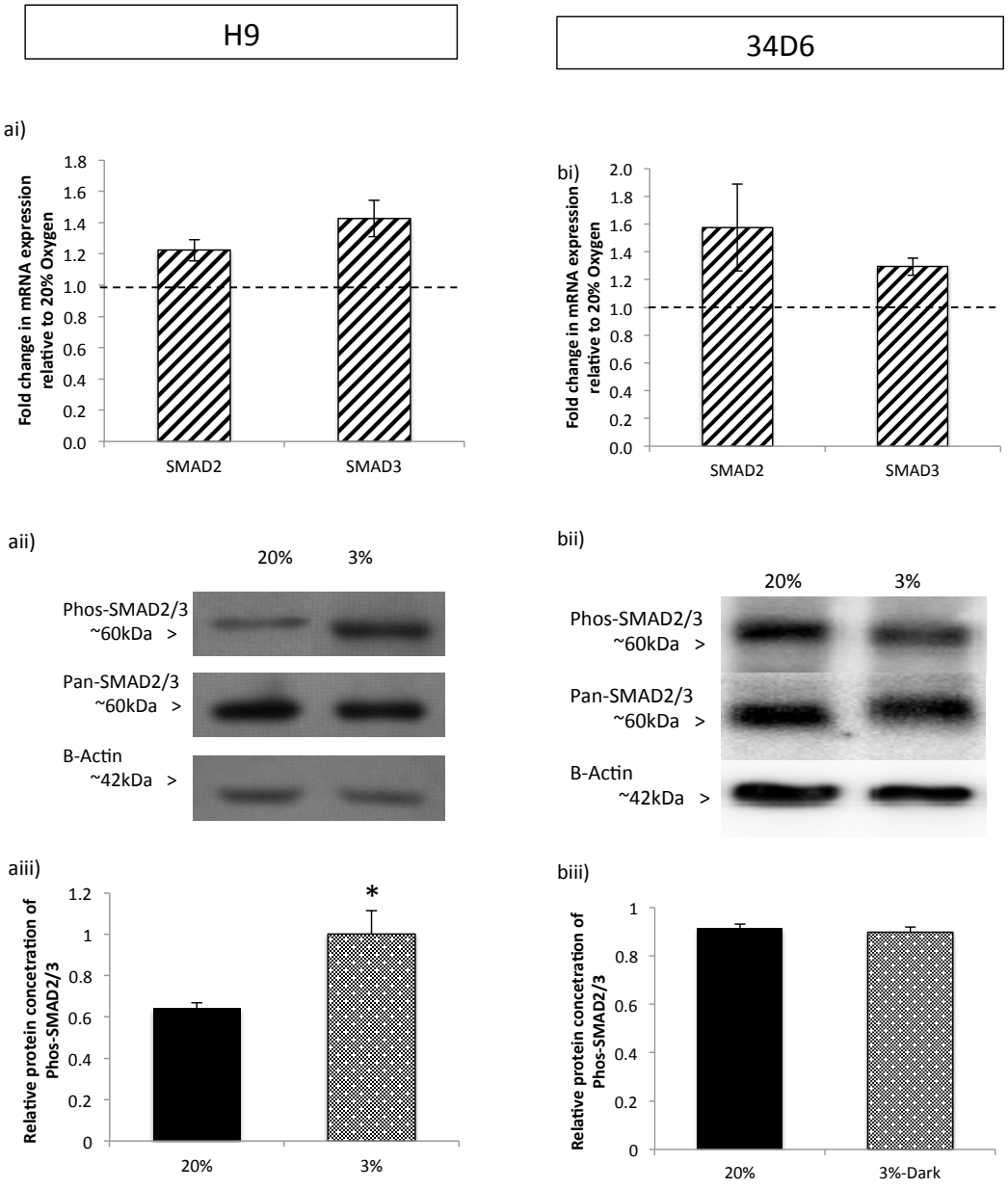

Figure 3.13 Downstream messengers of TGFβ signalling (SMAD2/3) showed a cell-line dependent activation response to 3% O_2. *Semi-quantitative PCR showed expression of SMAD2 and 3 at 3% O_2 increased relative to hESC at 20% O_2 (ai) and iPSC (bi) Upon TGFB receptor activation, phosphorylation of SMAD2/3 messengers signals activation and transcriptional regulation of downstream targets. A significant increase in phosphorylated SMAD2/3 (relative to phosphorylated and non-phosphorylated forms of the protein) in hESC at 3% O_2 was observed after 3 days in hESCs (aii, iii) but not in iPSCs (bii, iii).*

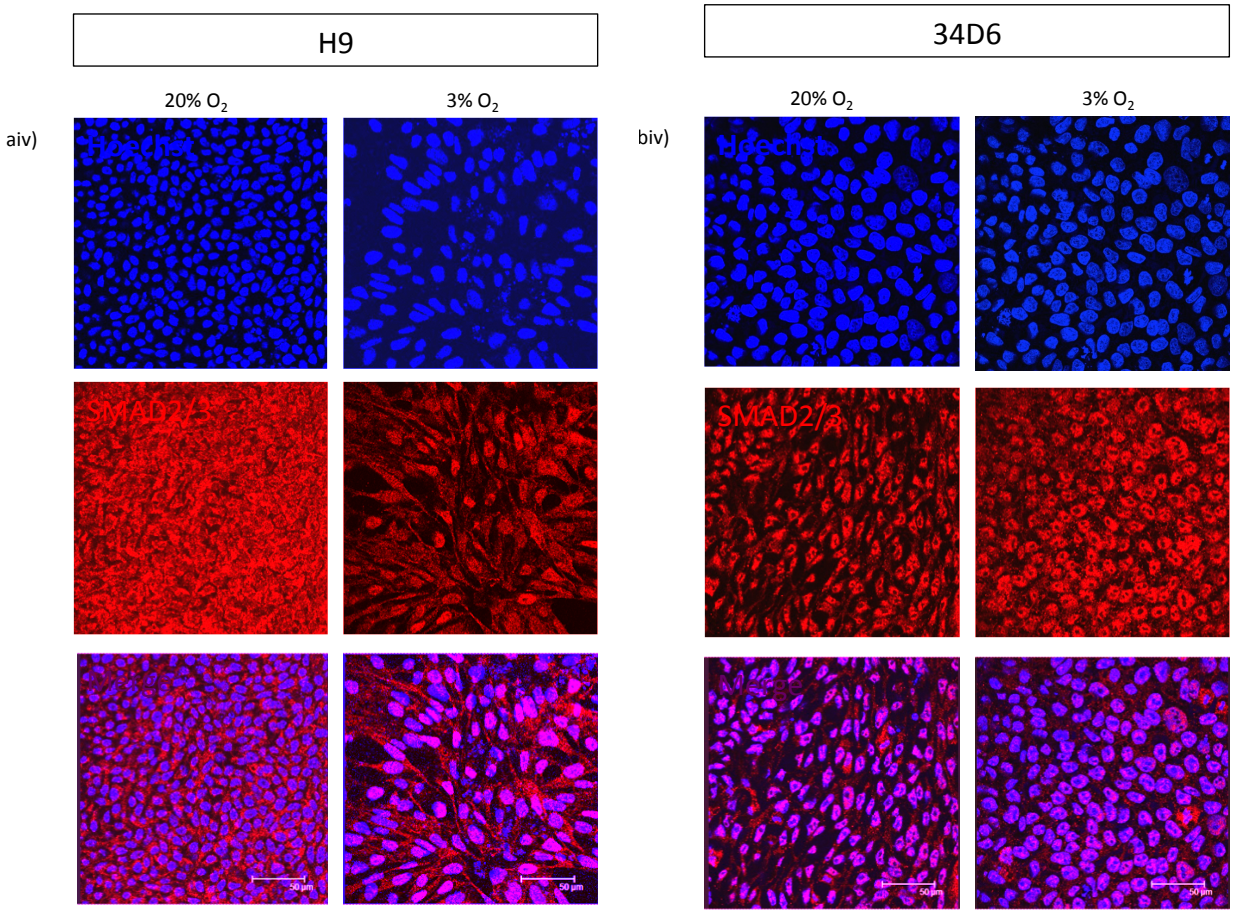

Figure 3.14. Low oxygen induced increased nuclear translocation of SMAD2/3 was cell line dependent. *Immunofluorescence of SMAD2/3 (red, staining both phosphorylated and non-phosphorylated forms) showed increased levels of co-localisation with nuclear stain (blue) at 3% O_2 in hESC (a) but not in iPSC (b).*

Previously, an increase in the relative amounts of gene transcription of NANOG, SOX2 and POU5F1 were observed in both the hESC (*3.10a*) and the iPSC lines (*3.10b*) but this was not reflected in the proportion of cells retaining expression of SSEA4. Confocal microscopy was used here to assess the intensity of protein staining of the aforementioned markers to see if an increase in transcription related to an increase in protein on a cell-by-cell level. Staining of both POU5F1 and NANOG appeared more intense at 3%-O_2 relative to 20% O_2 in hESCs (*3.12a*) but not in iPSC (*3.12b*). Staining of SOX2 remained constant in both cell lines, across both O_2 concentrations.

Upstream of NANOG and POU5F1 are a number of regulatory signalling networks. Previous reports suggested a direct interaction between HIF1A and SMAD3,

coordinating to drive gene transcription (Zhang et al. 2003; Sánchez-Elsner et al. 2001). As abolishment of SMAD2/3 phosphorylation has previously resulted in reduced NANOG and POU5F1 expression, both of which are now recognised as direct transcriptional targets of Phos-SMAD2/3, levels of SMAD2/3 signalling were examined here (Stewart et al. 2006; Xu et al. 2008; James et al. 2005),. Transcription of *SMAD2* and *SMAD3* was increased relative to that at 20% O2 in both hESC (*3.13ai*) and iPSC lines (*3.13bi*). Additional to augmented *SMAD2/3* transcription, western blots of hESC lysate showed an increase in the relative amount of SMAD2/3 phosphorylation (normalised to phosphorylated and non-phosphorylated forms of the protein) at 3% O2 (1.0±0.11) relative to 20% O2 (0.64±0.03, t(4)=3.1, p=0.036). Confocal microscopy of SMAD2/3 immunofluorescence also showed an increased tendency towards nuclear localisation (*3.14a*), correlating with a shift towards the active form of the protein. IPSC lysates showed no alteration to SMAD2/3 phosphorylation at 3% O2 (t(4)=0.52, p=0.63, biii) or in nuclear translocation (*3.14b*), indicating again, a cell line dependent response to reduced oxygen concentration.

3.3 Discussion

Maintaining pluripotent stem cells in a physiologically relevant oxygen concentration has great potential to aid the often costly and time-consuming process of culturing PSCs, in addition to improving cells for subsequent differentiation. Unfortunately, previous studies examining this issue were frequently contraindicatory, contributed to by the use of a variety of PSC lines and culture methods. Based on this, we confirmed that viability, proliferation and pluripotency of the H9 hESC line and 34D6 iPSC line were maintained during culture in low oxygen. Use of both ESC and iPSC lines allowed discrimination between those effects which may be uniform across PSCs and those which may be cell line specific.

3.3.1 Expression and nuclear translocation of HIFA and PHD subunits are responsive to 3% O_2.

The timeframe of HIF1A stabilisation in hESC in previous studies varied between 12-48 hours of low oxygen exposure before protein expression retreated to below detectable levels (Forristal et al. 2010; Francis & Wei 2010; Cameron et al. 2008). This variability was likely due to the use of multiple hESC lines (HUES7, UCO6 and HESCs and variations in the O_2 concentration applied (5%, 0.1% and 5%, respectively). Forristal et al also showed protein expression of 2A and 3A subunits to be up-regulated long term after exposure to low oxygen (Forristal et al. 2010). It is worth noting that definitions of the O_2 concentration refers to the gaseous phase of the chosen incubator only; the type of cell culture dishes, volume of media used and the confluency of the cells will all have contributed to determining the actual pericellular O_2 concentration. This study showed HIF1A stabilisation and nuclear localisation peaking between 2-12 hours in both PSC lines examined. In iPSCs, HIF2A protein was constitutively expressed at 20% O_2 with no up-regulation by 48 hours at 3% O_2 although nuclear localisation could not be determined. Cells at 20% O_2 also showed constitutive expression of HIF2A in hESCs, however, expression was variable after introduction to 3% O_2, with an initial observed reduction at 2 hours and a transient increase at ~6 hours. Unfortunately, immunofluorescence for HIF2A to determine nuclear translocation could not be performed as the antibodies examined showed non-specific staining which was non-responsive to HIF2A siRNA knock-down, hence not specifically binding the target protein. It is worth noting that the only paper examining both HIF1A and 2A expression in the H9 cell line also observed high HIF1A protein expression at 24 hours after introduction to 4% O_2 and residual expression 7 days after which is also contraindicatory to prior reports (Närvä et al. 2013). Likely this is partly underlain by variations in cell line identity drift, cell culture conditions or methods of controlling O_2 concentrations. That said, analysis of HIF1A and 2A expression profiles at low oxygen across multiple hESC and iPSC lines is worthy of further investigation.

Additional to a role for Prolyl-hydroxylases in marking HIFA subunits for pVHL mediated degradation in high oxygen, Jokilheto et al implicated PHD2 in the down-regulation of nuclear HIF1A in adenocarcinoma and HeLa cells, (Jokilehto et al. 2010). This was later observed in an osteosarcoma cell line, whereby forced nuclear expression of PHD2 inhibited HIF1A protein expression (Pientka et al. 2012). Here, PHD2 showed transient nuclear localisation in hESCs and iPSCs, peaking 2-6 hours after introduction to 3% O_2, retreating to cytoplasmic localisation by 24 hours. The corresponding timelines of nuclear localisation between HIF1A and PHD2 are concordant with this additional function for PHD2.

3.3.2 Apoptosis at 3% O_2 was augmented by exposure to light.

The use of reduced O_2 concentration was examined here in a bid to more accurately reflect the physiological O_2 concentration of PSCs and investigate the manipulation of O_2 in augmenting proliferation and self-renewal of PSCs. That said, it is recognised that restricting the oxygen concentration of cells *in vitro* often leads to increased apoptosis (Sermeus & Michiels 2011). HIF1A and 2A subunits have been linked to augmentation and suppression of pro-apoptotic factor p53 (Sermeus & Michiels 2011; Das et al. 2012) and although Mazumdar et al. reported a decrease in apoptosis of mESC at 5% O_2, no data on the viability of human PSCs have been reported (Mazumdar et al. 2010).

To maintain a consistently low oxygen environment throughout the entirety of the experimental timecourse, a fully enclosed workstation was used to allow constant gaseous environmental control during cell culture manipulation and incubation (*Figure 2.2*). Due to its transparent front screen, I additionally investigated whether exposure to light was negatively effecting cultures and underlying the high apoptosis rate observed throughout long term passaging experiments.

Initially, I assessed the proportion of live hESCs positive for the apoptotic marker AnnexinV, a process requiring dissociation of cells into a single cell suspension and live cell staining (phosphatidylserine is constitutively expressed on

the inner leaflet of the cell membrane, use of live cells ensured binding of AnnexinV to the outer leaflet only). Human PSCs are extremely sensitive to dissociation and the extremely high basal rates of apoptosis at 20% O_2 raised concerns over the suitability of the assay (Gauthaman et al. 2010). The use of TUNEL staining allowed for quantification of apoptosis rates whilst avoiding the trauma of colony dissociation. Whereas AnnexinV assays must be performed on a flow cytometer for accurate separation of apoptotic and non-apoptotic cells, the morphology associated with TUNEL positive cells allowed for high throughput image analysis. Using this method, adherent cells could be analysed with little departure from their normal state and significantly less interference from external sources. This hypothesis was confirmed through comparison of the two methods; a reduction from 13.2±2.2% AnnexinV+ cells to 1.43± 0.58% of TUNEL+ cells at 20% O2, more aptly reflecting the low levels of apoptosis observed throughout cell culture and signifying dissociation-related induction of apoptosis.

Exposure of cell culture to light has long been acknowledged as detrimental, inducing oxidative stress, chromosomal abnormalities and apoptosis through augmented ROS and H_2O_2 production (Wood et al. 2008; Grzelak et al. 2001; Halliwell 2003; Parshad et al. 1978). Although partially dependent on the constituents of cell culture media with inclusion of antioxidants such as glutathione and catalase attenuating phototoxicity (Parshad et al. 1978; Wood et al. 2008), studies in an array of cell lines showed light induced cytotoxicity occurring independent of the cell culture media (Grzelak et al. 2001; Parshad et al. 1978; Stoien & Wang 1974). Proportions of TUNEL+ cells between 20% and 3%-Dark were comparable in both cell lines, hence the heightened apoptosis at 3%-Light in both hESC and iPSC indicated light exposure was the underlying cause, and 3% O_2 was not the cause of reduced viability. This exposure to light also conceivably underlay the rise in apoptosis during long-term comparison of 20% and 3% O_2, which was performed at 3%-Light.

3.3.3. Proliferation of hESCs and iPSCs was differentially affected by 3% O_2.

Previous reports have outlined interactions between the HIFA subunits and cell cycle regulators, in addition to altered proliferation of cell lines at reduced O_2. Cancer and ESC lines deficient in HIF1A activity up-regulated p27 and p21 through attenuation of c-myc activity, triggering cell-cycle stall and G0/1 accumulation (Koshiji et al. 2004; Gardner et al. 2001; Carmeliet et al. 1998). HIF2A activity increased movement through the S-phase by boosting transcription of c-myc target genes (Gordan et al. 2007). Concordantly, silencing of HIF2A in hESCs resulted in reduction in cell number, colony diameter and Ki67 expression at 5% O_2 (Forristal et al. 2010). Additional studies on the proliferative effect of maintaining PSCs in reduced O_2 are mixed and often reliant on imprecise quantification methods (Ezashi et al. 2005; Forristal et al. 2010; Zachar et al. 2010; Cameron et al. 2008; Chen et al. 2009; Prasad et al. 2009; Mazumdar et al. 2010). Here, PSCs were precisely categorised as undergoing either G0/1 or G2/M. The hESC line was resistant to alterations in proliferative activity at 3% O_2, both in the long (15 days) and short (2 days) term, in the light and dark. However, the iPSC line consistently shifted cells towards cell duplication and division at 3% O_2, regardless of light exposure. Whether this inclination towards active proliferation was resultant of the reprogramming process itself has not been determined. Reprogramming of this line did involve random genomic integration of (amongst others) c-myc, hence feasibly having downstream effects on proliferation but silencing of the exogenous gene in the resulting pluripotent iPSC line was ensured (Bilican et al. 2012). That said, mesenchymal stromal cells reprogrammed without exogenous gene integration produced iPSC with augmented c-myc activity and reprogrammed MSCs showed augmented c-myc transcription at 5% O_2 (Foja et al. 2013; Marchetto et al. 2009). Further examination of c-myc activity in a wider range of hESC and iPSC lines was outside the scope of this study, but may clarify if this disparity in oxygen induced G2/M entry was resultant of the reprogramming process itself.

3.3.4. HESC at 3% O_2 showed augmented self-renewal signalling.

The main objective when maintaining pluripotency of stem cells in culture is to maximise the proportion of the population which have retained a pluripotent identity. To this end, many investigations have been made into optimising and homogenising cell culture techniques. (Dick et al. 2011; Rajala et al. 2010; Okada et al. 2010; van der Sanden et al. 2010). Pluripotent stem cells retain qualities reflective of a transient embryonic cell population formed *in vivo* at ~3-5% O_2 (Ottosen et al. 2006; Fischer & Bavister 1993; Kumar 2010), hence maintaining PSCs in low oxygen may support maintenance of a pluripotent state. This was addressed here by investigating the expression of key pluripotency regulators both at a transcriptional and translational level. As even minor (~2-fold) changes to protein levels of POU5F1 modulate directed differentiation towards endo- and meso-dermal lineages. (Z. Wang et al. 2012; Niwa et al. 2000), I focused on the proportion of cells which sustained expression of key pluripotency markers, in place of protein concentration throughout the entirety of the population through methods such as western blots.

Various pathways converge to maintain pluripotency of PSCs, including the Activin/Nodal arm of the TGFβ pathway. Once activated through phosphorylation, downstream transcription factors SMAD2 and 3 (Shi & Massagué 2003), act to regulate transcription of NANOG and POU5F1 directly (Stewart et al. 2006; Xu et al. 2008). The three key transcriptional regulators examined here, NANOG, POU5F1 and SOX2, also co-regulate expression of each other. POU5F1 and SOX2 have adjacent binding sites in the promoter region of NANOG (Kuroda et al. 2005; Rodda et al. 2005) and NANOG feeds back to modulate POU5F1 and SOX2, outlined in *Chapter 1.2* (Loh et al. 2006). In addition to regulatory control from other arms of the pluripotency signalling network, accumulating evidence indicates a critical role for HIF subunits in regulating the transcription of these genes. It's been shown that both POU5F1 and SOX2 contain HRE sites within their promoters which HIF2A binds (hypothesised to be as a heterodimer with HIFβ), resulting in augmented gene transcription (Moreno-Manzano et al. 2010; Covello et al. 2006). Cells under reduced O_2 or with constitutive HIFA expression have

correspondingly shown increased transcription of these three vital pluripotency regulators (Foja et al. 2013; Ji et al. 2009; Prasad et al. 2009; Forristal et al. 2010) although not all studies agree (Chen et al. 2009; Zachar et al. 2010). Here, transcription of NANOG, POU5F1 and SOX2 in hESCs and iPSCs was examined after 3 days introduction to 3% O_2 both in the light and dark and normalised to that at 20% O_2. Maintenance of hESCs at 3%-Light attenuated transcription of NANOG and POU5F1 compared to 3%-Dark, contrastingly to iPSC whereby transcription of all 3 genes at 3% O_2 was equivalent. Additionally, transcription of NANOG and POU5F1 at 3% O_2 exceeded a ratio of 1.0 in both iPSCs and hESCs at 3%-Dark with SOX2 transcription in iPSC also exceeding this limit, indicating transcription exceeded that at 20% O_2.

Although transcriptional data are useful, they do not necessarily equate to increased homogeneity of a pluripotent population. Little quantifiable data have been reported on whether reduced O_2 is useful in optimising the proportion of a population classified as 'pluripotent'. Maintenance of mesenchymal stem cells at 5% increased the number of NANOG+ and POU5F1+ cells (Foja et al. 2013) and HIF1A expression with hESC increased the number of Alkaline Phosphatase colonies but whether this was due to increased clonality is uncertain (Ji et al. 2009). The majority of remaining studies relied on morphological assessment of PSC colonies which, although a useful indicator, would be subject to bias (Chen et al. 2009; Chen et al. 2010; Prasad et al. 2009; Forristal et al. 2010; Zachar et al. 2010; Ezashi et al. 2005). Flow cytometry and confocal microscopy of immunofluorescence were used here to quantify the proportion of the population positive for POU5F1, NANOG, SOX2 and SSEA4, reliable markers for pluripotent stem cells (Adachi et al. 2010; Draper et al. 2002; Henderson et al. 2002; Rodda et al. 2005; Stewart et al. 2006; Thomson 1998; Z. Wang et al. 2012). Again, hESCs and iPSCs showed differing effects of 3% O_2. IPSC showed consistent decrease in the proportion of cells retaining SSEA4 expression at 3% O_2 and attenuated intensity of transcriptional regulators. Contrastingly, the percentage of SSEA4+ hESCs remained constant in the short-term and NANOG+, POU5F1+ and SOX2+ remained steady in the long-term, across O_2 concentrations. Additionally, intensity

of staining assessed by Confocal microscopy was constant or increased at 3% O_2. This outlines a differential response to reduced O_2 between the hESC and iPSC lines, with H9 being more resilient to changes in oxygen concentration.

Interestingly, a statistically significant decrease in SSEA4+ cells was seen at 3%-Dark, relative to 3%-Light in the iPSC line only (*3.11b*). One hypothesis is that exposure to light and a resulting increase in oxidative stress due to ROS and H_2O_2 production, acted as a population selector in this line. George et al. observed that pluripotent hESC had higher resilience towards light or H_2O_2 induced oxidative stress than their spontaneously differentiated progeny (George et al. 2009). It is feasible that cells which had undergone spontaneous differentiation at 3%-Light, underwent apoptosis more readily, therefore increased the proportion of pluripotent, SSEA4+ cells. Whether the differences between cell lines is based on intrinsic differences in how iPSC and hESC respond to cell stressors is unclear, and outside the scope of this study.

As NANOG, SOX2 and POU5F1 showed increased intensity of staining in hESCs but not iPSC, I examined an upstream regulator. In previous studies, human endothelial cells at 1% O_2 increased phosphorylation of upstream regulators SMAD2/3 with concordant nuclear translocation, outlining a process whereby HIF1A and SMAD3 directly interact to additively augment transcription of downstream targets (Zhang et al. 2003; Akman et al. 2001; Sánchez-Elsner et al. 2001). Chen et al also observed augmented SMAD2/3 phosphorylation in hESC at low O_2 (Chen et al. 2010). Transcription of *SMAD2* and *SMAD3* was increased at 3% O_2 in both cell lines, relative to 20% O_2. It is worth noting that SMADs primarily operate through phosphorylation mediated cycles of activation and inactivation and are not solely reliant on transcriptional up-regulation (Shi & Massagué 2003). HESC did show a significant shift in SMAD2/3 signalling towards the phosphorylated form at 3% O_2 relative to 20% O_2, both in the total protein concentration in the entirety of the population and through increased nuclear localisation, indicative of transcriptional activity. It is safe to assume that the increased phos-SMAD2/3 signalling contributed to the augmented NANOG, SOX2 and POU5F1 protein intensity and transcription.

The iPSC however showed no difference in either total protein or in nuclear localisation across oxygen concentrations. This lack of response in an upstream pluripotency regulator is concordant with the negligible alteration to observed NANOG, POU5F1, SOX2 protein intensity and the attenuated proportion of SSEA4+ cells.

3.4. Summary

Here, I sought to investigate and confirm the effects of 3% O_2 and light exposure using 2 separate pluripotent stem cell lines. It is evident from comparing cultures at 3% O_2 in the dark and exposed to light, that light exposure is detrimental to hESC and iPSC cultures. All future directed differentiation of hESC and iPSC will be undertaken in light protected incubation. 3% O_2 did not reduce apoptosis to below that at 20% O_2 in either cell line. Maintaining a pluripotent population was not enhanced by physiological oxygen levels in hESC, and was even detrimental in iPSCs with a significant decrease in the proportion of cells positive for the pluripotent stem cell marker SSEA4. An increase in the activation of TGFβ signalling was observed in hESCs at 3% O_2, possibly through a HIF1A dependent mechanism and possibly enhancing malleability for directed differentiation. This will be addressed in the following chapter, as it is feasible that embryonic O_2 levels are more relevant to development and patterning than to maintenance of a pluripotent state.

4. The role of physiological oxygen in early neuronal differentiation of hESC.

4.1 Introduction

Previously, I investigated the effect of 3% O_2 on maintaining pluripotent hESCs and iPSCs in short and long term timeframes (3 days and 15 days respectively) compared to culture at 20% O_2. Due to the equipment necessary for accurate control of oxygen concentration, cultures at 3% O_2 were exposed to light and a direct comparison of hESCs and iPSCs protected from and exposed to light at 3% O_2 confirmed augmented apoptosis due to light exposure. Consequently, all further experiments examining the effects of low oxygen on the neural patterning and differentiation of hESCs were performed at 3% O_2, protected from detrimental light exposure.

4.*1.1 Oxygen concentration and early neural development, in vivo.*

As detailed in section *1.9*, oxygen gradients and HIF response elements exist *in vivo* acting to regulate normal neural development, from post-fertilisation patterning through to response of adult NSCs after neurological trauma. During early embryonic development, oxygen concentration in the mouse brain was shown to reside at 1-3% O_2 (Mutoh et al. 2012; Lee et al. 2001; Chen et al. 1999; Zhou, Z 2004). These gradients in O_2 concentration have been heavily implicated in functionally and morphologically normal neural development. Although using non-physiological O_2 concentrations during the maturation of explanted blastocysts, in addition to HIF mouse knockouts, have extensively established an association between oxygen concentration and morphologically normal neural plate and tube formation, little work has been done translating these findings into an *in vitro* setting, particularly with human PSCs (Chen et al. 1999; Morriss & New 1979; Iyer et al. 1998; Ryan et al. 1998; Kozak et al. 1997; Tung & Winn 2011; B. Zhang et al. 2010). It has been shown that NPCs derived from mESCs formed higher densities

of rosettes, possibly due to augmented proliferation (Horie et al. 2008; Mondragon-Teran et al. 2009; Studer et al. 2000; Le Belle et al. 2011; Storch et al. 2001; Rodrigues et al. 2010). Additionally, Stacpoole et al also demonstrated increased numbers of NPCs produced at 3% O_2 (Stacpoole et al. 2011a). In light of this information, 3% O_2 was used here to reflect the estimated physiological oxygen concentration during the early neural induction of hESCs.

4.1.2 Neural induction of in vitro pluripotent stem cells.

Many protocols have been outlined for inducing PSCs towards a neural fate *in vitro (reviewed in section 1.8)*. As the state of pluripotency allows for direction towards any adult cell type, guiding cell fate specifically towards the formation of a consistent population with a homogenous identity can be a major obstacle, which previously required selection of NPCs from mixed populations. Reflecting the *in vivo* neuralising signals *in vitro* has since been shown to increase efficiency of neural induction. Addition of NOGGIN to hESCs, an inhibitor of BMP/TGFβ signalling known to be secreted by the Primitive Node *in vivo*, shortened the timeframe of NPC production and augmented efficiency of neuralisation (Gerrard, Rodgers, et al. 2005; Itsykson et al. 2005). This was further developed by the supplementary addition of SB431542, an inhibitor of Activin/Nodal/TGFβ signalling, inducing production of NPCs with little contamination of cell types from unwanted lineages (Chambers et al. 2009). It has since been demonstrated that by mimicking the dual inhibition of the Activin/Nodal and BMP arms of TGFβ signalling present during gastrulation *in vivo (section 1.7)*, PSCs *in vitro* were efficiently differentiated to form a homogenous population of NPC's and neural rosettes, reflective of the *in vivo* neural plate and tube (Chambers et al. 2009). Dual inhibition of TGFβ signalling using small molecule inhibitors was used here to induce formation of NPCs, both as a monolayer and embryoid bodies (EBs). By mimicking both trophic signalling and O_2 concentration, reflective of embryonic neural induction, I investigated whether O_2 could be used as an additional tool to drive a neural identity.

4.1.3 Defining a neuroectodermal identity.

A number of markers were used here to characterise NPC populations, namely PAX6, NESTIN and SOX2, co-expression of which have been widely recognised as markers of an early neuroectodermal identity (Chambers et al. 2009; Gerrard, Rodgers, et al. 2005; Cai & Grabel 2007; Zhao et al. 2013; Smukler et al. 2006; Malchenko et al. 2014).

PAX6 is recognised as a transcriptional regulator, classed as part of the 'paired-box' family of transcription factors which contain both a homeo-DNA binding domain and a paired-box domain allowing co-binding with other regulators (Jun & Desplan 1996). PAX6 becomes homogeneously expressed during the neural progenitor stage of development (X. Zhang et al. 2010). Expression emerges as the neural plate forms and is maintained through to when the neural tube becomes compartmentalized into fore-, mid-, hind-brain and spinal cord (Inoue et al. 2000). When the dorsal and ventral telencephalon separate, expression is retained throughout the border of the two territories as well as in the neurogenic dorsal ventricular zone, mostly regressing as cells mature (Hirata et al. 2002). Specific regions of the postnatal brain retain expression, including the SGZ and SVZ stem cell niches which bear responsibility for neurogenesis throughout adult life (Osumi et al. 2008). A role for this transcription factor in directly promoting neuronal differentiation has been indicated, $PAX6^{-}/^{-}$ mutant mice models showed drastically reduced neuron production (Osumi et al. 2008). Additionally, hESC lines with RNAi mediated PAX6 inhibition failed to form neuroepithelial cells or βIII-Tubulin positive neurons (X. Zhang et al. 2010). These disruptions to production of progenitors and neurons indicated a dual role for PAX6 in regulating proliferation and directing differentiation (Quinn et al. 2007). Therefore, PAX6 has been recognised as an early neural marker, specific to populations which have retained multipotent plasticity and remain malleable for further differentiation. As early neuroepithelial cells have been shown to express PAX6 earlier and in a more uniform manner than SOX1, it was used here as a reliable marker of neural progenitor cells in conjunction with NESTIN and SOX2 (X. Zhang et al. 2010).

The intermediate filament NESTIN, which has been implicated in normal development of the neural tube and has specific, transient expression in NPCs and NSCs *in vivo*, was also used here to classify cells as having a neuroectodermal identity. NESTIN has been characterised as an intermediate filament protein with two main functions. The first as a structural role in the cytoskeleton, involved in remodelling the intermediate filaments during mitosis (Michalczyk & Ziman 2005). Additionally, NESTIN has been implicated in viability and proliferation of the developing neural tube. NESTIN null mouse models developed with depleted levels of NSCs due to a loss of self-renewal and high rates of apoptosis. Its expression in neural cells was also linked exclusively with NPCs and NSCs, becoming down-regulated upon differentiation to terminal neurons (Park et al. 2010; Hendrickson et al. 2011)

Finally, as well as being representative of a pluripotent state when co-expressed with NANOG and POU5F1, sole expression of SOX2 has been widely recognised as representing a neuroectodermal identity with roles in regulating the self-renewal and proliferation of NSCs (Z. Wang et al. 2012; Zhang & Cui 2014; Graham et al. 2003; Bylund et al. 2003; Smukler et al. 2006). In the chick neural tube, forced expression of SOX2 prevented NPC differentiation (Graham et al. 2003; Bylund et al. 2003). Additionally, the ability of pro-neural factor NGN2 to trigger differentiation was dependent on inhibition and down-regulation of SOX2 (Bylund et al. 2003). Hence, SOX2 in conjunction with NESTIN and PAX6 was used to characterise cells as being neural progenitors, reflective of those found in the neural plate and tube.

By the application of Activin/Nodal and BMP TGFβ inhibition (hereafter referred to as dual-SMAD inhibition), investigation into the effect of early neural induction at 3% O_2 was performed. The combinatory use of the markers detailed above was used here to characterise the early NPC population produced, allowing investigation into whether the combination of physiologically relevant trophic signalling and O_2 concentration augmented homogeneity and efficiency of NPC production and hence, whether low oxygen was a useful tool for augmentation of neural induction.

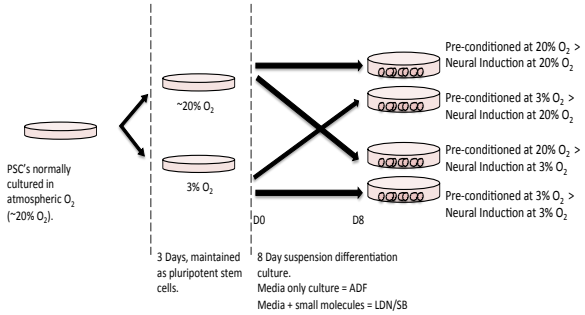

Figure 4.1. Experimental protocol with relevant nomenclature. *Pluripotent hESC (H9s) were preconditioned at 20% or 3% O_2 for 3 days, neuronal differentiation was then initiated in the same or alternative O_2 concentration.*

4.2 Results

4.2.1 Experimental cross-over between oxygen concentrations.

Dual inhibition of the Activin/Nodal and BMP arms of TGFβ signalling was applied here using combined treatment of 10μM SB431542 (an inhibitor of SMAD2/3 activation, repressing pluripotency) and 0.5nM LDN193189 (an inhibitor of SMAD1/5/8 activation, suppressing epidermal and neural crest differentiation from the ectoderm) (Inman et al. 2002; Hjelmeland et al. 2004; Boergermann et al. 2010; Ying & Smith 2003). As *Section 2.2* indicated augmented self-renewal in hESCs after 3 days at 3% O_2, I also investigated the effect of pre-conditioning at reduced O_2 prior to initiating neural induction. Pluripotent hESC were pre-conditioned at 20% or 3% O_2 for 3 days and subsequently underwent neural induction at either the same O_2 concentration or the other. The four combinations of oxygen pre-conditioning and differentiation are outlined in *Figure 4.1* and were defined as follows: 3% O_2 pre-conditioning, 3% O_2 neural induction (3>3); 3% O_2, 20% O_2 neural induction (3>20); 20% O_2 pre-conditioning, 20% O_2 neural induction (20>20); 20% O_2 pre-conditioning, 3% O_2 neural induction (20>3).

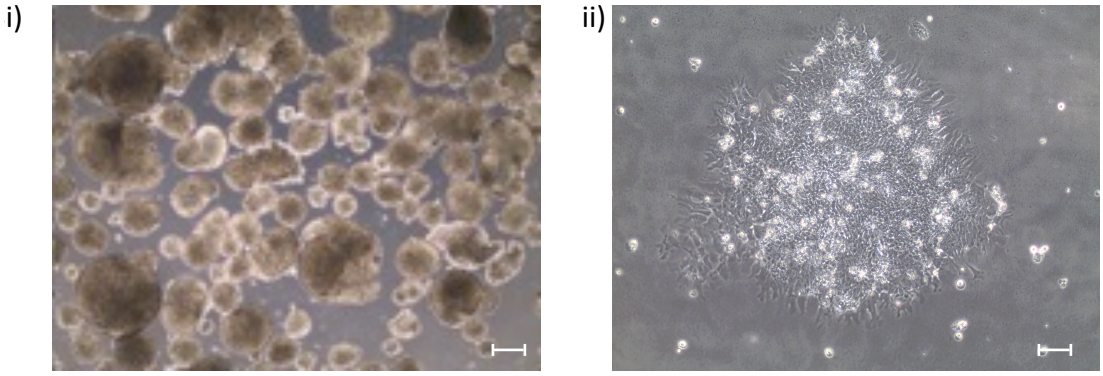

Figure 4.2 Representative images of hESCs after 8 day differentiation protocol under different conditions. *Upon initiation of dual SMAD inhibition, PSCs were either stimulated to form 3D cellular aggregates known as embryoid bodies (EBs) through culture in non-adherent plasticware (i) or maintained as monolayer colonies (ii). Scale bars show 200μm.4.2.2 Embryoid body based neural induction at reduced O_2.*

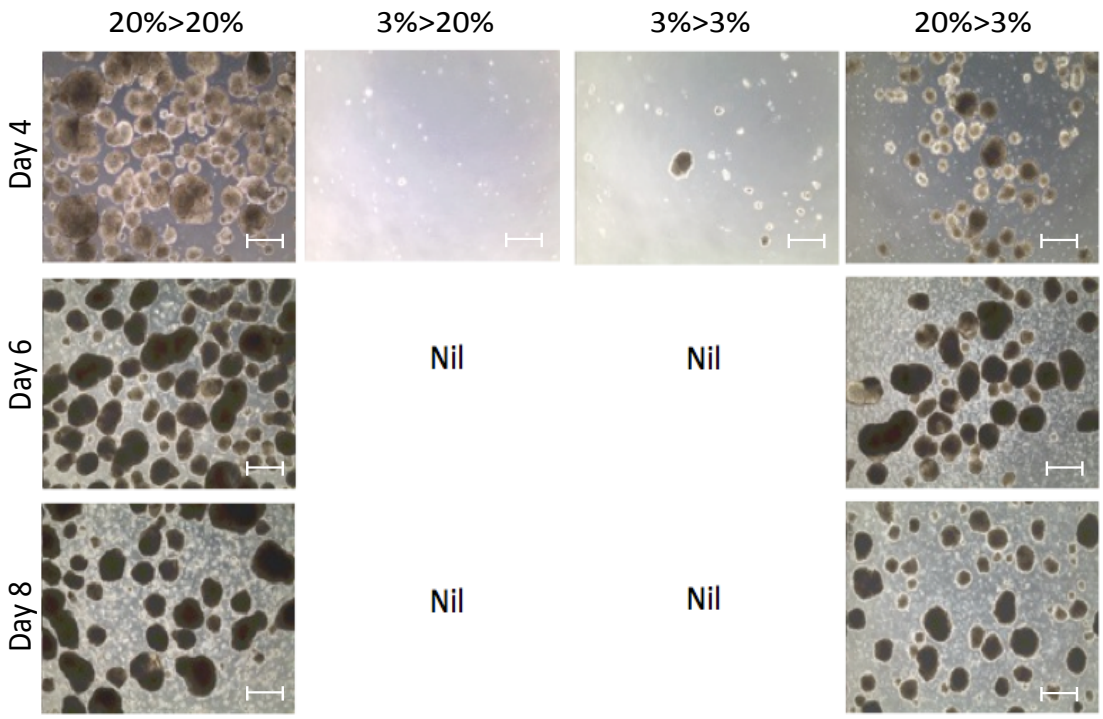

Figure 4.3. Pre-conditioning of hESCs at 3% O_2 was disadvantageous for neural differentiation in the form of Embryoid Bodies. *When differentiated as EBs with dual SMAD inhibition, those preconditioned in low oxygen (3>3 and 3>20) formed attenuated numbers of EBS. High oxygen pre-conditioned arms (20>20 and 20>3) formed typical embryoid bodies, n=2. Pictures are representative of EB density. Scale bars show 400μm.*

Traditionally, PSCs have often been differentiated as 3D suspension cultures, (*Figure 4.2i, section 1.8*) where cells in non-adherent culture conditions aggregate to form embryoid bodies (EBs). Initial experiments here aimed to induce EB formation at 20% and 3% O_2, after 3 days of pre-conditioning prior to dual SMAD inhibition

Surprisingly, pre-conditioning of H9 hESCs at 3% O_2, for three days prior to initiation of dual-SMAD inhibition, was severely detrimental to EB formation regardless of whether differentiation was later performed at 20% or 3% O_2. Both 3>3% and 3>20% O_2 showed a severe reduction of EB formation by D4 and a complete lack of EBs by D8 (*Figure 4.3*). Preconditioning at 20% O_2 showed no adverse effect on EB formation, whether neural induction was performed under 20% or 3% O_2.

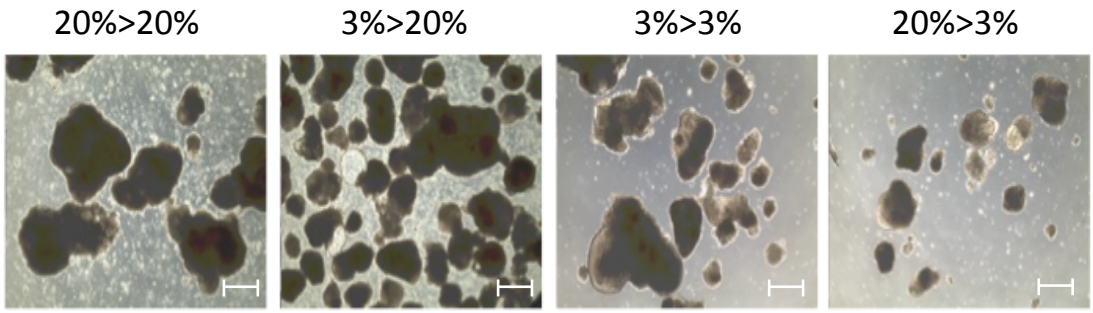

Figure 4.4. Pre-conditioning of hESCs at 3% O_2 was not disadvantageous for the formation of spontaneously differentiating embryoid bodies in basal media. *When induced to form embryoid bodies in basal media (i.e. without small molecule inhibition), all four arms formed and retained viable embryoid body structures up until the conclusion of the early 8-day differentiation protocol, although a reduction in number was observed after preconditioning at 3% O_2. Scale bars show 400μm.*

To investigate whether this attenuated EB formation was specific to neural induction, EB's were formed in basal media, without addition of dual SMAD inhibitors. After EB based differentiation in basal media *(Figure 4.4)*, EBs were formed in all four experimental conditions, although differentiation at 3% O_2 (experimental arms 20>3 and 3>3%) resulted in a marked decrease in the number of EBs obtained.

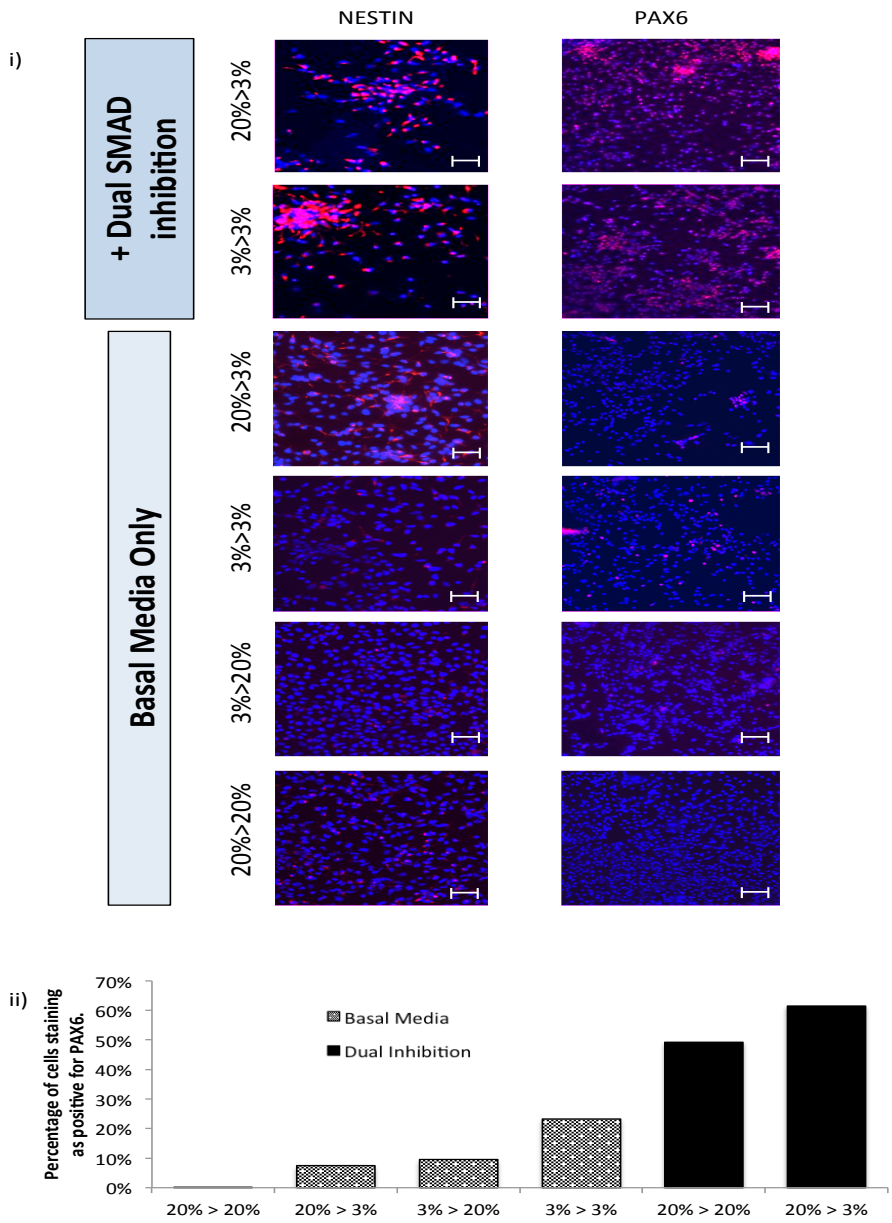

Figure 4.5 EB based differentiation performed at 3% O_2 tended towards increased production of PAX6+ cells. *At the conclusion of the 8 day, EB based, early neural differentiation protocol (both with and without dual SMAD inhibition), populations of cells characterised as neuroectodermal were formed (PAX6+, NESTIN+) in all combinations of oxygen concentration (i). The number of cells which stained positive for early neuroectodermal marker PAX6 (red) were counted, and normalised to all nuclei (blue). Differentiation performed at 3% O_2 resulted in augmented proportions of PAX6+ cells. n=2, statistics not performed. Scale bars show 50 μm.*

A number of markers have been shown to be indicative of multi-potent NPCs, *section 4.1.3*. Due to it's nuclear localisation, PAX6 was used here to quantify the

percentage of cells expressing this neuroectodermal marker. To allow quantification of the homogeneity of the population, at the conclusion of the 8-day differentiation protocol EB's were dissociated and reseeded onto glass coverslips for immunofluorescence (*section 2.1*). All 6 populations of cells formed PAX6+ and Nestin+ cells (*Figure 4.5i*). EBs produced in basal media showed an increase in the proportion of PAX6+ cells when pre-conditioned and differentiated at 3% O_2, up to 23.3% positive at 3>3 from ~8% positive in 20>3 and 3>20. When performed in conjunction with dual SMAD inhibition, the proportion of cells positive for PAX6 increased from 49.2% at 20>20 to 61.5% at 20>3 (*n=2, no significance testing*). Cell counts were performed using automated and unbiased software, which was technically difficult for use with cytoplasmically expressed proteins such as NESTIN, although rates of positive cells seemed comparable to that of PAX6.

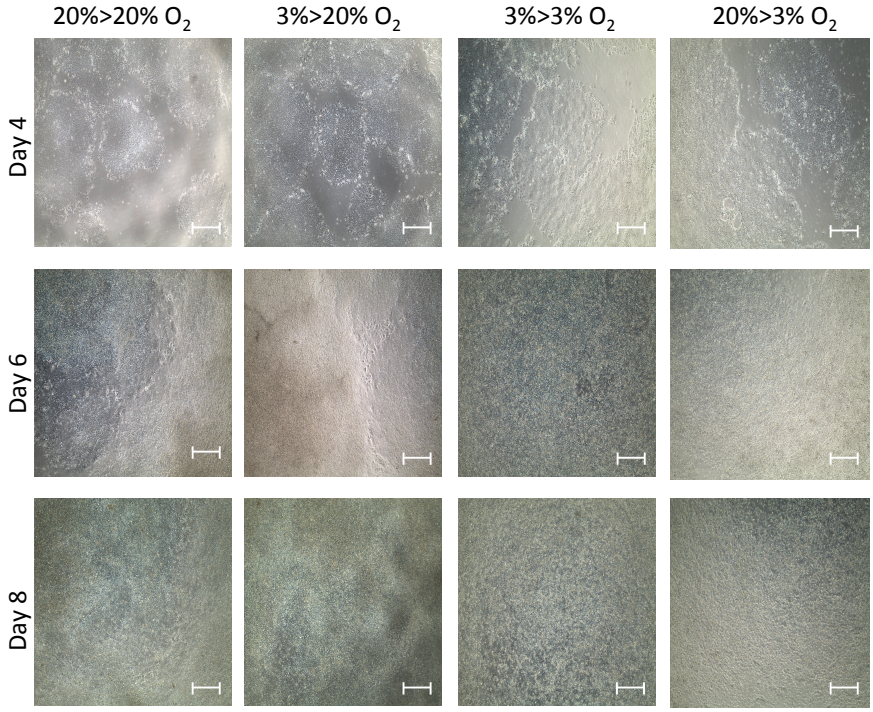

Figure 4.6 Monolayer neural differentiation of hESCs, with crossover between O_2 concentrations. *When neural differentiation was induced as monolayer cultures, all four experimental arms remained viable throughout. Scale bars indicate 200μm.*

4.2.3 Monolayer neural induction at 3% O_2.

It was indicated that neural induction at 3% O_2 augmented the production of NPCs. Upon further examination of D8 EB's, those formed at 3% O_2 were typically smaller and less numerous than those at 20% O_2. Hence, the augmented neural induction may have merely been a facet of relatively higher concentrations of SMAD inhibitors and not an effect due to reduced O_2. To circumvent this issue of EB based variability, dual-SMAD inhibition was applied as previously, but as a monolayer culture (*section 2.1, Figure 4.2ii*). When differentiation was performed as a monolayer instead of a 3D suspension culture *(Figures 4.2ii, 4.8)*, all four combinations of O_2 concentration continued to proliferate and remained viable up to D8, with no visible detrimental effect of preconditioning at 3% O_2 (*Figure 4.6*).

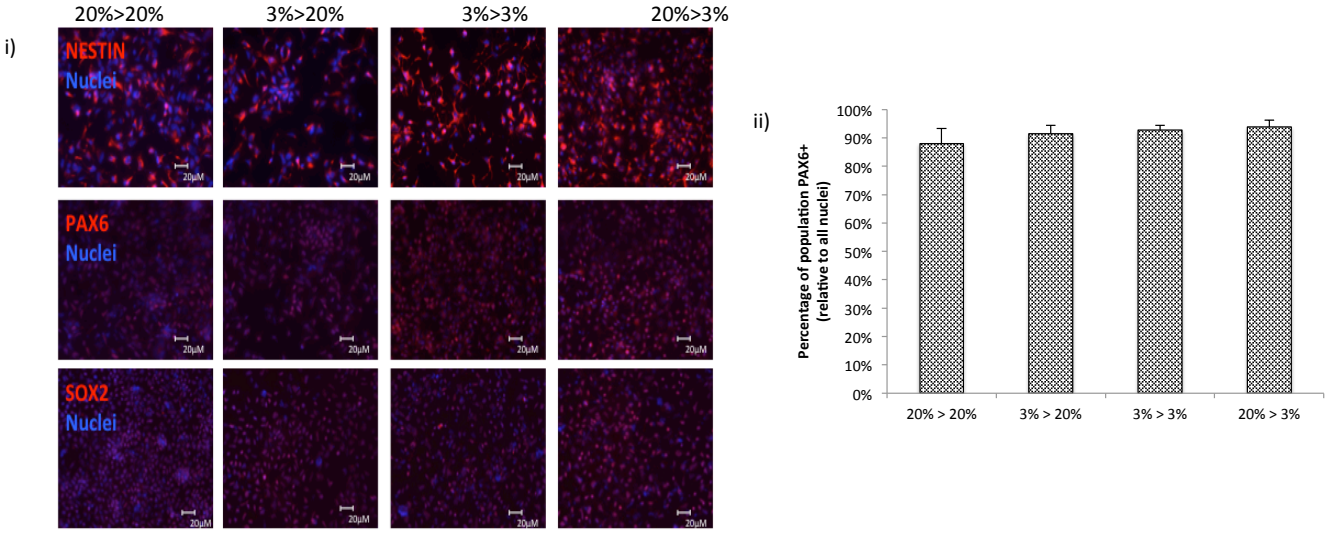

Figure 4.7. Formation of NPCs was comparable across O_2 concentrations. *All four O_2 combinations formed neuroectodermal populations in a highly reproducible and homogenous manner, with the vast majority of cells staining positive for PAX6, NESTIN and SOX2 (red) comparable to nuclei (blue) (i). The proportion of PAX6+ cells were comparable across O_2 concentrations (ii).*

All four combinations of O_2 concentration produced populations characterised as being of a homogenous neuroectodermal identity, with the vast majority of cells staining as positive for NESTIN, PAX6 and SOX2. Cell counts of the percentage of cells positive for PAX6 (relative to all nuclei) were comparable across O_2

concentrations, from 88.0±5.3% at 20>20 to 92.7±1.8% at 3>3. The proportion of cells expressing NESTIN could not be quantified, this intermediate filament showed typical cytoplasmic expression and hence accurate cell counts could not be attained. Additionally, as the vast majority of pluripotent H9 hESCs expressed SOX2 (*section 3.6, 3.7 and 3.12*), quantification of the proportion of SOX2 positive cells was deemed not to be specific to neuroectoderm, hence as a sole marker, unhelpful. However, as staining showed the vast majority of cells stained positive for both NESTIN and SOX2 in conjunction with the high rates of PAX6+ cells, the populations of cells were conclusively classed as being of an early neuroectodermal identity.

i)

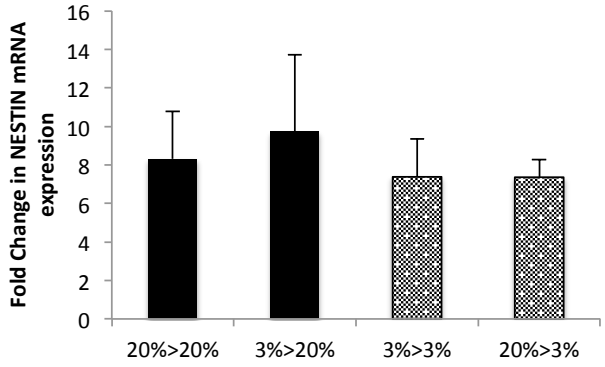

ii)

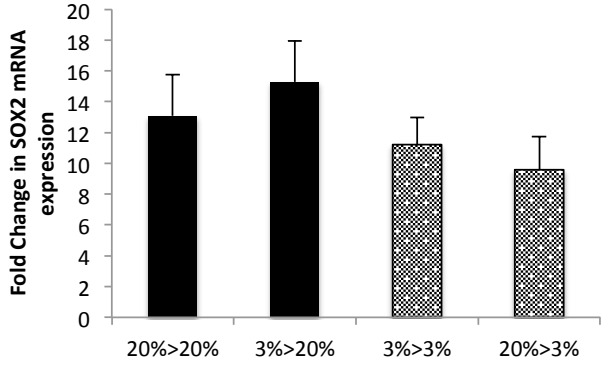

Figure 4.8. Neuroectodermal identity was consistent across all 4 experimental arms. *Semi-quantitative PCR of key neuroectodermal markers Nestin (i) and SOX2 (ii) showed no significant differences across experimental arms*

In addition to examining the proportion of cells expressing neuroectodermal protein markers, the transcription levels of these markers was also quantified, relative to a control sample (H9 hESCs differentiated to D8 without dual SMAD inhibition at 20% O_2) (*Figure 4.10*). Transcription of *NESTIN* (*i*) and *SOX2* (*ii*) was comparable across all O_2 concentrations, with no significant differences. Additionally, both genes showed transcription augmented far above a fold change

of 1, indicating augmented transcription of *NESTIN* and *SOX2* due to dual SMAD inhibition.

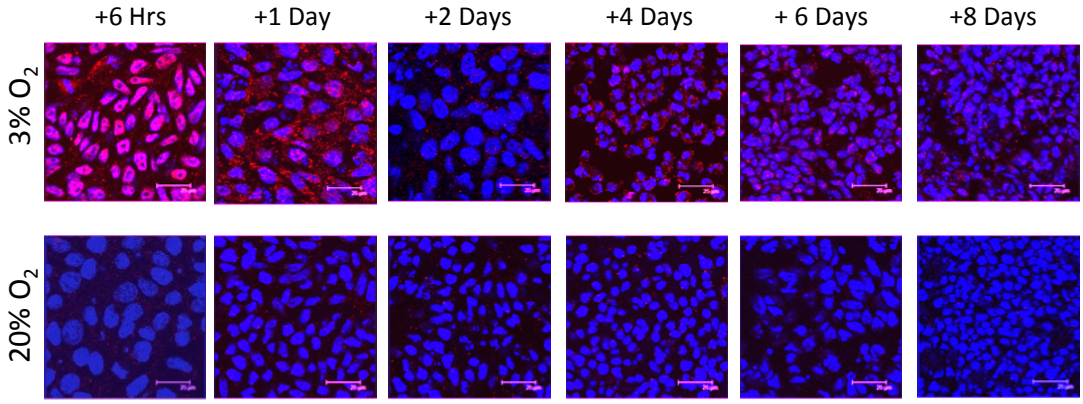

Figure 4.9. Stabilisation of HIF1A throughout differentiation protocol at 3% O_2. *The timeline of HIF1A induction was ascertained after introduction into 3% O_2, in concert with initiation of dual SMAD inhibition. Differentiation at 3% O_2 resulted in expected initial stabilisation of HIF1A (red) although low levels of expression persisted up to 8 days post introduction to 3% O_2. HIF1A expression was not evident at any point of differentiation at 20% O_2.*

4.2.4 HIF1A expression throughout early neural induction.

Roitbak et al. reported constitutive expression of HIF1A in telencephalic mouse NSC's, even when proliferated at atmospheric O_2 (Roitbak et al. 2008). This was concordant with HIF1A constitutive *in vivo* expression which was localised to neurogenic regions of the embryonic and adult brain, expression of which was required for NSC self-renewal and differentiation (Mazumdar et al. 2010; Huang et al. 2013). Hence, the expression of HIF1A in hESCs was examined during neural induction at 20% and 3% O_2. Reflective of pluripotent hESCs, NPCs at 20% O_2 showed no stabilisation or nuclear translocation of HIF1A throughout the differentiation process. When introduced into 3% O_2 in conjunction with initiation of dual SMAD inhibition, H9s showed typically high levels of HIF1A stabilisation and nuclear translocation, peaking after 6 hours. Protein levels subsided after this time but low levels of HIF1A expression, localised particularly in the nucleus, were observed in hESCs even after 8 days at 3% O_2.

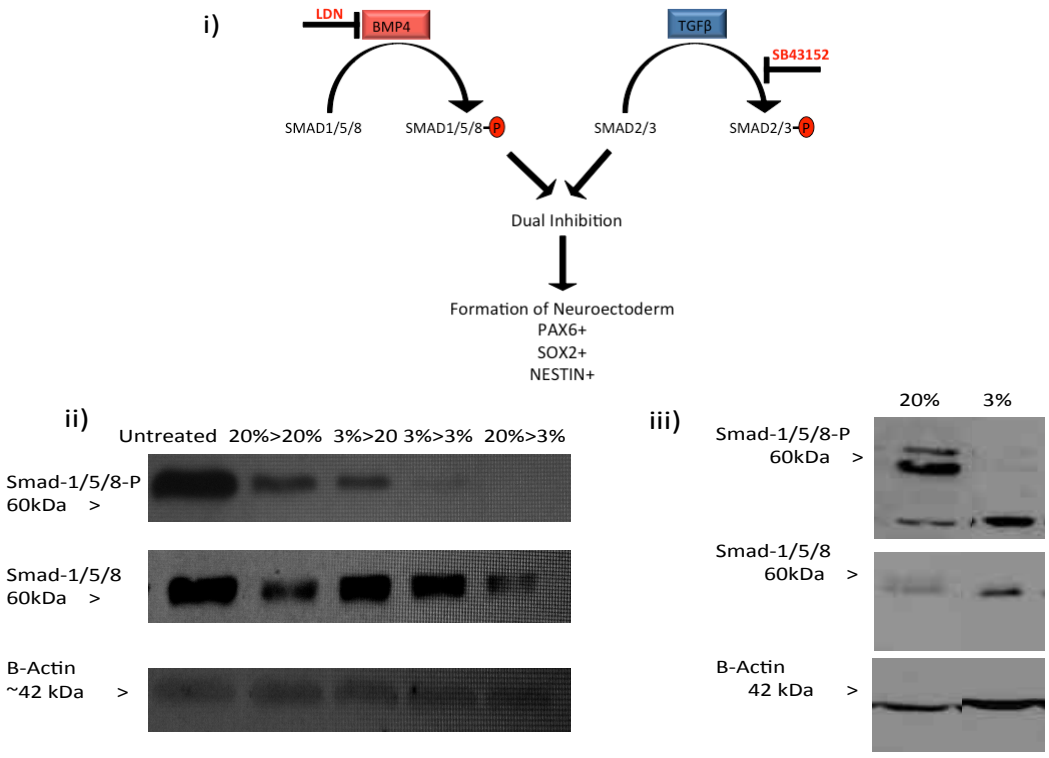

Figure 4.10 Differentiation at 3% O_2 augmented inhibition of BMP signalling, an essential aspect of neural induction. *Inhibition of BMP signalling is recognised as an essential step in formation of a neural identity (i), mimicked in vitro through use of small molecule inhibitor LDN193189. LDN193189 mediated inhibition reduced the amount of active messenger phosphorylated-SMAD1/5/8 compared to untreated control (ii) in all samples, but expression was completely inhibited by 3% O_2, regardless of preconditioning O_2 concentration. Concordantly, hESCs differentiated at 3% O_2 without exogenous BMP inhibition (iii) (basal media + SB431542 only) completely suppressed phosphorylation of SMAD1/5/8 in contrast to at 20% O_2 whereby phosphorylated SMAD1/5/8 persisted, n=2 for (iii) only.*

4.2.5 Inhibition of BMP signalling at 3% O_2.

As detailed in *figures 4.5* and *4.10*, inhibition of the Activin/Nodal and BMP arms of TGFβ SMAD signalling has been essential for induction of a neuroectodermal identity, increasing the proportion of cells classed as NPCs and transcription of genes critical for neural fate determination. Inhibition of SMAD2/3 phosphorylation has been shown to block the maintenance of pluripotency and inhibition of SMAD1/5/8 phosphorylation to block differentiation of neuroectoderm to epidermis and neural crest identities (Inman et al. 2002;

Hjelmeland et al. 2004; Boergermann et al. 2010; Ying & Smith 2003; Chambers et al. 2009). Here, addition of LDN193189 to hESC-derived NPC's reduced the levels of phosphorylated SMAD1/5/8 relative to an untreated sample (differentiated in basal media at 20% O_2) in all 4 O_2 concentrations. However, NPC's differentiated at 20% O_2 retained low levels of the phosphorylated protein whereas those produced at 3% O_2 showed complete repression of the active, phosphorylated form (*Figure 4.10ii*). Repression of SMAD1/5/8 phosphorylation at 3% O_2 persisted even without exogenous BMP inhibition (*Figure 4.10iii)* but was retained at 20% O_2. Probing for all forms of the protein, regardless of phosphorylation status after dual-SMAD inhibition (pan-SMAD1/5/8) revealed this was likely through repression of activation, and not through repression of *SMAD1/5/8* transcription, as pan-SMAD1/5/8 expression was largely retained in all combinations of O_2 concentration.

4.2.6 Proliferation and viability during neural induction at 3% O_2.

It was anecdotally observed that at the conclusion of the 8-day differentiation protocol, NPCs derived at 3% O_2 had a tendency towards lower cell numbers. As HIF1A and HIF2A subunits have been shown to stall and progress proliferation respectively in human cancer cell lines and mESCs, the rate of proliferation was assessed here after the initiation of dual SMAD inhibition (Gordan et al. 2007; Koshiji et al. 2004; Carmeliet et al. 1998). As pre-conditioning showed no effect on the production of a neuroectodermal population or the intensity of BMP inhibition, and the propensity for attenuated cell numbers was specific to those differentiated at low O_2, the remainder of experiments focused solely on differentiation at 20% or 3% O_2 (20%>20% or 20%>3%).

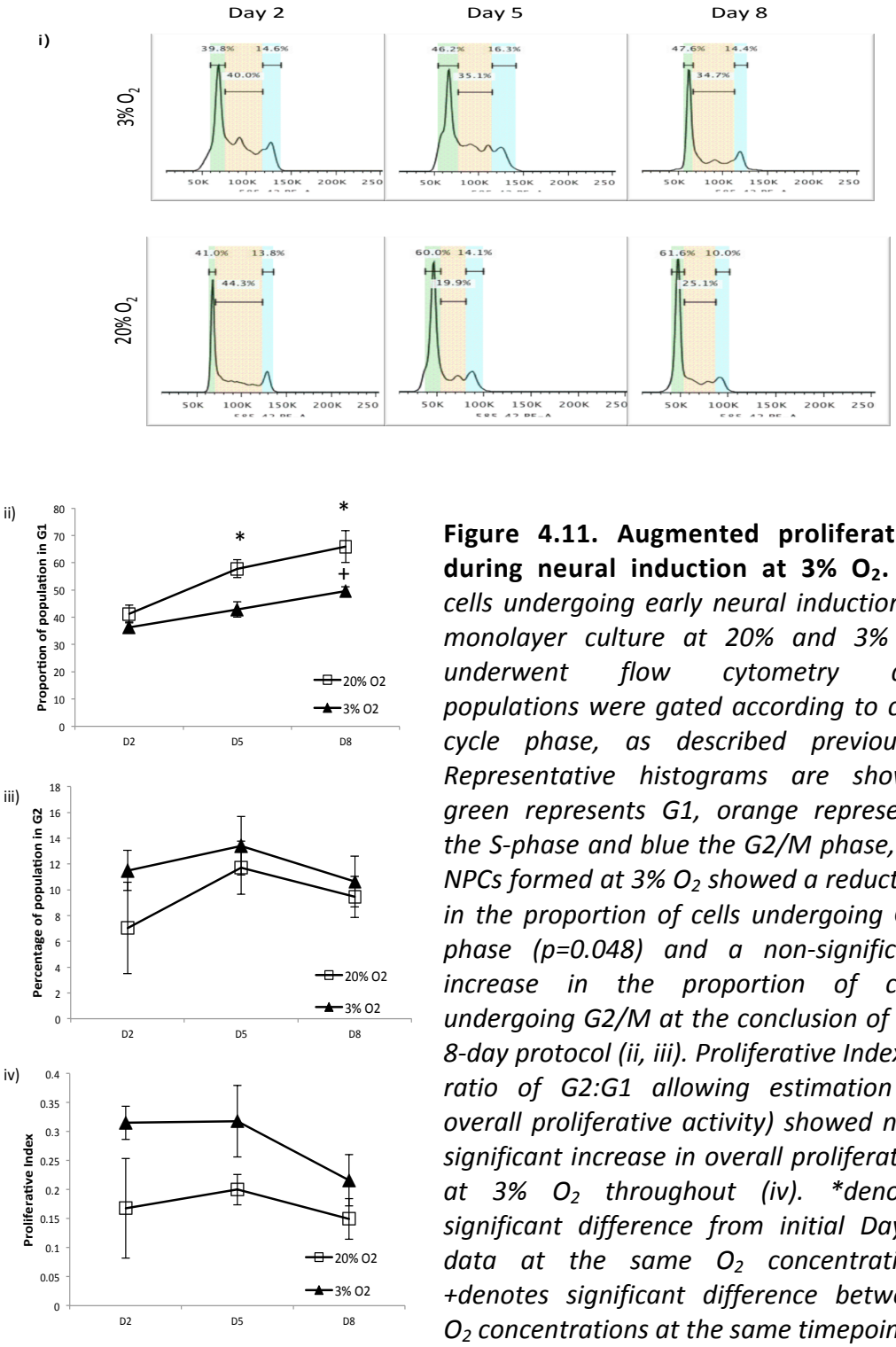

Figure 4.11. Augmented proliferation during neural induction at 3% O_2. *H9 cells undergoing early neural induction in monolayer culture at 20% and 3% O_2 underwent flow cytometry and populations were gated according to cell-cycle phase, as described previously. Representative histograms are shown, green represents G1, orange represents the S-phase and blue the G2/M phase, (i). NPCs formed at 3% O_2 showed a reduction in the proportion of cells undergoing G1-phase (p=0.048) and a non-significant increase in the proportion of cells undergoing G2/M at the conclusion of the 8-day protocol (ii, iii). Proliferative Index (a ratio of G2:G1 allowing estimation of overall proliferative activity) showed non-significant increase in overall proliferation at 3% O_2 throughout (iv). *denotes significant difference from initial Day 2 data at the same O_2 concentration. +denotes significant difference between O_2 concentrations at the same timepoint.*

At 20% O_2, the proportion of cells undergoing G1 significantly increased from 41.2±3.3% at Day 2, to 57.8±3.3% at Day 5 ($F(5, 12)=10.7$, $p=0.045$) and 66.0±5.9% at Day 8 ($p=0.003$) (*figure 4.11*). NPC's formed at 3% O_2 did not undergo this steady increase, with the proportion of cells in G0/1 steady from 36.3±1.9% at Day 2 to 49.6±1.6% at Day 8 ($p=0.134$). Hence, by Day 8, 20% O_2 had significantly

increased the proportion of non-dividing cells relative to those at 3% O_2 (p=0.048). Correlating with this, NPC's at 3% O_2 showed a consistently higher (although non-significant) proportion of cells actively dividing (*4.11ii*) and higher Proliferative Index, indicating higher overall rate of proliferation (*4.11iii*).

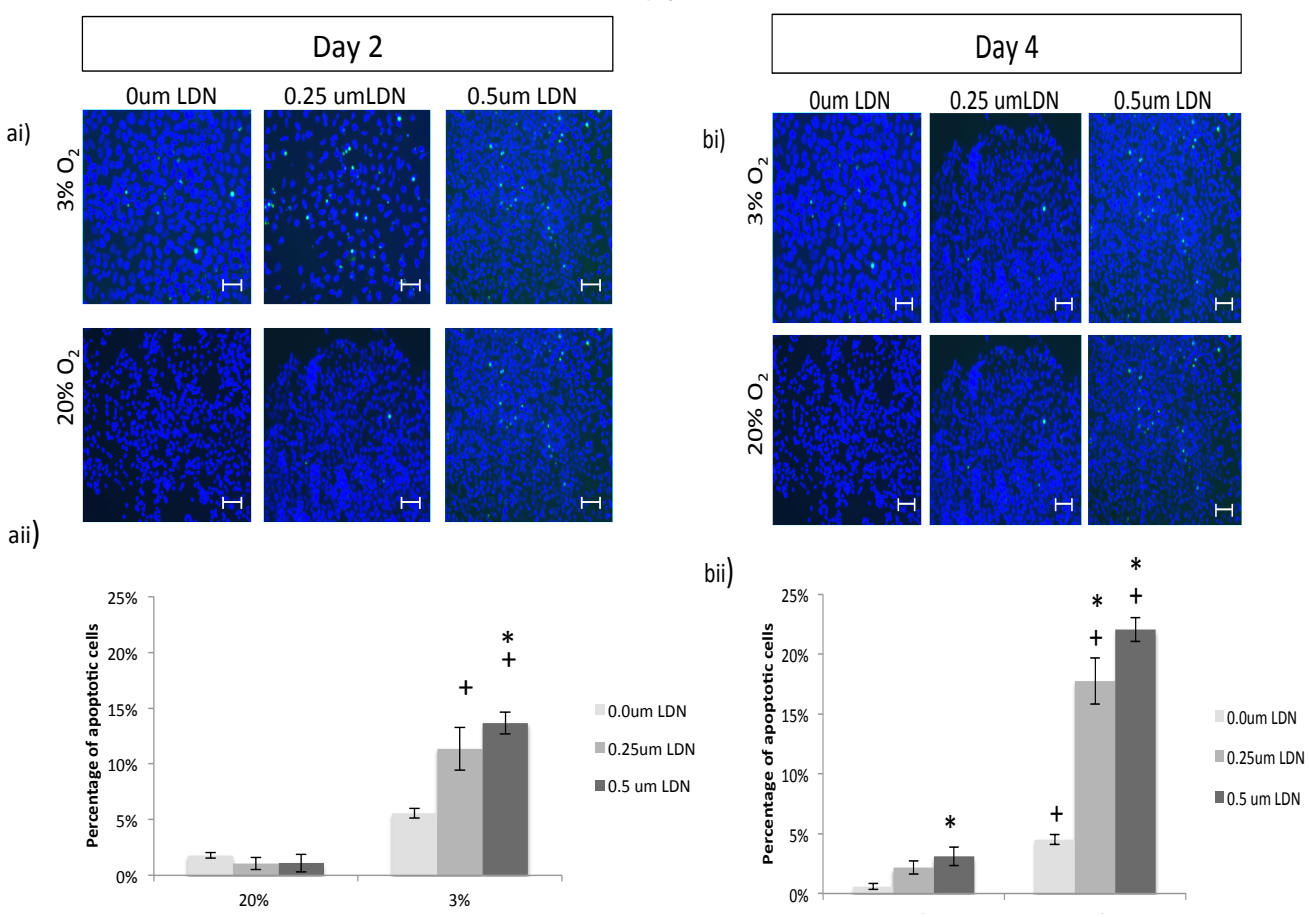

Figure 4.12. Augmented apoptosis was induced at 3% O_2 in a dose-independent manner. *Apoptosis at 3% O2 was assessed by quantifying the percentage of TUNEL+ cells (green) relative to all nuclei (blue, ai, bi) after 2 days (a) and 4 days (b) of neural induction at the following concentrations of BMP-inhibitor, LDN193189; 0μM, 0.25μM and 0.5μM. At both timepoints, apoptosis was augmented at each dose of LDN193189, after exposure to 3% O2 (aii, bii). At 20% O2, levels of apoptosis were steady across the LDN193189 dose range at Day 2 but at Day 4 showed a significant increase at 0.5μM LDN193189, comparable to 0μM. *denotes significant difference from initial Day 2 data at the same O2 concentration. +denotes significant difference between O2 concentrations at the same timepoint and dose. Scale bars show 50 μm.*

This increase in proliferation at 3% O_2 did not explain the anecdotally observed decrease in cell numbers at 3% O_2, therefore, the rates of apoptosis were also

examined. Prior to beginning dual SMAD inhibition, hESCs were reseeded onto glass coverslips, permitting periodic fixing and staining with TUNEL-FITC conjugate, through the binding and end-labelling of fragmented DNA in apoptotic cells (*section 2.1, 2.4*). It was also investigated as to whether levels of apoptosis were dependent on the applied dose of LDN193189 for BMP inhibition, at 0μM, 0.25μM and the normal dose, 0.5μM. Activin/Nodal inhibition with 10μM SB431542 was maintained, as detailed in section 2.1.

Without the influence of exogenous BMP inhibition, apoptosis at 3% O_2, was increased relative to 20% O_2 both at Day 2 (t(4)=2.0, p=0.111, n.s.) and at Day 4 (t(4)7.8, p=0.001, *figure 4.12*). At Day 2 of neural induction, apoptosis at 20% O_2 showed no change across the LDN193189 dose range, however at 3% O_2, a significant increase was observed upon addition of LDN193189. Both at 0.25μM (11.4±3.5%, t(4)=2.9, p=0.042) and 0.5μM (13.7±1.4%, t(4)=8.9, p=0.001) rates of apoptosis were increased relative to their counterparts at 20% O_2 (1.1±0.4% and 1.1±0.2% respectively). Only at 0.5μM LDN193189 did this increase at 3% O_2 deviate significantly from that at 0μM LDN193189 (t(4)=3.5, p=0.025).

By Day 4 of analysis, cells at 20% O_2 also showed an LDN193189 dependent increase in apoptosis whereby populations at 0.5μM LDN193189 had significantly increased rates of apoptotic cells (3.3±0.7%, t(4)=3.6, p=0.023) relative to 0μM LDN193189 (0.7±0.3%). Accordingly, at 3% O_2, apoptosis was induced at both 0.25μM (17.7±2.2%, t(4)=6.0, p=0.004) and 0.5μM LDN193189 (22.0±1.0%, t(4)=16.8, p=0.000074), relative to 0μM LDN193189 (4.3±0.3%).

Both 0.25μM and 0.5μM LDN193189 at low oxygen showed apoptosis augmented above corresponding treatment at high oxygen (t(4)=6.9, p=0.002 and t(4)=15.5, p=0.0001 respectively). As the reduced viability was observed in an LDN193189 dependent manner at 20% O_2 and an LDN193189-independent manner at 3% O_2, it seems feasible that the cell death observed at 3% O_2 was an oxygen-mediated, augmentation or acceleration of the neural induction induced apoptosis which was observed at 20% O_2.

4.3 Discussion

Although many of the existing protocols for differentiating hESCs and iPSCs towards a neural fate lineage are commonly performed at atmospheric oxygen, the physiological oxygen concentration in the adult and developing brain has been shown to be well below atmospheric oxygen concentration, varying across the brain from 0.8%-8% (Erecińska & Silver 2001; Lee et al. 2001; Lord et al. 1993; Chen et al. 1999). Here, this was reflected *in vitro* by differentiating hESCs at 3% O_2 to a neural progenitor identity reminiscent of the developmental stage of the neural plate and tube *in vivo*. The efficiency and homogeneity of neural induction was assessed by EB or monolayer differentiation of hESCs, in conjunction with signalling reflective of that present during gastrulation (dual SMAD inhibition).

4.3.1 Apoptosis was augmented at 3% O_2 during neural induction.

The structural and morphological development of EBs *in vitro* has been shown to reflect that present during early embryonic development, from the pre-implantation blastocyst through to the neuralisation of primitive ectoderm (Germain et al. 2010; Martin et al. 1977; ten Berge et al. 2008). Hence, I hypothesised that O_2 concentration and signalling reflective of that found *in vivo* during that developmental phase may be beneficial to the *in vitro* neural induction of human PSCs. Interestingly, pre-treatment of H9 hESCs at 3% O_2 prior to neural induction was severely detrimental to EB formation, with both 3>3% and 3>20% failing to sustain viability by the conclusion of the differentiation protocol. This effect was not observed when performed in basal medium (without dual SMAD inhibition), although both with and without TGFβ inhibition, EBs formed at 20>3% were typically smaller and less numerous than those at 20>20%. Upon investigation with monolayer differentiation, augmented apoptosis at 20>3% was observed both dependent and independent of, BMP-inhibition.

One cause of attenuated size and numbers of EBs after differentiation at 3% O_2 (20>20% vs 20>3%), was likely due to the pressure of additional internal oxygen gradients. Van Winkle et al detailed an inversely proportional decrease in O_2

concentration with increasing EB size; EBs with diameters of 800μm had an internal O_2 concentration 50% lower than those at 400μm (Van Winkle et al. 2012). This was also observed during EB based spontaneous differentiation of mESCs at 20%, whereby oxygen concentration dropped from ~130 mmHg to ~95 mmHg at an electrode depth of 400μm (Gassmann et al. 1996). EB formation in a reduced external oxygen concentration would logically reduce core O_2 further. It may be that once stabilised in low oxygen during the pre-conditioning period, the H9 line was unable to undergo any further adaptation to reduced O_2 necessary for stable EB formation. A dose-dependent relationship between pro-apoptotic factor p53 and hypoxia has also been acknowledged, with only severe oxygen restriction increasing p53 expression and activity (Sermeus & Michiels 2011). Therefore, it seems probable that the combination of internal EB oxygen gradients in conjunction with differentiation at 3% O_2 was inducing apoptosis in a combinatory manner, resulting in attenuated size and numbers of EBs. This correlates with reports of augmented cell death in hESC derived EBs and NSCs at reduced O_2 concentration (Cameron et al. 2008; Chen et al. 2010; Horie et al. 2008).

However, hESCs continued to show increased apoptosis at 3% O_2 even when differentiated as a monolayer. Therefore, the reduction in viable EBs was likely not wholly due to oxygen starvation in core cells. Indeed, a link between hypoxia, apoptosis and normal neural development has been previously reported. Chen et al outlined a process whereby the hypoxic microenvironment in the rat neural tube was essential for correct structural development, an O_2 concentration raised above physiological levels attenuated cell death, leading to gross abnormalities (Chen et al. 1999). *In vitro*, mouse NSCs and immortalised human NSCs exhibited an oxygen concentration dependent response, with increased apoptosis specifically at severe hypoxia (0-3% O_2) but not mild hypoxia (3-5% O_2) although additional reports indicated attenuated apoptosis in NSCs under low oxygen concentrations (Santilli et al. 2010; Studer et al. 2000; Horie et al. 2008). This laregely correlates with observations made in this study, of increased apoptosis after early neural induction at 3% O_2.

Apoptosis at 3% O_2 was additively increased in conjunction with exogenous BMP inhibition, both as EBs and monolayer cultures. As NPC's formed at 3% O_2 also showed increased suppression of SMAD1/5/8 phosphorylation, it is feasible that apoptosis and BMP inhibition are linked processes, although further investigation is required to confirm this. The use of neural induction protocols which are not reliant on exogenous BMP inhibition (such as Retinoic acid based neural induction) and additional hESC lines would clarify whether augmented apoptosis during neural induction at 3% O_2 was specific to dual-SMAD inhibition and/or the H9 hESC line.

4.3.2 NPC's formed at 3% O_2 showed reduction in non-actively dividing cells.

In conjunction with augmented apoptosis at 3% O_2, differentiating NPCs showed a shift in the proportion of cells actively dividing, with a reduced tendency to be in a non-dividing state (G1-phase) and a concurrent non-significant increase in the proportion of cells undergoing active cell division (G2-phase). Length of the cell-cycle has been inherently linked with the state of self-renewal in NSCs *in vivo*, mouse NSCs which had shifted to neuron producing cell division (asymmetrical divisions) concordantly showed an increase in the length of G1-phase relative to those continuing in rounds of self-renewing proliferation (symmetrical division) (Calegari et al. 2005). Lange et al. hypothesised that this was due to the production and organisation of additional factors required for neuronal differentiation, hence, rather than a side-effect of differentiation, a lengthened G1-phase may have been an underlying cause of differentiation (Lange & Calegari 2010). This has been extensively demonstrated elsewhere; forced lengthening of the G1-phase triggered a shift from symmetrical to asymmetrical division of embryonic human, mouse and Xenopus NSC's *in vivo*, consequently causing premature neural differentiation (Ohnuma & Harris 2003; Calegari & Huttner 2003; Calegari et al. 2005; Tapias et al. 2014; García-García et al. 2012). Therefore, the decreased tendency observed here for 3% O_2 NPCs to be in G1-phase may indicate a higher state of self-renewal than those at 20% O_2. This corresponds with previous studies, whereby progenitors cells maintained at low oxygen were

retained in a proliferative multipotent state, with a reduced proportion of cells undergoing G1-phase (Santilli et al. 2010; Baranov et al. 2013; Milosevic et al. 2007; Gustafsson et al. 2005). There is also a consideration to be made that the augmented proliferation at 3% O_2 was a reactionary event to the increase in apoptosis. The additional experiments outlined in *section 4.3.1* would also clarify this.

4.3.3 The proportion of PAX6+ cells was augmented at 3% O_2 when performed as EBs, but not as a monolayer.

In addition to oxygen gradients, Van Winkle et al also observed that EBs sustained concentration gradients of supplementary cytokines, in a manner dependent on the cytokines depletion rate; increased rates of depletion led to increased variability of concentrations from the core to the external layer (Van Winkle et al. 2012). As EBs formed at 3% O_2 were typically smaller than those at 20% O_2, this likely partly underlies the disparity in the homogeneity of NPC populations across oxygen concentration. EBs produced at 3% O_2 showed ~20% increase in the proportion of PAX6+ cells compared to those at 20% O_2 when generated when under the influence of dual SMAD inhibition, whereas induction as a monolayer formed comparable populations across all O_2 combinations. Monolayer differentiation also produced an increasingly homogenous population with >90% of cells classed as PAX6 positive. Thus, it is possible that EB induced gradients of dual SMAD inhibitors played a role not only in restricting drug access to core EB cells at 20% O_2 but concomitantly increasing exposure throughout the smaller EBs produced at 3% O_2. Confirmation of this could be achieved by performing immunofluorescence staining on cross-sections of EBs and examining the degree of phosphorylated SMAD1/5/8 expression.

However, EB based differentiation in basal media alone continued to form populations with increasing proportions of PAX6 positive cells after differentiation at low O_2, indicating an inherent link between reduced oxygen and a neural cell fate. This correlates with the reported repression and dysregulation of neural

induction due to the silencing of HIF1A (Iyer et al. 1998; Ryan et al. 1998; Kozak et al. 1997). The high efficiency of neural induction in monolayer cultures possibly outweighed the neuralising effect of low oxygen in EBs, correlating with Stacpoole et al.'s report of comparable NPC production (NESTIN+, SOX1+) at 3% O_2 (Stacpoole et al. 2011b). Interestingly, during neural induction through spontaneous differentiation of EBs, EBs which were smaller and rounder were found to be more neuralised, whilst EBs which were larger and more irregular retained OCT4+ niches (Joannides et al. 2007). Chen et al also observed hESC derived EB's at 2% O_2 which were smaller and more compact (Chen et al. 2010). This is concordant with the smaller EBs which formed here at 3% O_2.

4.3.4 Inhibition of BMP signalling was augmented at 3% O_2.

Dual inhibition of both the BMP and ACTIVIN/NODAL arms of TGFβ signalling is crucial for efficient neural differentiation. It was previously reported that sole inhibition of the ACTIVIN/NODAL arm to block self-renewal of monolayer hESCs resulted in differentiation to a trophoblast identity, in addition to suppressing mesodermal development (Chambers et al. 2009; Xu et al. 2002). Although hESCs which received sole inhibition of BMP or ACTIVIN/NODAL signalling formed NPCs, production was lengthier and a reduction in the proportion of NPCs produced was observed (Chambers et al. 2009; Gerrard, Rodgers, et al. 2005). Here, LDN193189 inhibited the kinase activity of ALK1/2/3/6 receptors, preventing activation of downstream transcriptional outputs through phosphorylation of SMAD1/5/8.

Pistollato et al clearly outlined a role for HIF1A in the repression of BMP signalling; SMAD1/5/8 phosphorylation in human NSCs at 20% O_2 was repressed after exposure to 2% O_2 and a BMP2 mediated drop in proliferation at 20% was derepressed at 2% O_2 (Pistollato et al. 2009). Forced expression of HIF1A in human fetal stromal cells and mESCs also resulted in attenuated BMP4 transcription and a resulting neuroectodermal identity in the former (Zhao et al. 2013; Ji et al. 2009). Here, the level of active BMP signalling, assessed by protein levels of phosphorylated SMAD1/5/8, was additively attenuated when dual SMAD

inhibition was combined with neural induction at 3% O_2. Low oxygen mediated suppression of BMP signalling was feasibly a cause of the increased neural induction of EB's in basal media at 3% O_2, in addition to the LDN193189 dependent increase in apoptosis at 3% O_2. Interestingly, it's been shown that sole inhibition of Activin/Nodal signalling in hESC derived EBs efficiently formed a population of caudal NPCs (Patani et al. 2009). Correlating with this, it was also shown that mESC differentiated at 20% O_2 efficiently formed neuroectoderm as EB's but to form neuroectoderm as a monolayer it was necessary to place them at 3% O_2 to recapitulate the hypoxic core present in EBs, which had been responsible for driving differentiation in a HIF1A dependent manner. Knockdown of HIF1A in EB's at 20% then abolished efficient neural induction and resulted in an increase in BMP4 protein and phosphorylation of SMAD1/5/8; forced expression of HIF1A subsequently reversed this phenotype (Zhao et al. 2014). This was reflected here; when differentiation at 3% O_2 was performed with ACTIVIN/NODAL inhibition only (i.e. no exogenous BMP inhibition) repression of SMAD1/5/8 phosphorylation was retained at low oxygen but not at high. Hence, there is solid evidence to suggest that an oxygen dependent suppression of BMP signalling was preserved during *in vitro* hESC differentiation. Additionally, it seems probable that here, due to the presence oxygen gradients, an internal hypoxic core was responsible for endogenously repressing BMP signalling during EB formation, aiding differentiation towards a neuroectodermal cell fate.

The protein expression of pan-SMAD1/5/8 appeared generally consistent across all oxygen concentrations, implying reduced SMAD1/5/8 phosphorylation may have been regulated by suppression of kinases or receptor activation. It is worth noting that occasional reductions in pan-SMAD1/5/8 protein concentration were observed (*Figure 4.10iii*) but this was inconsistent across multiple blots and hypothesised to be an effect of the stripping process required for repetitive blot probing, rather than a consistent downstream effect of neural induction at low oxygen.

4.4 Summary

Here, I applied a physiologically relevant O_2 concentration similar to that observed during early embryogenesis, to hESC culture and differentiation. In conjunction, differentiation was directed using exogenous signalling reflective of that observed *in vivo* during gastrulation and neural plate development. Although the proportion of NPCs produced in the form of EBs was augmented at 3% O_2, the efficiency of NPC production was greatly enhanced due to monolayer differentiation with >90% of cells positive for multipotent neural stem cell marker PAX6, however yield of NPCs remained consistent across oxygen concentrations. Although increased NPC production at 3% O_2 in EBs was likely also partly due to increased exposure to exogenous dual SMAD inhibition, differentiation in basal media continued to show increased PAX6+ cells. Additionally, monolayer differentiations consistently showed increased apoptosis at 3% O_2 relative to 20% O_2, both with and without exogenous BMP inhibition, the combination of which synergistically increased cell death. As NPC's at 3% O_2 consistently showed inhibition of BMP signalling above and beyond that at 20% O_2, this additive increase in cell death was feasibly linked to the observed hypoxia induced, endogenous BMP repression. Further work will investigate the existence of a link between HIF1A activity and BMP repression, as indicated by existing literature.

5. Maturation of hESC derived neurons at low oxygen.

5.1 Introduction.

5.1.1. Neuronal maturity assessed in terms of functional activity.

During the period of neurogenesis (outlined in section 1.7.5), axonal migration and synaptic integration bear responsibility for establishment of neuronal networks (Stiles & Jernigan 2010). The maturity and functionality of these neuronal networks can be evaluated in a number of ways *in vitro*. Previous studies examining the differentiation and maturity of neurons at reduced oxygen concentrations focused on the expression of structural markers recognised as specific to mature neurons, in addition to defining neuronal specification using protein expression of chosen neurotransmitters (Peng et al. 2000; Iyer et al. 1998; Horie et al. 2008; Studer et al. 2000; Clarke & van der Kooy 2009; Cunningham et al. 2012; Mutoh et al. 2012; Santilli et al. 2010; Stacpoole et al. 2011b; Stacpoole et al. 2011a; Mondragon-Teran et al. 2009).

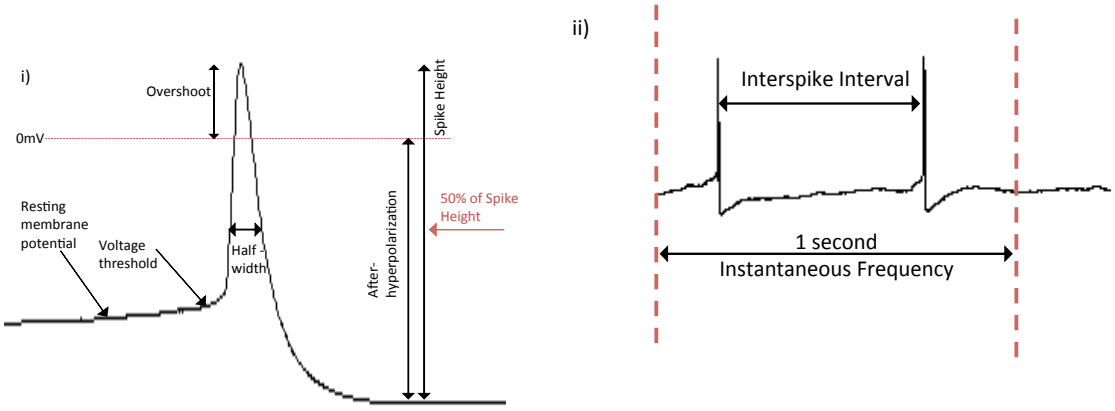

Figure 5.1 Contributory factors towards successful Action Potential generation and propagation *(i) Resting membrane potential was taken from the baseline current and voltage threshold (i.e. the voltage at which voltage gated Na^+ channels are activated) calculated using a triple differential. The overshoot was defined as the extent to which AP's exceed 0mv and the extent of afterhyperpolarisation defined as the degree of repolarisation below 0mV. Together, these form the AP spike height. The width of the AP was measured at half the spike height. Figure adapted from Bean, BP., 2007. (ii) The frequency of APs generated at resting membrane potential was quantified as the number of APs in one second, averaged over a 30 second period, known as the instantaneous frequency. The interspike interval was quantified as the time between APs, averaged over a 30 second period.*

Little examination has been paid as to whether low O2 during neurogenesis may also play a role in driving the synaptic integration and maturation of neuronal networks, assessed in terms of neuronal functionality and excitability.

The functionality of neurons can be defined by their ability to generate successful action potentials, the shape and frequency of which reflects neuronal maturity. Through dissection of the contributing factors that underlie formation of successful APs, the maturity of neuronal networks can be assessed (*see figure 5.1*). To be classed as a successful AP, depolarisation must exceed 0 mV (hence approaching E_{Na}), the extent to which it crosses this barrier is recognised as the 'overshoot'. Inactivation of voltage-gated Na^+ channels and the efflux of K^+ then additively contribute to the subsequent afterhyperpolarisation phase. Together, the overshoot and afterhyperpolarisation give the AP 'spike height'. The width of the AP at 50% of the spike height is classed as the 'half-width' (Molleman 2003; Westerlund et al. 2003). Faster rates of membrane depolarisation and repolarisation as a result of larger Na^+ and K^+ current densities result in increased AP overshoot, smaller half width, and often a more exaggerated after hyperpolarisation. These factors, which contribute to the shape and frequency of APs can be used to determine the relative maturity of a differentiating neuron (Johnson et al. 2007; Bain et al. 1995; Benninger et al. 2003; Picken Bahrey & Moody 2003; Gao & Ziskind-Conhaim 1998).

Although not a definitive correlation, neurons which produced APs with a reduced half-width also commonly displayed repetitive AP firing at high frequencies (Bean 2007). Firing frequency was calculated here as the number of successful APs per second, otherwise referred to as the instantaneous frequency (*figure 5.1ii*). In addition, measuring the time between successful APs quantified the interspike interval.

Maturation of mammalian neurons has been temporally linked to hyperpolarisation of the resting membrane potential (V_m) (Gao & Ziskind-Conhaim 1998; Johnson et al. 2007; Benninger et al. 2003; Westerlund et al. 2003). Concordantly, Input Resistance (R_{In}) is negatively correlated with the density of

membrane channels. This determines the degree of depolarising stimuli required to hit threshold for AP generation, hence a reduction is associated with a more mature excitable phenotype (Johnson et al. 2007; Benninger et al. 2003; Picken Bahrey & Moody 2003). As cell size increases due to synaptic and dendritic migration, the surface area of the cell and hence the membranes capacity for storing charge (Capacitance) has been observed to increase correspondingly (Johnson et al. 2007; Benninger et al. 2003; Picken Bahrey & Moody 2003).

The depolarisation and repolarisation phases of APs are caused by activation of Na^+ and K^+ channels respectively. Hence, an increase in channel density has been linked to an increase in the rates of depolarisation and repolarisation. This increased the rate and extent of AP overshoot and afterhyperpolarisation and reduced the AP half-width, resulting in APs with a more mature morphology. Channel density was assessed here by measuring the peak density of Na^+ and K^+ currents, (INa^+ Max and IK^+ Max respectively) both of which have previously been positively correlated with an increase in functional neuronal maturity (Johnson et al. 2007; Bain et al. 1995; Benninger et al. 2003; Picken Bahrey & Moody 2003; Gao & Ziskind-Conhaim 1998). It has also been reported that neurons with a more hyperpolarised voltage threshold produced APs with a more abrupt morphology of threshold activation, as a lesser degree of depolarising stimuli was required to trigger activation of voltage-gated Na^+ channels (Johnson et al. 2007; Benninger et al. 2003).

Mature neuronal populations also undergo synaptic integration, resulting in spontaneous propagation of APs across the neuronal network. As an initial indicator of synaptic integration, the degree of spontaneous AP generation and propagation is known to be indicative of neuronal maturity, as neurons undergoing synaptogenesis form inter-cell connections and networks (Heikkilä et al. 2009; Ban et al. 2007; Benninger et al. 2003; Illes et al. 2007). Production of AP trains (i.e. multiple APs in quick succession) are also indicative of AP propagation and are associated with neuronal maturity (Heikkilä et al. 2009; Illes et al. 2007; Johnson et al. 2007; Picken Bahrey & Moody 2003). Here, these aspects of neuronal AP generation and propagation have been examined in hESC derived

neurons produced at 20% and 3% O_2 to investigate the role of *in vivo* O_2 on *in vitro* neuronal maturation.

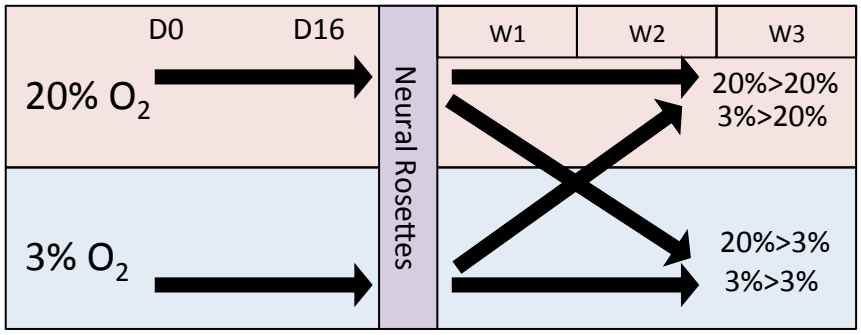

Figure 5.2 Schematic flow of O_2 concentration cross-over.

5.2 Results

5.2.1 Production and characterisation of neurons at 20% and 3% O_2.

As detailed in section 1.10, an association between reduced O_2 and the formation of a neural identity *in vitro* has been previously reported (Harms et al. 2010; Horie et al. 2008; Mondragon-Teran et al. 2009; Mutoh et al. 2012; Peng et al. 2000; Santilli et al. 2010; Stacpoole et al. 2011a; Stacpoole et al. 2011b; Studer et al. 2000; Tomita et al. 2003; Davila et al. 2013). Many of these studies have focused on the differentiation of explanted NSCs or mESCs, with little investigation into the neural differentiation of hESCs. Additionally, only Davila et al. and Francis & Wei. examined any effect of low oxygen on the functionality of neurons, although examination into the degree of spontaneous activity and excitability was not reported (Davila et al. 2013; Francis & Wei 2010).

In the previous chapter, hESC were driven towards a neuroectodermal identity (PAX6+, SOX2+, NESTIN+) using inhibition of both the TGFβ and BMP arms of SMAD signalling to form a highly homogenous population of NPCs. Here, those NPC's formed at either 20% or 3% O_2 (without pre-conditioning) were differentiated to neural rosettes and subsequently plated at a reduced density to

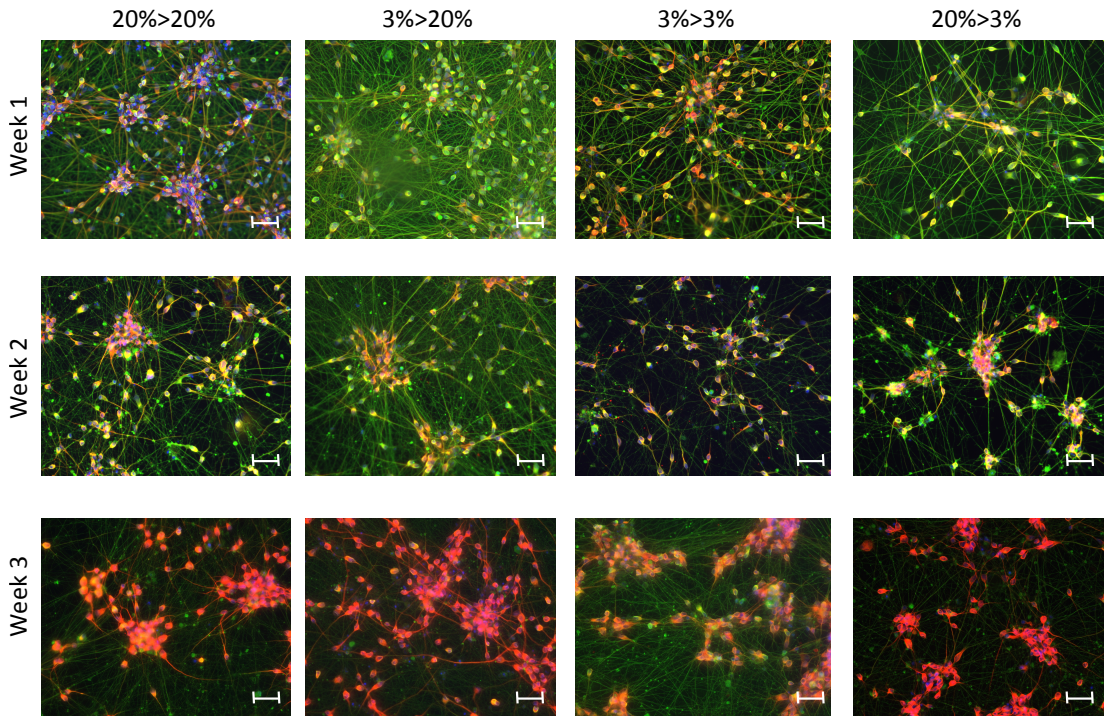

Figure 5.3. Differentiation of neural rosettes at 20% or 3% O_2 formed terminal neurons. *D16 rosettes formed at either 20% or 3% O_2 underwent the previously applied cross-over protocol after plating down for neuronal maturation. All 4 arms successfully formed populations positive for early neural marker BIII-Tubulin (green) with a high percentage positive for mature dendritic / cell body marker MAP2 (red), nuclei stained blue, scale bars show 50μm.*

induce differentiation to terminal neurons, in medium designed to augment neurogenesis (see *section 2.1.4*). As performed previously, neurons were maintained in either the same O_2 concentration or switched to the other (*Figure 5.2*). Post-platedown, neurons were examined at weeks 1, 2, 3 and 4. Expression of protein markers was then correlated with neuronal maturity, as assayed by patch-clamp. Due to technical constraints, patch-clamp analysis was only performed on neurons which underwent the entirety of the differentiation process at either 20% or 3% O_2.

A critical aspect of neuronal morphogenesis is recognised as the outgrowth and elongation of processes, forming axonal and dendritic neurites and allowing establishment of synaptic contacts between neurons (Sánchez et al. 2000). This cytoskeletal growth and rearrangement was shown to require

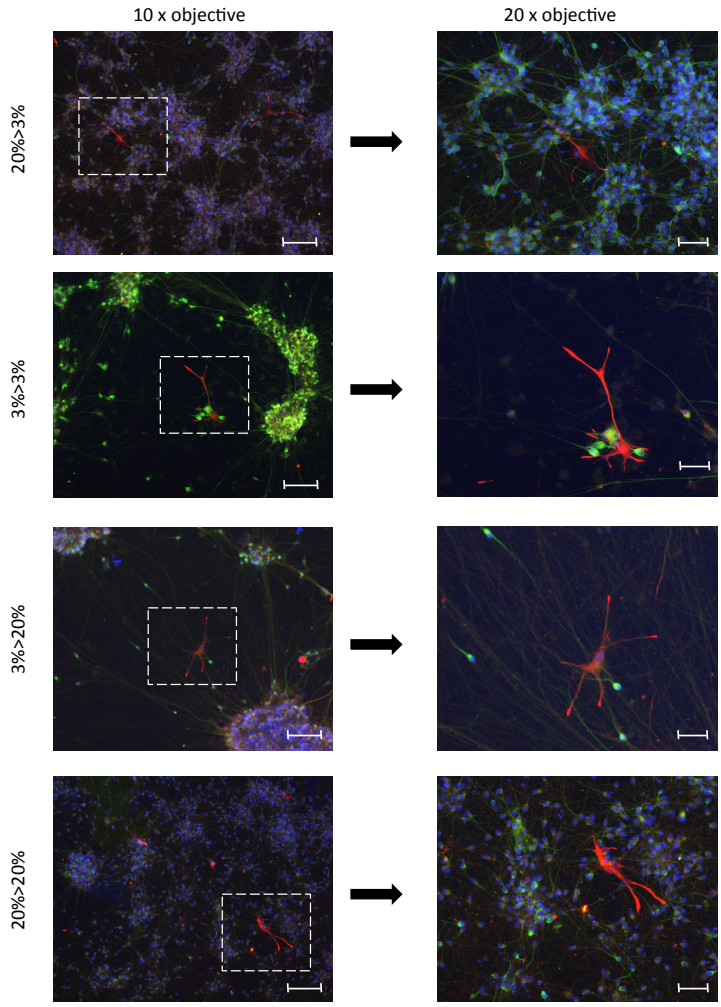

Figure 5.4. Neural differentiation at 20% or 3% O_2 formed a population of neurons with minimal astrocytic contamination. *All four populations of neurons showed a very small numbers of cells staining positive for reactive astrocyte marker S100β (red) and vast majority positive for mature neural marker MAP2 (green). Cells positive for S100β showed no co-staining for MAP2. Nuclei stained blue. At 10x objective scale bars show 100 μm, at 20x objective scale bars show 50 μm*

functional coordination of microfilaments, intermediate filaments and microtubules to synchronise cellular migration and differentiation (Sánchez et al. 2000; Katsetos et al. 2003). Expression of βIII-Tubulin has been shown to be largely specific to developing neurons with a very minor level of transient, non-neural expression (Katsetos et al. 2003). In the adult CNS, the βIII isotype was indicated to have a highly conserved expression pattern, exclusively neuron specific with no expression in glial cells (Katsetos et al. 2003). Microtubule assembly promoting protein -2 (MAP2) was also abundantly expressed in the

mammalian CNS as an integral component of the cytoskeletal structure (Sánchez et al. 2000). Its expression was recognised as largely specific to neurons and it's been implicated in the regulation of neurite outgrowth (Sánchez et al. 2000; Dehmelt & Halpain 2005). It was also shown that in NPC's, MAP2 expression was low, typically increasing after the up-regulation of βIII-Tubulin whereby it localised in dendritic processes and neuronal cell bodies (Dehmelt & Halpain 2005; Dehmelt & Halpain 2004). Here, high proportions of cells co-staining with both βIII-Tubulin and MAP2A/B (MAP2) demonstrated the highly efficient generation of homogenous populations of neurons in all cases. At 1 week, all cells were βIII-Tubulin positive with low levels of localised MAP2 expression in the cell bodies. By week 3, MAP2 expression had intensified and spread to include specific neurites, consistent with reports of dendritic localisation in mature neurons (*Figure 5.3*).

As previous studies reported an increase over time in the proportion of cells developing with an astrocytic identity *in vitro*, differentiating cultures were examined for astrocyte "contamination" (Erceg et al. 2008; Johnson et al. 2007). S100β is a signalling molecule produced by reactive astrocytes with a small amount of cross-reactivity with neuronal subtypes (Steiner et al. 2007). It is worth noting that S100β is not exclusively expressed in all astrocytes, but the consistently high levels of MAP2+ neurons allowed MAP2 to be used as a reference marker. All four populations of neurons showed minimal levels of astrocytic contamination. For each coverslip (constituting ~40-50,000 cells), a maximum of 5 cells per coverslip stained as positive for astrocytic marker S100β, with no evident co-staining between it and MAP2 (*Figure 5.4*).

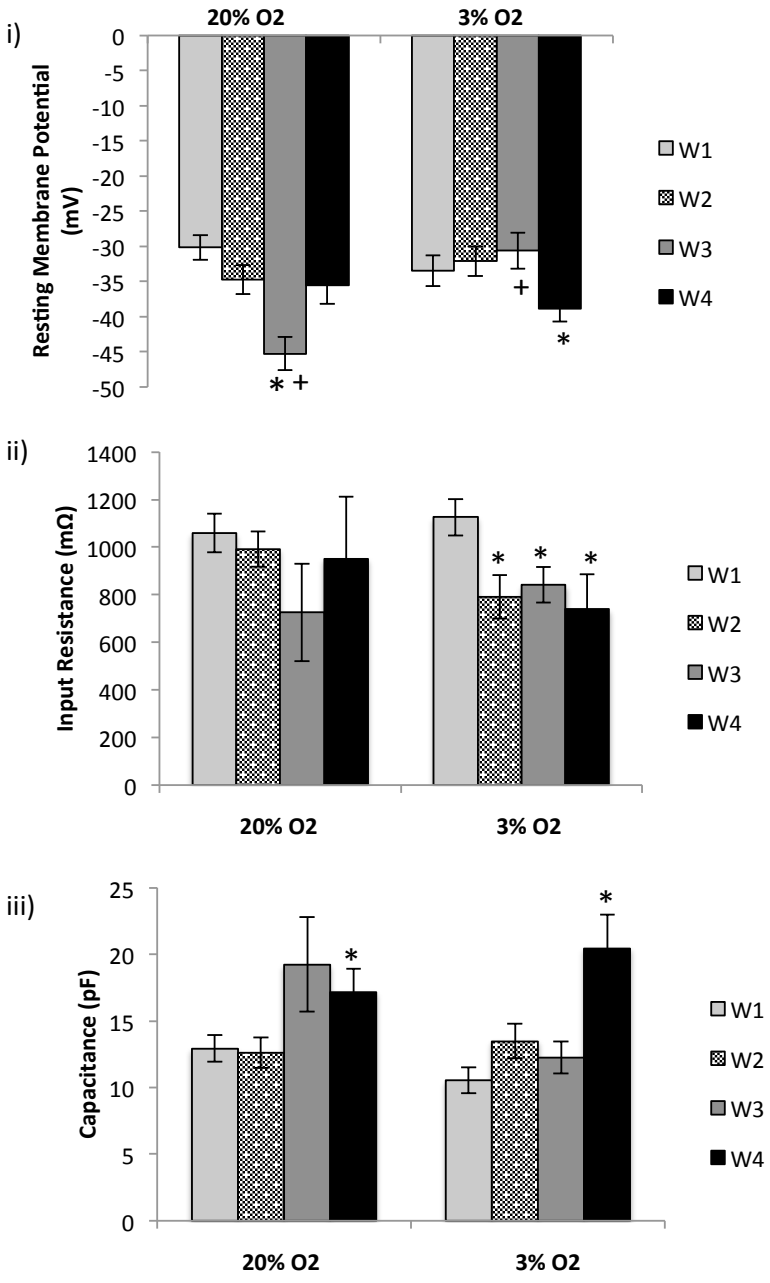

Figure 5.5. Resting membrane potential, Input resistance and cell capacitance showed progressive changes reflective of a more mature neuronal phenotype in neurons produced at 20% O_2 and 3% O_2. *Neurons formed at 20% and 3% O_2 showed hyperpolarised V_m (i) and augmented Cell Capacitance (iii) over 4 weeks of neuronal maturation. Only neuronal populations produced at 3% O_2 showed the expected attenuation of RIn throughout maturation (ii), with no significant change at 20% O_2. *denotes significantly different from Week 1 baseline data at the same O_2 concentration. +denotes a significant difference from the corresponding timepoint at contrasting O_2 concentration. Data are grouped by timepoint and O_2 concentration only, significance was set at $p<0.05$.*

5.2.2 Passive properties of neurons at 20% and 3% O_2.

A progressive hyperpolarisation of V_m has been reported to occur in a temporally linked manner with neuronal maturation (Gao & Ziskind-Conhaim 1998; Johnson et al. 2007; Benninger et al. 2003; Westerlund et al. 2003). Progressive hyperpolarisation of V_m (*Figure 5.5i*) in neurons produced at 20% O_2 peaked at Week 3 (-45.2±2.4 mV) relative to Week 1 (-30.1±1.8 mV, t(45)=5.2, p=0.000005), with a non-significant depolarising shift in V_m at week 4 (-35.5±2.6 mV, p=0.101). In contrast, at 3% O_2, hyperpolarisation of V_m was delayed with peak V_m occurring at Week 4. V_m was consistent between Week 1 (-33.5±2.2 mV) and Week 3 (-30.6±22.5 mV, t(46)=0.9, p=0.395), until a significant hyperpolarising shift at Week 4 (-38.9±1.8 mV, t(36)=2.3, p=0.028). This delayed V_m hyperpolarisation at 3% O_2 caused a significant difference in V_m across O_2 concentrations at Week 3 (t(43)=4.2, p=0.0001) but had equalised by Week 4 (t(23)=1.1, p=0.291).

A decrease in input resistance (R_{in}) due to increased channel density and activity has been linked to an increasingly mature neuronal phenotype (Johnson et al. 2007; Benninger et al. 2003; Picken Bahrey & Moody 2003). At 20% O_2, no significant difference was observed across the experimental period (*Figure 5.5ii*) from 1059.8±81.2 MΩ at Week 1 to 725.1±204.1 MΩ at Week 3 (t(42)=1.7, p=0.094) and 951.9±259.8 MΩ at Week 4 (t(34)=0.53, p=0.603). Contrastingly, those at 3% O_2 showed an initial significant decrease from 1126.0±77.3 MΩ at Week 1 to 791.5±91.3 MΩ at Week 2 (t(48)=1.7, p=0.008). No further decreases were observed from Week 2 onwards. RIn was also comparable across oxygen concentrations at each timepoint.

The synaptic and dendritic neural migration which has been shown to ensure an integrated and functional neuronal network also results in augmented cell size and complexity, assessed here through cell capacitance (Cp) (Johnson et al. 2007; Benninger et al. 2003; Picken Bahrey & Moody 2003). Both 20% and 3% O_2 showed a significant rise from baseline Week 1 values (*Figure 5.5ii,* 12.9±1.0 and

10.6±1.0 pF respectively) at Week 4 of neuronal maturation only (17.2±1.7 pF, t(33)=2.2, p=0.032 and 20.5±2.5, t(17)=3.7, p=0.002 for 20% and 3% respectively). No difference in Cp at contrasting O_2 concentrations was observed at any timepoint.

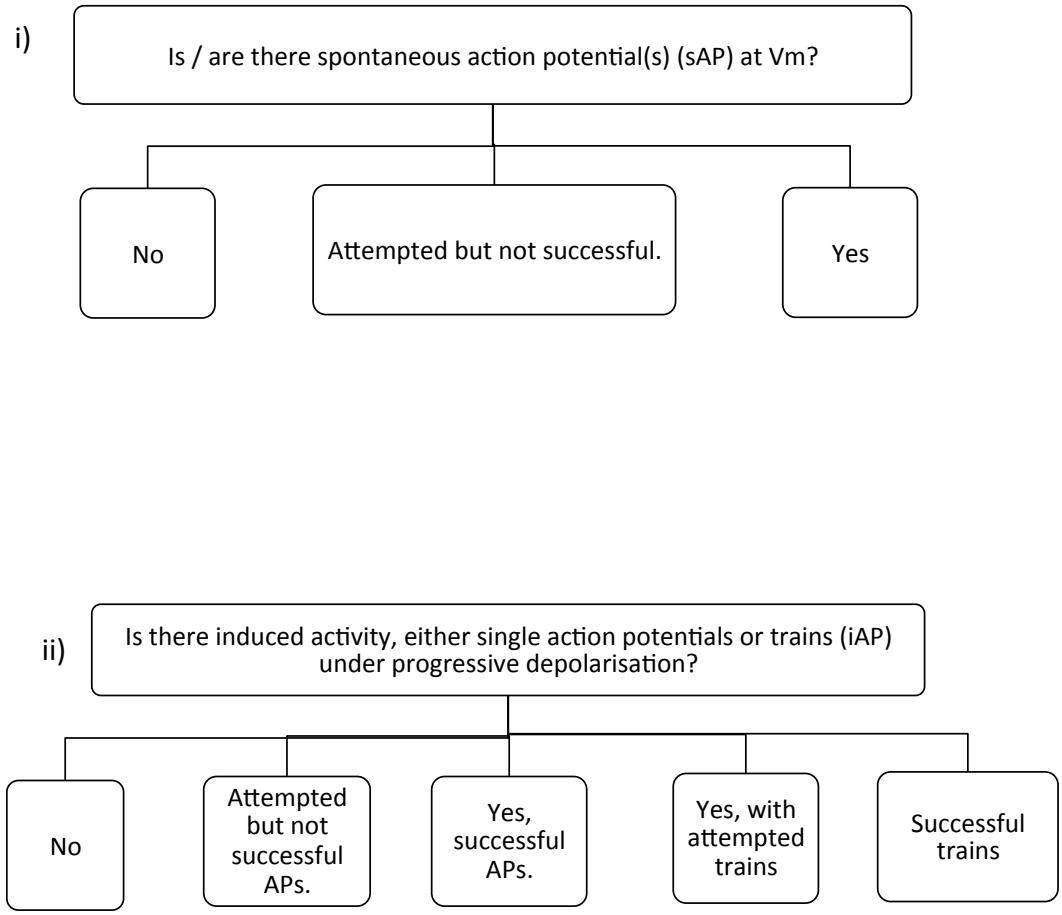

Figure 5.6. Data analysis process for each cell. *Each cell was initially categorised dependent on its levels of spontaneous activity at resting membrane potential (i). Spontaneous activity was defined as formation of one or more action potentials where depolarisation exceeded 0mV. Each cell was then sub-categorised dependent on induced activity under progressive membrane depolarisation (ii). A successful induced action potential was defined as previously outlined and a train of APs defined as two or more consecutive APs in close succession.*

Week 1 20% O_2 (n=26)		sAP type	n	sAP type	n	sAP type	n
		None		Attempted sAP		Full sAP	
	Cells within Group (%)	77%	20	19%	5	4%	1
iAP type (%)	None (%)	0%	0	0%	0	0%	0
	Attempted Single (%)	20%	4	20%	1	0%	0
	Single (%)	40%	8	20%	1	0%	0
	Attempted Train (%)	20%	4	60%	3	0%	0
	Train (%)	20%	4	0%	0	100%	1

Week 1 3% O_2 (n=24)		sAP type	n	sAP type	n	sAP type	n
		None		Attempted sAP		Full sAP	
	Cells within Group (%)	96%	23	0%	0	4%	1
iAP type (%)	None (%)	4%	1	0%	0	0%	0
	Attempted Single (%)	22%	5	0%	0	0%	0
	Single (%)	43%	10	0%	0	0%	0
	Attempted Train (%)	26%	6	0%	0	0%	0
	Train (%)	4%	1	0%	0	100%	1

Week 2 20% O_2 (n=25)		sAP type	n	sAP type	n	sAP type	n
		None		Attempted sAP		Full sAP	
	Cells within Group (%)	36%	9	36%	9	28%	7
iAP type (%)	None (%)	0%	0	0%	0	0%	0
	Attempted Single (%)	22%	2	11%	1	0%	0
	Single (%)	0%	0	33%	3	0%	0
	Attempted Train (%)	44%	4	33%	3	0%	0
	Train (%)	33%	3	22%	2	100%	7

Week 2 3% O_2 (n=26)		sAP type	n	sAP type	n	sAP type	n
		None		Attempted sAP		Full sAP	
	Cells within Group (%)	50%	13	12%	3	38%	10
iAP type (%)	None (%)	0%	0	0%	0	0%	0
	Attempted Single (%)	0%	0	33%	1	0%	0
	Single (%)	38%	5	33%	1	0%	0
	Attempted Train (%)	23%	3	33%	1	10%	1
	Train (%)	38%	5	0%	0	90%	9

Week 3 20% O_2 (n=21)		sAP type	n	sAP type	n	sAP type	n
		None		Attempted sAP		Full sAP	
	Cells within Group (%)	10%	2	24%	5	67%	14
iAP type (%)	None (%)	0%	0	20%	1	0%	0
	Attempted Single (%)	0%	0	0%	0	0%	0
	Single (%)	50%	1	0%	0	0%	0
	Attempted Train (%)	50%	1	40%	2	0%	0
	Train (%)	0%	0	40%	2	100%	14

Week 3 3% O_2 (n=24)		sAP type	n	sAP type	n	sAP type	n
		None		Attempted sAP		Full sAP	
	Cells within Group (%)	71%	17	8%	2	21%	5
iAP type (%)	None (%)	6%	1	0%	0	0%	0
	Attempted Single (%)	12%	2	50%	1	0%	0
	Single (%)	59%	10	0%	0	0%	0
	Attempted Train (%)	12%	2	0%	0	0%	0
	Train (%)	12%	2	50%	1	100%	5

Week 4 20% O_2 (n=11)		sAP type	n	sAP type	n	sAP type	n
		None		Attempted sAP		Full sAP	
	Cells within Group (%)	18%	2	18%	2	64%	7
iAP type (%)	None (%)	0%	0	0%	0	0%	0
	Attempted Single (%)	0%	0	0%	0	0%	0
	Single (%)	0%	0	0%	0	14%	1
	Attempted Train (%)	50%	1	50%	1	0%	0
	Train (%)	50%	1	50%	1	71%	5

Week 4 3% O_2 (n=14)		sAP type	n	sAP type	n	sAP type	n
		None		Attempted sAP		Full sAP	
	Cells within Group (%)	21%	3	21%	3	57%	8
iAP type (%)	None (%)	0%	0	0%	0	0%	0
	Attempted Single (%)	0%	0	0%	0	0%	0
	Single (%)	0%	0	0%	0	0%	0
	Attempted Train (%)	33%	1	67%	2	0%	0
	Train (%)	67%	2	33%	1	100%	8

Figure 5.7. Summary of spontaneous and induced activity in neurons formed at 20% and 3% O_2. *Cells were categorised dependent on spontaneous and induced activity at week 1 (i), week 2 (ii), week 3 (iii) and week 4 (iv) of analysis.*

Current-clamp recordings were used to regulate current across the membrane and measure the resulting changes in membrane potential. Measurements at V_m assessed the production of spontaneous action potentials (sAPs). Cells were initially classified as follows; (1) no sAPs, (2) attempted sAPs which did not exceed 0mV or (3) formation of successful sAPs, either singly or repetitively (*Figure 5.6*). Progressive depolarising steps (from 0 to 180mV in 10mV increments) increased current flow to induce generation of action potentials (iAPs). Induced APs were then classified as follows; (1) no iAPs, (2) attempted iAPs which did not exceed 0mV, (3) formation of single iAPs, (4) a single iAP with additional attempted iAPs

failing to exceed 0 mV or (5) multiple iAPs in quick succession, referred to hereafter as “trains”.

5.2.3. Active properties of induced Action Potentials at 20% and 3% O_2.

Current-clamp steps induced APs in all timepoints at both 20% and 3% O_2 (*Figures 5.7, 5.8*). The breakdown of the proportion of cells generating single or trains of iAPs is shown in *Figure 5.7*. Action potential trains were induced in both O_2 concentrations from Week 1 of differentiation onwards. The proportion of cells capable of producing iAP trains (regardless of spontaneous activity) increased throughout neuronal maturation, from 19.2% and 8.3% at Week 1 up to 63.6% and 78.6% at Week 4, when differentiated at 20% and 3% O_2 respectively. The intensity of iAPs can be analysed by dissecting the morphology of successful action potentials. Here, the first successful iAP or the first iAP in a successful train was analysed.

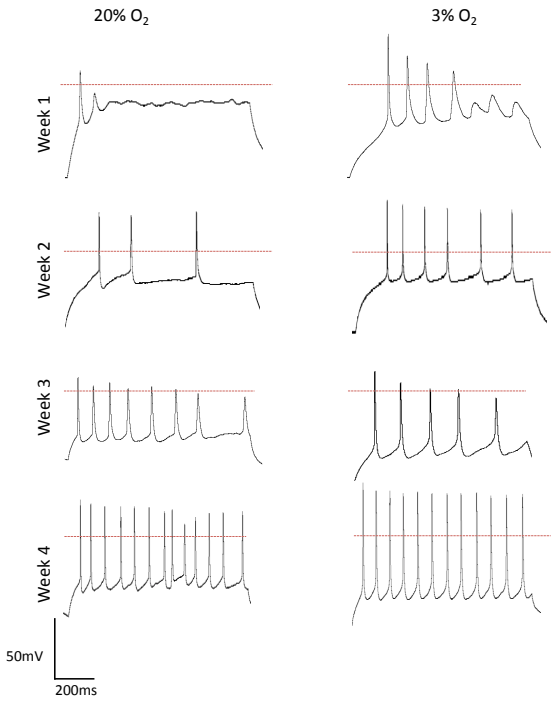

Figure 5.8. Representative traces of induced action potentials (iAP) at Weeks 1, 2, 3 and 4 in neurons produced at 20% and 3% O_2.

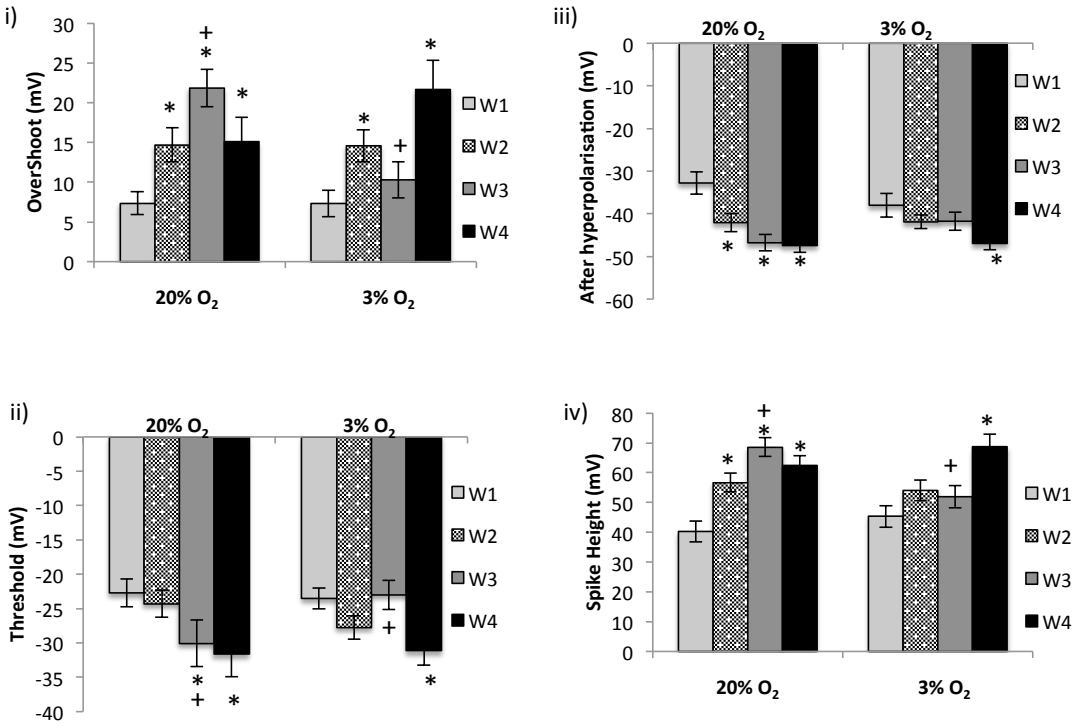

Figure 5.9. Action potential half-width, overshoot, after-hyperpolarisation and spike height reflect increasing maturity in neurons at both 20% and 3% O_2. *Neurons produced at both 20% and 3% O_2 showed temporal development of overshoot (i), threshold (ii), afterhyperpolarisation (iii) and spike height (iv) between Weeks 1 and 4, reflective of increasing neuronal maturity. *denotes significantly different from Week 1 baseline data at the same O_2 concentration. +denotes a significant difference from the corresponding timepoint at contrasting O_2 concentration. Data are grouped by timepoint and O_2 concentration only, significance was set at p<0.05.*

An increase in AP overshoot (commonly referred to as amplitude) is recognised as an indication of increased intensity of depolarisation and augmented neuronal maturity (*Figure 5.1*) (Molleman 2003; Westerlund et al. 2003). Here, both 20% and 3% O2 showed significantly increased overshoot from week 1 values, concordant with neuronal maturation (*figure 5.9i*). Neurons produced at 20% O_2 showed maximally increased overshoot at Week 3 (21.9±2.4 mV, t(41)=5.4, p=0.000003) comparatively to week 1 (7.3±1.4 mV) and the observed reduction in overshoot at Week 4 was non-significant (t(29)=1.7, p=0.095). Neurons produced

at 3% O_2 showed a similar increase from week 1 (7.3±1.7 mV) onwards although peak overshoot was delayed (relative to 20%), occurring at week 4 of the maturation period (21.7±3.7 mV, t(18)=3.6, p=0.002). Neurons at week 3 showed a consistent, short-lived drop in excitable activity. This ensured a disparity in overshoot between O_2 concentrations at Week 3 only (t(38)=3.5, p=0.001), this was transient and by Week 4 overshoot was once more equivalent between 20% and 3% O_2.

Alongside the increase in overshoot across the maturation period, the extent of afterhyperpolarisation was augmented throughout the maturation period in both populations. With no difference in the extent of afterhyperpolarisation between O_2 concentrations (*figure 5.9iii*), an increase was observed in the extent of afterhyperpolarisation from Week 1 to reach maximal values by Week 4 at 20% (-47.4±1.6 mV, t(32)=4.7, p=0.00005) and 3% O_2 (-46.9±1.5 mV, t(28)=2.8, p=0.008). In addition to augmentation of AP overshoot and after-hyperpolarisation, the spike height showed a progressively more mature phenotype throughout the neuronal maturation period, at both 20% and 3% O_2 (*figure 5.9iv*).

The extent of action potential overshoot and afterhyperpolarisation can be summed through assessment of spike height. Spike height at 20% O_2 reached maximal height at Week 3 (40.2±3.5 mV, t(41)=6.0, p=0.00001) with a non-significant decrease at Week 4 (62.4±3.4 mV, t(29)=1.3, p=0.230). At 3% O_2, maximal spike height was delayed until Week 4 (68.6±4.4 mV) from Week 1 values (45.3±3.6, t(32)=4.1, p=0.0003). Consistent with overshoot and threshold, the only significant difference between O_2 concentrations was observed at Week 3 due to a drop at 3% O_2 (t(38)=3.3, p=0.0002) with comparable spike height by Week 4 (t(23)=1.1, p=0.294).

Voltage threshold indicates the membrane potential at which voltage-gated Na^+ channels become active, allowing Na^+ influx into the cell and triggering membrane depolarisation. Typically, a more mature neuron would have a more hyperpolarised threshold, residing closer to V_m so requiring less incoming depolarisation signals to become active (Benninger et al. 2003). Those formed at 20% O_2 showed a minor hyperpolarising effect over the culture period, augmented

from -22.7±2.0mV at Week 1 to -30.0±3.4 mV at Week 3 (t(37)=2.4, p=0.022) and remaining steady from there onwards (*figure 5.9ii*). Again, a slight delay in maximal hyperpolarisation of AP Threshold was observed at 3% O_2, with only Week 4 (-31.1±2.1 mV) showing a significant departure from Week 1 (-22.7±2.0 mV, t(31)=2.9, p=0.007). This delayed reduction in threshold activation resulted in a significantly more hyperpolarised threshold at Week 3 in 20% O_2 comparable to that at 3% O_2 (t(38)=2.2, p=0.031), which was equivalent across O_2 concentrations by Week 4 of analysis.

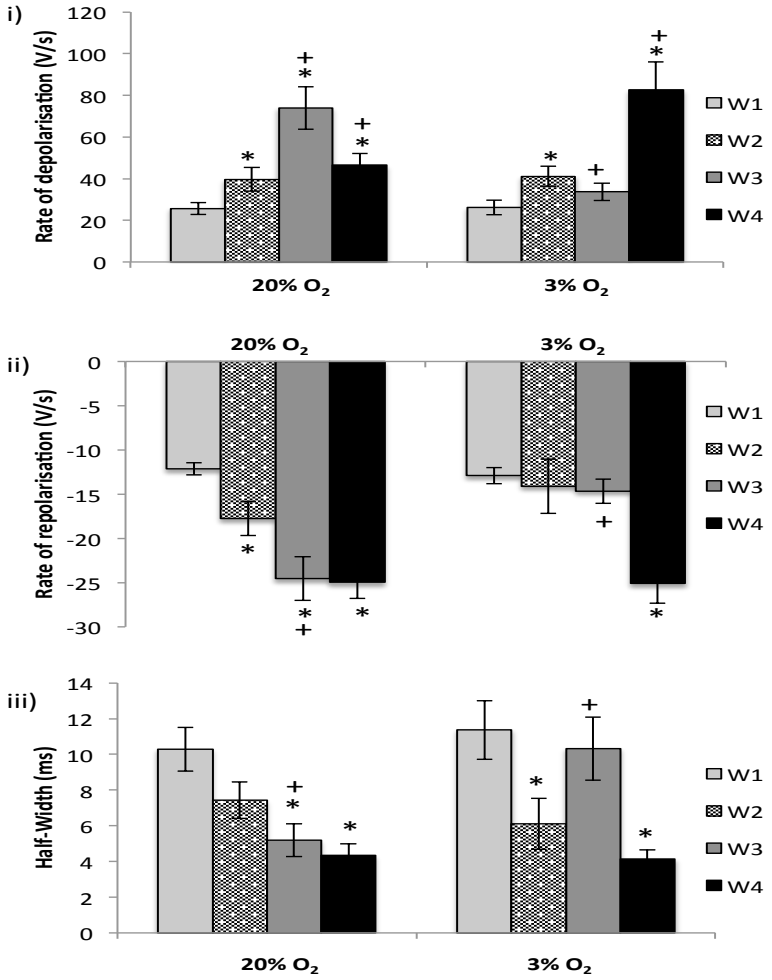

Figure 5.10. Augmented rates of depolarisation and repolarisation in induced action potentials resulted in reduced AP Half-Width at both 20% and 3% O_2. *Neurons produced at 20% and 3% O_2 showed augmented rates of AP depolarisation (i) and repolarisation (ii) reflected in reduced AP Half-width (iii) by Week 4 of neuronal maturation. *denotes significantly different from Week 1 baseline data at the same O_2 concentration. +denotes a significant difference from the corresponding timepoint at contrasting O_2 concentration. Data are grouped by timepoint and O_2 concentration only, significance was set at p<0.05.*

Throughout the maturation period, alterations to the morphology of action potentials can be observed, typically becoming sharper and narrower. Underlain by increased density of active Na^+ channels causing faster rates of depolarisation and hyperpolarisation, this augmented speed of signalling resulted in a narrowing of APs, quantified here as AP half-width (*figure 5.1, 5,10*). Throughout the maturation period, the average rate of AP depolarisation increased significantly at 20% O_2 (*Figure 5.10i*, 25.7±2.9 V/s at Week 1 to 73.9±10.3 V/s at Week 3, t(22)=4.5, p=0.0002) as did the rate of repolarisation (*Figure 5.10ii,* -12.1±0.7 V/s at Week 1 to -25.0±1.8 V/s at Week 4, t(13)=6.6, p=0.00002). As a result, AP Half-Width decreased accordingly from 10.3±1.2 ms at Week 1 to 4.3±0.7 ms at Week 4, (*Figure 5.10iii,* t(31)=4.3, p=0.0002).

Similarly, neurons at 3% O_2 also showed progressively faster rates of depolarisation (26.1±3.6 V/s to 82.5±13.5 V/s at Weeks 1 and 3 respectively, t(15)=4.0, p=0.001) and repolarisation (-12.9±0.9 V/s at Week 1 to -25.1±2.2 V/s at Week 4, t(17)=5.0, p=0.0001), resulting in a reduction of AP Half-Width from 11.4±1.6 ms at Week 1 to 4.1±0.5 ms at Week 4 (*Figure 5.12iii*, t(23)=4.2, p=0.0004). The temporary immature phenotype observed in neurons produced at 3% O_2 at Week 3 of maturation, seen as reduced spike height and depolarised threshold, was also reflected here (*figure 5.9*). At 3% O_2, both the rates of depolarisation and repolarisation did not increase until Week 4 of maturation, contrasting 20% O_2 which showed a significant increase by Week 3. A temporary increase in AP half-width was also observed at Week 3 compared to 20% O_2, although this dropped to minimal values by Week 4 of analysis.

In addition to increased rates of membrane depolarisation resulting in APs with increased spike height and reduced AP half-width, an increase in excitability has been shown to be correlative with increased intensity of Na^+ conductance (Heikkilä et al. 2009; Bain et al. 1995). This supports not only the production of AP trains, but also an increased number of APs within those trains, defined here as the spike frequency. During current injection between 60-120 pA, neurons produced at 3% O_2 produced significantly more AP's ($p<0.05$, up to 6.40±1.1 Hz)

than those at 20% O_2 (with a maximal spike frequency of 3.98±0.7 Hz), (*figure 5.11i*).

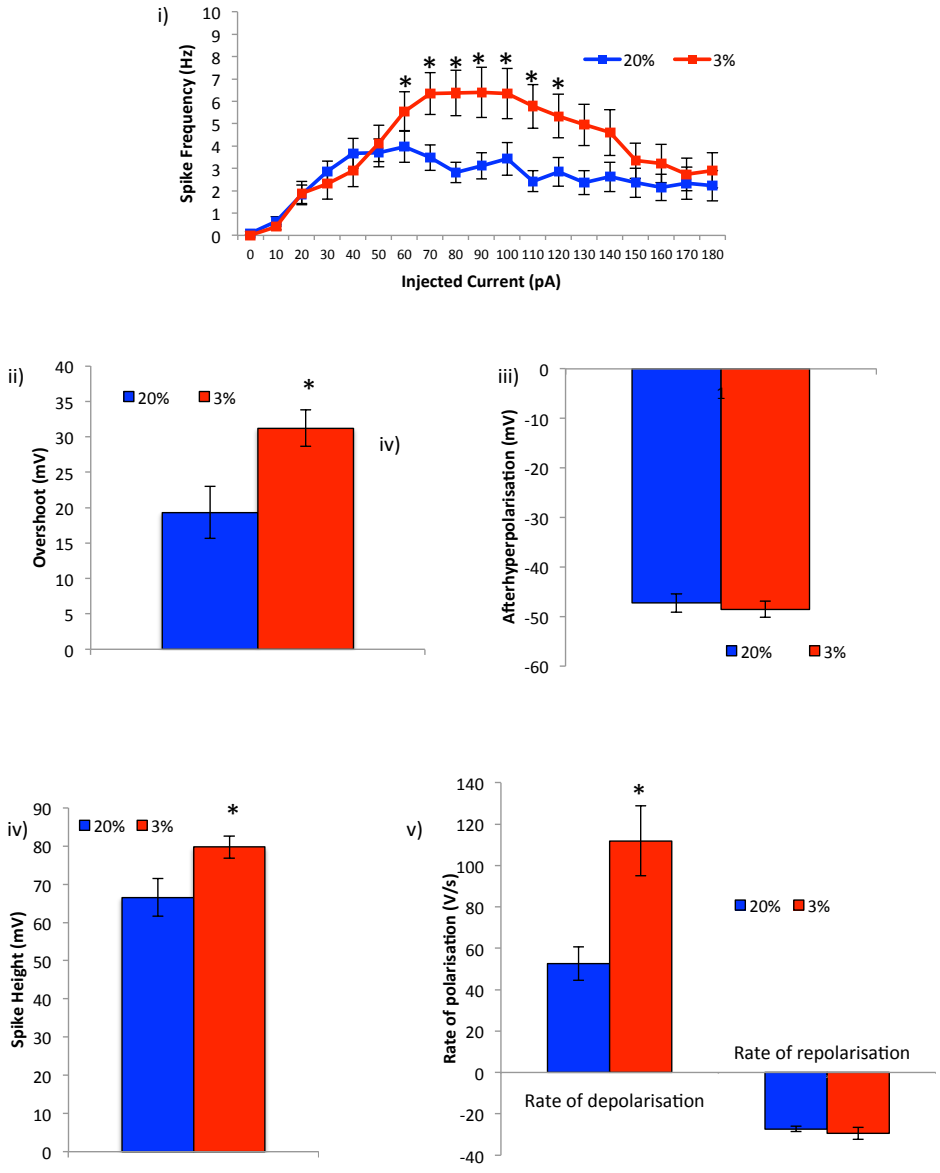

Figure 5.11. Increased induced excitability of neurons at 3% O2 relative to 20% O2. *Upon current injection, neurons at 3% O_2 generated a higher frequency of action potentials than those at 20% O_2 across the entirety of the experimental timeframe (i). In cells showing spontaneous activity at week 4 of neuronal maturation, iAPs in neurons at 3% O_2 showed augmented spike height (iv) due to an increase in overshoot (ii) with no change in the extent of afterhyperpolarisation (iii). This was associated with an escalated rate of membrane depolarisation (v) with steady rates of repolarisation at both 20% and 3% O_2. *denotes significant difference between O_2 concentrations, significance was set at p<0.05.*

Due to this pattern of augmented excitability at 3% O_2, active properties of iAPs were reanalysed. Data was segregated dependent on spontaneous activity, with only cells generating sAPs included (*figure 5.11 ii-v*). Concordantly with the previously described pattern of increased excitability, in neurons propagating sAPs at week 4, an increase in AP spike height was observed at 3% O_2 (79.7±2.9 mV) compared to 20% O_2 (*figure 5.11iv*, 66.6±4.9 mV, t(13)=2.9, p=0.013). This augmented spike height was due to a rise in the extent of AP overshoot at 3% O_2 (31.2±2.6 mV) relative to 20% O_2 (*figure 5.11ii*, 19.3±3.7 mV, t(13)=2.7, p=0.019). Afterhyperpolarisation was steady at 20% (-47.2±1.9 mV) and 3% O_2 (-48.5±1.7 mV, t(13)=0.5, p=0.62). This increase in overshoot was likely due to the observed 2-fold increase in the rate of membrane depolarisation at 3% O_2 (111.8±16.9 V/s) compared to 20% O_2 (*figure 5.11v*, 52.6±8.0 V/s, t(9)=3.3, p=0.010). Correlating with comparable afterhyperpolarisation, the rate of membrane repolarisation was steady across oxygen concentrations (-27.3±1.3 V/s and -29.4±2.9 V/s at 20% and 3% O_2 respectively, t(13)=0.6, p=0.552).

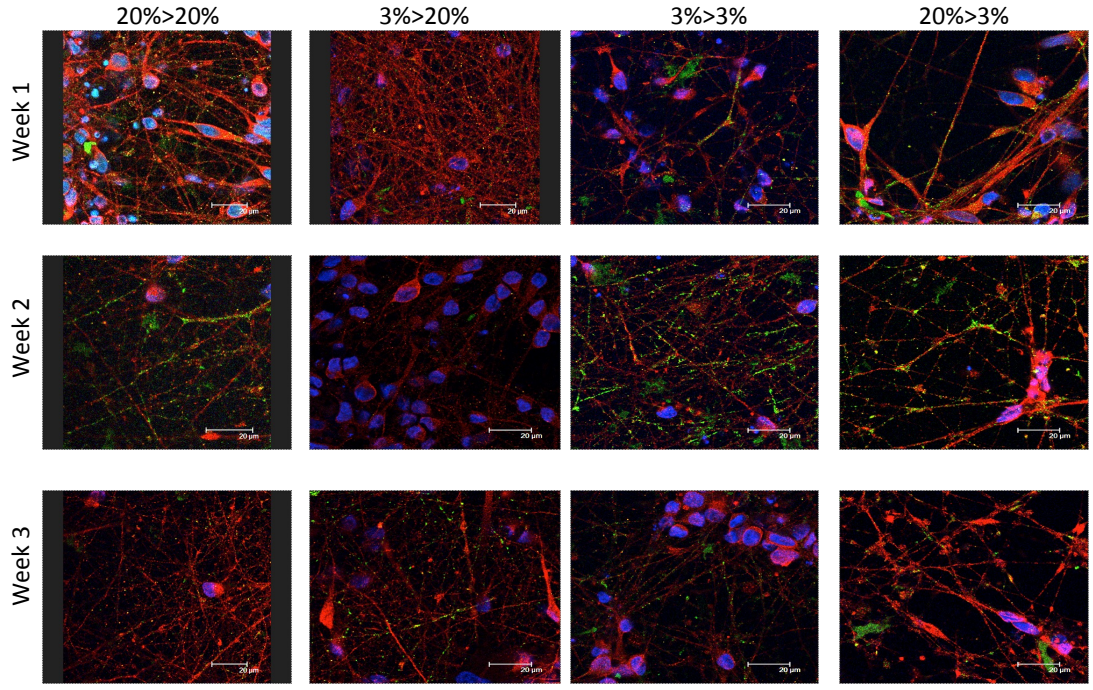

Figure 5.12. Terminal differentiation of neural rosettes at 3% O2 accelerated expression of pre-synaptic marker, Synaptophysin. *Presynaptic expression of Synaptophysin (green) showing co-localisation with PSD95 (red) occurred at Week 1 when differentiated at 3% O_2, those formed at 20% O_2 did not show synaptic co-localisation until Week 2 (nuclei, blue). Scale bars on images.*

5.2.4. Formation of synaptic terminals at 20% and 3% O_2.

It has been shown that as neuronal morphogenesis proceeds, the meeting and stabilisation of pre- and post-synaptic terminals (known as synaptogenesis) signals the starting step in the formation of an integrated neuronal network, a process requiring recruitment of specific factors intracellularly in both the pre and post-synaptic terminals. Hence, the number and type of synapses formed are essential in shaping the excitability and integration of the neuronal network. Synaptophysin, a protein constituting ~10% of total synaptic vesicle protein, has previously been recognised as a reliable pre-synaptic marker, with a reported role in the recycling of synaptic vesicles both during and after endocytosis and in the formation of synapses (Gordon et al. 2011; Kwon & Chapman 2011; Glantz et al. 2007; Tarsa & Goda 2002). Although KO mice showed no clear phenotype and seem to retain normal neurological function, Kwon et al showed a kinetic although non- deleterious effect on synaptic transmission in Synaptophysin $^{-/-}$ hippocampal neurons (Kwon & Chapman 2011; Eshkind & Leube 1995; McMahon et al. 1996).

Post-Synaptic Density Protein 95 (PSD95) has been found on the majority of post-synaptic synapses and shown to be present pre-natally, increasing post-natally to up until early adulthood (Glantz et al. 2007). Reported roles for PSD95 include co-ordination of ion channel receptor expression, synaptic stabilisation, maturation and synaptic plasticity, including up-regulation of pre-synaptic Synaptophysin expression (Glantz et al. 2007; El-Husseini et al. 2000; Prange et al. 2004). Here, co-staining of pre-synaptic marker Synaptophysin with post-synaptic marker PSD95 was used to indicate synapses comprising the necessary components required for synaptic connections (*figure 5.12*). Co-staining showed punctate co-registration of the two markers (i.e. staining on the same neurites but without direct overlay), indicating pre- and post-synaptic assembly. Interestingly, neurons differentiated at 3% O_2 showed Synaptophysin / PSD95 co-registration after only 1 week of neural differentiation, persisting through to week 2. Neuronal cultures at 20% O_2 displayed marker co-registration only at week 2 of differentiation, with expression receding in both O_2 concentrations by week 3.

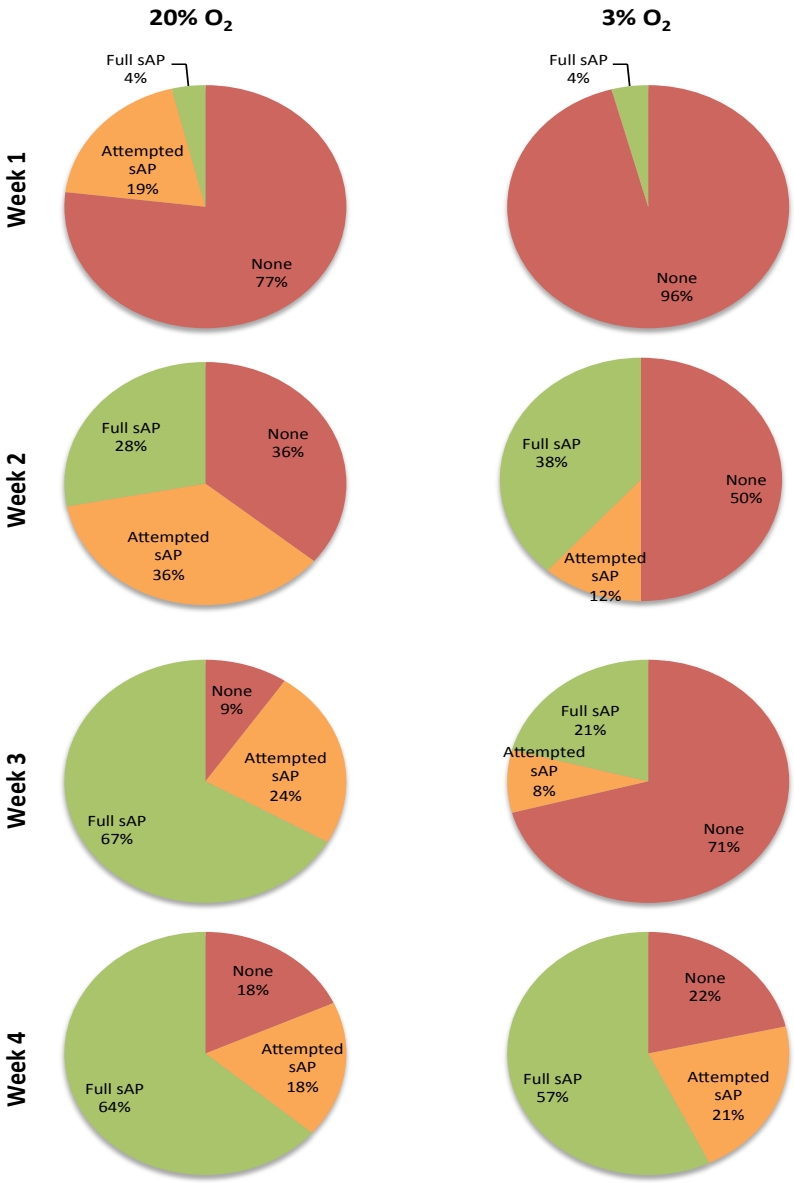

Figure 5.13. Spontaneous activity in neurons formed at 20% and 3% O_2. *Corresponding, categorical breakdown of spontaneous APs as follows; red, orange and green segments represent no sAPs, attempted sAPs and full sAPs respectively. Biological N=3.*

5.2.5 Spontaneous activity in neurons at 20% and 3% O_2.

Spontaneous firing of action potentials has been shown to be indicative of an integrated and functioning neuronal network As Synaptophysin/PSD95 co-staining indicated that synaptic formation was augmented at 3% O_2, continuous current-clamp recordings at resting membrane potential (V_m) were used to assess the generation and propagation of sAPs in neurons produced at 20% or 3% O_2

throughout the entirety of the differentiation protocol. (Heikkilä et al. 2009; Ban et al. 2007; Benninger et al. 2003; Illes et al. 2007). As AP generation in this context occurs independently of external current injection, spontaneous AP propagation was considered here as a further indicator of neuronal maturity.

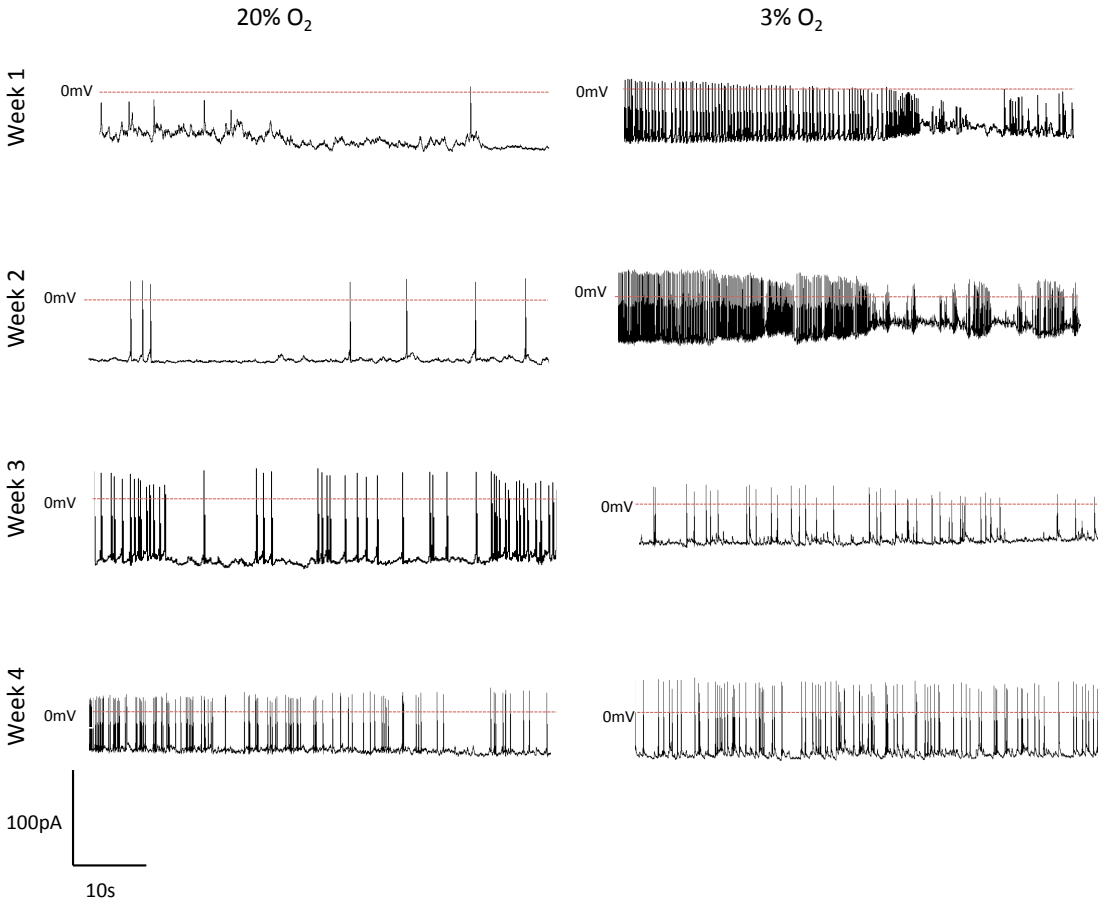

Figure 5.14. Neurons at 3% O_2 produced high frequency spontaneous action potentials. *Representative traces of sAP's at 20% and 3% in continuous current clamp recording at V_m for 60 seconds Biological N=3.*

Neurons at 20% and 3% showed a progressive increase in spontaneous activity over four weeks of neuronal maturation (*Figure 5.13, 5.14)*. The proportion of cells producing sAPs was consistent across oxygen concentrations, increasing from 4% at Week 1 to 64% and 57% at Week 4, at 20% and 3% O_2 respectively. Interestingly, neurons produced at 3% O_2 also consistently showed a transient

drop in spontaneous activity at Week 3 of analysis which recovered by Week 4, reflecting the drop observed in production of iAPs. This occurred consistently in all three separate sets of differentiations assessed here.

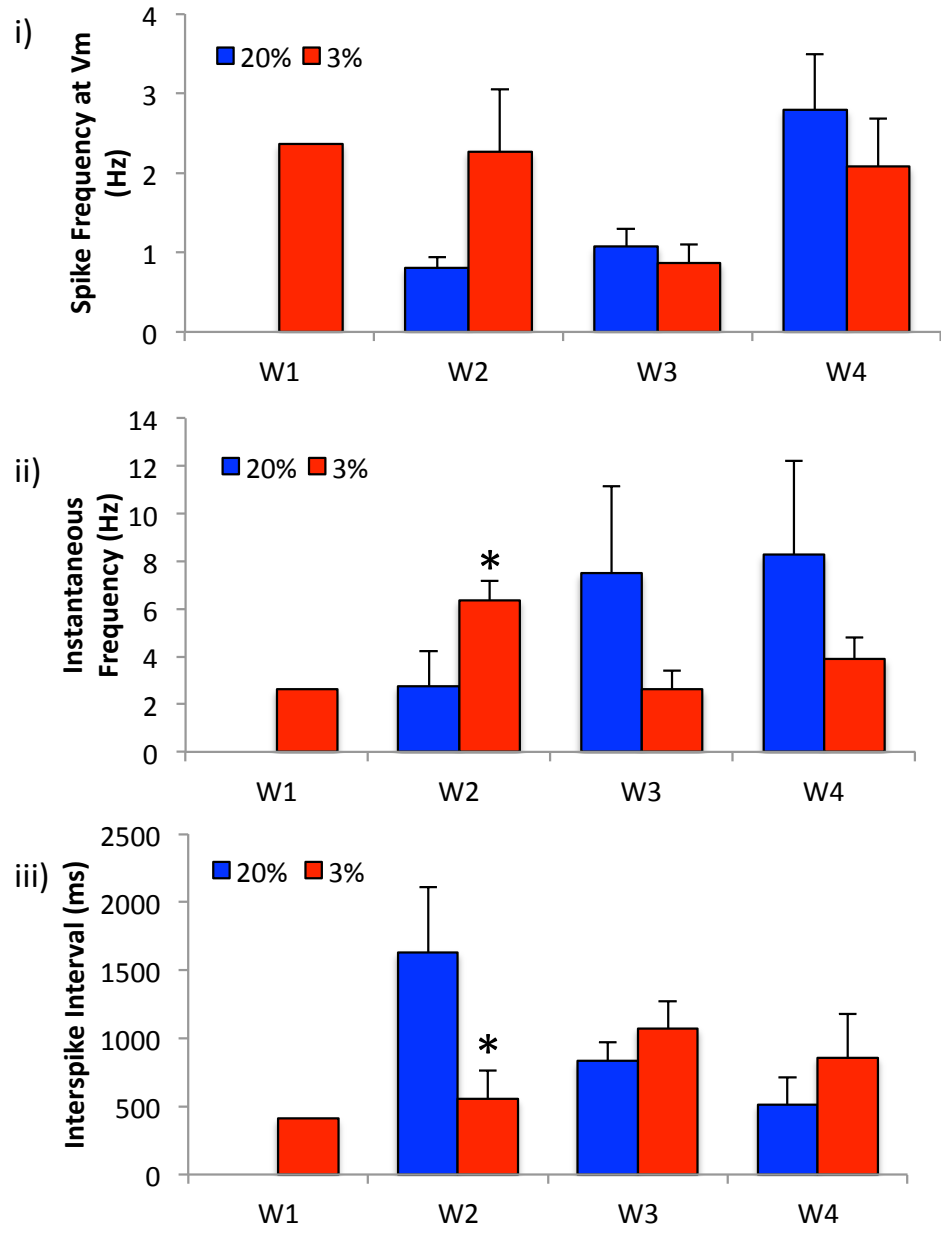

Figure 5.15. Increased excitability of neurons at 3% O_2 relative to 20% O_2. *At resting membrane potential, neurons demonstrating spontaneous activity at 3% O_2 produced AP trains at a higher spike frequency at weeks 1 and 2 of neuronal maturation (i) reflected with increased instantaneous frequency (ii) and reduced interspike interval (iii) *denotes significant difference between O_2 concentrations at the same current injection, significance was set at $p<0.05$.*

In neurons generating spontaneous activity at resting membrane potential, those matured at 3% O_2 showed far higher excitability and at much earlier timepoints than those at 20% O_2 (*figure 5.14, 5.15*). The number of successful APs during the first 30 seconds of gap-free recording at V_m was recorded and normalised per second (*figure 5.15i*). At week 1, spontaneous trains of APs were observed at 3% O_2 at 2.37 Hz (n=1) in contrast to 20% O_2 which showed just a single spontaneous action potential (*figures 5.7Ai, 5.14, 5.15i*). At week 2, spike frequency at 3% O_2 held steady at 2.27±0.8 Hz in comparison to reduced excitability at 20% O_2 (0.81±0.1 Hz, t(8)=1.2, p=0.272, n.s.). Spike frequency was also assessed using instantaneous frequency, whereby the number of APs per second was calculated and averaged over the first 30 seconds of recording (*figure 5.15ii*). Neurons produced at 20% O_2 did not show multiple sAPs at week 1 and repetitive firing was significantly retarded at week 2 (2.77±1.45 Hz, t(9)=2.7, p=0.026) comparatively to 3% O_2 (6.36±0.8 Hz). Both spike frequency and instantaneous frequency showed comparable spontaneous excitability across oxygen concentrations at week 3 and 4.

When assessing excitability, an additional useful factor to consider was the interval of time between successful APs, indicating the speed of propagation. The interval of time between spikes crossing the 0mV boundary (designated to classify a successful action potential) was consistently low at 3% O_2 from early on in the maturation period (409.1 ms at week 1 and 552.9±212.7 ms at week 2) whereas neurons at 20% O_2 showed lengthy interspike intervals at week 2 (1633.2±475.9 ms, t(9)=2.4, p=0.039). By week 4, 20% O_2 neurons reached comparable frequency to that observed at 3% O_2 (832.4±136.0 ms and 1073.4±195.7 ms respectively, t(10)=0.7, p=0.461). Hence, there is strong evidence to suggest that excitable neurons produced at 3% O_2 became functionally active in a shorter timeframe and to a greater degree than those at 20% O_2.

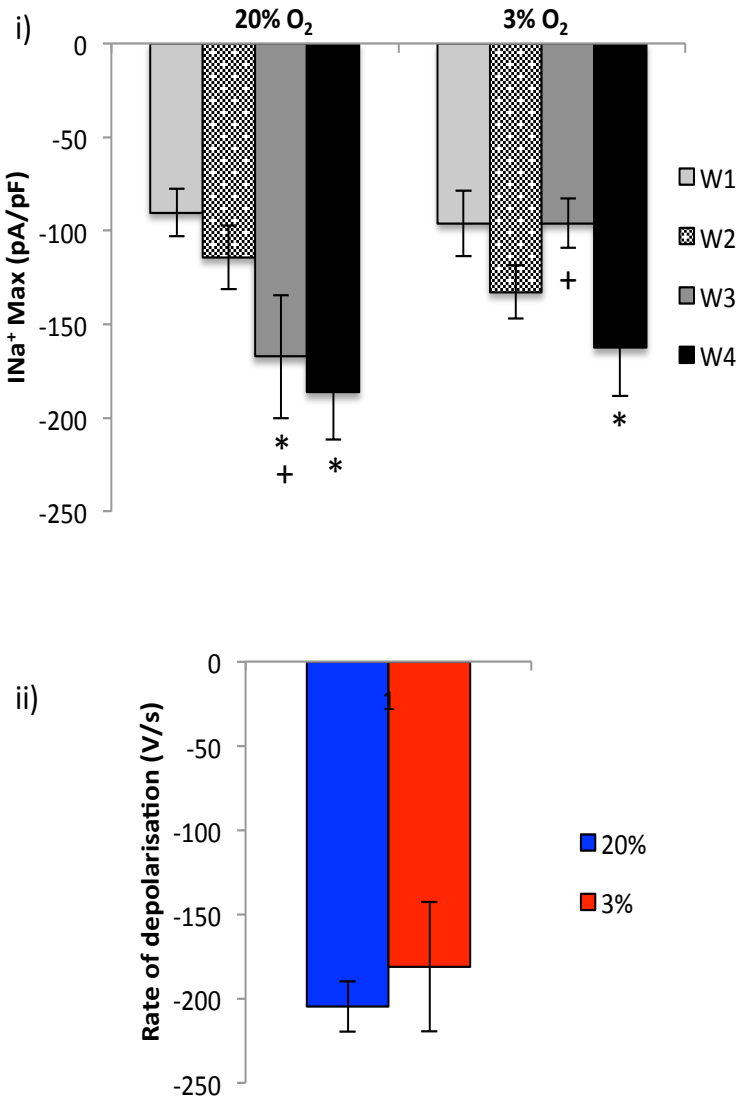

Figure 5.16. Peak Na^+ current density showed progressive increase over the four week maturation period at 20% and 3% O_2. *Upon examination of all cells which underwent patch-clamp analysis, peak Na^+ current density (INa^+ Max) showed progressive increase over Weeks 1 and 2, comparably between neurons produced at 20% and 3% O_2 with significant increase from baseline at Week 3 in neurons at 20% O_2 and Week 4 at 3% O_2 (i). When week 4 cells which showed spontaneous activity at resting membrane potential were focused on, this pattern continued with no significant differences across O_2 concentrations (ii). *denoted significantly different from Week 1 baseline data at the same O_2 concentration. +denoted a significant difference from the corresponding timepoint at contrasting O_2 concentration, significance was set at $p<0.05$.*

5.3.6 Activity of voltage-gated Na^+ and K^+ channels at 20% and 3% O_2.

Shown in *figure 5.10* was a characteristic progressive increase in the rate of depolarisation and repolarisation in neurons produced at both 20% and 3% O_2. Logically, an increase in the density of active ion channels may have been contributory towards this. An increase in the density of Na^+ and K^+ currents, INa^+ Max and IK^+ Max respectively, have previously been associated with a mature neuronal phenotype (Johnson et al. 2007; Bain et al. 1995; Benninger et al. 2003; Picken Bahrey & Moody 2003; Gao & Ziskind-Conhaim 1998). Here, voltage-clamp

was employed to assess peak channel activity and characterise the activation and inactivation of voltage-gated Na^+ channels.

The maximal density of active Na^+ currents (regardless of spontaneous activity at V_m) (*Figure 5.16i*) increased in a manner characteristic of neuronal maturation over the experimental period. Neural populations produced at 20% O_2 showed a progressive increase in INa^+ Max from Week 1 (-90.3±12.9 pA/pF) through to Week 3 (-167.2±33.0 pA/pF, t(17)=2.2, p=0.044), remaining steady at Week 4. Reflective of earlier analyses, neurons at 3% O_2 showed a delayed increase, with no significant deviation from Week 1 (-96.1±17.4 pA/pF) until Week 4 of the maturation period (-162.5±25.9 pA/pF, t(25)=2.1, p=0.046). Concordant with this, only at Week 3 was a difference observed between O_2 concentrations (t(30)=2.2, p=0.037). When analysis was performed solely on week 4 cells which had demonstrated spontaneous activity at V_m, (*figure 5.15ii*), INa^+ Max continued to be steady between 3% (-180.9±38.5 pA/pF) and 20% O_2 (-204.7±33.8 pA/pF, t(10)=0.5, p=0.653).

At both 20% and 3% O_2, cells with no spontaneous activity showed V_m lying outside of the (in)activation window (*figure 5.17)*, at a more depolarised position (*i*). Cells showing attempted (*ii*) and successful AP's (*iii*) had V_m generally lying within the (in)activation window. In cells attempting and producing sAPs at 3% O_2 (*ii, iii*), the mean V_m value was more centralised within the (in)activation window in comparison to those of 20% O_2, whereby mean V_m lay at an increasingly hyperpolarised position.

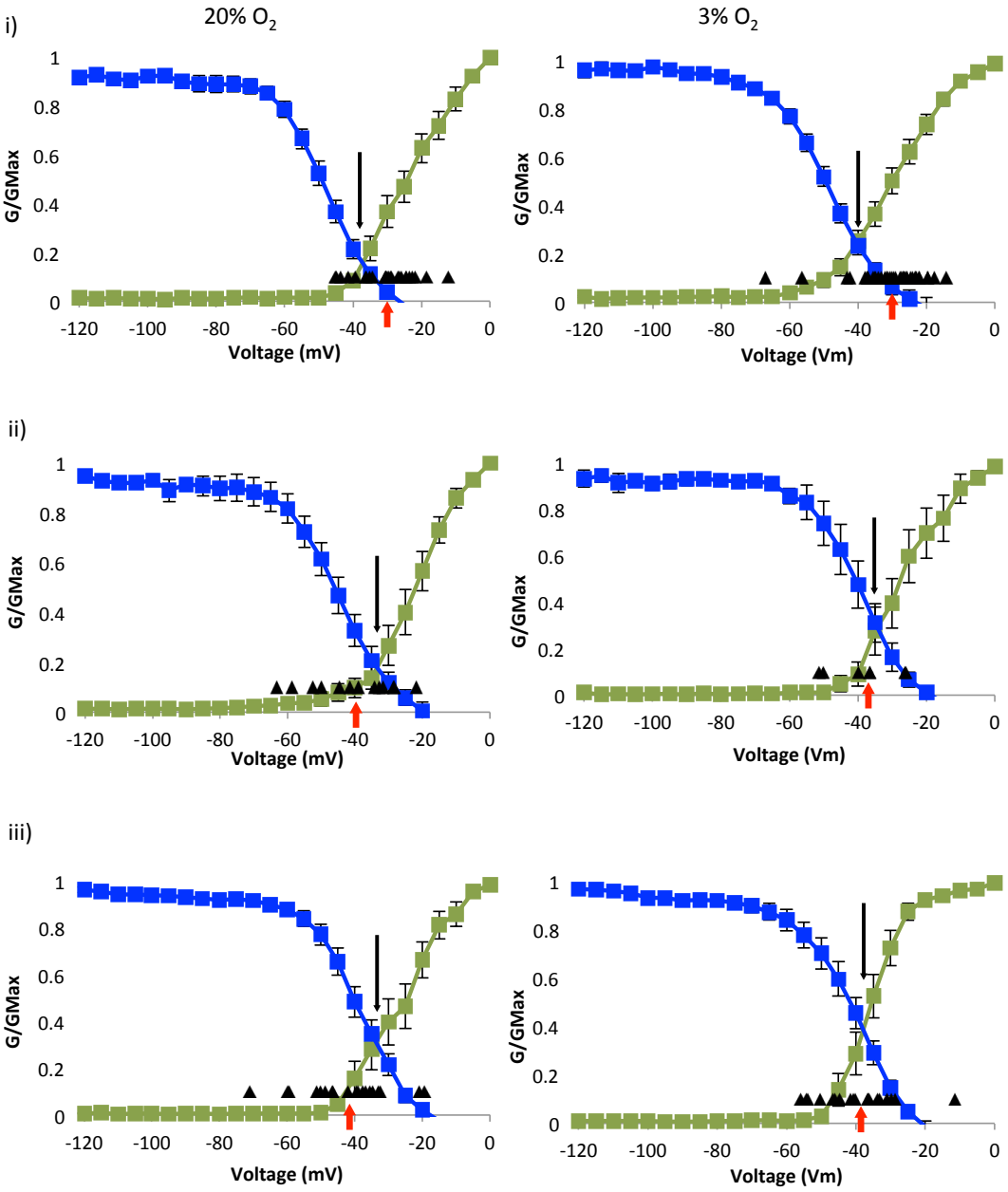

Figure 5.17. Sodium activation and inactivation plots. *Overlay of voltage-gated sodium activation (green) and inactivation (blue) give windows of activation (relative to input voltage), signified by downward black arrows indicating the cross-over, black triangles represent V_m for each cell analysed, upward red arrow signifies mean V_m value. Cells not attempting spontaneous action potentials at resting membrane potential (i) show mean V_m outside of (in)activation window. Those attempting sAPs (ii) showed a hyperpolarised shift in V_m as do those successfully forming sAPs (iii) at both 20% and 3% O_2. Data were grouped by O_2 concentration and spontaneous activity only and not separated dependent on timepoint of analysis.*

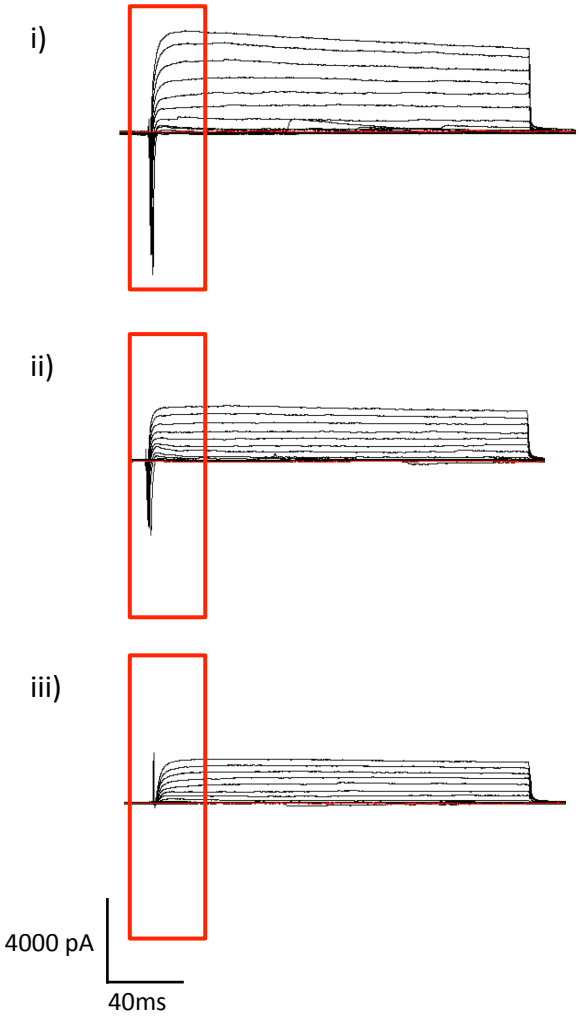

Figure 5.18. Activation of voltage-gated Na+ channels was successfully blocked by TTX. *The incoming positive current during voltage-clamp sweeps was confirmed to be due to the activation of voltage-gated Na^+ channels (i) by complete blockage with addition of 1μm Tetrodotoxin (TTX) (iii), an efficient inhibitor of Na^+ channels. Treatment with 1μm Nifedipine did not block incoming current, so depolarisation was not due to incoming calcium currents (ii).*

The inward current evoked by membrane depolarisation in untreated cells (*Figure 5.18i*) was confirmed to be due to activation of voltage gated Na^+ channels, demonstrated with a potent inhibitor of Na^+ channels, 1μm Tetrodotoxin (*iii*), and not due to Ca^{2+} channels, shown by the lack of effect of treatment with 1μm Nifedipine, an inhibitor of Calcium channels (*ii*).

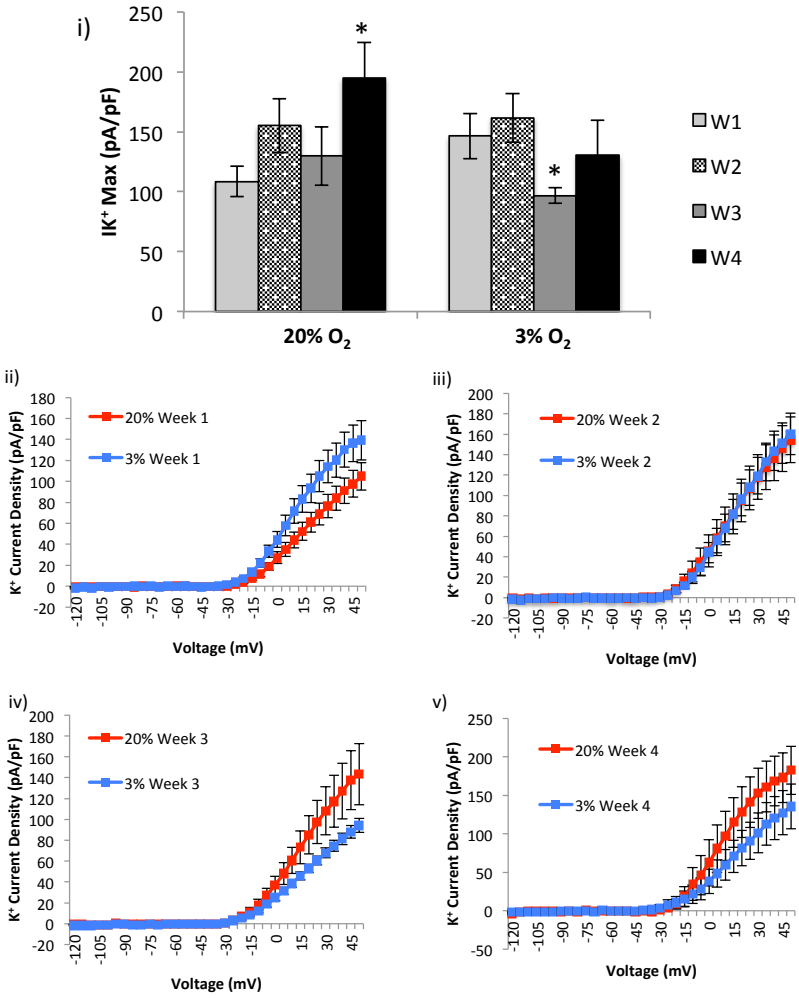

Figure 5.19. Maximal K^+ current density showed a limited response during neuronal maturation, with only neurons at 20% O_2 showing an increase in activity. *Peak K^+ current density (IK^+ Max) was increased at Week 4 comparatively to Week 1 at 20% O_2 although 3% O_2 had comparable IK^+ Max at Week 4 relative to Week 1. Week 3 showed a plateau at 20% O_2 and significant decrease at 3% O_2 (p=0.020). Data were grouped by timepoint and O_2 concentration only, significance was set at p<0.05.*

The peak density of active K^+ channels was more limited. A significant increase was observed at 20% O_2 between week 1 and week 4 (*Figure 5.19*, 108.4±12.6 pA/pF and 195.0±29.7 pA/pF, t(26)=3.1, p=0.004). 1 week old neurons at 3% O_2 had peak K^+ activity higher than at 20% O_2 although not significantly (141.7±20.8 pA/pF, t(33)=1.7, p=0.097) but the density of active K^+ channels at week 4 showed no significant difference to that at week 1 (130.6±28.8 pA/pF, t(16)=0.5, p=0.652).

Maximal K^+ activity was comparable across O_2 concentrations at all timepoints tested.

5.3 Discussion.

Use of pluripotent stem cells, particularly those from a human background whether ESC or iPSC, has increased exponentially over the last decade. With huge implications for readily produced *in vitro* terminal neurons in neurodegenerative disease modelling and toxicology, pressure for protocols producing large numbers of defined, fate specified, functionally relevant neurons is growing. Whilst much of the requirements are on producing a homogenous population of neurons patterned to a known specification, there is also a huge need for PSC-derived neurons whose excitability reflects that of neurons found *in vivo*. Here I have investigated in depth whether 3% O_2 was beneficial in augmenting the excitable and synaptic maturation of hESC derived terminal neurons.

5.3.1 Neural differentiation of hESCs at 3% and 20% O_2 formed a population of neurons in an efficient and reproducible manner.

Previous studies have implicated low O_2 in augmenting terminal neural differentiation *in vitro*. Commonly, a role in directing terminal specification has been the focus with an increase in the proportion of neurons expressing particular neurotransmitters reported, although little emphasis has been given to functionality (Krabbe et al. 2014; Stacpoole et al. 2011a; Horie et al. 2008; Studer et al. 2000; Kim et al. 2008). HESC derived NSCs, pre-conditioned at 0.1% O_2 for 12 hours prior to terminal neural differentiation showed no change in AP Overshoot, Half-Width or the number of APs generated (Francis & Wei 2010). Interestingly, direct neural reprogramming of human fibroblasts at 5% O_2 augmented the proportion of MAP2+ neurons and amplified levels of induced excitability although no investigation into the extent of synaptic integration was performed (Davila et al. 2013). Here, basic characterisation of neuronal cultures revealed consistency in the proportion of mature neurons produced (classed as βIII-Tubulin/MAP2+) at

20% and 3% O_2, with only a tiny subpopulation of astrocytes. This correlates with previous reports of no change in the efficiency of neural induction of mESC and rat NSCs at atmospheric and low O_2 (Mondragon-Teran et al. 2011; Jensen et al. 2011; Krabbe et al. 2014). Indeed, only Horie et al reported an increase in the proportion of terminal MAP2+ neurons produced from murine NSCs and the protocol used was one of extremely low efficiency, achieving less than 20% of neurons positive for βIII-Tubulin even at augmented production under low O_2 (Horie et al. 2008). MESCs and rodent NSCs differentiated at low O_2 showed a large increase in the proportion of the population with an immature βIII-Tubulin identity, but this did not induce an increase in mature MAP2+ cells (Mondragon-Teran et al. 2011; Krabbe et al. 2014). The extremely high efficiency of neural induction used here may have outweighed any effect of reduced O_2.

5.3.2. The proportion of excitable neurons was consistent across oxygen concentrations.

A previous study by Davila et al. reported that neural reprogramming of fibroblasts at low O_2 doubled the proportion of neurons generating induced APs, relative to an atmospheric O_2 concentration (Davila et al. 2013). In terms of the functional activity observed here, the proportion of neurons firing spontaneous action potentials and induced APs (both single and AP trains) was comparable across O_2 concentrations. Indeed, by Week 3 of analysis, 100% of cells at both 20% and 3% O_2 generated iAPs in current clamp steps. Hence, the high efficiency protocol used to generate populations of mature neurons may have also outweighed any effect of reduced O_2 on increasing or accelerating the proportion of neurons which became excitable.

At Week 3 of analysis, neuronal populations produced at 3% O_2 consistently showed a reduction in functional activity, which showed signs of rebounding by Week 4 of analysis. As analysis of those at 20% O_2 in Week 4 indicated a similar pattern in both passive and active functional components (depolarised V_m, reduced overshoot and a deceleration of the rate of depolarisation, *figures 5.9,*

5.10), it is possible that this was a technical issue. Anecdotally, prolonged maintenance of stem cell derived neurons *in vitro* is a recognised issue within the field, hence the temporal disparity may have been a combinatory effect of reduced O_2 hastening this drop in excitability. Alternatively, neuronal maturation at 3% O_2 to augment excitability was a transient temporal requirement, and movement to a higher oxygen concentration after two weeks is necessary for further maturation. Further work is required to investigate whether switching to higher O_2 will further synaptic integration and neuronal excitability. Use of a microelectrode array would allow switches between oxygen concentrations to be investigated in a high throughput manner.

5.3.3 Formation of synaptic terminals and spontaneous activity was accelerated at 3% O_2.

For formation of an integrated and functional neuronal network, the meeting of neuronal terminals and subsequent assembly of synapses is an essential step. Synaptophysin and PSD95 have been demonstrated as reliable markers of pre- and post-synaptic terminals respectively (Gordon et al. 2011; Kwon & Chapman 2011; Glantz et al. 2007; El-Husseini et al. 2000; Prange et al. 2004). Here, co-staining of these markers showed clear punctate co-registration on neuronal terminals, with PSD95 expression present from 1 Week onwards. Interestingly, neurons at 3% O_2 showed accelerated expression of Synaptophysin at week 1 with expression delayed to Week 2 in 20% O_2. As Synaptophysin has reportedly played a role in the formation of synapses and in the recycling of synaptic vesicles, its fast-tracked appearance here indicated that structural meeting of pre- and post-synaptic synapses may have occurred earlier at 3% O_2 in comparison to 20% O_2 (Gordon et al. 2011; Kwon & Chapman 2011; Glantz et al. 2007; Tarsa & Goda 2002). Although this did not result in an increase in the proportion of cells propagating spontaneous activity at 3% O_2, it may underlie the augmented excitability observed at 3% O_2. When held at resting membrane potential, cells produced at 3% O_2 showed vastly higher levels of repetitive firing, even at Week 1 of neuronal maturation (*figures 5.14, 5.15*). This was reflected in the increased spike frequency

at 3% O_2 in iAP trains (*figure 5.11*). It is feasible that an increase in synaptic recycling through augmented Synaptophysin expression supported the increased AP firing frequency. It is worth noting that the accelerated Synaptophysin expression at 3% O_2 occurred regardless of O_2 prior to neuronal plate-down, suggesting that the observed increased excitability due to 3% O_2 was specific to the period of neurogenesis itself. Unfortunately, due to time constraints it was not possible to perform electrophysiology on all 4 conditions to confirm this, although this will be performed in future experiments. Additionally, use of a microelectrode array to assess synaptic transmission of action potentials would clarify whether accelerated Synaptophysin expression at 3% O_2 correlated with increased formation of a synaptic network or whether the increase in spontaneous repetitive AP firing was a result of increased excitability on an individual cell basis. Scholl analysis of dendritic outgrowth at 20% and 3% oxygen would also further clarify levels of dendritic migration.

5.3.4 Increased AP firing in spontaneously excitable neurons at 3% O_2.

Although the proportion of neurons which showed spontaneous and induced excitability was comparable across oxygen concentrations, the degree of excitability was significantly enhanced by differentiation at low oxygen. Not only did neurons demonstrate greater frequencies of induced action potentials, but the intensity of spontaneous activity was also enhanced and accelerated at low oxygen, with augmented frequency of AP firing and reduction of intervals between APs (*figure 5.11, 5.15*). After 4 weeks of maturation, the rate of membrane depolarisation was boosted to such a degree that AP overshoot was significantly increased. This highlights oxygen as an essential tool for increasing excitability of neurons. Previous reports have indicated a role in low oxygen influencing the phenotype of stem cell derived neurons (Mutoh et al. 2012; Studer et al. 2000; Horie et al. 2008; Kim et al. 2008; Y. Wang et al. 2013). Regional specification of neurons produced at 3% and 20% O_2 was deemed outside of the scope of this study, but investigation into the patterned identity of neurons matured in low oxygen may clarify if this was a general effect in neuronal maturation or due to an

influence on regional identities. As an increase in the rate of depolarisation was also observed, additional determination of voltage gated Na^+ channel expression in terms of RNA transcription and protein expression would also be beneficial.

5.3.5 Increasingly co-ordinated resting membrane potential and ion channel activity in neurons produced at 3% O_2.

A number of factors are contributory to the formation and propagation of a successful action potential. High density of voltage gated Na^+ channels would theoretically allow for more rapid charging of capacitance and accelerated membrane depolarisation. Additionally, a hyperpolarised resting membrane potential residing within the (in)activation window of voltage-gated Na^+ channels gives the potential for repetitive firing under the necessary incoming stimuli. It's been shown previously that as the number of membrane channels increased, the resistance to current flow across a membrane decreases, giving an inverse relationship between channel density and Input Resistance (Johnson et al. 2007; Benninger et al. 2003; Picken Bahrey & Moody 2003). In addition to augmenting the density of channels responding to incoming depolarising signals and subsequent Na^+ influx, increased density of K^+ channels would accelerate repolarisation, aiding fast repetitive firing. RIn in neurons produced at 3% O_2 was significantly reduced at all timepoints from Week 2 onwards whereas those at 20% did not deviate from baseline Week 1 values throughout neuronal maturation. That said, this did not seem to have any large functional benefit until week 4 of maturation whereby cells at 3% O_2 showed acceleration in the rate of depolarisation. Additionally, although resting membrane potential at 3% O_2 showed no significant hyperpolarisation until Week 4 of analysis, cells which attempted or succeeded in propagating sAPs also had V_m which resided within the Na^+ current in(activation) window at 3% O_2 (*figure 5.17*). Those which were spontaneously active at week 4 in 3% O_2 also had iAPs with augmented overshoot and rates of depolarisation. Together, this evidence indicates that low oxygen was contributory towards providing and organising the required machinery for

functional, highly excitable neurons; with indications of accelerated synaptogenesis, increased membrane ion channels and augmented excitability.

5.4 Summary

Here, I sought to define the characteristics of neuronal maturity in hESC-derived neurons, and to investigate in depth whether production of neurons under O_2 reminiscent of that present during embryonic and post-natal synaptogenesis played a role in accelerating or enhancing the excitability and functionality of neurons. Neural populations at both high and low oxygen differentiated with a clear pattern of progressive excitable phenotype, with hyperpolarised V_m, voltage threshold and afterhyperpolarisation, reduced RIn and AP half-width and augmented overshoot and membrane polarisation rates, compared to basal week 1 values. Although Synaptophysin expression was accelerated in neurons produced at 3% O_2, indicating augmented formation of synaptic junctions, this did not correlate with an increase in the proportion of cells producing spontaneous or induced action potentials. However, neurons with spontaneous activity at 3% O_2 consistently showed increased excitability reflected by heightened spike frequency of iAPs. It was also observed that at V_m, neurons formed at 3% O_2 produced spontaneous trains in an accelerated timeframe with augmented firing frequency. Neurons produced at 3% O_2 demonstrated increased rates of membrane depolarisation and attenuated input resistance. Additionally, V_m appeared to be hyperpolarised and hence lay within the (in)activation window of voltage gated Na^+ channels, likely contributing to the observed increased excitability. Future work will consider further manipulation of the O_2 applied in addition to using Micro Electrode Arrays for additional, high throughput assessment of spontaneous synaptic transmission.

6. Validation of media de-oxygenation, in conjunction with Baker-Ruskinn.

The following white paper was produced in conjunction with Baker-Ruskinn for validation of the HypoxyCOOL™.

Abstract

Application of reduced O_2 for the *in vitro* maintenance of mammalian cells and tissues is widespread, bringing with it certain practical challenges. In this paper we demonstrate the validation of a systematic approach to removing dissolved oxygen (DO) from cell culture medium. The HypoxyCOOL™ predictably deoxygenated DMEM, MEM and IMDM basal media to 0.60±0.23 mg/L O_2 (1.25±0.47%), 0.67±0.23 mg/L O_2 (1.37±0.47%) and 0.74±0.34 mg/L O_2 (1.45±0.66%) respectively, over a standard 3 hour cycle. In comparison, deoxygenation of medium using the traditional method of incubation in a hypoxic workstation was prolonged, with only minimal reduction of DO, from 7.81±0.76 to 6.24±0.43 mg/L over a 6-hour period. HypoxyCOOL deoxygenated media showed ~2-fold increase 24 hours post-deoxygenation, remaining stable with reduced O_2 for up to 6 weeks thereafter. The HypoxyCOOL is an efficient and reproducible method for deoxygenating large volumes of cell culture media.

Introduction

Oxygen is recognised as an inherently essential molecule for life with all major organisms dependent on it for energy production. In addition to its role as a vital electron acceptor during ATP production (Karp 2009), it has also been highlighted for its critical function as an *in vivo* signalling molecule (Simon & Keith 2008; Semenza 2000; Iyer et al. 1998). Although oxygen constitutes ~21% of atmospheric air (160 mmHg), this concentration drops rapidly upon inhalation and entry into the circulatory system, with most adult tissues operating at ~5% O_2 (~40 mmHg) (Singh 2008). An increase in metabolic rate and distance away from

vascular networks has been correlated with additional attenuation of pericellular and intracellular oxygen concentrations (Singh 2008; Pettersen et al. 2005). These gradients in oxygen concentration exist from post-fertilization onwards through to adulthood, acting to regulate both normal cellular identity and proliferation in addition to a pathogenic role in many disease states such as vascularisation of hypoxic tumours and excessive inflammation (Bartels et al. 2013; Semenza 2011b; Simon & Keith 2008). With current developments in tissue culture modelling, necessary consideration must be given to accurately replicating the *in vivo* environment for *in vitro* maintenance of cells and tissues, particularly during the examination of oxygen sensitive signalling pathways.

In this context, consistency and stability of *in vitro* experimental oxygen concentrations is key. Widespread use of hypoxic and anaerobic workstations has ensured consistency of environment throughout long-term experiments, allowing accurate and physiologically relevant modelling of *in vivo* O_2 concentrations. To avoid fluctuating O_2 during maintenance of cell cultures, a common practice is de-oxygenation of the liquids required for cell cultures through incubation in a gaseous low oxygen environment prior to use, a process which (dependent on the scale required) may be time-consuming and inaccurate. HypoxyCOOL™ (Baker-Ruskinn, UK) is a pre-conditioning unit designed to supplement *in vitro* experiments in low oxygen or anoxia, reducing the concentration of dissolved oxygen (DO) in media and other cell culture reagents to the desired level, in order to maintain consistency of O_2 exposure. Initial experiments detailed here were employed to assess the efficiency, reproducibility and stability of media preconditioning, in addition to validating the deoxygenation process in media with a range of salinity.

Materials and Methods

Controlled deoxygenation of media.

The HypoxyCOOL™ was designed to reduce the concentration of dissolved oxygen through agitation and cooling at reduced gaseous O_2 concentration. Each

variable was set by the end-user and operated within a set range: 2-6°C, 0.5-15% gaseous O_2, 0-10% gaseous CO_2 and 40-120 rpm agitation. Here, a standard cycle of 1% O_2, 5% CO_2, 4°C and 120rpm was used for deoxygenation cycles unless stated otherwise. Three media types with varying dissolved salt (NaCl) content were used throughout experiments; Dulbecco's Modified Eagle Medium at 6.329g/L NaCl, rounded to 6g/L (DMEM, BE12-709F), Modified Eagle Medium at 8g/L NaCl (MEM, BE12-127F) and Iscove's Modified Dulbecco's Medium at 4.505g/l NaCl, rounded to 5g/L (IMDM, BE12-722F) all from Lonza, UK. Dissolved oxygen concentration in media was measured before and after deoxygenation of media. For HypoxyCOOL™ deoxygenation, media bottle caps were replaced with vented sterile caps (10133532, Fisher-Scientific, UK) to allow gas transfer into the headspace of media bottles. For measurements of long-term stability, caps were replaced with original media bottle caps, bottles were then stored at 4-8°C until conclusion of stability study.

Defining measurements of gaseous and dissolved O_2.

The amount of oxygen present in either a gaseous or liquid mixture can be understood and defined in a number of ways. The partial pressure of a gas is the pressure exerted by that gas in a mixture of gases (measured in mmHg). Concordantly, the ideal gas law states that the partial pressure of each gas is dependent and proportional to the number of gas molecules present, hence is equivalent to the concentration of that gas. Dalton's Law of Partial Pressures rules that the pressure of an individual gas within a mixed gas population within a set volume is the same as if it was the only gas present within the same system. Hence, the total pressure of a mixture of non-reactive gases is equal to the sum of the partial pressure of each individual gas.

The degree to which oxygen dissolves within a liquid is dependent on its partial pressure in the gaseous phase. Henry's Law states that at a constant temperature, the concentration of a given gas in a given liquid is directly proportional to the partial pressure at which the gas is applied. As pressure above the liquid increases, the amount of dissolved oxygen within the liquid increases proportionally, until

reaching equilibrium between the two phases. This point of equilibrium is defined as maximal saturation and is dependent on altitude, salinity and temperature of the liquid.

An increase in altitude and the corresponding decrease in barometric pressure reduces the overall number of gas molecules present in the gaseous phase; the percentage of those which are O_2 will remain constant although the absolute concentration may drop considerably. Any change in gaseous pO_2 will have downstream effects on the achievable dissolved oxygen concentration (Lighton 2008). The solubility of oxygen within a liquid is also inversely proportional to temperature and salinity of the liquid, with the maximum possible oxygen saturation occurring at low temperature and salinity.

The concentration of a gas dissolved in a liquid can be defined in 2 general ways; absolute and relative measurements. Absolute measurements quantify the number of oxygen molecules present, such as, parts per million (ppm), milligram per litre (mg/L) or micromoles (μM). Relative measurements convey this in terms of a fraction of the whole, for example, O_2 constitutes 20.9% of atmospheric air as it contributes 160 mmHg towards a total barometric pressure of 760 mmHg. Comparably, the percentage of dissolved oxygen in a solution is relative to the maximum saturation possible in water at fixed temperature, salinity and pressure. For example, pure water is capable of holding 10.07 mg/L O_2 at 15°C, dropping to 7.54 mg/L O_2 at 30°C (FAO.org n.d.). Water holding half the possible amount of oxygen at both temperatures will continually show as 50% saturated, although the concentration between temperatures has changed vastly.

Method of measuring dissolved oxygen.

For all measurements of DO in medium, media bottles were placed inside a sterile, low oxygen workstation (SCI-tive, Baker-Ruskinn) set at 3% O_2 and 5% CO_2. Measurements of dissolved oxygen were performed with an electrochemical probe (HI2400 Dissolved Oxygen meter (HANNA, HANNA Instruments) derived from the original Clark electrode, current was produced by oxidative reduction in a

manner whereby current output was proportional to partial pressure (Clark et al. 1953). Segregation of a cathode and anode away from the test solution by an oxygen permeable membrane, ensured the oxygen 'starved' cathode reduced all O_2 exposed to it (Lighton 2008). The HANNA underwent weekly 2-point calibration between zero and atmospheric O_2 using a solution of 1-3% sodium metabisulfite (HI-7040, HANNA Instruments) and calibration in air respectively. Inserting the probe into media for 1-3 minutes allowed temperature to settle and thermal equilibrium to occur between external test solution and internal electrolyte, necessary for accurate measurements. Dissolved oxygen was recorded as absolute (parts per million) and relative (percentage) measurements. As the calibration curve ran from 0-21% O_2 but readout was between 0-100%, the following linear equation was applied, to scale values down to be representative of 0-21% O2; where x=% data readout, [(x/100)*21].

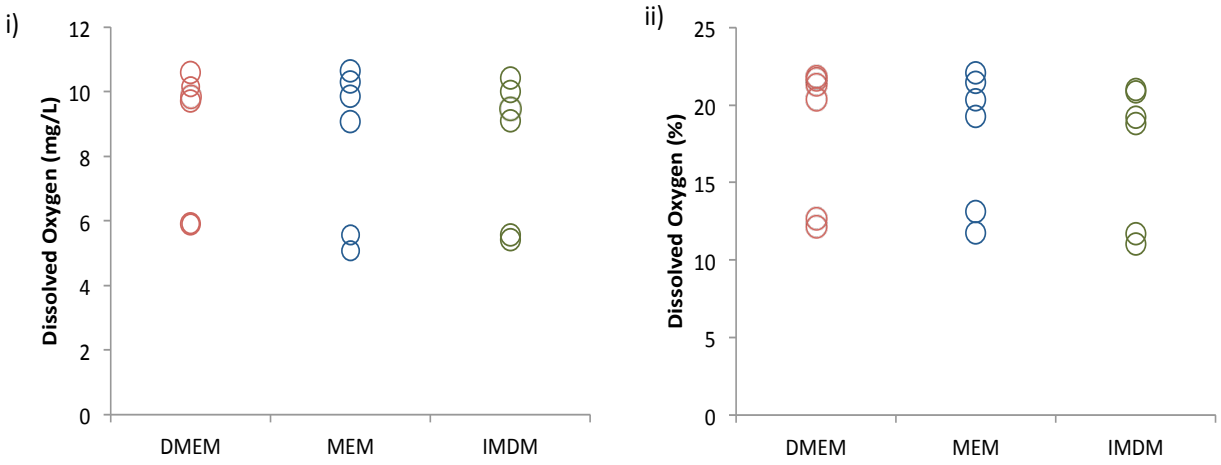

Figure 1. Fresh bottles of media show large variation in dissolved oxygen content. *Fresh, previously unopened bottles of DMEM, MEM and IMDM media showed large variations in DO concentration when measured either with the HANNA as mg/L (i) or percentage (ii), n=6, each circle represents an independent bottle.*

Results

Prior to pre-conditioning, fresh, previously unopened media bottles were assessed for starting DO concentration. All three media types tested showed large, inter-bottle variation in DO content (*Figure 1*), ranging from 5.9-10.5 mg/L in DMEM, 5.08-10.65 mg/L in MEM and 5.43-10.43 mg/L in IMDM.

Initial tests had outlined a preliminary test cycle for investigation into HypoxyCOOL media de-oxygenation using the following setpoints; 1% O_2, 5% CO_2, 4°C and 120RPM agitation for 3 hours. We sought to determine how efficient and reproducible this cycle was in removing DO from multiple media types with a range of salinities. All three media types showed consistent and efficient removal of DO after application of the standard cycle (*Figures 2-4*). Absolute measurements showed <1mg/L DO after deoxygenation across all media types, with removal of DO in DMEM from 8.68±2.18 to 0.60±0.23 mg/L (*figure 2.A*), MEM from 8.42±2.46 to 0.67±0.23 mg/L (*figure 2.B*) and IMDM from 8.33±2.24 to 0.74±0.34 mg/L (*figure 2.C*). This pattern was reflected with relative percentage measurements post-conditioning; DMEM at 1.25±0.47%, MEM at 1.37±0.47%, IMDM at 1.45±0.66

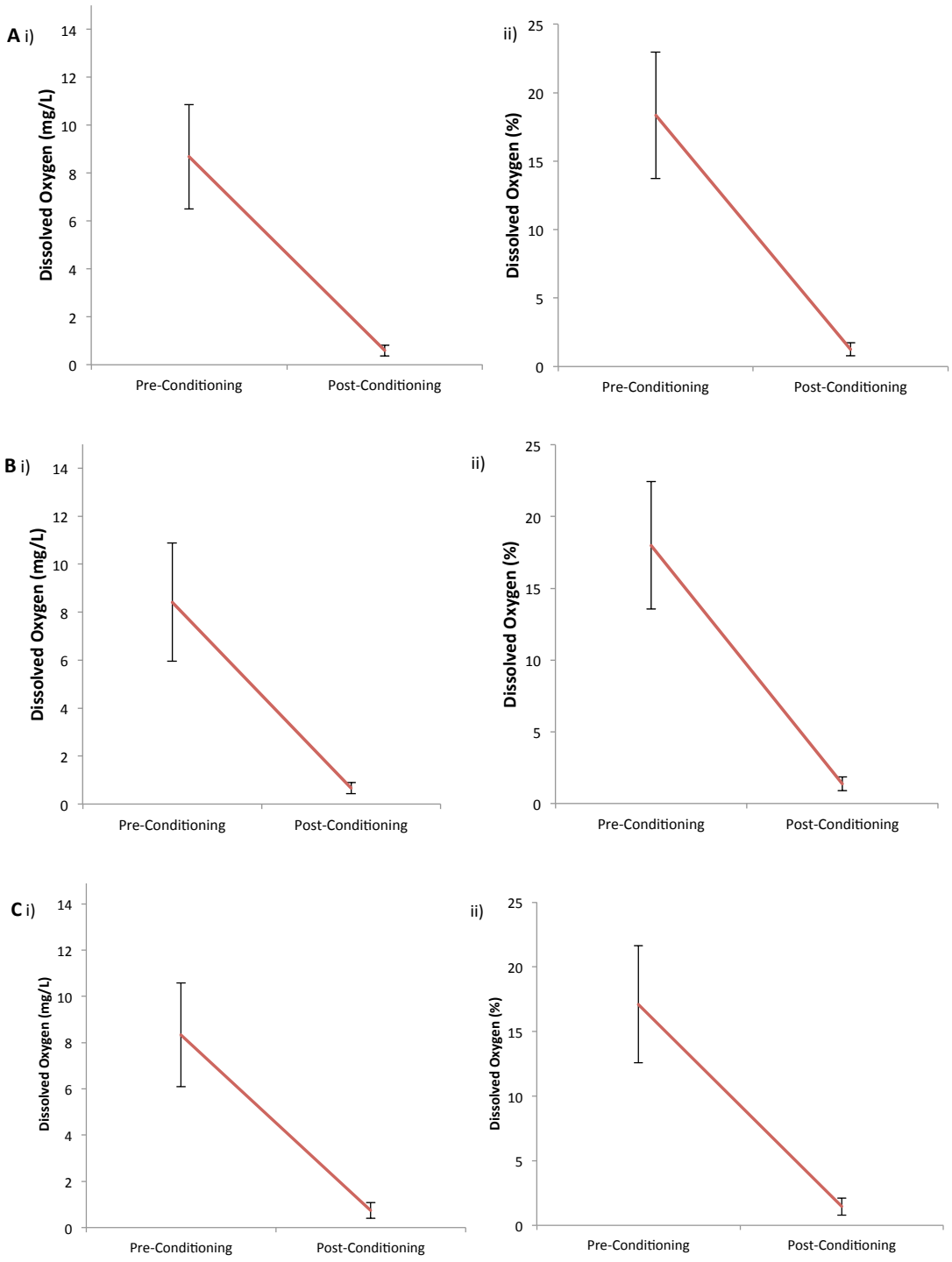

Figure 2. Controlled deoxygenation of DMEM, MEM and IMDM media. *After a standard HypoxyCOOL cycle (1% O_2, 5% CO_2, 120RPM, 4°C for 3 hours), the dissolved oxygen concentration was assessed in multiple media types across a range of salinities. DMEM media (A) deoxygenated from 0.60±0.23 mg/L O_2 (i) or 1.25±0.47% O_2 (ii) n=6. MEM media (B) deoxygenated from 0.67±0.23 mg/L O_2 (i) or 1.37±0.47% O_2 (ii), n=6. IMDM media (C) deoxygenated from 0.74±0.34 mg/L O_2 (i) or 1.45±0.66% O_2 (ii), n=6, data displayed as mean±SD*

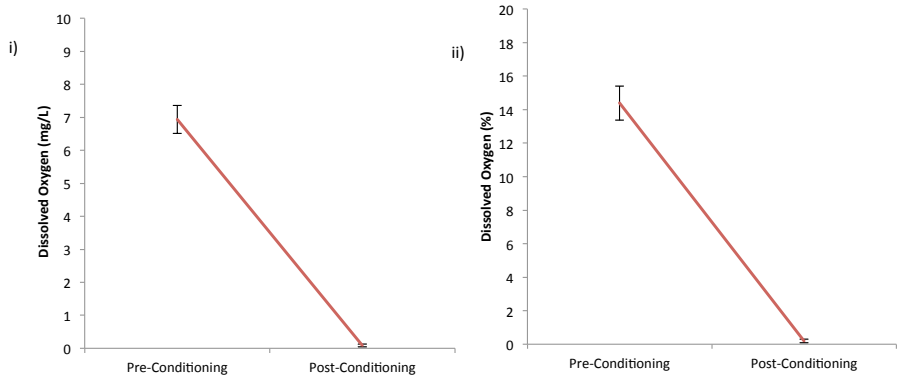

Figure 3. Controlled deoxygenation of DMEM media down to less than 0.5% Dissolved Oxygen. *Using a HypoxyCOOL cycle of 0.5% O_2, 5% CO_2, 120RPM, 4°C for 5 hours, DMEM media was brought down to 0.09±0.05 mg/L O_2 (i) or 0.20±0.0.11% O_2 (ii), n=3, data displayed as mean±SD*

As research in the field of low oxygen has commonly focused on cells and tissues functioning at <1% O_2 (relative to comparable DO in water at the same salinity), we aimed to reduce DO in cell culture medium to below this level (Simon & Keith 2008). By reducing the O_2 setpoint to 0.5% O_2 and extending the cycle length to a total of 5 hours, the relative DO concentration of DMEM was reduced to 0.20±0.11% and the absolute concentration to 0.09±0.05 mg/L (*figure 3*). In addition to demonstrating the ability of the HypoxyCOOL to efficiently deoxygenate media to minimal levels, this clearly emphasized the requirement for end-user optimisation of HypoxyCOOL cycles to reach their desired O_2 concentration.

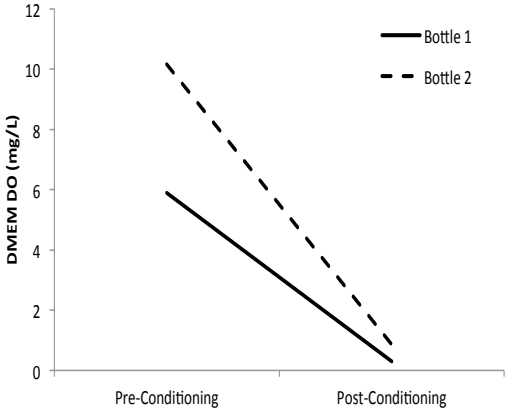

Figure 4. Dissolved oxygen concentration prior to deoxygenation was contributory to DO concentration achieved post-conditioning. *Using a HypoxyCOOL cycle of 1% O_2, 5% CO_2, 120RPM, 4°C for 3 hours, DMEM media was pre-conditioned to reduce oxygen content. Bottle 1 had initial DO content of 5.9mg/L and reduced to 0.29mg/L whereas with a starting concentration of 10.15mg/L DO concentration of 0.86mg/L was obtained (Bottle 2).*

It was also observed that the efficiency of de-oxygenation was impingent on the starting DO content. *Figure 4* shows data representative of the entirety of the data set; post-conditioning, DO content was nearly three-fold higher in Bottle 2 than Bottle 1 (0.86mg/L and 0.29mg/L respectively) after a two-fold higher starting DO concentration (10.15mg/L and 5.9mg/L). Regardless of the range of starting concentrations tested, all samples showed consistent reduction of DO content to <1mg/L *(see figure 2)*.

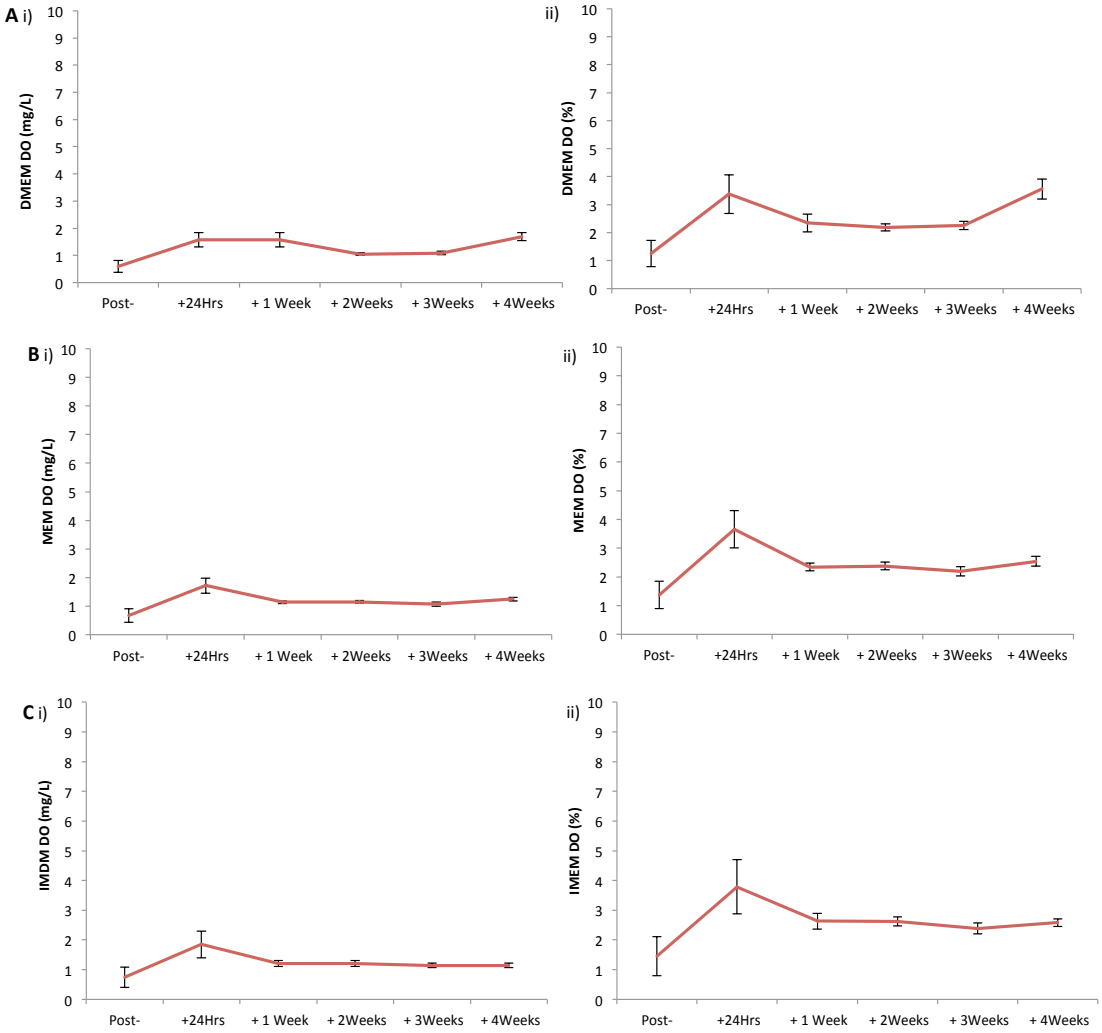

Figure 5. Post-conditioning, dissolved oxygen concentration in DMEM, MEM and IMDM remained stable for up to 4 weeks. *HypoxyCOOL mediated deoxygenation reduced DO concentration in DMEM (A), MEM (B) and IMDM (C) to 0.60±0.23 mg/L, 0.67±0.23 mg/L and to 0.74±0.34 mg/L O_2 respectively. This reduced concentration was largely retained for up to 4 weeks post-conditioning at 1.70±0.39 mg/L, 1.24±0.07 mg/L and 1.14±0.07 mg/L O_2, n=6 each.*

Previous studies outlined the passive movement of O_2 across the polyethylene terephthalate plastic commonly used in the manufacture of media bottles(Papkovsky & Dmitriev 2013; Siró et al. 2010; Prattipati et al. 2005). Hence, we deemed it prudent to determine the stability of DO concentration after media deoxygenation, expecting it to be short-term and transient, before rising to equilibrate with atmospheric O_2. Surprisingly, reduced DO concentration was shown to be relatively stable long-term, with the observed increase in DO concentration during the initial 24 hours post-deoxygenation being retained for up to 4 weeks at 1.70±0.39 mg/L, 1.65±0.69 mg/L and 2.67±0.19 mg/L for DMEM, MEM and IMDM respectively (*figure 5*).

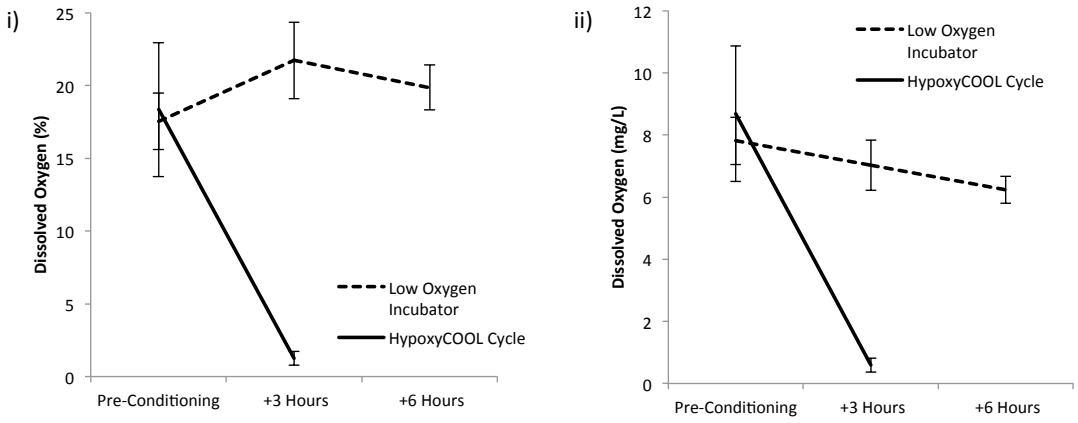

Figure 6. Deoxygenation via the HypoxyCOOL was more rapid, efficient and reliable in comparison to deoxygenation through incubation in a low oxygen incubator. *Fresh 500ml bottles of DMEM were reliably brought down to 1.25±0.47 % (i) or 0.60±0.23 mg/L (ii) using a standard 3 hour HypoxyCOOL cycle. Contrastingly, incubation of 500ml bottles with gas permeable lids inside a workstation programmed to 3% O_2, 5% CO_2 showed very mild deoxygenation over 6 hours, reaching 7.03±0.23 mg/L and 6.24±0.43 mg/L after 3 and 6 hours respectively (ii), n=3. No drop in percentage was observed after 6 hours (i), this relates back to percentage of the maximum possible dissolved oxygen saturation at that temperature, salinity and pressure; as temperature increases, the solubility of oxygen decreases such that the observed small reductions in oxygen concentration are negligible when compensating for the above factors. Data displayed as mean±SD, n=3.*

The majority of researchers working within a low oxygen environment maintain consistency of oxygen concentration in cell cultures by incubating liquids in a low oxygen incubator or workstation prior to use. Here, 500ml bottles of media were left for up to 6 hours in a workstation operating at 3% O_2 and 5% CO_2 to determine the efficiency of deoxygenating liquids in this method. Even after 6 hours, absolute DO content had only dropped to 6.24±0.43 mg/L from a starting concentration of 7.81±0.76 mg/L, in comparison to 0.60±0.23 mg/L achieved by the HypoxyCOOL™ in 3 hours, from a starting concentration of 8.68±2.18 mg/L.

Timepoint	***Temperature (°C)***	***Maximum O_2 saturation (mg/L)***	***Absolute O_2 saturation (mg/L)***	***Absolute / Maximum O_2 saturation (%)***	***HANNA O_2 saturation readout (%).***
Pre-conditioning	*16*	*9.512*	*8.10*	*85.2*	*85.5*
+ 3 hours	*34*	*6.822*	*7.03*	*103.0*	*103.4*

Figure 7. Relative vs absolute measurements of dissolved oxygen. *The observed increase in temperature over three hours of incubation at 3% O_2 and subsequent decrease in the defined maximum O_2 saturation led to an increase in the relative O_2 saturation, masking the reduction of absolute DO from 8.10mg/L to 7.03 mg/L.*

It was interesting to observe that the minimal decreases in absolute DO concentration over 6 hours (*figure 6ii*), were not observed when quantifying DO in relative terms (*figure 6i*). This is an excellent example of why measurements in absolute terms are essential for accurate assessment of DO concentration. Output in terms of 'percentage' relate back to the percentage of the maximum possible dissolved oxygen saturation of water at fixed altitude, temperature and salinity. As temperature increased, the solubility of oxygen decreased such that the observed small reductions in oxygen concentration were negligible when compensated for the above factors. As an example, see *figure 7* for a breakdown of the 3 hour timepoint in *figure 6i* and *ii*; at 34°C in a liquid with 6mg/L salinity, the maximum possible DO saturation is 6.822mg/L. With the absolute readout of 7.03mg/L,

conversion to a relative readout [(7.03 / 6.828)*100] equals 102.9%, closely correlating to the HANNA relative measurement of 103.4%. This can be explained by examining the temperature change due to 3 hours incubation in a 37°C workstation after refrigerated storage, equating to a decrease in the maximum possible oxygen saturation of water, essentially cancelling out the clear although small decrease of DO in absolute terms.

Discussion

Here, we examined the deoxygenation of multiple media types using the HypoxyCOOL™, in addition to determination of stability of dissolved oxygen post-conditioning. Deoxygenation of all media types tested was reliable and reproducible and could be performed in a manner that maintained integrity of medium, for future use in cell cultures. No obvious signs of microbiological contamination (clouding of media, visible acidification etc.) were observed throughout although comprehensive microbiological analysis was deemed outside the scope of this study. Deoxygenation in this manner bought DO content down to a predictable level in a manner partly dependent on the starting concentration as seen in *Figure 4*, although regardless of DO concentrations tested, all samples showed reduction in DO concentration to below 1mg/L or 1-1.5% in the standard cycle and DMEM down to 0.09mg/L with optimisation of the applied cycle. Whilst DO concentration rose marginally in the first 24 hours post-conditioning (0.74±0.34 to 1.85±0.45 mg/L in DMEM for example), this concentration was largely retained for up to 4 weeks post-deoxygenation.

The DO sensor tested here had a mechanistic basis in the Clark electrode, whereby cathodic oxidative reduction generated a current output correlative to DO concentration. A number of issues occurred whilst measuring very low concentrations of DO in a sterile setting. Electrochemical oxygen quantification was reliant on oxidative reduction at the cathode, consuming the oxygen present and forming hydroxyl ions (OH^-) in its stead (Lighton 2008). Whilst rates of O_2 consumption were relatively low, this did present issues when working at very low

DO concentrations as further removal of DO from the test sample may have contributed to measurement inconsistencies.

Assessing the rate of deoxygenation in volumes applicable to small-scale cultures (50-250ml) is a vital next step. Removing the DO from medium by incubation in a low oxygen environment is pervasive, here, investigation using a 500ml media bottle displayed slow and marginal deoxygenation over a 6 hour time period. Frequently, the required volumes would be far smaller and hence deoxygenation presumably quicker. Future work will examine this using optical DO sensors which in addition to not being oxygen consumptive also do not require immersion of a probe into a small volume and may be more appropriate to a sterile, cell culture application.

7. Thesis Conclusions and Future Directions

In this study I have examined whether the use of an oxygen concentration reminiscent of that present during early embryonic development and neurogenesis, was a useful tool in maintaining the self-renewal and directing the differentiation of human pluripotent stem cells. Here I have recapitulated the key findings of this study and outlined further work.

7.1 Low oxygen did not increase self-renewal of the H9 hESC or 34D6 iPSC lines.

Here, comparison of H9 hESCs and 34D6 iPSCs showed contrasting responses to maintaining pluripotency at 3% O_2, consistent with the variable responses reported previously. This cements the necessity for each PSC line to undergo assessment prior to differentiation at low oxygen. Both showed stabilisation and nuclear translocation of HIF1A and expression of HIF2A, and in a novel finding, up-regulation and nuclear translocation of PHD2 was observed in a timeline that correlated with nuclear HIF1A expression. Additionally, neither line suffered reduced viability at 3% O_2 (once light exposure was removed as an apoptotic inducer). That said, only the 34D6 line showed an oxygen dependent increase in the actively dividing population, in addition to a reduction in the proportion of cells retaining SSEA4 expression, an acknowledged marker of self-renewing cells (Adachi et al. 2010; Fong, K. a Hohenstein, et al. 2008; Z. Wang et al. 2012). Additionally, the H9 hESC line alone increased signalling of upstream pluripotency regulators through augmented phosphorylation and subsequent nuclear translocation of SMAD2/3 and increased transcription of *NANOG* and *POU5F1*. An associated role for HIF1A in regulating SMAD2/3 transcriptional activity has been previously reported in vascular cell lines and mouse ESC, but not in human ESC. However, even with the observed increase in TGFβ signalling, the proportion of hESCs classified as pluripotent was unaltered.

Examination of whether these differing responses across cell lines was due to cell line variability or an inherent difference between ESCs and iPSCs merits further investigation. As neither line showed an increase in the proportion of cells classified as pluripotent, it is likely that the use of low oxygen to maintain self-renewal is superfluous due to recent developments in defined media formulations.

7.1.2 Future work

Differentiation of multiple hESC lines to a somatic identity and subsequent reprogramming back to a pluripotent state would clarify if the variable responses observed here between the H9 hESC and 34D6 iPSC line were a facet of genetic differences or an inherent effect due to the reprogramming process. The following assays could then be performed:

- Cell-cycle analysis, with the expected observation of continued increase in active cell division in iPSCs, independent of effect on parent hESCs, which would likely be variable across lines.
- Silencing of HIF1A and HIF2A and subsequent analysis of SMAD2/3 phosphorylation state at low oxygen. This would likely result in consistent attenuation of SMAD2/3 phosphorylation with variability across iPSC lines.

7.2 Differentiation of hESCs to a neuroectodermal fate at low oxygen did not improve efficiency of neural induction, but did augment BMP inhibition above that at atmospheric oxygen.

Here, early neural induction of H9 hESCs using dual-SMAD inhibition augmented production of PAX6+ cells when performed as EBs but not as a monolayer, in conjunction with reduced EB production at low oxygen. When differentiated as a monolayer at reduced O_2, the percentage of cells with a

neuroectodermal cell fate was extremely efficient and equivalent, with no additive increase due to differentiation at low oxygen.

However, at 3% O_2 NPCs developed with augmented suppression of SMAD1/5/8 phosphorylation above that which was observed at atmospheric O_2. Suppression of phosphorylation was still observed at 3% O_2 without exogenous BMP inhibition, hence the disparity between neural induction as EBs and monolayer was likely contributed to by endogenous inhibition of BMP signalling at 3% O_2. As H9s differentiated with Activin/Nodal inhibition only retained inhibition of SMAD1/5/8 phosphorylation at 3% O_2, it is feasible that a high proportion of neuroectodermal cells would continue to be produced, but would likely not be more efficient than exogenous BMP inhibition via LDN193189 treatment.

Additionally, an increase in apoptosis was observed at low oxygen, both in a BMP-inhibition dependent and independent manner. HESC derived neural progenitors also underwent a significant decrease in the proportion of cells not dividing, indicating a rise in cell proliferation at 3% O_2 during neural differentiation. As increased proliferation was not observed in pluripotent hESCs at low O_2, it seems feasible that it is specific to the neural differentiation process, although whether a reactionary event to increased apoptosis warrants further investigation. These are novel findings in the context of hESC differentiation.

7.2.2 Future work

The efficiency of neural induction at 3% O_2 showed variability when performed as a monolayer or as EBs, the following would clarify if this related to concentration gradients of oxygen and small molecule inhibitors:

- Perform cryosections of EBs for histology staining of phosphorylated SMAD1/5/8, HIF1A and TUNEL. Compare with EBs, chopped at regular intervals to maintain consistent size across oxygen concentrations. Gradients of BMP activity and HIF1A expression would likely present in a manner dependent on EB size at 20% O_2. A higher proportion of TUNEL+

cells and augmented SMAD1/5/8 phosphorylation would likely be retained at 3% O_2.

Augmented inhibition of BMP signalling occurred concurrently with increased apoptosis at 3% O_2 and was increased by exogenous BMP inhibition, the following assays would clarify this apparent connection:

- Neural induction of hESCs without exogenous BMP inhibition, for example through the use of Retinoic acid. Augmented BMP inhibition and increased apoptosis would likely be retained at low oxygen, higher than that at high oxygen.

7.3 Differentiation of hESCs at 3% O_2 increased neuronal excitability.

Use of 3% O_2 for neural differentiation of hESCs produced neurons with augmented and accelerated excitability. Whilst the proportion of neurons showing spontaneous and induced excitable activity was comparable across oxygen concentrations, neurons at 3% O_2 also showed co-registration of Synaptophysin and PSD95 earlier than those at high O_2. Additionally, they formed trains of action potentials at an earlier timepoint in the maturation process and at a higher frequency than those at high oxygen. This was likely contributed to by the observed faster rate of membrane depolarisation seen by week 4 and resting membrane potentials which lay within the sodium (in)activation window. This would have aided repetitive firing as a lesser degree of incoming depolarising signals would be required to hit voltage threshold. These are novel findings, which highlight low oxygen as an essential tool for increasing excitability of neurons, *in vitro*.

7.3.2 Future work.

Synaptophysin expression was accelerated at 3% O_2 concordantly with augmented spontaneous excitability. The following experiments would clarify if this was indicative of increased synaptogenesis:

- Use of a microelectrode array for assessment of action potential propagation across the synaptic network, expected to result in increased synaptic integration due to neuronal maturation at low O_2.

The intensive time requirement required for patch clamp analysis restricted further investigation into manipulation of oxygen concentration for augmentation of neuronal maturation.

- Use of a microelectrode array would allow for high throughput analysis of the time period and oxygen concentration required to further optimise maturation of neurons at low oxygen.
- Scholl analysis would also be beneficial to investigate dendritic outgrowth and axon length, which would be expected to increase at low oxygen.

7.4 A low oxygen environment during in vitro cell culture must be carefully controlled.

Through this collaboration with Baker-Ruskinn, it has become apparent that numerous technical aspects of low oxygen culture must be carefully controlled. Many low oxygen workstations (including the one used here) have transparent front screens to allow cell culture processes to be performed without disturbing gas concentration levels. Both the 34D6 iPSC line and H9 hESC line showed vast increases in cell death due to this resultant light exposure, a factor which had not previously been recognised to be an issue within the company. A screen cover has now been made available to end-users to prevent this issue in the future.

Through development of the HypoxyCOOL media preconditioning unit, knowledge of dissolved oxygen has also been disseminated throughout the company. This must be considered and controlled for through pre-incubation of all cell culture liquids prior to use. The time required for pre-incubation was also

largely shown to be dependent on the volume of liquids and the final oxygen concentration required.

8. Appendix and Bibliography

8.1 Appendix

Table 8.1 Summary of data obtained from whole cell patch clamp of hESC derived neurons at week 1 in 20% and 3% O_2.

Week 1 **NOX** (n=26)		sAP type		n	sAP type		n	sAP type		n
		None			**Attempted sAP**			**Full sAP**		
	Cells within Group (%)	77%		20	19%		5	4%		1
iAP type (%)	None (%)	0%		0	0%		0	0%		0
	Attempted Single (%)	20%		4	20%		1	0%		0
	Single (%)	40%		8	20%		1	0%		0
	Attempted Train (%)	20%		4	60%		3	0%		0
	Train (%)	20%		4	0%		0	100%		1
		Mean	SEM	n	Mean	SEM	n	Mean	SEM	n
Passive	Vm (mV)	-28.2	1.6	20	-34.49978	4.5	5	-30.1338	N/A	1
	Rin (MΩ)	960.9	81.8	20	1433.172	139.6	5	1471.47	N/A	1
	Cp (pF)	13.7	1.2	18	10.3908	1.9	5	14.82	N/A	1
Spike Analysis	Threshold (mV)	-24.5	2.6	14	-19.4	0.3	5	-19.6	N/A	1
	Overshoot (mV)	7.2	1.6	17	8.1	2.7	5	10.0	N/A	1
	Afterhyperpolaization (mV)	-35.0	3.0	17	-30.3	3.8	5	-19.6	N/A	1
	Spike Height (mV)	42.2	4.0	17	38.4	5.6	5	29.5	N/A	1
	Depolarization rate (V/S)	25.9	3.4	17	22.1	1.7	5	12.2	N/A	1
	Repolarization rate (V/S)	-12.2	0.7	17	-11.8	2.4	5	-9.2	N/A	1
	Half Width (ms)	9.0	1.1	17	14.5	3.5	5	26.0	N/A	1
		Mean	SEM	n	Mean	SEM	n	Mean	SEM	n
Currents	INa_{Max} (pA/pF)	-85.3	15.7	13	-99.8	22.3	4	0.0	N/A	1
	IK_{+60} (pA/pF)	112.1	13.1	13	110.9	31.6	4	0.0	N/A	1

Week 1 **HOX** (n=24)		sAP type		n	sAP type		n	sAP type		n
		None			**Attempted sAP**			**Full sAP**		
	Cells within Group (%)	96%		23	0%		0	4%		1
iAP type (%)	None (%)	4%		1	0%		0	0%		0
	Attempted Single (%)	22%		5	0%		0	0%		0
	Single (%)	43%		10	0%		0	0%		0
	Attempted Train (%)	26%		6	0%		0	0%		0
	Train (%)	4%		1	0%		0	100%		1
		Mean	SEM	n	Mean	SEM	n	Mean	SEM	n
Passive	Vm (mV)	-33.4	1.7	23				-36.7098	N/A	1
	Rin (MΩ)	1,144.2	77.9	23				706.177	N/A	1
	Cp (pF)	10.6	1.0	22				10.25	N/A	1
Spike Analysis	Threshold (mV)	-24.0	1.3	20				-37.0	N/A	1
	Overshoot (mV)	6.4	1.1	18				30.9	N/A	1
	Afterhyperpolaization (mV)	-39.5	2.1	19				-58.6	N/A	1
	Spike Height (mV)	45.9	2.2	19				89.5	N/A	1
	Depolarization rate (V/S)	24.2	2.0	19				82.4	N/A	1
	Repolarization rate (V/S)	-12.2	0.7	19				-24.4	N/A	1
	Half Width (ms)	11.5	1.6	19				4.2	N/A	1
		Mean	SEM		Mean	SEM	n	Mean	SEM	n
Currents	INa_{Max} (pA/pF)	-91.1	17.6	15				-200.8	N/A	1
	IK_{+60} (pA/pF)	145.4	21.0	15				154.0	N/A	1

Table 8.2 Summary of data obtained from whole cell patch clamp of hESC derived neurons at week 2 in 20% and 3% O_2.

Week 2 **NOX** (n=25)		sAP type		n	sAP type		n	sAP type		n
		None			**Attempted sAP**			**Full sAP**		
	Cells within Group (%)	36%		9	36%		9	28%		7
iAP type (%)	None (%)	0%		0	0%		0	0%		0
	Attempted Single (%)	22%		2	11%		1	0%		0
	Single (%)	0%		0	33%		3	0%		0
	Attempted Train (%)	44%		4	33%		3	0%		0
	Train (%)	33%		3	22%		2	100%		7
		Mean	SEM	n	Mean	SEM	n	Mean	SEM	n
Passive	Vm (mV)	-32.9	3.0	9	-36.0	3.6	9	-34.7	4.7	7
	Rin (MΩ)	1,013.5	73.0	8	989.4	177.6	9	943.3	121.4	7
	Cp (pF)	11.8	1.7	9	13.1	1.7	7	25.2	1.7	6
Spike Analysis	Threshold (mV)	-25.3	3.1	7	-23.0	3.4	8	-44.0	1.8	7
	Overshoot (mV)	9.8	1.7	7	9.1	2.5	8	15.1	3.0	7
	Afterhyperpolaization (mV)	-43.7	3.7	7	-38.7	4.2	8	-53.3	2.8	7
	Spike Height (mV)	53.5	3.7	7	47.9	4.8	8	68.4	3.6	7
	Depolarization rate (V/S)	29.2	4.6	7	30.2	3.2	8	91.6	9.4	7
	Repolarization rate (V/S)	-13.5	2.0	7	-15.6	1.0	8	-36.6	3.3	7
	Half Width (ms)	9.2	1.2	7	8.8	2.2	8	2.1	0.7	7
		Mean	SEM	n	Mean	SEM	n	Mean	SEM	n
Currents	INa_{Max} (pA/pF)	-86.0	15.7	9	-122.1	24.7	5	0.0	41.9	6
	IK_{+60} (pA/pF)	141.4	24.3	9	213.6	73.0	5	0.0	24.0	6
Week 2 **HOX** (n=26)		sAP type		n	sAP type		n	sAP type		n
		None			**Attempted sAP**			**Full sAP**		
	Cells within Group (%)	50%		13	12%		3	38%		10
iAP type (%)	None (%)	0%		0	0%		0	0%		0
	Attempted Single (%)	0%		0	33%		1	0%		0
	Single (%)	38%		5	33%		1	0%		0
	Attempted Train (%)	23%		3	33%		1	10%		1
	Train (%)	38%		5	0%		0	90%		9
		Mean	SEM	n	Mean	SEM	n	Mean	SEM	n
Passive	Vm (mV)	-27.8	2.3	13	-26.1	12.3	3	-20.2	4.3	10
	Rin (MΩ)	901.2	138.7	13	660.1	150.5	3	954.3	172.1	10
	Cp (pF)	12.1	1.7	11	8.4	5.2	3	18.3	0.2	10
Spike Analysis	Threshold (mV)	-25.2	2.6	13	-33.2	N/A	2	-24.6	1.5	10
	Overshoot (mV)	9.0	1.8	13	11.6	N/A	2	40.3	1.7	10
	Afterhyperpolaization (mV)	-40.0	2.1	13	-41.8	N/A	2	-34.4	1.3	10
	Spike Height (mV)	44.4	4.2	13	53.4	N/A	2	74.7	3.4	10
	Depolarization rate (V/S)	29.9	2.4	13	45.8	N/A	2	97.6	3.8	10
	Repolarization rate (V/S)	-12.9	1.0	13	-15.3	N/A	2	-33.6	1.9	10
	Half Width (ms)	9.4	1.3	13	3.9	N/A	2	2.5	0.5	10
		Mean	SEM		Mean	SEM	n	Mean	SEM	n
Currents	INa_{Max} (pA/pF)	-100.9	18.5	11	-166.6	22.8	3	-217.8	4.3	8
	IK_{+60} (pA/pF)	129.7	27.2	11	320.5	36.1	3	59.7	13.9	8

Table 8.3 Summary of data obtained from whole cell patch clamp of hESC derived neurons at week 3 in 20% an d 3% O_2.

Week 3 **NOX** (n=21)		sAP type		n	sAP type		n	sAP type		n
		None			**Attempted sAP**			**Full sAP**		
	Cells within Group (%)	10%		2	24%		5	67%		14
iAP type (%)	None (%)	0%		0	20%		1	0%		0
	Attempted Single (%)	0%		0	0%		0	0%		0
	Single (%)	50%		1	0%		0	0%		0
	Attempted Train (%)	50%		1	40%		2	0%		0
	Train (%)	0%		0	40%		2	100%		14
		Mean	SEM	n	Mean	SEM	n	Mean	SEM	n
Passive	Vm (mV)	-34.1	N/A	2	-49.4	4.8	5	-45.4	2.9	14
	Rin (MΩ)	843.3	N/A	2	1,322.8	864.0	4	506.2	91.0	12
	Cp (pF)	9.3	N/A	2	14.2	2.7	5	22.7	5.2	13
Spike Analysis	Threshold (mV)	-31.8	N/A	2	-23.6	5.3	4	-31.7	3.7	14
	Overshoot (mV)	20.5	N/A	2	10.2	4.8	4	25.4	2.5	14
	Afterhyperpolaization (mV)	-46.8	N/A	2	-44.2	1.4	4	-47.4	2.5	14
	Spike Height (mV)	67.3	N/A	2	54.4	5.7	4	72.8	3.5	14
	Depolarization rate (V/S)	79.4	N/A	2	31.3	9.4	4	85.3	12.3	14
	Repolarization rate (V/S)	-24.4	N/A	2	-13.7	1.5	4	-27.7	2.9	14
	Half Width (ms)	4.4	N/A	2	10.9	3.1	4	3.7	0.4	14
		Mean	SEM	n	Mean	SEM	n	Mean	SEM	n
Currents	INa_{Max} (pA/pF)	-231.7	N/A	2	-109.5	19.2	3	-172.1	42.7	9
	IK_{+60} (pA/pF)	133.6	N/A	2	145.4	51.8	3	123.7	34.6	9

Week 3 **HOX** (n=24)		sAP type		n	sAP type		n	sAP type		n
		None			**Attempted sAP**			**Full sAP**		
	Cells within Group (%)	71%		17	8%		2	21%		5
iAP type (%)	None (%)	6%		1	0%		0	0%		0
	Attempted Single (%)	12%		2	50%		1	0%		0
	Single (%)	59%		10	0%		0	0%		0
	Attempted Train (%)	12%		2	0%		0	0%		0
	Train (%)	12%		2	50%		1	100%		5
		Mean	SEM	n	Mean	SEM	n	Mean	SEM	n
Passive	Vm (mV)	-26.4	2.6	17	-38.3	N/A	2	-41.8	4.5	5
	Rin (MΩ)	914.8	97.6	17	680.7	N/A	2	651.8	66.6	5
	Cp (pF)	10.6	1.2	16	12.8	N/A	2	17.3	3.2	5
Spike Analysis	Threshold (mV)	-21.9	2.6	11	-19.7	N/A	1	-26.8	3.0	5
	Overshoot (mV)	4.5	1.0	14	16.8	N/A	1	25.1	3.6	5
	Afterhyperpolaization (mV)	-38.4	2.6	14	-47.5	N/A	1	-49.7	2.4	5
	Spike Height (mV)	42.9	2.9	14	64.4	N/A	1	74.8	2.6	5
	Depolarization rate (V/S)	24.4	3.3	14	42.7	N/A	1	58.0	6.8	5
	Repolarization rate (V/S)	-11.6	0.8	14	-21.4	N/A	1	-22.0	3.1	5
	Half Width (ms)	12.9	2.3	14	4.3	N/A	1	4.4	0.5	5
		Mean	SEM	n	Mean	SEM	n	Mean	SEM	n
Currents	INa_{Max} (pA/pF)	-92.7	20.0	11	-66.5	N/A	2	-115.0	15.7	5
	IK_{+60} (pA/pF)	93.4	10.2	11	110.1	N/A	2	98.7	7.3	5

Table 8.4 Summary of data obtained from whole cell patch clamp of hESC derived neurons at week 4 in 20% and 3% O2.

Week 4 **NOX** (n=11)		sAP type		n	sAP type		n	sAP type		n
		None			**Attempted sAP**			**Full sAP**		
	Cells within Group (%)	18%		2	18%		2	64%		7
iAP type (%)	None (%)	0%		0	0%		0	0%		0
	Attempted Single (%)	0%		0	0%		0	0%		0
	Single (%)	0%		0	0%		0	14%		1
	Attempted Train (%)	50%		1	50%		1	0%		0
	Train (%)	50%		1	50%		1	71%		5
		Mean	SEM	n	Mean	SEM	n	Mean	SEM	n
Passive	Vm (mV)	-26.3	N/A	2	-28.7	N/A	2	-27.1	0.8	7
	Rin (MΩ)	1,019.1	N/A	2	95.8	N/A	2	416.6	116.5	7
	Cp (pF)	13.3	N/A	2	11.9	N/A	2	21.7	2.4	7
Spike Analysis	Threshold (mV)	-45.7	N/A	2	-33.8	N/A	2	-35.5	2.7	7
	Overshoot (mV)	8.9	N/A	2	12.6	N/A	2	24.3	3.7	7
	Afterhyperpolaization (mV)	-52.8	N/A	2	-46.3	N/A	2	-45.7	1.9	7
	Spike Height (mV)	61.7	N/A	2	58.9	N/A	2	70.0	4.9	7
	Depolarization rate (V/S)	49.6	N/A	2	21.4	N/A	2	61.1	8.0	7
	Repolarization rate (V/S)	-25.9	N/A	2	-12.2	N/A	2	-33.6	1.3	7
	Half Width (ms)	3.8	N/A	2	6.5	N/A	2	2.5	0.3	7
		Mean	SEM	n	Mean	SEM	n	Mean	SEM	n
Currents	INa_{Max} (pA/pF)	-222.3	N/A	2	-104.9	N/A	2	0.0	14.9	6
	IK_{+60} (pA/pF)	284.3	N/A	2	107.8	N/A	2	0.0	17.2	6

Week 4 **HOX** (n=14)		sAP type		n	sAP type		n	sAP type		n
		None			**Attempted sAP**			**Full sAP**		
	Cells within Group (%)	21%		3	21%		3	57%		8
iAP type (%)	None (%)	0%		0	0%		0	0%		0
	Attempted Single (%)	0%		0	0%		0	0%		0
	Single (%)	0%		0	0%		0	0%		0
	Attempted Train (%)	33%		1	67%		2	0%		0
	Train (%)	67%		2	33%		1	100%		8
		Mean	SEM	n	Mean	SEM	n	Mean	SEM	n
Passive	Vm (mV)	-39.4	1.5	3	-32.8	5.5	3	-41.0	2.1	8
	Rin (MΩ)	1,126.0	451.3	3	1,041.9	412.8	3	479.9	97.2	8
	Cp (pF)	18.3	5.3	3	16.5	3.6	3	22.7	3.8	8
Spike Analysis	Threshold (mV)	-35.6	9.9	3	-29.6	3.9	3	-30.0	1.0	8
	Overshoot (mV)	10.8	5.6	3	7.3	5.6	3	31.2	2.6	8
	Afterhyperpolaization (mV)	-46.8	3.3	3	-42.8	4.3	3	-48.5	1.7	8
	Spike Height (mV)	57.6	2.3	3	50.0	9.7	3	79.7	2.9	8
	Depolarization rate (V/S)	44.8	6.2	3	42.3	14.2	3	111.8	16.9	8
	Repolarization rate (V/S)	-17.8	3.1	3	-20.9	1.3	3	-29.4	2.9	8
	Half Width (ms)	5.7	1.0	3	5.1	1.5	3	3.2	0.4	8
		Mean	SEM	n	Mean	SEM	n	Mean	SEM	n
Currents	INa_{Max} (pA/pF)	-152.9	N/A	2	-116.6	N/A	2	-180.9	38.5	6
	IK_{+60} (pA/pF)	220.1	N/A	2	135.9	N/A	2	99.0	20.9	6

Figure 8.1 Additional HIF2A western blots in the H9 cell line.

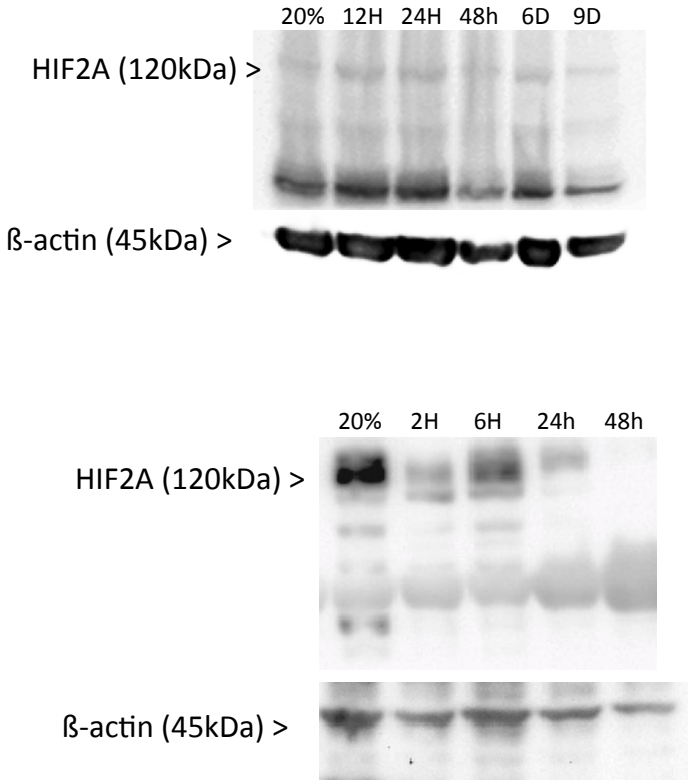

8.2 Bibliography.

Aaku-Saraste, E., Hellwig, A. & Huttner, W.B., 1996. Loss of occludin and functional tight junctions, but not ZO-1, during neural tube closure--remodeling of the neuroepithelium prior to neurogenesis. *Developmental biology*, 180(2), pp.664–79.

Abouna, G.M., 2008. Organ shortage crisis: problems and possible solutions. *Transplantation proceedings*, 40(1), pp.34–8.

Abranches, E. et al., 2009. Neural differentiation of embryonic stem cells in vitro: a road map to neurogenesis in the embryo. *PloS one*, 4(7), p.e6286.

Adachi, K. et al., 2010. Role of SOX2 in maintaining pluripotency of human embryonic stem cells. *Genes to cells : devoted to molecular & cellular mechanisms*, 15(5), pp.455–70.

Akman, H.O. et al., 2001. Response to hypoxia involves transforming growth factor-beta2 and Smad proteins in human endothelial cells. *Blood*, 98(12), pp.3324–31.

De Almeida, P.E. et al., 2014. Transplanted terminally differentiated induced pluripotent stem cells are accepted by immune mechanisms similar to self-tolerance. *Nature communications*, 5, p.3903.

Amit, M. et al., 2000. Clonally derived human embryonic stem cell lines maintain pluripotency and proliferative potential for prolonged periods of culture. *Developmental biology*, 227(2), pp.271–8.

Andersen, P. et al., 2012. Non-canonical Notch signaling: emerging role and mechanism. *Trends in cell biology*, 22(5), pp.257–65.

Appelhoff, R.J. et al., 2004. Differential function of the prolyl hydroxylases PHD1, PHD2, and PHD3 in the regulation of hypoxia-inducible factor. *The Journal of biological chemistry*, 279(37), pp.38458–65.

Armstrong, L. et al., 2006. The role of PI3K/AKT, MAPK/ERK and NFkappabeta signalling in the maintenance of human embryonic stem cell pluripotency and viability highlighted by transcriptional profiling and functional analysis. *Human molecular genetics*, 15(11), pp.1894–913.

Aubert, J. et al., 2002. Functional gene screening in embryonic stem cells implicates Wnt antagonism in neural differentiation. *Nature biotechnology*, 20(12), pp.1240–5.

Augstein, A. et al., 2011. Cell-specific and hypoxia-dependent regulation of human HIF-3α: inhibition of the expression of HIF target genes in vascular cells. *Cellular and molecular life sciences : CMLS*, 68(15), pp.2627–42.

Aulisio, M.P., Devita, M. & Luebke, D., 2007. Taking values seriously: Ethical challenges in organ donation and transplantation for critical care professionals. *Critical care medicine*, 35(2 Suppl), pp.S95–101.

Avery, S. et al., 2006. Embryonic Stem Cells. , 740, pp.729–740.

Avilion, A. et al., 2003. Multipotent cell lineages in early mouse development depend on SOX2 function. *Genes & development*, 17(1), pp.126–40.

Baba, M. et al., 2003. Loss of von Hippel-Lindau protein causes cell density dependent deregulation of CyclinD1 expression through hypoxia-inducible factor. *Oncogene*, 22(18), pp.2728–38.

Bain, G. et al., 1995. Embryonic stem cells express neuronal properties in vitro. *Developmental biology*, 168(2), pp.342–57.

Baker, J.C., Beddington, R.S. & Harland, R.M., 1999. Wnt signaling in Xenopus embryos inhibits bmp4 expression and activates neural development. *Genes & development*, 13(23), pp.3149–59.

Baker, M., 2009. Unregulated stem cell transplant causes tumours. *Nature Reports Stem Cells*.

Bales, K.R., 2012. The value and limitations of transgenic mouse models used in drug discovery for Alzheimer's disease: an update. *Expert opinion on drug discovery*, 7(4), pp.281–97.

Ban, J. et al., 2007. Embryonic stem cell-derived neurons form functional networks in vitro. *Stem cells (Dayton, Ohio)*, 25(3), pp.738–49.

Baranov, P., Tucker, B.A. & Young, M.J., 2013. Low Oxygen Culture Conditions Extend the Multipotent Properties of Human Retinal Progenitor Cells. *Tissue engineering. Part A*.

Bartels, K., Grenz, A. & Eltzschig, H.K., 2013. Hypoxia and inflammation are two sides of the same coin. *Proceedings of the National Academy of Sciences of the United States of America*, 110(46), pp.18351–2.

Bean, B.P., 2007. The action potential in mammalian central neurons. *Nature reviews. Neuroscience*, 8(6), pp.451–65.

Beaudoin, G.M.J. et al., 2012. Culturing pyramidal neurons from the early postnatal mouse hippocampus and cortex. *Nature protocols*, 7(9), pp.1741–54.

Becker, K.A. et al., 2007. Establishment of histone gene regulation and cell cycle checkpoint control in human embryonic stem cells. *Journal of cellular physiology*, 210(2), pp.517–26.

Becker, K.A. et al., 2010. Human embryonic stem cells are pre-mitotically committed to self-renewal and acquire a lengthened G1 phase upon lineage programming. *Journal of cellular physiology*, 222(1), pp.103–10.

Becker, K.A. et al., 2006. Self-renewal of human embryonic stem cells is supported by a shortened G1 cell cycle phase. *Journal of cellular physiology*, 209(3), pp.883–93.

Bell, E.L. et al., 2007. Mitochondrial reactive oxygen species trigger hypoxia-inducible factor-dependent extension of the replicative life span during hypoxia. *Molecular and cellular biology*, 27(16), pp.5737–45.

Le Belle, J.E. et al., 2011. Proliferative neural stem cells have high endogenous ROS levels that regulate self-renewal and neurogenesis in a PI3K/Akt-dependant manner. *Cell stem cell*, 8(1), pp.59–71.

Belmokhtar, C.A., Hillion, J. & Ségal-Bendirdjian, E., 2001. Staurosporine induces apoptosis through both caspase-dependent and caspase-independent mechanisms. *Oncogene*, 20(26), pp.3354–62.

Ben-Hur, T. et al., 2004. Transplantation of human embryonic stem cell-derived neural progenitors improves behavioral deficit in Parkinsonian rats. *Stem cells (Dayton, Ohio)*, 22(7), pp.1246–55.

Benninger, F. et al., 2003. Functional integration of embryonic stem cell-derived neurons in hippocampal slice cultures. *The Journal of neuroscience : the official journal of the Society for Neuroscience*, 23(18), pp.7075–83.

Berchner-Pfannschmidt, U. et al., 2008. Nuclear oxygen sensing: induction of endogenous prolyl-hydroxylase 2 activity by hypoxia and nitric oxide. *The Journal of biological chemistry*, 283(46), pp.31745–53.

Ten Berge, D. et al., 2008. Wnt signaling mediates self-organization and axis formation in embryoid bodies. *Cell stem cell*, 3(5), pp.508–18.

Bernardi, M.L., Fléchon, J.E. & Delouis, C., 1996. Influence of culture system and oxygen tension on the development of ovine zygotes matured and fertilized in vitro. *Journal of reproduction and fertility*, 106(2), pp.161–7.

Berra, E. et al., 2003. HIF prolyl-hydroxylase 2 is the key oxygen sensor setting low steady-state levels of HIF-1alpha in normoxia. *The EMBO journal*, 22(16), pp.4082–90.

Besser, D., 2004. Expression of nodal, lefty-a, and lefty-B in undifferentiated human embryonic stem cells requires activation of Smad2/3. *The Journal of biological chemistry*, 279(43), pp.45076–84.

Bhattacharya, S. et al., 1999. Functional role of p35srj, a novel p300/CBP binding protein, during transactivation by HIF-1. *Genes & development*, 13(1), pp.64–75.

Bilican, B. et al., 2012. Mutant induced pluripotent stem cell lines recapitulate aspects of TDP-43 proteinopathies and reveal cell-specific vulnerability. *Proceedings of the National Academy of Sciences of the United States of America*, 109(15), pp.5803–8.

Boergermann, J.H. et al., 2010. Dorsomorphin and LDN-193189 inhibit BMP-mediated Smad, p38 and Akt signalling in C2C12 cells. *The international journal of biochemistry & cell biology*, 42(11), pp.1802–7.

Bontekoe, S. et al., 2012. Low oxygen concentrations for embryo culture in assisted reproductive technologies (Review) Low oxygen concentrations for embryo culture in assisted reproductive technologies. , (7).

Boyer, L.A. et al., 2005. Core transcriptional regulatory circuitry in human embryonic stem cells. *Cell*, 122(6), pp.947–56.

Brahimi-Horn, C., Mazure, N. & Pouysségur, J., 2005. Signalling via the hypoxia-inducible factor-1alpha requires multiple posttranslational modifications. *Cellular signalling*, 17(1), pp.1–9.

Brederlau, A. et al., 2006. Transplantation of human embryonic stem cell-derived cells to a rat model of Parkinson's disease: effect of in vitro differentiation on graft survival and teratoma formation. *Stem cells (Dayton, Ohio)*, 24(6), pp.1433–40.

Brons, I.G.M. et al., 2007. Derivation of pluripotent epiblast stem cells from mammalian embryos. *Nature*, 448(7150), pp.191–5.

Bylund, M. et al., 2003. Vertebrate neurogenesis is counteracted by Sox1-3 activity. *Nature neuroscience*, 6(11), pp.1162–8.

Cai, C. & Grabel, L., 2007. Directing the differentiation of embryonic stem cells to neural stem cells. *Developmental dynamics : an official publication of the American Association of Anatomists*, 236(12), pp.3255–66.

Cai, J. et al., 2007. Transplantation of embryonic stem cell-derived cardiomyocytes improves cardiac function in infarcted rat hearts. *Cytotherapy*, 9(3), pp.283–91.

Calegari, F. et al., 2005. Selective lengthening of the cell cycle in the neurogenic subpopulation of neural progenitor cells during mouse brain development. *The Journal of neuroscience : the official journal of the Society for Neuroscience*, 25(28), pp.6533–8.

Calegari, F. & Huttner, W.B., 2003. An inhibition of cyclin-dependent kinases that lengthens, but does not arrest, neuroepithelial cell cycle induces premature neurogenesis. *Journal of cell science*, 116(Pt 24), pp.4947–55.

Camarasa, M.V. et al., 2012. Optimized protocol for derivation of human embryonic stem cell lines. *Stem cell reviews*, 8(3), pp.1011–20.

Cameron, C.M. et al., 2008. Activation of hypoxic response in human embryonic stem cell-derived embryoid bodies. *Experimental biology and medicine (Maywood, N.J.)*, 233(8), pp.1044–57.

Caniggia, I. et al., 2000. Hypoxia-inducible factor-1 mediates the biological effects of oxygen on human trophoblast differentiation through TGFbeta(3). *The Journal of clinical investigation*, 105(5), pp.577–87.

Carmeliet, P. et al., 1998. Role of HIF-1alpha in hypoxia-mediated apoptosis, cell proliferation and tumour angiogenesis. *Nature*, 394(6692), pp.485–90.

Caspi, O. et al., 2007. Transplantation of human embryonic stem cell-derived cardiomyocytes improves myocardial performance in infarcted rat hearts. *Journal of the American College of Cardiology*, 50(19), pp.1884–93.

Cejudo-Martin, P. & Johnson, R.S., 2005. A new notch in the HIF belt: how hypoxia impacts differentiation. *Developmental cell*, 9(5), pp.575–6.

Chambers, S.M. et al., 2009. Highly efficient neural conversion of human ES and iPS cells by dual inhibition of SMAD signaling. *Nature biotechnology*, 27(3), pp.275–80.

Chandel, N.S. et al., 1998. Mitochondrial reactive oxygen species trigger hypoxia-induced transcription. *Proceedings of the National Academy of Sciences of the United States of America*, 95(20), pp.11715–20.

Chandel, N.S. et al., 2000. Reactive oxygen species generated at mitochondrial complex III stabilize hypoxia-inducible factor-1alpha during hypoxia: a mechanism of O2 sensing. *The Journal of biological chemistry*, 275(33), pp.25130–8.

Chen, E.Y. et al., 1999. Hypoxic Microenvironment Within an Embryo Induces Apoptosis and Is Essential for Proper. *Teratology*, 60(4), pp.215–225.

Chen, G. et al., 2011. Chemically defined conditions for human iPSC derivation and culture. *Nature methods*, 8(5), pp.424–9.

Chen, H.-F. et al., 2009. A reduced oxygen tension (5%) is not beneficial for maintaining human embryonic stem cells in the undifferentiated state with short splitting intervals. *Human reproduction (Oxford, England)*, 24(1), pp.71–80.

Chen, H.-F. et al., 2010. Hypoxic culture maintains self-renewal and enhances embryoid body formation of human embryonic stem cells. *Tissue engineering. Part A*, 16(9), pp.2901–13.

Cho, E.-G. et al., 2011. MEF2C enhances dopaminergic neuron differentiation of human embryonic stem cells in a parkinsonian rat model. *PloS one*, 6(8), p.e24027.

Clark, L.C. et al., 1953. Continuous recording of blood oxygen tensions by polarography. *Journal of applied physiology*, 6(3), pp.189–93.

Clarke, L. & van der Kooy, D., 2009. Low oxygen enhances primitive and definitive neural stem cell colony formation by inhibiting distinct cell death pathways. *Stem cells (Dayton, Ohio)*, 27(8), pp.1879–86.

Clarkson, E.D., 2001. Fetal tissue transplantation for patients with Parkinson's disease: a database of published clinical results. *Drugs & aging*, 18(10), pp.773–85.

Conklin, J.F. & Sage, J., 2009. Keeping an eye on retinoblastoma control of human embryonic stem cells. *Journal of cellular biochemistry*, 108(5), pp.1023–30.

Conley, B.J. et al., 2005. Mouse embryonic stem cell derivation, and mouse and human embryonic stem cell culture and differentiation as embryoid bodies. *Current protocols in cell biology / editorial board, Juan S. Bonifacino ... [et al.]*, Chapter 23, p.Unit 23.2.

Covello, K.L. et al., 2006. HIF-2alpha regulates Oct-4: effects of hypoxia on stem cell function, embryonic development, and tumor growth. *Genes & development*, 20(5), pp.557–70.

Cunningham, L.A., Candelario, K. & Li, L., 2012. Roles for HIF-1α in neural stem cell function and the regenerative response to stroke. *Behavioural brain research*, 227(2), pp.410–7.

Curchoe, C.L., Russo, J. & Terskikh, A. V, 2012. hESC derived neuro-epithelial rosettes recapitulate early mammalian neurulation events; an in vitro model. *Stem cell research*, 8(2), pp.239–46.

D'Angelo, G. et al., 2003. Hypoxia up-regulates prolyl hydroxylase activity: a feedback mechanism that limits HIF-1 responses during reoxygenation. *The Journal of biological chemistry*, 278(40), pp.38183–7.

Dahéron, L. et al., 2004. LIF/STAT3 signaling fails to maintain self-renewal of human embryonic stem cells. *Stem cells (Dayton, Ohio)*, 22(5), pp.770–8.

Dai, W. et al., 2007. Survival and maturation of human embryonic stem cell-derived cardiomyocytes in rat hearts. *Journal of molecular and cellular cardiology*, 43(4), pp.504–16.

Das, B. et al., 2012. HIF-2α suppresses p53 to enhance the stemness and regenerative potential of human embryonic stem cells. *Stem cells (Dayton, Ohio)*, 30(8), pp.1685–95.

Davila, J. et al., 2013. Acute reduction in oxygen tension enhances the induction of neurons from human fibroblasts. *Journal of neuroscience methods*, 216(2), pp.104–9.

Dee, C.T. et al., 2007. A change in response to Bmp signalling precedes ectodermal fate choice. *The International journal of developmental biology*, 51(1), pp.79–84.

Dehmelt, L. & Halpain, S., 2004. Actin and microtubules in neurite initiation: are MAPs the missing link? *Journal of neurobiology*, 58(1), pp.18–33.

Dehmelt, L. & Halpain, S., 2005. The MAP2/Tau family of microtubule-associated proteins. *Genome biology*, 6(1), p.204.

Delaune, E., Lemaire, P. & Kodjabachian, L., 2005. Neural induction in Xenopus requires early FGF signalling in addition to BMP inhibition. *Development (Cambridge, England)*, 132(2), pp.299–310.

Detrick, R.J., Dickey, D. & Kintner, C.R., 1990. The effects of N-cadherin misexpression on morphogenesis in xenopus embryos. *Neuron*, 4(4), pp.493–506.

Dhara, S. & SL., S., 2009. Neural Differentiation of Human Embryonic Stem Cells. *Journal of Cellular Biochemistry*, 105(3), pp.633–640.

Dick, E. et al., 2011. Two new protocols to enhance the production and isolation of human induced pluripotent stem cell lines. *Stem cell research*, 6(2), pp.158–67.

Ding, V.M.Y. et al., 2010. FGF-2 modulates Wnt signaling in undifferentiated hESC and iPS cells through activated PI3-K/GSK3beta signaling. *Journal of cellular physiology*, 225(2), pp.417–28.

Doi, D. et al., 2012. Prolonged maturation culture favors a reduction in the tumorigenicity and the dopaminergic function of human ESC-derived neural cells in a primate model of Parkinson's disease. *Stem cells (Dayton, Ohio)*, 30(5), pp.935–45.

Draper, J.S. et al., 2002. Surface antigens of human embryonic stem cells: changes upon differentiation in culture. *Journal of anatomy*, 200(Pt 3), pp.249–58.

Duff, K. & Suleman, F., 2004. Transgenic mouse models of Alzheimer's disease: how useful have they been for therapeutic development? *Briefings in functional genomics & proteomics*, 3(1), pp.47–59.

Dunnett, S.B. et al., 1997. Neuronal cell transplantation for Parkinson's and Huntington's diseases. *British medical bulletin*, 53(4), pp.757–76.

Dutta, D. et al., 2008. Activation of the VEGFR1 chromatin domain: an angiogenic signal-ETS1/HIF-2alpha regulatory axis. *The Journal of biological chemistry*, 283(37), pp.25404–13.

Ebert, A.D., Liang, P. & Wu, J.C., 2012. Induced pluripotent stem cells as a disease modeling and drug screening platform. *Journal of cardiovascular pharmacology*, 60(4), pp.408–16.

Eiselleova, L. et al., 2009. A complex role for FGF-2 in self-renewal, survival, and adhesion of human embryonic stem cells. *Stem cells (Dayton, Ohio)*, 27(8), pp.1847–57.

El-Husseini, A.E. et al., 2000. PSD-95 involvement in maturation of excitatory synapses. *Science (New York, N.Y.)*, 290(5495), pp.1364–8.

Elkabetz, Y. et al., 2008. Human ES cell-derived neural rosettes reveal a functionally distinct early neural stem cell stage. , pp.152–165.

Elkabetz, Y. & Studer, L., 2008. Human ESC-derived neural rosettes and neural stem cell progression. *Cold Spring Harbor symposia on quantitative biology*, 73, pp.377–87.

Ema, M. et al., 1997. A novel bHLH-PAS factor with close sequence similarity to hypoxia-inducible factor 1alpha regulates the VEGF expression and is potentially involved in lung and vascular development. *Proceedings of the National Academy of Sciences of the United States of America*, 94(9), pp.4273–8.

Erceg, S. et al., 2008. Differentiation of human embryonic stem cells to regional specific neural precursors in chemically defined medium conditions. *PloS one*, 3(5), p.e2122.

Erecińska, M. & Silver, I. a, 2001. Tissue oxygen tension and brain sensitivity to hypoxia. *Respiration physiology*, 128(3), pp.263–76.

Eshkind, L.G. & Leube, R.E., 1995. Mice lacking synaptophysin reproduce and form typical synaptic vesicles. *Cell and tissue research*, 282(3), pp.423–33.

Evans, M.J. & Kaufman, M.H., 1981. Establishment in culture of pluripotential cells from mouse embryos. *Nature*, 292(5819), pp.154–156.

Ezashi, T., Das, P. & Roberts, R.M., 2005. Low O2 tensions and the prevention of differentiation of hES cells. *Proceedings of the National Academy of Sciences of the United States of America*, 102(13), pp.4783–8.

Faast, R. et al., 2004. Cdk6-cyclin D3 activity in murine ES cells is resistant to inhibition by p16(INK4a). *Oncogene*, 23(2), pp.491–502.

Fadok, V.A. et al., 1998. The role of phosphatidylserine in recognition of apoptotic cells by phagocytes. *Cell death and differentiation*, 5(7), pp.551–62.

Fandrey, J., Gorr, T.A. & Gassmann, M., 2006. Regulating cellular oxygen sensing by hydroxylation. *Cardiovascular research*, 71(4), pp.642–51.

FAO.org, FAO.org. *http://www.fao.org/docrep/field/003/ac183e/ac183e04.htm*.

Fernandes, T.G. et al., 2010. Different stages of pluripotency determine distinct patterns of proliferation, metabolism, and lineage commitment of embryonic stem cells under hypoxia. *Stem cell research*, 5(1), pp.76–89.

Fischer, B. & Bavister, B., 1993. Oxygen tension in the oviduct and uterus of rhesus monkeys, hamsters and rabbits. *Journal of reproduction and fertility.*, 99(2).

Foja, S. et al., 2013. Hypoxia supports reprogramming of mesenchymal stromal cells via induction of embryonic stem cell-specific microRNA-302 cluster and pluripotency-associated genes. *Cellular reprogramming*, 15(1), pp.68–79.

Fong, H., Hohenstein, K. a & Donovan, P.J., 2008. Regulation of self-renewal and pluripotency by Sox2 in human embryonic stem cells. *Stem cells (Dayton, Ohio)*, 26(8), pp.1931–8.

Fong, H., Hohenstein, K.A. & Donovan, P.J., 2008. Regulation of self-renewal and pluripotency by Sox2 in human embryonic stem cells. *Stem cells (Dayton, Ohio)*, 26(8), pp.1931–8.

Forristal, C.E. et al., 2010. Hypoxia inducible factors regulate pluripotency and proliferation in human embryonic stem cells cultured at reduced oxygen tensions. *Reproduction (Cambridge, England)*, 139(1), pp.85–97.

Forsyth, N.R. et al., 2006. Physiologic oxygen enhances human embryonic stem cell clonal recovery and reduces chromosomal abnormalities. *Cloning and stem cells*, 8(1), pp.16–23.

Francis, K.R. & Wei, L., 2010. Human embryonic stem cell neural differentiation and enhanced cell survival promoted by hypoxic preconditioning. *Cell death & disease*, 1(2), p.e22.

Freedman, S.J. et al., 2003. Structural basis for negative regulation of hypoxia-inducible factor-1alpha by CITED2. *Nature structural biology*, 10(7), pp.504–12.

Fukuda, H. et al., 2006. Fluorescence-activated cell sorting-based purification of embryonic stem cell-derived neural precursors averts tumor formation after transplantation. *Stem cells (Dayton, Ohio)*, 24(3), pp.763–71.

Gao, B.-X. & Ziskind-Conhaim, L., 1998. Development of Ionic Currents Underlying Changes in Action Potential Waveforms in Rat Spinal Motoneurons. *J Neurophysiol*, 80(6), pp.3047–3061.

García-García, E. et al., 2012. Intermediate progenitors are increased by lengthening of the cell cycle through calcium signaling and p53 expression in human neural progenitors. *Molecular biology of the cell*, 23(7), pp.1167–80.

Gardner, L.B. et al., 2001. Hypoxia inhibits G1/S transition through regulation of p27 expression. *The Journal of biological chemistry*, 276(11), pp.7919–26.

Gassmann, M. et al., 1996. Oxygen supply and oxygen-dependent gene expression in differentiating embryonic stem cells. *Proceedings of the National Academy of Sciences of the United States of America*, 93(7), pp.2867–72.

Gauthaman, K., Fong, C.-Y. & Bongso, A., 2010. Effect of ROCK inhibitor Y-27632 on normal and variant human embryonic stem cells (hESCs) in vitro: its benefits in hESC expansion. *Stem cell reviews*, 6(1), pp.86–95.

Genbacev, O., 1997. Regulation of Human Placental Development by Oxygen Tension. *Science*, 277(5332), pp.1669–1672.

George, S. et al., 2009. Comparison of the response of human embryonic stem cells and their differentiated progenies to oxidative stress. *Photomedicine and laser surgery*, 27(4), pp.669–74.

Germain, N., Banda, E. & Grabel, L., 2010. Embryonic stem cell neurogenesis and neural specification. *Journal of cellular biochemistry*, 111(3), pp.535–42.

Gerrard, L., Zhao, D., et al., 2005. Stably transfected human embryonic stem cell clones express OCT4-specific green fluorescent protein and maintain self-renewal and pluripotency. *Stem cells (Dayton, Ohio)*, 23(1), pp.124–33.

Gerrard, L., Rodgers, L. & Cui, W., 2005. Differentiation of human embryonic stem cells to neural lineages in adherent culture by blocking bone morphogenetic protein signaling. *Stem cells (Dayton, Ohio)*, 23(9), pp.1234–41.

Gilbert, S., 2006. *Developmental Biology* 8th ed.,

Glantz, L.A. et al., 2007. Synaptophysin and postsynaptic density protein 95 in the human prefrontal cortex from mid-gestation into early adulthood. *Neuroscience*, 149(3), pp.582–91.

Goda, N. et al., 2003. Hypoxia-Inducible Factor 1 ‚, Is Essential for Cell Cycle Arrest during Hypoxia. , 23(1), pp.359–369.

Goldberg, J.S. & Hirschi, K.K., 2009. Diverse roles of the vasculature within the neural stem cell niche. *Regenerative medicine*, 4(6), pp.879–97.

Gomes Sobrinho, D.B. et al., 2011. IVF/ICSI outcomes after culture of human embryos at low oxygen tension: a meta-analysis. *Reproductive biology and endocrinology : RB&E*, 9(1), p.143.

Gordan, J.D. et al., 2007. HIF-2alpha promotes hypoxic cell proliferation by enhancing c-myc transcriptional activity. *Cancer cell*, 11(4), pp.335–47.

Gordon, S.L., Leube, R.E. & Cousin, M.A., 2011. Synaptophysin is required for synaptobrevin retrieval during synaptic vesicle endocytosis. *The Journal of neuroscience : the official journal of the Society for Neuroscience*, 31(39), pp.14032–6.

Graham, V. et al., 2003. SOX2 functions to maintain neural progenitor identity. *Neuron*, 39(5), pp.749–65.

Grzelak, A., Rychlik, B. & Bartosz, G., 2001. Light-dependent generation of reactive oxygen species in cell culture media. *Free radical biology & medicine*, 30(12), pp.1418–25.

Gu, Y.Z. et al., 1998. Molecular characterization and chromosomal localization of a third alpha-class hypoxia inducible factor subunit, HIF3alpha. *Gene expression*, 7(3), pp.205–13.

Guillaumond, F. et al., 2013. Strengthened glycolysis under hypoxia supports tumor symbiosis and hexosamine biosynthesis in pancreatic adenocarcinoma. *Proceedings of the National Academy of Sciences of the United States of America*, 110(10), pp.3919–24.

Gultice, A.D., Kulkarni-Datar, K. & Brown, T.L., 2009. Hypoxia-inducible factor 1alpha (HIF1A) mediates distinct steps of rat trophoblast differentiation in gradient oxygen. *Biology of reproduction*, 80(1), pp.184–93.

Gustafsson, M. V et al., 2005. Hypoxia requires notch signaling to maintain the undifferentiated cell state. *Developmental cell*, 9(5), pp.617–28.

Halliwell, B., 2003. Oxidative stress in cell culture: an under-appreciated problem? *FEBS letters*, 540(1-3), pp.3–6.

Hardwick, L.J.A. et al., 2014. Cell cycle regulation of proliferation versus differentiation in the central nervous system. *Cell and tissue research*.

Harms, K.M., Li, L. & Cunningham, L.A., 2010. Murine neural stem/progenitor cells protect neurons against ischemia by HIF-1alpha-regulated VEGF signaling. *PloS one*, 5(3), p.e9767.

Harvey, A.J. et al., 2004. Oxygen-regulated gene expression in bovine blastocysts. *Biology of reproduction*, 71(4), pp.1108–19.

Heikkilä, M. et al., 2011. Roles of the human hypoxia-inducible factor (HIF)-3α variants in the hypoxia response. *Cellular and molecular life sciences : CMLS*, 68(23), pp.3885–901.

Heikkilä, T.J. et al., 2009. Human embryonic stem cell-derived neuronal cells form spontaneously active neuronal networks in vitro. *Experimental neurology*, 218(1), pp.109–16.

Henderson, J.K. et al., 2002. Preimplantation human embryos and embryonic stem cells show comparable expression of stage-specific embryonic antigens. *Stem cells (Dayton, Ohio)*, 20(4), pp.329–37.

Hendrickson, M.L. et al., 2011. Expression of nestin by neural cells in the adult rat and human brain. C. Combs, ed. *PloS one*, 6(4), p.e18535.

Hierholzer, A. & Kemler, R., 2010. Beta-catenin-mediated signaling and cell adhesion in postgastrulation mouse embryos. *Developmental dynamics : an official publication of the American Association of Anatomists*, 239(1), pp.191–9.

Hill, D.S. et al., 2010. Teratogenic effects of antiepileptic drugs. *Expert review of neurotherapeutics*, 10(6), pp.943–59.

Hirata, T. et al., 2002. Mosaic development of the olfactory cortex with Pax6-dependent and -independent components. *Brain research. Developmental brain research*, 136(1), pp.17–26.

Hjelmeland, M.D. et al., 2004. SB-431542 , a small molecule transforming growth factor- β -receptor antagonist , inhibits human glioma cell line proliferation and motility factor-B-receptor antagonist , inhibits human glioma cell line proliferation and motility. , pp.737–745.

Hoch, R. V, Rubenstein, J.L.R. & Pleasure, S., 2009. Genes and signaling events that establish regional patterning of the mammalian forebrain. *Seminars in cell & developmental biology*, 20(4), pp.378–86.

Hoffmeyer, K. et al., 2012. Wnt/β-catenin signaling regulates telomerase in stem cells and cancer cells. *Science (New York, N.Y.)*, 336(6088), pp.1549–54.

Horie, N. et al., 2008. Effects of oxygen concentration on the proliferation and differentiation of mouse neural stem cells in vitro. *Cellular and molecular neurobiology*, 28(6), pp.833–45.

Hou, P. et al., 2013. Pluripotent stem cells induced from mouse somatic cells by small-molecule compounds. *Science (New York, N.Y.)*, 341(6146), pp.651–4.

Hovatta, O. et al., 2003. A culture system using human foreskin fibroblasts as feeder cells allows production of human embryonic stem cells. *Human reproduction (Oxford, England)*, 18(7), pp.1404–9.

Hu, C., Wang, L., Chodosh, L., et al., 2003. Differential Roles of Hypoxia-Inducible Factor 1α (HIF-1α) and HIF-2α in Hypoxic Gene Regulation. *Molecular cell biology*, 23(24), pp.9361–74.

Hu, C., Sataur, A. & Wang, L., 2007. The N-terminal transactivation domain confers target gene specificity of hypoxia-inducible factors HIF-1α and HIF-2α. *Molecular biology of the …*, 18(November), pp.4528–4542.

Hu, C., Wang, L. & Chodosh, L., 2003. Differential roles of hypoxia-inducible factor 1α (HIF-1α) and HIF-2α in hypoxic gene regulation. *Molecular and cellular …*, 23(24), pp.9361–9374.

Hu, X. et al., 2008. Transplantation of hypoxia-preconditioned mesenchymal stem cells improves infarcted heart function via enhanced survival of implanted cells and angiogenesis. *The Journal of thoracic and cardiovascular surgery*, 135(4), pp.799–808.

Huang, Z. et al., 2013. Necdin controls proliferation and apoptosis of embryonic neural stem cells in an oxygen tension-dependent manner. *The Journal of neuroscience : the official journal of the Society for Neuroscience*, 33(25), pp.10362–73.

Hughes, C.S., Postovit, L.M. & Lajoie, G.A., 2010. Matrigel: a complex protein mixture required for optimal growth of cell culture. *Proteomics*, 10(9), pp.1886–90.

Ietta, F. et al., 2006. Dynamic HIF1A regulation during human placental development. *Biology of reproduction*, 75(1), pp.112–21.

Iliopoulos, O. et al., 1996. Negative regulation of hypoxia-inducible genes by the von Hippel-Lindau protein. *Proceedings of the National Academy of Sciences of the United States of America*, 93(20), pp.10595–9.

Illes, S. et al., 2007. Development and pharmacological modulation of embryonic stem cell-derived neuronal network activity. *Experimental neurology*, 207(1), pp.171–6.

Inman, G.J. et al., 2002. SB-431542 Is a Potent and Specific Inhibitor of Transforming Growth Factor- ɴʟ Superfamily Type I Activin Receptor-Like. , 62(1), pp.65–74.

Inoue, T., Nakamura, S. & Osumi, N., 2000. Fate mapping of the mouse prosencephalic neural plate. *Developmental biology*, 219(2), pp.373–83.

Isaacs, J.S. et al., 2002. Hsp90 regulates a von Hippel Lindau-independent hypoxia-inducible factor-1 alpha-degradative pathway. *The Journal of biological chemistry*, 277(33), pp.29936–44.

Israel, M. a et al., 2012. Probing sporadic and familial Alzheimer's disease using induced pluripotent stem cells. *Nature*, 482(7384), pp.216–20.

Itsykson, P. et al., 2005. Derivation of neural precursors from human embryonic stem cells in the presence of noggin. *Molecular and cellular neurosciences*, 30(1), pp.24–36.

Iyer, N. V et al., 1998. Cellular and developmental control of O2 homeostasis by hypoxia-inducible factor 1 alpha. *Genes & development*, 12(2), pp.149–62.

James, D. et al., 2005. TGFbeta/activin/nodal signaling is necessary for the maintenance of pluripotency in human embryonic stem cells. *Development (Cambridge, England)*, 132(6), pp.1273–82.

Jensen, P. et al., 2011. Enhanced proliferation and dopaminergic differentiation of ventral mesencephalic precursor cells by synergistic effect of FGF2 and reduced oxygen tension. *Experimental cell research*, 317(12), pp.1649–62.

Ji, L. et al., 2009. Self-renewal and pluripotency is maintained in human embryonic stem cells by co-culture with human fetal liver stromal cells expressing hypoxia inducible factor 1alpha. *Journal of cellular physiology*, 221(1), pp.54–66.

Jiang, P.-C. et al., 2013. A clinical trial report of autologous bone marrow-derived mesenchymal stem cell transplantation in patients with spinal cord injury. *Experimental and therapeutic medicine*, 6(1), pp.140–146.

Joannides, A.J. et al., 2007. A scaleable and defined system for generating neural stem cells from human embryonic stem cells. *Stem cells (Dayton, Ohio)*, 25(3), pp.731–7.

Johnson, M.A. et al., 2007. Functional neural development from human embryonic stem cells: accelerated synaptic activity via astrocyte coculture. *The Journal of neuroscience : the official journal of the Society for Neuroscience*, 27(12), pp.3069–77.

Jokilehto, T. et al., 2010. Retention of prolyl hydroxylase PHD2 in the cytoplasm prevents PHD2-induced anchorage-independent carcinoma cell growth. *Experimental cell research*, 316(7), pp.1169–78.

Jun, S. & Desplan, C., 1996. Cooperative interactions between paired domain and homeodomain. *Development (Cambridge, England)*, 122(9), pp.2639–50.

Karp, G., 2009. *Cell and Molecular Biology*,

Kashyap, V. et al., 2009. Regulation of stem cell pluripotency and differentiation involves a mutual regulatory circuit of the NANOG, OCT4, and SOX2 pluripotency transcription factors with polycomb repressive complexes and stem cell microRNAs. *Stem cells and development*, 18(7), pp.1093–108.

Katsetos, C.D. et al., 2003. Class III beta-tubulin isotype: a key cytoskeletal protein at the crossroads of developmental neurobiology and tumor neuropathology. *Journal of child neurology*, 18(12), pp.851–66; discussion 867.

Kaushansky, K., 2006. Lineage-specific hematopoietic growth factors. *The New England journal of medicine*, 354(19), pp.2034–45.

Kazanis, I. et al., 2013. *The Neural Stem Cell Microenvironment.*,

Ke, Q. & Costa, M., 2006. Hypoxia-inducible factor-1 (HIF-1). *Molecular pharmacology*, 70(5), pp.1469–80.

Kearney, N. & Richardson, A., 2005. *Nursing Patients with Cancer: Principles and Practice*,

Kelly, C. et al., 2000. Maternally controlled (beta)-catenin-mediated signaling is required for organizer formation in the zebrafish. *Development (Cambridge, England)*, 127(18), pp.3899–911.

Kelly, O.G., Pinson, K.I. & Skarnes, W., 2004. The Wnt co-receptors Lrp5 and Lrp6 are essential for gastrulation in mice. *Development (Cambridge, England)*, 131(12), pp.2803–15.

Keramari, M. et al., 2010. Sox2 is essential for formation of trophectoderm in the preimplantation embryo. *PloS one*, 5(11).

Kim, K. et al., 2010. Epigenetic memory in induced pluripotent stem cells. *Nature*, 467(7313), pp.285–90.

Kim, T.-S. et al., 2008. Increase in dopaminergic neurons from mouse embryonic stem cell-derived neural progenitor/stem cells is mediated by hypoxia inducible factor-1alpha. *Journal of neuroscience research*, 86(11), pp.2353–62.

Klingensmith, J. et al., 1999. Neural induction and patterning in the mouse in the absence of the node and its derivatives. *Developmental biology*, 216(2), pp.535–49.

Koopman, G. et al., 1994. Annexin V for flow cytometric detection of phosphatidylserine expression on B cells undergoing apoptosis. *Blood*, 84(5), pp.1415–20.

Koshiji, M. et al., 2004. HIF-1alpha induces cell cycle arrest by functionally counteracting Myc. *The EMBO journal*, 23(9), pp.1949–56.

Kozak, K.R., Abbott, B. & Hankinson, O., 1997. ARNT-deficient mice and placental differentiation. *Developmental biology*, 191(2), pp.297–305.

Krabbe, C. et al., 2014. Influence of oxygen tension on dopaminergic differentiation of human fetal stem cells of midbrain and forebrain origin. *PloS one*, 9(5), p.e96465.

Krieg, M. et al., 2000. Up-regulation of hypoxia-inducible factors HIF-1alpha and HIF-2alpha under normoxic conditions in renal carcinoma cells by von Hippel-Lindau tumor suppressor gene loss of function. *Oncogene*, 19(48), pp.5435–43.

Kühl, S.J. & Kühl, M., 2012. On the role of Wnt/β-catenin signaling in stem cells. *Biochimica et biophysica acta*.

Kumar, R., 2010. *Textbook of Human Embryology*,

Kuroda, T. et al., 2005. Octamer and Sox elements are required for transcriptional cis regulation of Nanog gene expression. *Molecular and cellular biology*, 25(6), pp.2475–85.

Kwon, S.E. & Chapman, E.R., 2011. Synaptophysin regulates the kinetics of synaptic vesicle endocytosis in central neurons. *Neuron*, 70(5), pp.847–54.

Lamb, T. et al., 1993. Neural induction by the secreted polypeptide noggin. *Science*, 262(5134), pp.713–718.

Lambert, J.-C. & Amouyel, P., 2011. Genetics of Alzheimer's disease: new evidences for an old hypothesis? *Current opinion in genetics & development*, 21(3), pp.295–301.

Lange, C. & Calegari, F., 2010. Cdks and cyclins link G1 length and differentiation of embryonic, neural and hematopoietic stem cells. *Cell cycle (Georgetown, Tex.)*, 9(10), pp.1893–900.

Lau, K.W. et al., 2007. Target gene selectivity of hypoxia-inducible factor-alpha in renal cancer cells is conveyed by post-DNA-binding mechanisms. *British journal of cancer*, 96(8), pp.1284–92.

Launay, C. et al., 1996. A truncated FGF receptor blocks neural induction by endogenous Xenopus inducers. *Development (Cambridge, England)*, 122(3), pp.869–80.

Lawrence, P. et al., 2011. *Principles of Development* 4th ed.,

Le, R. et al., 2014. Enhanced telomere rejuvenation in pluripotent cells reprogrammed via nuclear transfer relative to induced pluripotent stem cells. *Cell stem cell*, 14(1), pp.27–39.

Lee, H. et al., 2007. Directed differentiation and transplantation of human embryonic stem cell-derived motoneurons. *Stem cells (Dayton, Ohio)*, 25(8), pp.1931–9.

Lee, Y.M. et al., 2001. Determination of hypoxic region by hypoxia marker in developing mouse embryos in vivo: a possible signal for vessel development. *Developmental dynamics : an official publication of the American Association of Anatomists*, 220(2), pp.175–86.

Lengner, C.J. et al., 2010. Derivation of pre-X inactivation human embryonic stem cells under physiological oxygen concentrations. *Cell*, 141(5), pp.872–83.

Leor, J. et al., 2007. Human embryonic stem cell transplantation to repair the infarcted myocardium. *Heart (British Cardiac Society)*, 93(10), pp.1278–84.

Levine, A.J. & Brivanlou, A.H., 2007. Proposal of a model of mammalian neural induction. *Developmental biology*, 308(2), pp.247–56.

Li, J. et al., 2007. MEK/ERK signaling contributes to the maintenance of human embryonic stem cell self-renewal. *Differentiation; research in biological diversity*, 75(4), pp.299–307.

Lighton, J.R.B., 2008. *Measuring Metabolic Rates : A Manual for Scientists: A Manual for Scientists*, Oxford University Press.

Lipton, P., 1999. Ischemic Cell Death in Brain Neurons. *Physiol Rev*, 79(4), pp.1431–1568.

Liu, S. et al., 2009. Generation of dopaminergic neurons from human fetal mesencephalic progenitors after co-culture with striatal-conditioned media and exposure to lowered oxygen. *Brain research bulletin*, 80(1-2), pp.62–8.

Loh, Y.-H. et al., 2006. The Oct4 and Nanog transcription network regulates pluripotency in mouse embryonic stem cells. *Nature genetics*, 38(4), pp.431–40.

Lord, E.M. et al., 1993. Detection of Hypoxic Cells by Monoclonal Antibody Recognizing 2-Nitroimidazole Adducts Detection of Hypoxic Cells by Monoclonal Antibody Recognizing 2-Nitroimidazole. , pp.5721–5726.

Lowry, W.E. et al., 2008. Generation of human induced pluripotent stem cells from dermal fibroblasts. *Proceedings of the National Academy of Sciences of the United States of America*, 105(8), pp.2883–8.

Ludwig, T. & Thomson, A., 2007. Defined, feeder-independent medium for human embryonic stem cell culture. *Current protocols in stem cell biology*, Chapter 1, p.Unit 1C.2.

Makino, Y. et al., 2002. Inhibitory PAS domain protein (IPAS) is a hypoxia-inducible splicing variant of the hypoxia-inducible factor-3alpha locus. *The Journal of biological chemistry*, 277(36), pp.32405–8.

Malchenko, S. et al., 2014. Onset of rosette formation during spontaneous neural differentiation of hESC and hiPSC colonies. *Gene*, 534(2), pp.400–7.

Mallon, B.S. et al., 2006. Toward xeno-free culture of human embryonic stem cells. *The international journal of biochemistry & cell biology*, 38(7), pp.1063–75.

Maltepe, E. et al., 1997. Abnormal angiogenesis and responses to glucose and oxygen deprivation in mice lacking the protein ARNT. *Nature*, 386(6623), pp.403–7.

Marchetto, M.C.N. et al., 2009. Transcriptional signature and memory retention of human-induced pluripotent stem cells. *PloS one*, 4(9), p.e7076.

Martin, G.R., 1981. Isolation of a pluripotent cell line from early mouse embryos cultured in medium conditioned by teratocarcinoma stem cells. *Proceedings of the National Academy of Sciences of the United States of America*, 78(12), pp.7634–8.

Martin, G.R., Wiley, L.M. & Damjanov, I., 1977. The development of cystic embryoid bodies in vitro from clonal teratocarcinoma stem cells. *Developmental biology*, 61(2), pp.230–44.

Maynard, M.A. et al., 2003. Multiple splice variants of the human HIF-3 alpha locus are targets of the von Hippel-Lindau E3 ubiquitin ligase complex. *The Journal of biological chemistry*, 278(13), pp.11032–40.

Mazumdar, J. et al., 2010. O2 regulates stem cells through Wnt/β-catenin signalling. *Nature cell biology*, 12(10), pp.1007–13.

McCord, A.M. et al., 2009. Physiologic oxygen concentration enhances the stem-like properties of CD133+ human glioblastoma cells in vitro. *Molecular cancer research : MCR*, 7(4), pp.489–97.

McMahon, H.T. et al., 1996. Synaptophysin, a major synaptic vesicle protein, is not essential for neurotransmitter release. *Proceedings of the National Academy of Sciences of the United States of America*, 93(10), pp.4760–4.

Michalczyk, K. & Ziman, M., 2005. Nestin structure and predicted function in cellular cytoskeletal organisation. *Histology and histopathology*, 20(2), pp.665–71.

Milosevic, J. et al., 2007. Lack of hypoxia-inducible factor-1 alpha impairs midbrain neural precursor cells involving vascular endothelial growth factor signaling. *The Journal of neuroscience : the official journal of the Society for Neuroscience*, 27(2), pp.412–21.

Mitsui, K. et al., 2003. The homeoprotein Nanog is required for maintenance of pluripotency in mouse epiblast and ES cells. *Cell*, 113(5), pp.631–42.

Molleman, A., 2003. *Patch Clamping : An Introductory Guide to Patch Clamp Electrophysiology*, Wiley.

Mondragon-Teran, P. et al., 2013. Oxygen-controlled automated neural differentiation of mouse embryonic stem cells. *Regenerative medicine*, 8(2), pp.171–82.

Mondragon-Teran, P. et al., 2011. The full spectrum of physiological oxygen tensions and step-changes in oxygen tension affects the neural differentiation of mouse embryonic stem cells. *Biotechnology progress*, 27(6), pp.1700–8.

Mondragon-Teran, P., Lye, G. & Veraitch, F., 2009. Lowering oxygen tension enhances the differentiation of mouse embryonic stem cells into neuronal cells. *Biotechnology progress*, 25(5), pp.1480–8.

Moreno-Manzano, V. et al., 2010. FM19G11, a new hypoxia-inducible factor (HIF) modulator, affects stem cell differentiation status. *The Journal of biological chemistry*, 285(2), pp.1333–42.

Morizane, A. et al., 2011. Small-molecule inhibitors of bone morphogenic protein and activin/nodal signals promote highly efficient neural induction from human pluripotent stem cells. *Journal of neuroscience research*, 89(2), pp.117–26.

Morriss, G.M. & New, D.A., 1979. Effect of oxygen concentration on morphogenesis of cranial neural folds and neural crest in cultured rat embryos. *Journal of embryology and experimental morphology*, 54, pp.17–35.

Mukhopadhyay, M. et al., 2001. Dickkopf1 is required for embryonic head induction and limb morphogenesis in the mouse. *Developmental cell*, 1(3), pp.423–34.

Muñoz-Sanjuán, I. & Brivanlou, A.H., 2002. Neural induction, the default model and embryonic stem cells. *Nature reviews. Neuroscience*, 3(4), pp.271–80.

Mutoh, T. et al., 2012. Oxygen levels epigenetically regulate fate switching of neural precursor cells via hypoxia-inducible factor 1α-notch signal interaction in the developing brain. *Stem cells (Dayton, Ohio)*, 30(3), pp.561–9.

Nakagawa, M. et al., 2008. Generation of induced pluripotent stem cells without Myc from mouse and human fibroblasts. *Nature biotechnology*, 26(1), pp.101–6.

Närvä, E. et al., 2013. Continuous Hypoxic Culturing of Human Embryonic Stem Cells Enhances SSEA-3 and MYC Levels. *PloS one*, 8(11), p.e78847.

Nazıroğlu, M. & Yürekli, V.A., 2013. Effects of antiepileptic drugs on antioxidant and oxidant molecular pathways: focus on trace elements. *Cellular and molecular neurobiology*, 33(5), pp.589–99.

Nguyen, L.K. et al., 2013. A dynamic model of the hypoxia-inducible factor 1α (HIF-1α) network. *Journal of cell science*, 126(Pt 6), pp.1454–63.

Nichols, J. et al., 1998. Formation of pluripotent stem cells in the mammalian embryo depends on the POU transcription factor Oct4. *Cell*, 95(3), pp.379–91.

Niecknig, H. et al., 2012. Role of reactive oxygen species in the regulation of HIF-1 by prolyl hydroxylase 2 under mild hypoxia. *Free radical research*, 46(6), pp.705–17.

Nishi, H. et al., 2004. Hypoxia-Inducible Factor 1 Mediates Upregulation of Telomerase (hTERT). , 24(13), pp.6076–6083.

Niwa, H., Miyazaki, J. & Smith, A.G., 2000. Quantitative expression of Oct-3/4 defines differentiation, dedifferentiation or self-renewal of ES cells. *Nature genetics*, 24(4), pp.372–6.

Nordhoff, V. et al., 2001. Comparative analysis of human, bovine, and murine Oct-4 upstream promoter sequences. *Mammalian genome : official journal of the International Mammalian Genome Society*, 12(4), pp.309–17.

O'Leary, T. et al., 2013. Derivation of human embryonic stem cells using a post-inner cell mass intermediate. *Nature protocols*, 8(2), pp.254–64.

O'Malley, J., Woltjen, K. & Kaji, K., 2009. New strategies to generate induced pluripotent stem cells. *Current opinion in biotechnology*, 20(5), pp.516–21.

Ohnuma, S. & Harris, W.A., 2003. Neurogenesis and the cell cycle. *Neuron*, 40(2), pp.199–208.

Okabe, S. et al., 1996. Development of neuronal precursor cells and functional postmitotic neurons from embryonic stem cells in vitro. *Mechanisms of development*, 59(1), pp.89–102.

Okada, M., Oka, M. & Yoneda, Y., 2010. Effective culture conditions for the induction of pluripotent stem cells. *Biochimica et biophysica acta*, 1800(9), pp.956–63.

Oshima, R., 1978. Stimulation of the clonal growth and differentiation of feeder layer dependent mouse embryonal carcinoma cells by beta-mercaptoethanol. *Differentiation; research in biological diversity*, 11(3), pp.149–55.

Osumi, N. et al., 2008. Concise review: Pax6 transcription factor contributes to both embryonic and adult neurogenesis as a multifunctional regulator. *Stem cells (Dayton, Ohio)*, 26(7), pp.1663–72.

Ottosen, L.D.M. et al., 2006. Observations on intrauterine oxygen tension measured by fibre-optic microsensors. *Reproductive biomedicine online*, 13(3), pp.380–5.

Pan, G. et al., 2006. A negative feedback loop of transcription factors that controls stem cell pluripotency and self-renewal. *FASEB journal : official publication of the Federation of American Societies for Experimental Biology*, 20(10), pp.1730–2.

Panopoulos, A.D. et al., 2012. The metabolome of induced pluripotent stem cells reveals metabolic changes occurring in somatic cell reprogramming. *Cell research*, 22(1), pp.168–77.

Papkovsky, D.B. & Dmitriev, R.I., 2013. Biological detection by optical oxygen sensing. *Chemical Society reviews*, 42(22), pp.8700–32.

Park, D. et al., 2010. Nestin is required for the proper self-renewal of neural stem cells. *Stem cells (Dayton, Ohio)*, 28(12), pp.2162–71.

Park, I.-H. et al., 2008. Reprogramming of human somatic cells to pluripotency with defined factors. *Nature*, 451(7175), pp.141–6.

Park, K.I. et al., 2006. Acute injury directs the migration, proliferation, and differentiation of solid organ stem cells: evidence from the effect of hypoxia-ischemia in the CNS on clonal “reporter” neural stem cells. *Experimental neurology*, 199(1), pp.156–78.

Parshad, R. et al., 1978. Fluorescent light-induced chromosome damage and its prevention in mouse cells in culture. *Proceedings of the National Academy of Sciences of the United States of America*, 75(4), pp.1830–3.

Patani, R. et al., 2009. Activin/Nodal inhibition alone accelerates highly efficient neural conversion from human embryonic stem cells and imposes a caudal positional identity. *PloS one*, 4(10), p.e7327.

Patel, S.A. & Simon, M.C., 2008. Biology of Hypoxia-Inducible Factor-2Ļ in Development and Disease HHMI Author Manuscript. *Cell death and differentiation*, 15(24), pp.628–634.

Peng, J. et al., 2000. The transcription factor EPAS-1/hypoxia-inducible factor 2alpha plays an important role in vascular remodeling. *Proceedings of the National Academy of Sciences of the United States of America*, 97(15), pp.8386–91.

Pera, E. & De Robertis, E.M., 2000. A direct screen for secreted proteins in Xenopus embryos identifies distinct activities for the Wnt antagonists Crescent and Frzb-1. *Mechanisms of Development*, 96(2), pp.183–95.

Perdew, G., Vanden-Heuvel, J. & Peters, J., 2006. *Regulation of Gene Expression: Molecular Mechanisms*,

Perrier, A.L. et al., 2004. Derivation of midbrain dopamine neurons from human embryonic stem cells. *Proceedings of the National Academy of Sciences of the United States of America*, 101(34), pp.12543–8.

Petruzzelli, R. et al., 2014. HIF-2α Regulates NANOG Expression in Human Embryonic Stem Cells following Hypoxia and Reoxygenation through the Interaction with an Oct-Sox Cis Regulatory Element. *PloS one*, 9(10), p.e108309.

Pettersen, E.O. et al., 2005. Pericellular oxygen depletion during ordinary tissue culturing, measured with oxygen microsensors. *Cell proliferation*, 38(4), pp.257–67.

Pfaffl, M.W., 2001. A new mathematical model for relative quantification in real-time RT – PCR. , 29(9), pp.16–21.

Picken Bahrey, H.L. & Moody, W.J., 2003. Early development of voltage-gated ion currents and firing properties in neurons of the mouse cerebral cortex. *Journal of neurophysiology*, 89(4), pp.1761–73.

Pientka, F.K. et al., 2012. Oxygen sensing by the prolyl-4-hydroxylase PHD2 within the nuclear compartment and the influence of compartmentalisation on HIF-1 signalling. *Journal of cell science*, 125(Pt 21), pp.5168–76.

Pirkmajer, S. & Chibalin, A. V, 2011. Serum starvation: caveat emptor. *American journal of physiology. Cell physiology*, 301(2), pp.C272–9.

Pistollato, F. et al., 2009. Hypoxia and HIF1alpha repress the differentiative effects of BMPs in high-grade glioma. *Stem cells (Dayton, Ohio)*, 27(1), pp.7–17.

POST, 2013. *Organ Donation and Transplants*,

Prange, O. et al., 2004. A balance between excitatory and inhibitory synapses is controlled by PSD-95 and neuroligin. *Proceedings of the National Academy of Sciences of the United States of America*, 101(38), pp.13915–20.

Prasad, S.M. et al., 2009. Continuous hypoxic culturing maintains activation of Notch and allows long-term propagation of human embryonic stem cells without spontaneous differentiation. *Cell proliferation*, 42(1), pp.63–74.

Prattipati, V. et al., 2005. Effect of compatibilization on the oxygen-barrier properties of poly(ethylene terephthalate)/poly(m-xylylene adipamide) blends. *Journal of Applied Polymer Science*, 97(3), pp.1361–1370.

Pringle, K.G. et al., 2010. Beyond oxygen: complex regulation and activity of hypoxia inducible factors in pregnancy. *Human reproduction update*, 16(4), pp.415–31.

Quail, D.F. et al., 2011. Low oxygen levels induce the expression of the embryonic morphogen Nodal. *Molecular biology of the cell*, 22(24), pp.4809–21.

Quinn, J.C. et al., 2007. Pax6 controls cerebral cortical cell number by regulating exit from the cell cycle and specifies cortical cell identity by a cell autonomous mechanism. *Developmental biology*, 302(1), pp.50–65.

Rajala, K. et al., 2010. A defined and xeno-free culture method enabling the establishment of clinical-grade human embryonic, induced pluripotent and adipose stem cells. *PloS one*, 5(4), p.e10246.

Ramírez-Bergeron, D.L. et al., 2006. HIF-dependent hematopoietic factors regulate the development of the embryonic vasculature. *Developmental cell*, 11(1), pp.81–92.

Ren, G. et al., 2012. Concise review: mesenchymal stem cells and translational medicine: emerging issues. *Stem cells translational medicine*, 1(1), pp.51–8.

Reubinoff, B.E., Pera, M.F., Fong, C.Y., Trounson, a, et al., 2000. Embryonic stem cell lines from human blastocysts: somatic differentiation in vitro. *Nature biotechnology*, 18(4), pp.399–404.

Reubinoff, B.E., Pera, M.F., Fong, C.Y., Trounson, A., et al., 2000. Embryonic stem cell lines from human blastocysts: somatic differentiation in vitro. *Nature biotechnology*, 18(4), pp.399–404.

Reubinoff, B.E. et al., 2001. Neural progenitors from human embryonic stem cells. *Nature biotechnology*, 19(12), pp.1134–40.

Reynolds, B.A. & Weiss, S., 1996. Clonal and population analyses demonstrate that an EGF-responsive mammalian embryonic CNS precursor is a stem cell. *Developmental biology*, 175(1), pp.1–13.

Richard, D.E. et al., 1999. p42/p44 mitogen-activated protein kinases phosphorylate hypoxia-inducible factor 1alpha (HIF-1alpha) and enhance the transcriptional activity of HIF-1. *The Journal of biological chemistry*, 274(46), pp.32631–7.

Rodda, D.J. et al., 2005. Transcriptional regulation of nanog by OCT4 and SOX2. *The Journal of biological chemistry*, 280(26), pp.24731–7.

Rodesch, F. et al., 1992. Oxygen measurements in endometrial and trophoblastic tissues during early pregnancy. *Obstetrics and gynecology*, 80(2), pp.283–5.

Rodrigues, C.A. V et al., 2010. Hypoxia enhances proliferation of mouse embryonic stem cell-derived neural stem cells. *Biotechnology and bioengineering*, 106(2), pp.260–70.

Roitbak, T., Li, L. & Cunningham, L.A., 2008. Neural stem/progenitor cells promote endothelial cell morphogenesis and protect endothelial cells against ischemia via HIF-1alpha-regulated VEGF signaling. *Journal of cerebral blood flow and metabolism : official journal of the International Society of Cerebral Blood Flow and Metabolism*, 28(9), pp.1530–42.

Roitbak, T., Surviladze, Z. & Cunningham, L., 2011. Continuous expression of HIF-1alpha in neural stem/progenitor cells. *Cell and molecular neurobiology*, 31(1), pp.119–33.

Rossant, J., 2004. Lineage development and polar asymmetries in the peri-implantation mouse blastocyst. *Seminars in cell & developmental biology*, 15(5), pp.573–81.

Ryan, H.E., Lo, J. & Johnson, R.S., 1998. HIF-1 alpha is required for solid tumor formation and embryonic vascularization. *The EMBO journal*, 17(11), pp.3005–15.

Saha, K. & Jaenisch, R., 2009. Technical Challenges in Using Human Induced Pluripotent Stem Cells to Model Disease. *Cell Stem Cell*, 5(6), pp.584–595.

Salceda, S. et al., 1997. Complex role of protein phosphorylation in gene activation by hypoxia. *Kidney International*, 51(2), pp.556–559.

Sánchez, C., Díaz-Nido, J. & Avila, J., 2000. Phosphorylation of microtubule-associated protein 2 (MAP2) and its relevance for the regulation of the neuronal cytoskeleton function. *Progress in neurobiology*, 61(2), pp.133–68.

Sánchez-Elsner, T. et al., 2001. Synergistic cooperation between hypoxia and transforming growth factor-beta pathways on human vascular endothelial growth factor gene expression. *The Journal of biological chemistry*, 276(42), pp.38527–35.

Van der Sanden, B. et al., 2010. Optimizing stem cell culture. *Journal of cellular biochemistry*, 111(4), pp.801–7.

Santilli, G. et al., 2010. Mild hypoxia enhances proliferation and multipotency of human neural stem cells. *PloS one*, 5(1), p.e8575.

Sato, N. et al., 2004. Maintenance of pluripotency in human and mouse embryonic stem cells through activation of Wnt signaling by a pharmacological GSK-3-specific inhibitor. *Nature medicine*, 10(1), pp.55–63.

Savatier, P. et al., 1994. Contrasting patterns of retinoblastoma protein expression in mouse embryonic stem cells and embryonic fibroblasts. *Oncogene*, 9(3), pp.809–18.

Scheiner, Z.S., Talib, S. & Feigal, E.G., 2014. The potential for immunogenicity of autologous induced pluripotent stem cell-derived therapies. *The Journal of biological chemistry*, 289(8), pp.4571–7.

Schipani, E. et al., 2001. Hypoxia in cartilage: HIF-1alpha is essential for chondrocyte growth arrest and survival. *Genes & development*, 15(21), pp.2865–76.

Schuldiner, M. et al., 2001. Induced neuronal differentiation of human embryonic stem cells. *Brain research*, 913(2), pp.201–5.

Schulz, T.C. et al., 2004. Differentiation of human embryonic stem cells to dopaminergic neurons in serum-free suspension culture. *Stem cells (Dayton, Ohio)*, 22(7), pp.1218–38.

Schwartz, S.D. et al., 2012. Embryonic stem cell trials for macular degeneration: a preliminary report. *Lancet*, 379(9817), pp.713–20.

Scortegagna, M. et al., 2003. Multiple organ pathology, metabolic abnormalities and impaired homeostasis of reactive oxygen species in Epas1-/- mice. *Nature genetics*, 35(4), pp.331–40.

Sela-Donenfeld, D. & Kalcheim, C., 1999. Regulation of the onset of neural crest migration by coordinated activity of BMP4 and Noggin in the dorsal neural tube. *Development (Cambridge, England)*, 126(21), pp.4749–62.

Semenza, G.L., 2011a. HIF-1 : upstream and downstream of cancer metabolism. , 20(1), pp.1–10.

Semenza, G.L., 2000. HIF-1 and human disease: one highly involved factor. *Genes & development*, 14(16), pp.1983–91.

Semenza, G.L., 2011b. Oxygen sensing, homeostasis, and disease. *The New England journal of medicine*, 365(6), pp.537–47.

Semenza, G.L. & Wang, G.L., 1992. A nuclear factor induced by hypoxia via de novo protein synthesis binds to the human erythropoietin gene enhancer at a site required for transcriptional activation. *Molecular and cellular biology*, 12(12), pp.5447–54.

Sermeus, A. & Michiels, C., 2011. Reciprocal influence of the p53 and the hypoxic pathways. *Cell death & disease*, 2, p.e164.

Shen, Q. et al., 2008. Adult SVZ stem cells lie in a vascular niche: a quantitative analysis of niche cell-cell interactions. *Cell stem cell*, 3(3), pp.289–300.

Shi, Y. & Massagué, J., 2003. Mechanisms of TGF-β Signaling from Cell Membrane to the Nucleus. *Cell*, 113(6), pp.685–700.

Shimada, H. et al., 2012. Accelerated generation of human induced pluripotent stem cells with retroviral transduction and chemical inhibitors under physiological hypoxia. *Biochemical and biophysical research communications*, 417(2), pp.659–64.

Sies, H. & Bruene, B., 2007. *Oxygen Biology and Hypoxia (Methods in Enzymology)*,

Simon, M.C. & Keith, B., 2008. The role of oxygen availability in embryonic development and stem cell function. *Nature reviews. Molecular cell biology*, 9(4), pp.285–96.

Singh, I., 2008. *Anatomy and Physiology for Nurses*,

Siró, I., Plackett, D. & Sommer-Larsen, P., 2010. A comparative study of oxygen transmission rates through polymer films based on fluorescence quenching. *Packaging Technology and Science*, 23(6), pp.301–315.

Smukler, S.R. et al., 2006. Embryonic stem cells assume a primitive neural stem cell fate in the absence of extrinsic influences. *The Journal of cell biology*, 172(1), pp.79–90.

Spemann, H. & Mangold, H., 1924. Induction of embryonic primordia by implantation of organizers from a different species. *The International journal of developmental biology*, 45(1), pp.13–38.

Stacpoole, S.R.L. et al., 2011a. Derivation of neural precursor cells from human ES cells at 3% O(2) is efficient, enhances survival and presents no barrier to regional specification and functional differentiation. *Cell death and differentiation*, 18(6), pp.1016–23.

Stacpoole, S.R.L. et al., 2011b. Efficient derivation of NPCs, spinal motor neurons and midbrain dopaminergic neurons from hESCs at 3% oxygen. *Nature protocols*, 6(8), pp.1229–40.

Stacpoole, S.R.L. et al., 2013. Neural precursor cells cultured at physiologically relevant oxygen tensions have a survival advantage following transplantation. *Stem cells translational medicine*, 2(6), pp.464–72.

Stead, E. et al., 2002. Pluripotent cell division cycles are driven by ectopic Cdk2, cyclin A/E and E2F activities. *Oncogene*, 21(54), pp.8320–33.

Steiner, J. et al., 2007. Evidence for a wide extra-astrocytic distribution of S100B in human brain. *BMC neuroscience*, 8(1), p.2.

Stewart, R., Stojkovic, M. & Lako, M., 2006. Mechanisms of self-renewal in human embryonic stem cells. *European journal of cancer (Oxford, England : 1990)*, 42(9), pp.1257–72.

Stiles, J. & Jernigan, T.L., 2010. The basics of brain development. *Neuropsychology review*, 20(4), pp.327–48.

Stoien, J.D. & Wang, R.J., 1974. Effect of near-ultraviolet and visible light on mammalian cells in culture II. Formation of toxic photoproducts in tissue culture medium by blacklight. *Proceedings of the National Academy of Sciences of the United States of America*, 71(10), pp.3961–5.

Storch, A. et al., 2001. Long-term proliferation and dopaminergic differentiation of human mesencephalic neural precursor cells. *Experimental neurology*, 170(2), pp.317–25.

Studer, L. et al., 2000. Enhanced proliferation, survival, and dopaminergic differentiation of CNS precursors in lowered oxygen. *The Journal of neuroscience : the official journal of the Society for Neuroscience*, 20(19), pp.7377–83.

Sugimoto, K. et al., 2013. Effects of hypoxia on pluripotency in murine iPS cells. *Microscopy research and technique*, 76(10), pp.1084–92.

Sumi, T. et al., 2004. STAT3 is dispensable for maintenance of self-renewal in nonhuman primate embryonic stem cells. *Stem cells (Dayton, Ohio)*, 22(5), pp.861–72.

Szabó, G.V. et al., 2013. Peripheral blood-derived autologous stem cell therapy for the treatment of patients with late-stage peripheral artery disease-results of the short- and long-term follow-up. *Cytotherapy*, 15(10), pp.1245–52.

Tachibana, M. et al., 2013. Human embryonic stem cells derived by somatic cell nuclear transfer. *Cell*, 153(6), pp.1228–38.

Takahashi, K. et al., 2007. Induction of pluripotent stem cells from adult human fibroblasts by defined factors. *Cell*, 131(5), pp.861–72.

Takahashi, K. & Yamanaka, S., 2006. Induction of Pluripotent Stem Cells from Mouse Embryonic and Adult Fibroblast Cultures by Defined Factors. *Cell*, 126(4), pp.663–676.

Talks, K.L. et al., 2000. The Expression and Distribution of the Hypoxia-Inducible Factors HIF-1α and HIF-2α in Normal Human Tissues, Cancers, and Tumor-Associated Macrophages. *The American Journal of Pathology*, 157(2), pp.411–421.

Tapias, A. et al., 2014. Trrap-dependent histone acetylation specifically regulates cell-cycle gene transcription to control neural progenitor fate decisions. *Cell stem cell*, 14(5), pp.632–43.

Tarsa, L. & Goda, Y., 2002. Synaptophysin regulates activity-dependent synapse formation in cultured hippocampal neurons. *Proceedings of the National Academy of Sciences of the United States of America*, 99(2), pp.1012–6.

Tavazoie, M. et al., 2008. A specialized vascular niche for adult neural stem cells. *Cell stem cell*, 3(3), pp.279–88.

Tervit, H.R., Whittingham, D.G. & Rowson, L.E.A., 1972. SUCCESSFUL CULTURE IN VITRO OF SHEEP AND CATTLE OVA. *Reproduction*, 30(3), pp.493–497.

Tesar, P.J. et al., 2007. New cell lines from mouse epiblast share defining features with human embryonic stem cells. *Nature*, 448(7150), pp.196–9.

Theus, M.H. et al., 2008. In vitro hypoxic preconditioning of embryonic stem cells as a strategy of promoting cell survival and functional benefits after transplantation into the ischemic rat brain. *Experimental Neurology*, 210(2), pp.656–670.

Thomson, J. a., 1998. Embryonic Stem Cell Lines Derived from Human Blastocysts. *Science*, 282(5391), pp.1145–1147.

Thomson, J.A., 1995. Isolation of a Primate Embryonic Stem Cell Line. *Proceedings of the National Academy of Sciences*, 92(17), pp.7844–7848.

Tian, H., McKnight, S.L. & Russell, D.W., 1997. The hypoxia-responsive transcription factor EPAS1 is essential for catecholamine homeostasis and protection against heart failure during embryonic development. *Genes & development*, 11(1), pp.72–82.

Tomita, S. et al., 2003. Defective brain development in mice lacking the Hif-1alpha gene in neural cells. *Molecular and cellular biology*, 23(19), pp.6739–49.

Tung, E.W.Y. & Winn, L.M., 2011. Valproic acid increases formation of reactive oxygen species and induces apoptosis in postimplantation embryos: a role for oxidative stress in valproic acid-induced neural tube defects. *Molecular pharmacology*, 80(6), pp.979–87.

Vallier, L. et al., 2009. Activin/Nodal signalling maintains pluripotency by controlling Nanog expression. *Development (Cambridge, England)*, 136(8), pp.1339–49.

Vallier, L., Alexander, M. & Pedersen, R. a, 2005. Activin/Nodal and FGF pathways cooperate to maintain pluripotency of human embryonic stem cells. *Journal of cell science*, 118(Pt 19), pp.4495–509.

Vazin, T. et al., 2008. Assessment of stromal-derived inducing activity in the generation of dopaminergic neurons from human embryonic stem cells. *Stem cells (Dayton, Ohio)*, 26(6), pp.1517–25.

Verani, R. et al., 2007. Expression of the Wnt inhibitor Dickkopf-1 is required for the induction of neural markers in mouse embryonic stem cells differentiating in response to retinoic acid. *Journal of neurochemistry*, 100(1), pp.242–50.

Wang, G.L. et al., 1995. Hypoxia-inducible factor 1 is a basic-helix-loop-helix-PAS heterodimer regulated by cellular O2 tension. *Proceedings of the National Academy of Sciences of the United States of America*, 92(12), pp.5510–4.

Wang, G.L. & Semenza, G.L., 1993. Characterization of hypoxia-inducible factor 1 and regulation of DNA binding activity by hypoxia. *The Journal of biological chemistry*, 268(29), pp.21513–8.

Wang, J. et al., 2006. A protein interaction network for pluripotency of embryonic stem cells. *Nature*, 444(7117), pp.364–8.

Wang, J., Levasseur, D.N. & Orkin, S.H., 2008. Requirement of Nanog dimerization for stem cell self-renewal and pluripotency. *Proceedings of the National Academy of Sciences of the United States of America*, 105(17), pp.6326–31.

Wang, S. et al., 2013. Umbilical Cord Mesenchymal Stem Cell Transplantation Significantly Improves Neurological Function in Patients with Sequelae of Traumatic Brain Injury. *Brain research*, 1532, pp.76–84.

Wang, S., Qu, X. & Zhao, R.C., 2012. Clinical applications of mesenchymal stem cells. *Journal of hematology & oncology*, 5(1), p.19.

Wang, Y. et al., 2013. Hypoxia promotes dopaminergic differentiation of mesenchymal stem cells and shows benefits for transplantation in a rat model of Parkinson's disease. H. Cai, ed. *PloS one*, 8(1), p.e54296.

Wang, Z. et al., 2012. Distinct lineage specification roles for NANOG, OCT4, and SOX2 in human embryonic stem cells. *Cell stem cell*, 10(4), pp.440–54.

Watanabe, K. et al., 2007. A ROCK inhibitor permits survival of dissociated human embryonic stem cells. *Nature biotechnology*, 25(6), pp.681–6.

Watson, J. V, Chambers, S.H. & Smith, P.J., 1987. A pragmatic approach to the analysis of DNA histograms with a definable G1 peak. *Cytometry*, 8(1), pp.1–8.

Wenger, R.H., 2002. Cellular adaptation to hypoxia: O2-sensing protein hydroxylases, hypoxia-inducible transcription factors, and O2-regulated gene expression. *FASEB journal : official publication of the Federation of American Societies for Experimental Biology*, 16(10), pp.1151–62.

Wessely, O. et al., 2001. Neural induction in the absence of mesoderm: beta-catenin-dependent expression of secreted BMP antagonists at the blastula stage in Xenopus. *Developmental biology*, 234(1), pp.161–73.

Westerlund, U. et al., 2003. Stem cells from the adult human brain develop into functional neurons in culture. *Experimental cell research*, 289(2), pp.378–83.

White, J. & Dalton, S., 2005. Cell cycle control of embryonic stem cells. *Stem cell reviews*, 1(2), pp.131–8.

White, J.R. et al., 2004. Genetic amplification of the transcriptional response to hypoxia as a novel means of identifying regulators of angiogenesis. *Genomics*, 83(1), pp.1–8.

Wiesener, M.S. et al., 2002. Widespread, hypoxia-inducible expression of HIF-2α in distinct cell populations of different organs. , (1).

Wilson, S.I. et al., 2001. The status of Wnt signalling regulates neural and epidermal fates in the chick embryo. *Nature*, 411(6835), pp.325–30.

Van Winkle, A., Gates, I. & Kallos, M., 2012. Mass transfer limitations in embryoid bodies during human embryonic stem cell differentiation. *Cells Tissues Organs*, 196(1).

Wood, J.P.M. et al., 2008. The influence of visible light exposure on cultured RGC-5 cells. *Molecular vision*, 14, pp.334–44.

Wu, S.M. & Hochedlinger, K., 2011. Harnessing the potential of induced pluripotent stem cells for regenerative medicine. *Nature cell biology*, 13(5), pp.497–505.

Wu, W. et al., 2010. Transplantation of neural stem cells expressing hypoxia-inducible factor-1alpha (HIF-1alpha) improves behavioral recovery in a rat stroke model. *Journal of clinical neuroscience : official journal of the Neurosurgical Society of Australasia*, 17(1), pp.92–5.

Xu, C. et al., 2001. Feeder-free growth of undifferentiated human embryonic stem cells. *Nature biotechnology*, 19(10), pp.971–4.

Xu, R.-H. et al., 2002. BMP4 initiates human embryonic stem cell differentiation to trophoblast. *Nature biotechnology*, 20(12), pp.1261–4.

Xu, R.-H. et al., 2008. NANOG is a direct target of TGFbeta/activin-mediated SMAD signaling in human ESCs. *Cell stem cell*, 3(2), pp.196–206.

Ye, Z. et al., 2009. Human-induced pluripotent stem cells from blood cells of healthy donors and patients with acquired blood disorders. *Blood*, 114(27), pp.5473–80.

Ying, Q.-L. & Smith, A.G., 2003. Defined conditions for neural commitment and differentiation. *Methods in enzymology*, 365, pp.327–41.

Yoshida, Y. et al., 2009. Hypoxia enhances the generation of induced pluripotent stem cells. *Cell stem cell*, 5(3), pp.237–41.

Yoshikawa, Y. et al., 1997. Evidence that absence of Wnt-3a signaling promotes neuralization instead of paraxial mesoderm development in the mouse. *Developmental biology*, 183(2), pp.234–42.

Yu, A.Y. et al., 1998. Temporal, spatial, and oxygen-regulated expression of hypoxia-inducible factor-1 in the lung. *The American journal of physiology*, 275(4 Pt 1), pp.L818–26.

Yue, X. & Tomanek, R.J., 1999. Stimulation of coronary vasculogenesis/angiogenesis by hypoxia in cultured embryonic hearts. *Developmental dynamics : an official publication of the American Association of Anatomists*, 216(1), pp.28–36.

Zachar, V. et al., 2010. The effect of human embryonic stem cells (hESCs) long-term normoxic and hypoxic cultures on the maintenance of pluripotency. *In vitro cellular & developmental biology. Animal*, 46(3-4), pp.276–83.

Zeng, X. et al., 2004. Dopaminergic differentiation of human embryonic stem cells. *Stem cells (Dayton, Ohio)*, 22(6), pp.925–40.

Zeng, X. & Rao, M.S., 2007. Human embryonic stem cells: long term stability, absence of senescence and a potential cell source for neural replacement. *Neuroscience*, 145(4), pp.1348–58.

Zhang, B., Wang, X. & Nazarali, A.J., 2010. Ascorbic acid reverses valproic acid-induced inhibition of hoxa2 and maintains glutathione homeostasis in mouse embryos in culture. *Cellular and molecular neurobiology*, 30(1), pp.137–48.

Zhang, H. et al., 2003. Cellular response to hypoxia involves signaling via Smad proteins. *Blood*, 101(6), pp.2253–60.

Zhang, S. & Cui, W., 2014. Sox2, a key factor in the regulation of pluripotency and neural differentiation. *World journal of stem cells*, 6(3), pp.305–11.

Zhang, S.C. et al., 2001. In vitro differentiation of transplantable neural precursors from human embryonic stem cells. *Nature biotechnology*, 19(12), pp.1129–33.

Zhang, X. et al., 2010. Pax6 is a human neuroectoderm cell fate determinant. *Cell stem cell*, 7(1), pp.90–100.

Zhao, Y. et al., 2013. Dual Functions of Hypoxia Inducible Factor-1 alpha for the Commitment of Mouse Embryonic Stem Cells Toward a Neural Lineage. *Stem cells and development*.

Zhao, Y. et al., 2014. Dual Functions of Hypoxia-Inducible Factor 1 Alpha for the Commitment of Mouse Embryonic Stem Cells Toward a Neural Lineage. *Stem cells and development*.

Zhou, Z, Z., 2004. Histology and Embryology. *Peoples Medicine Press*.

Ziegler, U., 2004. Morphological Features of Cell Death. *News in Physiological Sciences*, 19(3), pp.124–128.